Absorption of Nitric Oxide from Flue Gas Using Ammoniacal Cobalt(II) Solutions

by

Hesheng Yu

A thesis
presented to the University of Waterloo
in fulfillment of the
thesis requirement for the degree of
Doctor of Philosophy
in
Mechanical Engineering

Waterloo, Ontario, Canada, 2012

Author's Declaration

I hereby declare that I am the sole author of this thesis. This is a true copy of the thesis, including any required final revisions, as accepted by my examiners.

I understand that my thesis may be made electronically available to the public.

Hesheng Yu

Abstract

Air emissions from the combustion of fossil fuel, including carbon dioxide, sulfur dioxide, nitrogen dioxide and nitric oxide, have caused severe health and environmental problems. The post-combustion wet scrubbing has been employed for control of carbon dioxide and sulfur dioxide emissions. However, it is restricted by the sparingly water soluble nitric oxide, which accounts for 90-95% of nitrogen oxides. It is desirable and cost-effective to remove nitric oxide from flue gas by existing wet scrubbers for reduced capital costs and foot prints.

In this research, absorption of nitric oxide from simulated flue gas using three different absorbents was first conducted in a bubble column system at room temperature and atmospheric pressure. Through performance comparison, ammoniacal cobalt(II) solutions were chosen as the optimum absorbent for nitric oxide absorption. Then the effects of fresh absorbent composition, pH value and temperature on nitric oxide absorption were investigated. Experimental results showed that the best initial NO removal efficiency of 96.45% was measured at the inlet flow rate of 500 $mL \cdot min^{-1}$; the room temperature of 292.2 K; the pH value of 10.50; and the concentrations of cobalt(II) solution, NO and O_2 of 0.06 $mol \cdot L^{-1}$, 500 ppmv and 5.0%, respectively.

For in-depth understanding of NO absorption into ammoniacal cobalt(II) complexes, equilibrium constants of reactions between nitric oxide and penta- and haxa-amminecobalt(II) solutions, respectively were determined using a bubble column reactor, in which the operation was performed continuously with respect to gas phase and batch-wise with respect to liquid phase. The experiments were conducted at temperatures from 298.2 to 310.2 K and pH from 9.06 to 9.37, all under atmospheric pressure. All experimental data fitted well to the following equations: $K_{NO}^{5} = 1.90 \times 10^{7}\exp(\frac{3598.5}{T})$ and $K_{NO}^{6} = 3.56 \times 10^{11}\exp(\frac{1476.4}{T})$, which give the enthalpy of reactions between NO and penta- and hexa-amminecobalt (II) nitrates as $\Delta H^{5} = -29.92\ kJ \cdot mol^{-1}$ and $\Delta H^{6} = -12.27\ kJ \cdot mol^{-1}$.

In kinetic study, a number of experiments were conducted in a home-made double-stirred reactor at temperatures of 298.2 and 303.2 K and pH from 8.50 to 9.87 under atmospheric pressure. The reaction rate constants were calculated with the use of enhancement factor derived for gas absorption accompanied by parallel chemical reactions. The reaction between NO and pentaaminecobalt(II) was first order with respect to NO and pentaamminecobalt(II) ion, respectively. Similarly, the reaction between NO and hexaaminecobalt(II) was also first order with respect to NO and hexaamminecobalt(II) ion, respectively. The forward reaction rate constants of these two reactions

were 6.43×10^6 and 1.00×10^7 $L \cdot mol^{-1} \cdot s^{-1}$, respectively at 298.2 K, and increased to 7.57×10^6 and 1.12×10^7 $L \cdot mol^{-1} \cdot s^{-1}$, respectively at 303.2 K.

Furthermore, regeneration of used absorbent was attempted but fails. None of the additives tested herein including potassium iodide (KI), sodium persulphate ($Na_2S_5O_8$) and activated carbon (AC) showed capability of regeneration at room temperature and atmospheric pressure. In addition, the effect of oxygen was investigated. With ammoniacal cobalt(II) compounds a positive effect of oxygen on NO absorption was observed. Calculated NO amount absorbed into the aqueous solution showed that with the oxygen the absorption reaction could be considered as irreversible. This fact was probably the reason for the failure of regeneration of the tested reagents.

Last but not least, volumetric liquid-phase mass transfer coefficient, k_La, in some popular industrial absorbers including bubble column (BC), conventional stirred tank reactor (CSTR) and gas-inducing agitated tank (GIAT) were determined by modeling removal of oxygen from water. The experimental results could be well interpreted by mathematical models with 90% of deviations less than ± 10 %.

Acknowledgements

I would like to acknowledge my supervisor, Dr. Zhongchao Tan, for his guidance, supervision, and patience throughout the course of this research project. His encouragement and support are greatly appreciated. I would also like to thank other members of my thesis examining committee, Drs. Eric Croiset, Xiangguo Li, Mark J. Rood, and John Z. Wen, for their contributions to this dissertation. In addition, support from Dr. Qunyi Zhu in Harbin Institute of Technology is highly acknowledged.

Thank you is also extended to Professor Guangyuan Xie, Dr. Jimmy Yu and Ms. Lin Wu. My dream of studying overseas could not be realized without their encouragement and assistance. I am grateful to them from my very bottom of heart.

Financial support and scholarships from Natural Sciences and Engineering Research Council of Canada (NSERC), Imperial Oil Ltd., Enersul Inc., the University of Calgary, and the University of Waterloo are also highly appreciated.

I would also like to thank Jim Baleshta, Jason Benninger, Charlie Boyle and Mark Kuntz for their technical support. To those I have worked with during my PhD program both in Calgary and Waterloo, Dr. Sudong Yin, Grace Pan, Chao Yan, Harry Lei, Ke Zhang, Stephen Kuan, Zhe Li, Fang Liu, Raheleh Givhechi and Qixia Zhang, thank you for your assistance, friendship and a pleasant studying environment. Rose Jin, Hanwen Liu, Jianchen Tao and Yuzan Yang, thanks for your friendship over the course of my degree.

I would like to thank all my family members, my parents, my parents-in-law, my sister and brother-in-law. This thesis could not be completed without your great understanding and unconditional support. I especially thank Qianqian Nie, my dear wife, for her love, patience and consistent encouragement she gave so that I could concentrate on studying and working on this project. Her trust is the source of power that drives me to courageously face any challenges.

Dedication

To my loving wife Qianqian and my parents

Table of Contents

List of Figures

List of Tables

List of Symbols

Notation	Term	Unit
a	specific gas-liquid interfacial area	m^{-1}
a_w	water activity	-
A	cross-sectional area	m^2
B	liquid bulk concentration	$mol \cdot L^{-1}$
c, [ ]	concentration	$mol \cdot L^{-1}$
c_1 and c_2	constants in Eq. 2.28	-
d_I	impeller diameter	m
d_P	pipe diameter	m
d_T	vessel diameter	m
	or square tank width	
d_{vs}	Sauter mean bubble diameter	m
D	molecular diffusivity of solute gas in liquid phase	$m^2 \cdot s^{-1}$
E	enhancement factor	-
f	friction factor	-
f_{NH_3}	the activity coefficient of the ammonia	-
g	gravitational acceleration	$m \cdot s^{-2}$
G_m	total molar flow rate of gas	$mol \cdot s^{-1}$
H	Henry's constant	$L \cdot atm \cdot mol^{-1}$
I	ionic strength	$mol \cdot L^{-1}$
k	reaction rate constants	
	or salting-out parameter in Equation 4.11	$L \cdot mol^{-1}$
k_i	defined in Eq. 7.16	
k_G	gas-phase mass transfer coefficient	$mol \cdot s^{-1} \cdot m^{-2} \cdot atm^{-1}$
k_L	liquid-phase mass transfer coefficient	$m \cdot s^{-1}$
k_La	volumetric liquid-phase mass transfer coefficient	s^{-1}
$k_{NH_4^+}$	the acid dissociation constant of ammonium ion	$mol \cdot L^{-1}$

K	equilibrium constant	$L \cdot mol^{-1}$ or $L^3 \cdot mol^{-3}$
K^0	constant in Eq. 2.16	-
M	molar mass of the solution	$g \cdot mol^{-1}$
	quantity defined in Eq.s 2.26 and 5.6	
m, n, p, q	reaction orders with respect to reactant, unless otherwise stated	
n	stirring speeds in Eq.s 5.8 and 5.9	rpm
	or amount of NO absorbed	mol
N	absorption rate	$mol \cdot m^{-2} \cdot s^{-1}$
N_{cd}	minimum impeller speed for gas complete dispersion	Hz
N_{cr}	critical impeller speed for gas induction	Hz
N_I	impeller speed	Hz
P	pressure	Pa
dp/dz	pressure drop per unit length of pipeline	$Pa \cdot m^{-1}$
P_c	power consumption in a stirred tank	W
P_c/V_L	power input per unit liquid volume	$W \cdot m^{-3}$
Q	volumetric flow rate	$m^3 \cdot s^{-1}$
Q_I	gas induction rate	$m^3\ s^{-1}$
R	gas constant	$= 0.08205\ L \cdot atm \cdot K^{-1} \cdot mol^{-1}$
		$= 8.314\ J \cdot K^{-1} \cdot mol^{-1}$
R_I	impeller radius	m
s	impeller submergence	m
S	perimeter	m
S_A	cross-sectional area of the double-stirred reactor	m^2
t	time	s
T	temperature	K
u	fluid phase velocity in pipe	$m\ s^{-1}$
U	fluid phase superficial velocity in tank	$m\ s^{-1}$
	or uncertainty	dependent on quantity

V	volume	m^3
V_{bA}	molar volume of solute A at its normal boiling temperature	$cm^2 \cdot mol^{-1}$
W	impeller vertical width	m
x	contribution to salting-out parameter	$L \cdot mol^{-1}$
y	concentration of NO in the gas phase	ppmv
z	axial distance	m
	or ionic valence	-

Greek letters

α	Busen absorption coefficient	cm^3 of gas · cm^{-3} of solution
	significance level of Grubbs' test	-
ΔH	reaction enthalpy	$kJ \cdot mol^{-1}$
ε	phase holdup	-
	the characteristic Lennard-Jones energy	J
η	efficiency	%
θ	subtended angle in Figure 7-4	rad
κ	Boltzmann's constant	$J \cdot K^{-1}$
μ	dynamic viscosity	Pa·s
ν	kinematic viscosity	$m^2 \cdot s^{-1}$
ϵ	frictional energy dissipation	Pa s^{-1}
ρ	phase density	$kg \cdot m^{-3}$
σ	surface tension	$N \cdot m^{-1}$
	characteristic length	Å
τ	shear stress	Pa
φ	association factor of solvent	-
Ω_D	diffusion collision integral	-

Superscripts

0	reference state at which ammonium nitration concentration =0 and T = 303.2 K

5	reaction between penta-amminecobalt(II) nitrate and NO
6	reaction between hexa-amminecobalt(II) nitrate and NO

Subscripts

1	NH_4NO_3, in Eq. 4.9
2	$Co(NO_3)_2$, in Eq. 4.9 2^{nd} reaction order elsewhere
5	penta-amminecobalt(II) nitrate
6	hexa-amminecobalt(II) nitrate
a	anion
A,B	substances A and B
c	cation
chem	chemical absorption
con	continuous
e	equilibrium state
G	gas phase
GI	gas-inducing agitated tank
i	gas-liquid interphase
I	impeller
in	inlet
j	j species
L	liquid phase
multiple	multiple reactions
n	the number of reaction, n = 1 – 6, unless otherwise stated
NO	nitric oxide
out	outlet
p	horizontal pipe
parallel	parallel reactions

r	recirculation of gas-liquid dispersion
s	interfacial or saturated
S	superficial
single	single reaction
SB	semi-batch
T	tank
	or total
TPF	two-phase flow
w	wall
	or water

Abbreviation

AC	activated carbon
CAA	Clean Air Act
CPP	combined plasma photolysis
CSTR	conventional stirred tank reactor
DBD	dielectric barrier discharge
DO	dissolved oxygen
FGT	flue gas treatment
GIAT	gas-inducing agitated tank
HCCI	homogeneous charge compression ignition
ID	inner diameter
Mt	million metric tons
NO	nitric oxide
NO_x	nitrogen oxides
RHS	right-hand side
SCR	selective catalytic reduction
SNCR	selective non-catalytic reduction
TPF	two-phase flow

WBG World Bank Group

Dimensionless Groups

Gas flow number $Fl = \frac{Q_G}{N_I d_I^3}$

Froude number $Fr = \frac{N_I^2 d_I}{g}$

Reynolds number $Re = \frac{d_p u \rho_G}{\mu_G}$

Chapter 1
Introduction

1.1 Research Motivations

Nitrogen oxides, denoted as NO_x, represent seven oxides of nitrogen: nitric oxide (NO), nitrogen dioxide (NO_2), nitrous oxide (N_2O), dinitrogen dioxide (N_2O_2), dinitrogen trioxide (N_2O_3), dinitrogen tetroxide (N_2O_4) and dinitrogen pentoxide (N_2O_5). However, NO_x are referred to as NO and NO_2 only by the US Environmental Protection Agency (EPA) as these two gases are significant contributors to air pollution [1]. The mobile and stationary sources contribute to nearly half the total NO_x emission [2]. Selective catalytic reduction (SCR) [3] and homogeneous charge compression ignition (HCCI) [4, 5] are two popular technologies that have been well employed for mobile source. However, controversy over the optimal NO_x control method for stationary source has arisen for a long time as more sectors are included. According to statistics of U.S. Energy Information Administration (EIA) [6], NO_x emissions from thermal plants were as high as 3.3 million metric tons in U.S. in 2008, which was approximately 40% of the NO_x emissions from stationary sources.

The formation of NO_x is almost inevitable in all combustion processes due to the nitrogen element contained in fuel and nitrogen in the air. At a high temperature, especially when it is above 1373.2 K, thermal NO_x is formed by the reaction between nitrogen and oxygen [1, 2]. At a lower temperature, prompt NO_x is expected to be produced by a fast reaction between nitrogen and oxygen molecules and hydrocarbon radicals. At the same time, fuel NO_x may also be generated from direct oxidation of organically bound nitrogen in fuels such as coal and heavy oil. In most industrial combustion processes, thermal NO_x is the predominant among these three types of NO_x, of which approximately 95% is nitric oxide [7]. It makes the reduction of nitric oxide crucial to the success of NO_x emission control.

NO_x can negatively impact human health and the environment. Firstly, nitrogen oxides are health hazards. NO is a colorless poisonous gas which can cause irritation to the eyes and throat, tightness of the chest, nausea and headache. Prolonged exposure to high concentration NO could be fatal. NO_2 is a red-brown, highly toxic gas that has a suffocating odor. It is able to irritate lungs and to deteriorate one's resistance to respiratory infections [8]. Secondly, tropospheric ozone and smog are produced by reactions of NO_2 in the atmosphere. Stratospheric ozone in the upper atmosphere protects us from high-intensity ultraviolet (UV) rays from the sun, while tropospheric ozone in the ambient air that we breathe can cause respiratory issues. NO_2 also reacts with air with the presence of UV to form ozone

and NO. Furthermore, NO_2 and unburned volatile organic compounds (VOC) under the influence of sunlight will give rise to photochemical smog. Thirdly, acid rain is formed by reaction between NO_2 and water vapor in the atmosphere. Even though NO is dominant in the NO_x from industrial combustion, NO reacts with oxygen in the air to create NO_2. NO_2 is highly reactive with water to form nitrous acid (HNO_2) and nitric acid (HNO_3). Acid rain is harmful to plants, trees and structures.

Governmental regulations around the world have been issued since the first Clean Air Act (CAA) of 1970 was established in the USA. The lowest achievable emission rate (LAER) of NO_x established by US Environmental Protection Agency (EPA) is 3-15 ppmv. In Japan, the NO_x emission limits are set below15, 30 and 60 ppmv for new large gas-, oil- and coal-fired thermal plants by most local governments. In Europe, counterpart NO_x emission limits are 30-50, 55-75, and 50-100 ppmv, respectively [9].

In response to government regulations, many NO_x abatement and control technologies have been developed. Typical technologies for NO_x reduction are summarized in **Table 1-1**. They mainly fall into two categories: 1) suppression of NO_x formation in the combustion process and 2) flue gas treatment involving chemical reactions with post-combustion NO_x. NO_x suppression can be fuel switching, for example, substituting low-nitrogen fuels, such as natural gas or propane for coal to create less "fuel NO_x" or by combustion modification which focuses on minimizing peak combustion temperature and residence time at peak temperature to generate less "thermal NO_x". Flue gas treatment technologies include selective catalytic reduction (SCR), selective non-catalytic reduction (SNCR) and wet scrubbing. From a practical standpoint, it is currently very challenging to completely replace coal with natural gas for power generation. Statistics from EIA show that coal for generating electric power constantly provided around 50% of total net generation annually from 1997 to 2008 in the U.S. [6].

Table 1-1: Summary of NO_x control technology

Representative Technologies		Principles
Fuel switching		Fuel switching involves the replacement of fuels having high nitrogen content like coal and heavy oils with low nitrogen fuels such as natural gas [10].
Combustion Modification	Less Excess Air (LEA)	Peak temperature is decreased by reducing excessive oxygen at the burner flame. It reduces the amount of air introduced into the boiler leading to an increase in thermal efficiency if stoichiometric requirements are met [1].
	Staged combustion (SC)	SC burns the fuel in two steps. A fuel-rich condition is created near the primary flame by introducing insufficient air in the first step. Then, the rest of combustion air is filled to complete the combustion. Both deficiency of oxygen in the first step and low temperature in the second step result in NOx reduction [10].
	Flue gas recirculation (FGR)	FGR redirects partial flue gases back to the combustion chamber. The recycled flue gas mixes with secondary air, lowering the flame temperature and diluting oxygen as well, accordingly reducing NOx formed [11-15].
	Low-NOx burners (LNB)	These special burners are developed based on the combination of LEA, SC and FGR [1, 2].
	Water/steam injection	The suppression of NOx formed in combustion is completed by both lowering peak temperature and the residence time at the peak temperature [10, 16].
Post-combustion Flue Gas treatment	SCR	SCR uses ammonia or ammonia-based agents to convert NOx into N_2 and H_2O at relatively low temperatures in the presence of a catalyst [17].

Table 1-1: Summary of NO_x control technology (continued)

Representative Technologies		Operational Principle
Post-combustion Flue Gas treatment	Selective non-catalytic reduction (SNCR)	SNCR involves the reaction between injected ammonia- or urea-based compounds and NO_x to form nitrogen and water at relatively high temperatures [10, 16].
	Combined plasma photolysis (CPP)	CPP is the combination of the use of a dielectric barrier discharge (DBD) plasma and ultraviolet radiation [18, 19].
	Activated Carbon (AC)	Except being used in SCR, AC itself can adsorb NO_x emissions to form complexes, and then desorb them by heating or microwave irradiation [20-23].
	Wet scrubbing	Wet scrubbing is using an absorbent to react with NO_x, forming by-product commodity [24].

1.2 Research Opportunities

Combustion modifications are extensively applied to reduce NO_x emissions. Nevertheless, post-combustion flue gas treatment (FGT) is indispensable in order to meet the increasingly stringent emission standards. Firstly, combustion modifications involve retrofit to existing systems or design of new units. This is a long-term investment and it takes years to complete. FGT is necessary during the implementation of combustion modifications to ensure that NO_x are treated before being emitted. Secondly, the NO_x reduction efficiencies of combustion modifications are not high enough to meet the emission limits. Usually, the removal efficiencies are less than 50% [10], which cannot lower the NO_x concentration to around 15 ppmv; and FGT process can be a good supplement to any combustion modifications since they are located downstream of combustion zone. A combination of a combustion modification and a FGT will for sure meet the severe NO_x emission control. In addition, the FGT technologies can be applied to non-combustion sources of NO_x such as chemical manufacturing and metal processing. Therefore, FGT deserves more developmental attentions in both the short and long terms.

As seen in **Table 1-1**, selective catalytic reduction (SCR), selective non-catalytic reduction (SNCR) and wet scrubbing are three representative FGTs. SCR uses ammonia or ammonia-based agents to convert NO_x into nitrogen and water at a relatively low temperature in the presence of a catalyst such as platinum, vanadium and titanium dioxide. Typical operating temperatures of these three catalysts

are 477.6 K, 672 K and 810.9 K, respectively. SCR can reach a NO_x reduction efficiency of 60-90% at a relatively high cost of US $40-80/kW according to a report by World Bank Group (WBG). And, the catalyst is easy to get poisoned by fly ash rich in arsenic and/or alkali and the disposal of consumed toxic catalysts is another issue [25]. SNCR involves reactions among injected ammonia- or urea-based compounds and NO_x to form nitrogen and water at relatively high temperatures. Generally, it can reach a removal efficiency of 60-70% at a cost of US $10-20/kW; the process is rather sensitive to temperature. The optimum temperature range is from 1144 K to 1422 K. Efficiencies at temperatures outside of this range are greatly deteriorated [10, 16].

Activated carbon has been commonly used in SCR as a catalyst [20], and it can adsorb NO_x by forming carbon-based complexes at temperatures between 343.2 and 393.2 K and desorb NO_x through heating at around 413.2 to 423.2 K [22] or via microwave irradiation [21]. In addition, the combined plasma photolysis (CPP) technology developed by Rood's Group could achieve simultaneous removal efficiencies for SO_2 and NO of 29% and 79%, respectively [19].

Different from the aforementioned dry technologies, wet scrubbing using an absorbent in liquid offers an alternative approach to FGT [24]. Wet FGT mainly includes two methods: (1) direct absorption of NO_x or (2) conversion of insoluble NO into NO_2 using a strong oxidant, followed by removal of NO_2. It is comparatively insensitive to flue gas particulate matter and has been widely employed by chemical manufacturers. Wet scrubbing technologies are potentially able to achieve high NO_x reduction efficiency owing to the high reaction rate between absorbents and NO_x. In addition, most absorbent has the ability to simultaneously remove SO_2 and NO_x and flue gas desulphurization (FGD) devices, which are wet scrubbing reactors, have been extensively applied in power plant to remove SO_2. It is expected to be simple to adapt to NO_x abatement.

The selection of suitable absorbent is important to wet scrubbing. First of all, since inactive NO accounts for more than 90-95% of NO_x, the realization of NO_x control by wet scrubbing rests primarily on the successful removal of NO. It requires that the absorbent must fast react with NO. In addition, an excellent absorbent should also be easily regenerated or recycled, which will reduce the operating cost. Several solvents have been reported for NO_x absorption. A summary of some commonly used absorbents is presented in **Table 1-2**.

As shown in Eq. 1.1, wet scrubbing using a strong oxidant such as ClO_2/$NaClO_2$ or $KMnO_4$ to convert NO into soluble NO_2 leads to a challenge because by-product NO penetrates the scrubber as part of the exhaust air. As a result, direct absorption of NO by reaction with an agent like $FeSO_4$ and Fe(II)EDTA to form a complex is preferred.

$$3NO_2 + H_2O \rightarrow 2HNO_3 + NO\uparrow \quad (1.1)$$

Table 1-2: Absorbents used for NOx reduction

Absorbents	**Operating Conditions**	**References**
$KMnO_4$-NaOH	$KMnO_4$: 0.089 – 0.243 mol·L^{-1}; NaOH: 0.5 - 2.5 mol·L^{-1}; NO: 1.5 – 20%; T: 298.2 K	Sada et al. [26]
$NaClO_2$-NaOH	$NaClO_2$: 0.21-1.5 mol·L^{-1}; NaOH: 0.05-0.5 mol·L^{-1}; NO: 0.8-15%; T: 298.2 K	Sada et al. [27, 28]
H_2O_2	H_2O_2: 0.107 – 0.566 mol·L^{-1}; NO: 6.9–24.7 %; T: 288.2 – 303.2 K	Baveja et al. [29]
Fe(II)EDTA-Na_2SO_3	Fe(II)EDTA: 0.01-0.02 mol·L^{-1}; Na_2SO_3: 0.25-0.125 mol·L^{-1}; NO: 510- 2330 ppmv; T: 278.2 – 323.2 K	Teramoto [30]
$FeSO_4$-H_2SO_4	$FeSO_4$: 0.25 – 1 mol·L^{-1}; H_2SO_4: 0.25 to 0.50 mol·L^{-1}; Pure NO; T: 298.2 K	Bosio et al. [31]
$Co(NH_3)_6Cl_2$-KI	$Co(NH_3)_6Cl_2$: 0.01 – 0.04 mol·L^{-1}; KI: 0.01 mol·L^{-1} with/out UV; NO: 250-900 ppmv; SO_2: 0 -2500 ppmv; O_2: 0-5.2%; T: 323.2 K	Long [32]
ClO_2	ClO_2: sufficient; NO: 150-1180 ppmv; SO_2: 0 - 1800 ppmv; T: 318.2 K	Deshwal [33]
$Co(NH_3)_6Cl_2$-Activated carbon	$Co(NH_3)_6Cl_2$: 0.01 mol·L^{-1}; NO: 600 ppmv; SO_2: 1500 ppmv; NaOH: 0.25 – 0.60 mol·L^{-1}; Activated carbon: 40g; T: 333.2 K	Cheng [34]

Transitional metal chelate like Fe(II)-EDTA combines with NO to form a complex more effectively than $FeSO_4$ does. The coordination reactions between NO and Fe(II)-EDTA and $FeSO_4$ are as follows:

$$Fe^{II}EDTA + NO \rightleftharpoons Fe^{II}(NO)EDTA \quad (1.2)$$

$$FeSO_4 + NO \rightleftharpoons Fe(NO)SO_4 \quad (1.3)$$

The chemical equilibrium constant of Reaction (1.2) is in the order of 10^6 L·mol^{-1} at 298.2 K [30], while that of Reaction (1.3) is only in the order of 10^2 L·mol^{-1} [35]. Recently, Long's group reported that the application of hexaamminecobalt (II) solution could effectively remove NO from simulated

flue gas. The absorbent could also be regenerated by KI solution with ultraviolet light or activated carbon (modified by KOH) or electrochemical measures [36]. The main by-products nitrite and nitrate were sources of fertilizers. Thus, hexamminecobalt(II) solution can be considered as a candidate absorbent for wet FGT technology.

Although Long's group discovered hexaamminecobalt(II) solution, key parameters such as equilibrium constant and reaction rate constant are questionable or unknown, thereby preventing the further development of this technology. Furthermore, as oxygen plays an important part in flue gas treatment, the effect of oxygen on NOx absorption is worth investigation. In addition, earlier research was conducted using small bench-top reactors such as packed column with 18mm inner diameter. It is of importance to conduct some trials in relatively large reactors towards commercialization.

1.3 Research Objectives

Given the severe health and environmental impact caused by flue gas, which contains carbon dioxide, sulfur oxides and nitrogen dioxide, emitted from fuel combustion, control of these air emissions is currently necessary and urgent. Of these gases, nitric oxide is the bottleneck of the emission control technology. The post-combustion capture of carbon dioxide by using an amine-based absorbent has been well developed and rapid stride has been made [37, 38]. Sulfur dioxide can be easily treated by flue gas desulfurization (FGD) process with a removal efficiency of 95% or higher [39-41]. The reduction of nitrogen oxides, however, remains a challenge primarily due to the inactive nitric oxide, which accounts for 90-95% of nitrogen oxides.

As sulfur dioxide can be well controlled by wet scrubbing, it is desired and cost-effective to remove nitric oxide from flue gas by existing wet absorbers or scrubbers. Specifically, this project principally concentrated on the removal of nitric oxide from simulated flue gas using ammoniacal cobalt(II) solutions; following tasks were accomplished.

a) Comparison between different absorbents in a bubble column reactor system to show the feasibility of using hexaamminecobalt (II) solution for de-NO.

b) Equilibrium study of reaction between ammoniacal cobalt(II) complex and nitric oxide.

c) Kinetic study of reaction between ammoniacal cobalt(II) complex and nitric oxide.

d) Investigations on absorbent regeneration and effect of oxygen on NO absorption.

e) Study of mass transfer in industrial gas-liquid contactors for further development and commercialization of this technology.

1.4 Thesis Structure

This thesis work includes literature review, selection of absorbent, determination of equilibrium constants, kinetic study and the determination of volumetric liquid-phase mass transfer coefficients of some large scale scrubbers.

In the literature review, the characterization of nitric oxides is first introduced, followed by existing abatement technologies. It is concluded that post-combustion technology is indispensable in response to increasingly stringent legitimated regulation. Through comparative study on different nitric oxide absorbents, ammoniacal cobalt(II) was identified as a promising absorbent for wet scrubbing. Then the mechanism of absorption of nitric oxide into ammoniacal cobalt(II) solutions was investigated systematically. Finally, the state-of-art of mass transfer in the potential industrial gas-liquid contactors for NO absorption was elaborated for further investigation of this technology.

In the selection of absorbent, absorption of nitric oxide from simulated flue gas using three different absorbents was conducted in a bubble column system at room temperature and atmospheric pressure. The ammoniacal cobalt(II) solutions were then chosen as an optimum absorbent for nitric oxide reduction. Meanwhile, the effects of fresh absorbent composition, pH value and temperature on nitric oxide removal are discussed.

The equilibrium constants of reactions between nitric oxide and penta- and haxa-amminecobalt(II) solutions, respectively were determined in a bubble column reactor; experiments were conducted continuously with respect to gas phase and batch-wise with respect to liquid phase. Experimental setup, absorbent preparation, and experimental procedures were first described in detail. Then original data were analyzed. At last, equilibrium constants at different temperatures were determined and presented in the van't Hoff equation.

The kinetic study was conducted in a home-made stainless steel double-stirred reactor and the corresponding reaction rate constants were calculated using enhancement factor. As information on ammoniacal cobalt(II) coordination reaction was only available for temperatures from 295.2 to 303.2 K, and higher temperatures were not in favor of the absorption of nitric oxide into ammoniacal cobalt(II) solutions, experimentations were conducted only at 298.2 and 303.2 K.

The mass transfer coefficients in various gas-liquid contactors were determined by both experimental investigation and mathematic modeling of degassing performance of these contactors. All the validated correlations are expected to be able to guide apparatus scale-up in the future.

Conclusions and original contributions of this thesis project are presented in the last chapter. Meanwhile, several recommendations are given for future work.

1.5 Original Contributions

This thesis project focuses on the absorption of NO into ammoniacal cobalt(II) solutions, and following original contributions have been achieved:

(1) The analysis of cobalt(II) - ammonia system in solution with concentrated ammonium salt was systematically introduced and applied to NO absorption into ammoniacal cobalt(II) solutions.

(2) The reactivity of ammoniacal cobalt(II) complexes with NO was determined, and the nature of reactions between NO and penta- and hexa-amminecobalt(II) ions at room temperature or above was validated.

(3) The equilibrium constants of reactions between NO and penta- and hexa-amminecobalt(II) ions were determined in a bubble column.

(4) The reaction rate constants of reactions between NO and penta- and hexa-amminecobalt(II) ions were experimentally determined for the first time in a home-made double-stirred tank.

(5) A correlation for the estimate of volumetric liquid-phase mass transfer, k_La, in a gas-inducing agitated tank is proposed. Furthermore, optimum correlations for the evaluation of values of k_La in conventionally stirred tank reactor and bubble column were selected by investigating removal of oxygen from water.

Chapter 2
Literature Review

2.1 Characterization of Nitrogen Oxides

2.1.1 Definition and Source of Nitrogen Oxides

Nitrogen oxides (NO_x) represent a family of seven chemical compounds tabulated in **Table 2-1** with physical properties in the order of nitrogen valence [2]. Nitrogen oxide (NO) and nitrogen dioxide (NO_2) accounts for the majority of NO_x emitted into the ambient air by fuel combustion and chemical manufacturing [1, 10]. Approximately 95% of the NOx emissions from stationary sources are in the form of NO [1, 2, 42].

Table 2-1: Compounds of nitrogen oxides

Formula	Terminology	Physical Properties	Nitrogen valence
N_2O	nitrous oxide	colorless gas water soluble	1
NO N_2O_2	nitric oxide dinitrogen dioxide	colorless gas sparingly water soluble	2
N_2O_3	dinitrogen trioxide	black solid water soluble, decomposes in water	3
NO_2 N_2O_4	nitrogen dioxide dinitrogen tetroxide	yellowish-orange to reddish-brown gas fairly water soluble, decomposes in water	4
N_2O_5	dintrogen pentoxide	white solid fairly water soluble, decomposes in water	5

Both natural and anthropogenic sources contribute to the NOx emissions. The natural sources including biological process in soil and water, lightning and volcanic activity, forest fire, grass fire, trees, bushes, grasses and even yeasts, represent nearly 90% of the total NOx emissions. The rest is from anthropogenic sources, almost equally halved by mobile and stationary sources [10]. The largest stationary source is power plants, accounting for 40% or so [2].

2.1.2 Formation of NO_x in Fuel Combustion

NO_x is generated by the chemical combination of nitrogen and oxygen during the fuel combustion process. Three separate mechanisms, thermal NO_x, fuel NOx and prompt NO_x, have been identified

for generating NO_x in the fuel combustion process [1, 2, 16]. They all produce mainly NO as the short residence time usually does not allow a great amount of oxidation of NO into NO_2 to take place.

Thermal NO_x is produced by the thermal fixation of molecular nitrogen in the air at high temperatures, known as Zeldovich mechanism [42]:

$$2N_{2(g)} + 3O_{2(g)} \rightarrow 2NO_{(g)} + 2NO_{2(g)} + heat \qquad (2.1)$$

The concentration of thermal NO_x is greatly dependent upon the combustion temperature and less sensitive to nitrogen and oxygen concentrations. Thermal NO_x extraordinarily increases with temperature. Almost all thermal NO_x is formed at the region of the flame at the highest temperature. It is generally the predominant mechanism for NO_x formation in combustion at temperatures above 1373.2 K [1, 10]. It is generally not a major concern to biomass combustion because of the relatively low combustion temperature.

Fuel NO_x is resulted from the oxidation of organically bound nitrogen in such fuels as biomass, heavy oil and coal. It is not an issue for fuels with less or no organically bound nitrogen, for example, natural gas and propane. The simplified mechanism of fuel NO_x formation can be presented as [42]:

$$2f - N_{(s)} + 2O_{2(g)} \rightarrow NO_{(g)} + NO_{2(g)} + f - O_{(s)} + heat \qquad (2.2)$$

Contrary to the thermal NO_x formation, the conversion of fuel-bound nitrogen is relatively independent of temperature. Instead, the availability of free oxygen molecules plays a critical role in the conversion. Additionally, mixing pattern and the nitrogen content of the fuel also affect the concentration of fuel NO_x [42].

Prompt NO_x was first introduced by Fenimore to describe NO_x formed by the fast reaction between nitrogen, oxygen and hydrocarbon radicals in the flame front [43].

$$CH_{4(s)} + 3.5\ O_{2(g)} + N_{2(g)} \rightarrow NO_{(g)} + NO_{2(g)} + CO_{2(g)} + 2H_2O + trace\ speices \qquad (2.3)$$

The amount is relatively small and only of interest in accomplishing ultra-low NO_x emission levels with high-quality nitrogen-free fuels. Prompt NO_x becomes more important under fuel-rich conditions in lower-temperature combustion [43]. The respective contribution of those three NO_x from a certain power plant cannot be calculated theoretically and it varies with combustion conditions, the type of burner and the type of fuel [2,16].

2.1.3 Negative Impacts of NO_x

Nitric oxides may negatively affect public health and the environment. Firstly, NO is a colorless but poisonous gas which can cause irritation to the eyes and throat, tightness of the chest, nausea and headache. Prolonged exposure to NO could be fatal. NO_2 is a reddish-brown, highly toxic gas that has a suffocating odor. It is able to irritate lungs and to deteriorate one's resistance to respiratory infections [2]. The US federal primary air quality standard for NO_2 is set as 0.053 ppmv, annual arithmetic mean concentration [8]. Secondly, tropospheric ozone and smog are produced by reactions of NO_2 in the atmosphere. Stratospheric ozone in the upper atmosphere protects the lives on the earth from high-intensity ultraviolet (UV) rays from the sun, while tropospheric ozone in the ambient air is an irritant to the eyes, noses and throats. NO_2 reacts with air in the presence of UV to form ozone and NO as well. The NO will be easily recycled to NO_2 by oxidation. Thus, each molecule of NO_2 can produce ozone multiple times. In addition, NO_2 and unburned volatile organic compounds (VOC) under the influence of sunlight will give rise to photochemical smog that causes respiratory diseases. Thirdly, acid rain is formed by reaction between NO_2 and water in the atmosphere. NO_2 is highly reactive with water to produce nitrous acid (HNO_2) and nitric acid (HNO_3). Although NO is the dominant product in the NO_x from industrial combustion, it reacts with oxygen in the air to create NO_2. Acid rain is harmful to plants, trees and even constructions. The acidification of groundwater and lakes caused by acid rain leads to terrible consequences such as "dead lakes" for locations where there is few alkaline substances in the soil and rocks [44]. Meanwhile, nutrient enrichment of water bodies may arise with the increase of concentration of nitrates or phosphates, which incurs algal bloom and plant growth, leading to the death of other plants in the water due to the depletion of oxygen [44].

2.2 NO_x Abatement Technologies

Effective control of NO_x emissions from both mobile and stationary sources requires different technologies. This thesis project concentrates primarily on the reduction of NO_x emitted from stationary sources. As prompt NO_x only constitutes small portion, most NO_x abatement technologies are directed towards thermal NO_x and fuel NO_x. The existing techniques either aim to suppress the NO_x formation during the fuel combustion or manage to treat the post-combustion flue gas. These approaches are briefly introduced as follows.

2.2.1 Fuel Switching

Fuel switching is to switch conventional fuels such as coal and heavy oil with high-quality natural gas. Coal and oil contain organically-bound nitrogen compounds which react with oxygen to form

fuel NO_x. Switching fuels with nitrogen-free or low-nitrogen natural gas can reduce the fuel NO_x to the most extent. It was reported that a natural-gas-fired plant produces 60% less NO_x emissions than a coal-fired plant [10].

2.2.2 Combustion Modification

Combustion modifications are based on NO_x formation chemistry and may involve any of three strategies: (a) minimizing peak combustion temperatures; (b) minimizing gas residence time at peak temperature; (c) reducing oxygen concentration in the combustion zone [10].

2.2.2.1 Less Excess Air (LEA) Combustion

Less excess air (LEA) combustion is a simple yet effective method for the reduction of NO_x formation. It reduces the total amount of excess air supplied for combustion, resulting in lower peak flame temperature and thus less NO_x formation. Therefore, it is commonly used in new and retrofit plants. The ultimate level of excess air is related to the onset of smoke or carbon monoxide emission. Fouling and slagging caused by low levels of excess air are typical side effects of this technology. LEA combustion is usually the first option for utility boilers. It could achieve an average reduction of 16-21% [1].

2.2.2.2 Off-stoichiometric or Staged Combustion

Off stoichiometric or staged combustion (OSC) reduces NO_x emissions by burning fuels in two or more steps (or zones). Fuel is first burned with less than stoichiometric amount of air to form a primary fuel-rich zone. The deficiency of oxygen in the first zone and the low temperature in the second zone both result in less NO_x formation. It was reported that OSC could reduce the NO_x emissions by 20-50% and corrosion and slagging might limit the potential of OSC technology [2].

2.2.2.3 Flue Gas Recirculation (FGR)

Flue gas recirculation (FGR) is recycling a portion of the flue gas back to the furnace, which is usually applied to large coal, oil or gas boilers. The recycled flue gas mixes with secondary air entering the combustion chamber, lowering both the furnace air temperature and the oxygen concentration. FGR can reduce NO_x emission by 20-50%. Although the relatively high cost somewhat limits its application, FGR can also reduce NO_x emission and is beneficial to CO_2 capture and storage [11-15]

2.2.2.4 Reduced Air Preheat Operation (RAP) and Reduced Firing Rate (RFR)

Reduced air preheat (RAP) operation and reduced firing rate (RFR) control NO_x emission through lowering the peak temperature of primary combustion zone. As a result, the thermal NO_x formation is reduced. Nevertheless, this strategy is rarely used in practice due to the significant energy penalty and low thermal efficiency [1, 2].

2.2.2.5 Steam and Water Injection

Steam or water injection (WI) is applied to lower flame temperature, thus giving rise to less thermal NO_x formation. It is especially effective for internal combustion engines and gas turbines. For a gas turbine, it could achieve a NO_x reduction efficiency of 80% at a WI rate of 2% with an energy penalty of 1%. For a utility boiler, however, the corresponding energy penalty can be up to 10% [10, 16].

2.2.3 Post-combustion Flue Gas Treatment

2.2.3.1 Selective Catalytic Reduction

In a selective catalytic reduction (SCR) system, flue gas stream from the combustion process is cooled and ammonia-containing air is injected into the flue gas prior to its passing over a catalyst. Typical catalysts are a mixture of titanium dioxide, vanadium pentoxide and tungsten trioxide [17]. The catalyst promotes the reaction between NO_x and ammonia to form nitrogen and water vapor. SCR systems can remove 50-90% of NO_x from flue gas if properly designed and operated [2]. Several drawbacks including disposal of spent catalysts, high capital and operating costs and complexity of the system limit its application [25].

2.2.3.2 Selective Non-Catalytic Reduction (SNCR)

Selective non-catalytic reduction (SNCR) systems use gas phase homogeneous chemical reactions to chemically reduce a portion of the NO_x emissions. Ammonia- or urea-based compounds are commonly reducing agents. A SNCR system can reduce NO_x from flue gas by 30-70% [2]. Its capital cost is much less than that of SCR. However, SNCR systems are sensitive to operating temperature. The desired reaction takes places in the range of 1600 to 2000 ^oF [1, 10, 16]. Temperatures outside this range are likely to negatively affect the NO_x removal efficiency.

2.2.3.3 Combined plasma photolysis (CPP)

Combined plasma photolysis (CPP) is in fact the integration of dielectric barrier discharge (DBD) plasma and ultraviolet radiation. The DBD technology using 20–40 kV voltages and alternating current can generate a great amount of ozone. The UV radiation is used to enhance the generation of

gas-phase radicals in the gas stream. Thus, SO_2 and NO can be simultaneously removed through gas-phase oxidation [18, 45] It was reported that the removal efficiencies for SO_2 and NO could reach as high as 29% and 79%, respectively.[19]

2.2.3.4 Adsorption/Desorption by Activated Carbon

Activated carbon (AC) is able to directly adsorb NO_x from the flue gas [20, 23]. The adsorption-desorption concept proposed by Rubel et al. [22] was a typical process for NO_x reduction using AC. NO_x emissions were removed from flue gas by using AC to form carbon-NO_x complexes at temperatures from 343.2 to 393.2 K, followed by desorption of NO_x from the complexes via heating to temperatures at about 413.2 to 423.2 K. Recently, Ma et al. [21] reported that AC desorption could also be achieved through microwave irradiation. However, the treatment of captured pure NO_x is another issue. Unlike carbon dioxide, it is unrealistic to store NO_x in underground geologic formations. Also, the disposal of AC raises attention.

2.2.3.5 Wet Scrubbing

Wet scrubbing using an absorbent offers an alternative approach to FGT [24]. Wet FGT mainly includes two methods: (1) direct of absorption of NO_x and (2) conversion of insoluble NO into NO_2 using a strong oxidant, followed by removal of NO_2. It is relatively insensitive to flue gas particulates and has been widely employed by chemical manufacturers such as nitric acid plants. Wet scrubbing is potentially able to achieve high NOx reduction efficiency for the right absorbents. Flue gas desulphurization (FGD) devices, which are wet scrubbing reactors, have been well developed for removal of SO_2 from power plant flue gas. It is desirable to adapt or share the existing FGD devices for simultaneous SO_2 and NO_x abatement. This new approach to multiple air pollution control has been studied globally in the past decades.

2.3 Selection of NO Absorbent

An effective absorbent for wet scrubbing should be able to react with inactive NO and to be easily regenerated as well. The selection of absorbent is based on a compromise of last two principles. There have been several NO_x absorbents developed and they are summarized as follows.

2.3.1 H_2O_2

Hydrogen peroxide (H_2O_2) was considered as a NO reactive solvent and subsequent liquid treatment is relatively simple. The primary products of reactions between NO and H_2O_2 are water and nitric acid, as shown in Reaction 2.4. Baveja et al. [29] investigated the kinetics of absorption of NO into aqueous H_2O_2 solution in a 10.15 cm I.D. glass stirred cell at temperatures between 288.2 and 303.2

K. The concentrations of relevant NO and H_2O_2 solutions were 7-25% and 0.107 to 0.566 mol·L^{-1}, respectively.

$$2NO + 3H_2O_2 \rightarrow 2HNO_3 + 2H_2O \quad (2.4)$$

The absorption reaction between NO and aqueous H_2O_2 was identified to be first order with respect to both reactants. The second order reaction rate constant can be expressed as a function of T as below,

$$\ln(1000k_2) = 36.4 - 6900/T \quad (2.5)$$

Calculated value of k_2 from Eq. 2.5 is 5.72 ×10^2 L·mol^{-1}·s^{-1} at 298.2 K, which is far below 1.7×10^8 L·mol^{-1}·s^{-1} of Fe(II)-EDTA [30]. It might be a suitable oxidant for nitric acid plants due to its ability to convert NO into HNO_3; however, its absorption rate and performance is definitely significantly inferior to other absorbents which will be introduced afterwards for combustion flue gas treatment. It is reasonable to eliminate it from potential de-NO absorbents here.

2.3.2 $FeSO_4$ + H_2SO_4

Although the NO absorption capacity is low, $FeSO_4$ has been extensively investigated as a NO absorbent due to its moderate absorption rate, easy regeneration and low cost. Hikita et al. [46] conducted experiments in a liquid-jet column and a wetted-wall column to study the kinetics of reaction between pure NO and $FeSO_4$ with 0.005 mol·L^{-1} H_2SO_4 solution under atmospheric pressure and at temperatures from 288.2 to 308.2 K. The liquid volumetric flow rates in both columns were remained at 3.8 mL·s^{-1}, while liquid exposure time to the gas varied from 0.0012-0.023 seconds for the former and 0.057-1 seconds for the latter. Prepared $FeSO_4$ concentrations were from 0.0625 to 0.5 mol·L^{-1}. The chemical equilibrium constant, K, and forward second order rate constant k_2 of Reaction 2.6 were

$$FeSO_4 + NO \rightleftharpoons Fe(NO)SO_4 \quad (2.6)$$

$$logK = -2.672 + 0.0666I + 1546/T \quad (2.7)$$

$$\log k_2 = 10.303 + 0.124I - 1337/T \quad (2.8)$$

The values of K and k_2 are 364 L·mol^{-1} and 8×10^5 L·mol^{-1}·s^{-1}, respectively, in a 0.125 mol·L^{-1} $FeSO_4$ solution at 298.2 K [46].

Sada et al. [47] further studied the absorption of NO by an acidic $FeSO_4$ solution under more broad operating conditions: NO concentration of 100 ppmv – 99% (by volume) and exposure time of 0.2 –

5000 seconds. The values of enhancement factor were reported and interpreted by a theory of mass transfer accompanied with reversible reaction.

The regeneration of $FeSO_4$ could be completed by heating the formed nitrosyl complex to a certain temperature, at which the nitrosyl decomposed to NO and $FeSO_4$ again. Rich NO is captured for other use while $FeSO_4$ is recycled to a wet scrubber [48].

2.3.3 Fe(II)-EDTA

From Eq. 2.7 it can be seen that the equilibrium constant value of $FeSO_4$ solution used to absorb NO is in the order of 10^2, which means that the capacity of $FeSO_4$ of absorbing NO is not high. Teramoto et al. [30] studied the removal of NO by ferrous chelate, Fe(II)EDTA, rather than ferrous salt. The reaction between Fe(II)-EDTA and NO is,

$$Fe(II) - EDTA + NO \rightleftharpoons Fe(NO)EDTA \qquad (2.9)$$

Experiments were run in two sorts of reactors, a bubble column with 2.5-cm I.D. and a 7.5-cm I.D. double-stirred vessel equipped with four vertical baffles. They found that the value of K was in the order 10^6 L·mol^{-1} (1.6×10^6) for Fe(II)EDTA, which is about four orders of magnitude greater than that for $FeSO_4$. They calculated the reaction rate constant based on the penetration model and stated that the reaction rate constant was 1.7×10^8 L·mol^{-1}·s^{-1} at 298.2 K for the pH ranging from 4.6 to 8.0. Apparently, at the same temperature, this rate constant is much higher than that of $FeSO_4$ solution. Therefore, Fe(II)EDTA is deemed superior to $FeSO_4$ as a NO absorbent in terms of capacity and reaction rate.

The regeneration of Fe(II)EDTA can be fulfilled by chemical reaction or non-chemical methods. The chemical reaction approach consumes chemicals like Na_2SO_3 [30] or $Na_2S_2O_4$ [49], and the cost is high. Among the non-chemical approaches, heterogeneous electron transfer using transition metal complex ions has been well investigated for decades [50]. A non-chemical reactivation of Fe(II)EDTA was developed by DOW Chemical Company with greatly lower cost for solvent regeneration [49]. Chang's group [25, 51] also carried on investigations on other ferrous chelates, such as iron (II) dithicarbonates, $Fe(II)(DMPS)_2$. They appeared to be more economically competitive.

Admittedly, Fe(II)EDA can effectively remove NO from flue gases and the absorbent can be generated under the condition free of oxygen. However, a typical flue gas contains 2-6% of oxygen by volume [52, 53]. The performance of Fe(II)EDTA is highly sensitive to oxygen due to the oxidation of Fe(II)EDTA to Fe(III)EDTA which is inactive towards NO. Meanwhile, oxygen will

react with the activated nitrosyl and create undesired nitrogen-sulfur compounds [51, 54]. The presence of 5% oxygen will greatly deteriorate the NO removal capacity by as high as 83% [25] The negative effect of oxygen on NO absorption capacity of other ferrous chelates was also significant, for example, 5% oxygen would result in a reduction of 44% to a thiolated iron(II) chelate, Fe(II)-$(DMPS)_2$ [25].

2.3.4 Hexaamminecobalt (II) Solution

Cobalt (II) is another transition metal whose chelates can act as a NO absorbent. The first report of reaction between cobalt(II) chelate and NO to form nitrosyl can date back to one century ago [55]. Recently, Long's group has conducted some experimental studies on removal of dilute nitric oxide from flue gas using various cobalt chelates [32, 56-59]. Long et al. [32] carried out absorption NO tests in a 18 mm I.D. × 1000 mm long packed column scrubber at 323.2 K under an aerobic condition with oxygen, NO and SO_2 concentrations of 5 -5.2%, 250-900 ppmv and 0-2500 ppmv, respectively. The simulated flue gases entered the laboratorial scale reactor base at 0.2 – 0.4 $L \cdot min^{-1}$ and counter-currently contacted with scrubbing solvent from the top at 25 $mL \cdot min^{-1}$. Results showed the advantages of ammoniacal cobalt(II) complex over other absorbents such as Fe(II)EDTA and H_2O_2. Similar conclusion was made by Yu et al. [60] later through a systematic comparison between several potential solvents. The positive effect of oxygen on NO absorption is one of the most impressive strengths of this absorbent. Oxygen in the flue gas first tends to react with ammonical cobalt(II) compounds to form a binuclear cobalt complex ion [61] which has a strong oxidization similar to hydrogen peroxide instead of directly oxidizing reactive cobalt(II) absorbent ion to inactive cobalt(II) chelate. Long's group also attempted the regeneration of $[Co(NH_3)_6]^{2+}$ solution using KI solution irradiated by ultraviolet light and using (modified) activated carbon. Favorable by-products like nitrite and nitrate, which are sources of fertilizer, rather than unwanted nitrogen-sulfur compounds, were found.

2.4 Coordination Chemistry of Ammoniacal Cobalt(II) Solutions

2.4.1 Cobalt(II) – Ammonia System

Several investigations have been conducted on the ammoniacal cobalt (II) complex since 1950s. It is well-acknowledged in coordination chemistry that one cobalt (II) ion is able to attach up to six ammonia molecules. A series of step equilibria exist in solutions containing ammonia and cobalt (II) salts. In order to determine the consecutive equilibrium constants in the cobalt (II) – ammonia system, Bjerrum [62] conducted experiments by adding ammonia into solutions with small concentrations of

cobalt(II) nitrate and at a high concentration of ammonium nitrate up to 2 $mol \cdot L^{-1}$. The presence of ammonium nitrate is to form $NH_4NO_3/NH_3 \cdot H_2O$ buffer solution to ensure a ready supply of NH_3 ligand while avoiding the formation of hydroxide and the precipitation of cobalt hydroxide. Six reversible step reactions, as summarized in **Table 2-2**, are involved in the investigated solution. The ultimate cobalt (II) – ammonia system greatly depends on pH value, temperature and the concentration of ammonium nitrate. This theoretical analysis of cobalt (II) - ammonia system method has been experimentally confirmed by Yatsimirskii and Volchenskova using absorption spectra [63] and has been successfully used by Simplicio and Wilkins [61] and Ji et al. [36].

Table 2-2: Step reversible reactions involved in the cobalt (II) – ammonia system

Reaction	Number
$Co(H_2O)_6{}^{2+} + NH_3 \rightleftharpoons Co(NH_3)(H_2O)_5{}^{2+} + H_2O$	(1)
$Co(NH_3)(H_2O)_5{}^{2+} + NH_3 \rightleftharpoons Co(NH_3)_2(H_2O)_4{}^{2+} + H_2O$	(2)
$Co(NH_3)_2(H_2O)_4{}^{2+} + NH_3 \rightleftharpoons Co(NH_3)_3(H_2O)_3{}^{2+} + H_2O$	(3)
$Co(NH_3)_3(H_2O)_3{}^{2+} + NH_3 \rightleftharpoons Co(NH_3)_4(H_2O)_2{}^{2+} + H_2O$	(4)
$Co(NH_3)_4(H_2O)_2{}^{2+} + NH_3 \rightleftharpoons Co(NH_3)_5(H_2O)^{2+} + H_2O$	(5)
$Co(NH_3)_5(H_2O)^{2+} + NH_3 \rightleftharpoons Co(NH_3)_6{}^{2+} + H_2O$	(6)

The equilibrium constants of the six step reversible reactions in **Table 2-2** can be described as follows.

$$K_1 = \frac{\left[Co(NH_3)(H_2O)_5{}^{2+}\right]}{\left[Co(H_2O)_6{}^{2+}\right][NH_3]} \cdot \frac{a_w}{f_{NH_3}} \tag{2.10}$$

$$K_2 = \frac{\left[Co(NH_3)_2(H_2O)_4{}^{2+}\right]}{[Co(NH_3)(H_2O)_5][NH_3]} \cdot \frac{a_w}{f_{NH_3}} \tag{2.11}$$

$$K_3 = \frac{\left[Co(NH_3)_3(H_2O)_3{}^{2+}\right]}{\left[Co(NH_3)_2(H_2O)_4{}^{2+}\right][NH_3]} \cdot \frac{a_w}{f_{NH_3}} \tag{2.12}$$

$$K_4 = \frac{\left[Co(NH_3)_4(H_2O)_2{}^{2+}\right]}{\left[Co(NH_3)_3(H_2O)_3{}^{2+}\right][NH_3]} \cdot \frac{a_w}{f_{NH_3}} \quad (2.13)$$

$$K_5 = \frac{[Co(NH_3)_5H_2O^{2+}]}{\left[Co(NH_3)_4(H_2O)_2{}^{2+}\right][NH_3]} \cdot \frac{a_w}{f_{NH_3}} \quad (2.14)$$

$$K_6 = \frac{\left[Co(NH_3)_6{}^{2+}\right]}{[Co(NH_3)_5H_2O^{2+}][NH_3]} \cdot \frac{a_w}{f_{NH_3}} \quad (2.15)$$

where K_n = the equilibrium constant of the nth reaction in **Table 2-2** (n = 1-6), L·mol^{-1};

[ ] = corresponding concentration, mol·L^{-1};

a_w = water activity, - ;

f_{NH_3} = the activity coefficient of free ammonia, -.

The corresponding equilibrium constants at temperatures ranged from room temperature (295.2 K) to 303.2 K can be described as [62]:

$$log_{10}K_n = log_{10}K_n{}^0 + 0.062[NH_4^+] + 0.005(303.2 - T) \quad (2.16)$$

where $K_n{}^0$ = empirical constant (n=1–6), and the values of $\log_{10}(K_n{}^0)$ are summarized in **Table 2-3** [62]; T = temperature, K.

Table 2-3: The values of $\log_{10}(K_n{}^0)$

Quantity	**$\log_{10}(K_1{}^0)$**	**$\log_{10}(K_2{}^0)$**	**$\log_{10}(K_3{}^0)$**	**$\log_{10}(K_4{}^0)$**	**$\log_{10}(K_5{}^0)$**	**$\log_{10}(K_6{}^0)$**
Value	1.99	1.51	0.93	0.64	0.06	-0.74

The free ammonia concentration required in Eqs. 2.10 – 2.15 can be given by the acid dissociation constant of the ammonium described in Eq. 2.17.

$$k_{NH_4^+} = \frac{[NH_3][H^+]}{[NH_4^+]} \quad (2.17)$$

where $k_{NH_4^+}$ = acid dissociation constant of the ammonium, mol·L^{-1}.

It is noteworthy that the available data of $k_{NH_4^+}$ in literatures are usually applicable to solutions of ionic strength nearly zero [64], where the influence of electrolyte is not included. The corresponding values for 2 mol·L^{-1} NH_4NO_3 solution at 295.2 and 303.2 K, respectively, were experimentally determined by Bjerrum [62]. Hence, values in or close to this temperature interval can be estimated by interpolation.

As for the determination of factors, a_w and f_{NH_3}, which are the active mass of the water and the activity coefficient of the ammonia, respectively, the assumption of unity can only be valid in 2 mol·L^{-1} NH_4NO_3 solution with low ammonia concentration (smaller than 1 mol·L^{-1}); otherwise, it leads to erroneous results [61, 62]. A recommended way to estimate the values for ammonia concentrations is interpolation according to a number of experimental data obtained between 1.010 and 10.57 mol·L^{-1} [62, 65].

With known [NH_3], a_w and f_{NH_3}, K_n (n=1-6), the respective concentration of various ammoniacal cobalt(II) compounds is given by mass conservation of cobalt(II) ion,

$$[Co^{2+}]_T = \sum_{j=0}^{6} \left[Co(NH_3)_i(H_2O)_{6-j}{}^{2+}\right] \tag{2.18}$$

where $[Co^{2+}]_T$ = the total concentration of cobalt(II) ion, mol·L^{-1}.

It can be seen that the final cobalt(II) – ammonia system is associated with pH value, temperature and the concentration of ammonium nitrate. As an example, **Figure 2-1**, given by the coding in Appendix A.1, describes the ammonia-cobalt(II) system at T = 303.2 K and c(NH_4^+) = 2 mol·L^{-1} for different pH values with simplicity of a_w =1 and f_{NH3} =1. It shows that complexes with large coordination number tend to exist at high pH values and a small pH value favors the generation of compounds of small coordination number.

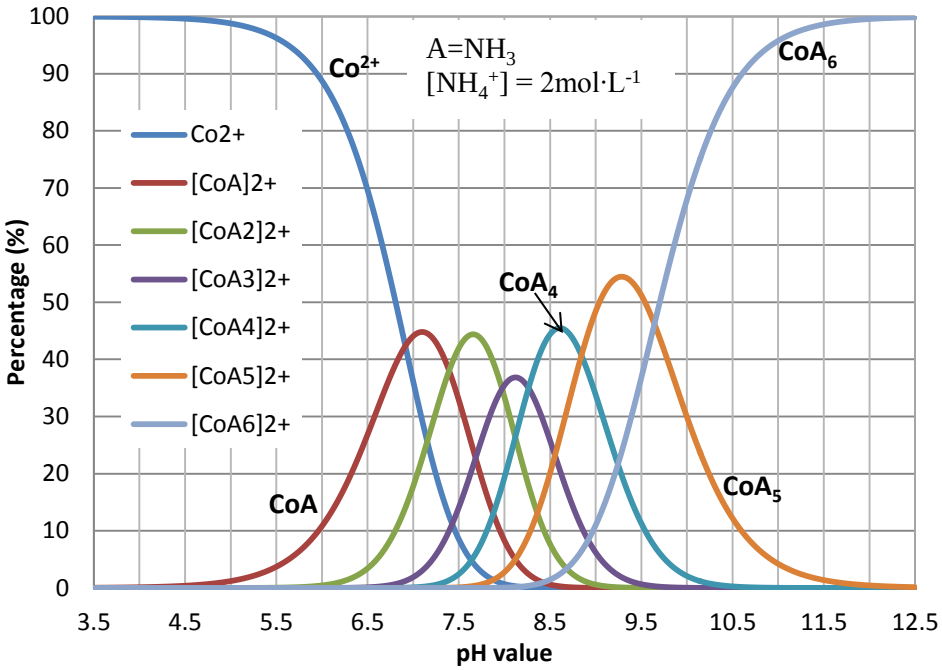

Figure 2-1: Cobalt-ammonia system for different pH values at T=303.2 K

2.4.2 Structure of Cobalt Nitrosyl

Among the complexes with different coordination numbers in the cobalt (II) – ammonia system, only penta- and hexa-ammoniacobalt (II) ions were referred to as reactants that react with NO to form nitrosyl by Ford and Lorkovic [66], Asmussen et al. [67] and Gans [68]. And, it has been reported by Simplicio and Wilkins [61] that penta- and hexa-ammoniacobalt (II) nitrates were the only reactive compounds towards oxygen. A test performed at pH =7.5 or so and T = 303.2 K was able to confirm the reactive substances in a cobalt (II) – ammonia system due to the fact that the system nearly contains only complexes with coordination number less than 5 at pH = 7.5 according to the analysis of cobalt (II) – ammonia system (**Figure 2-1**). It can be verified that only penta- and hexa-amminecobalt(II) ions have the ability to react with nitric oxide if no evident absorption of nitric oxide occurs at pH values close to 7.5.

Additionally, there have been a number of studies about the preparation [69-71] and structure [67, 68, 72-82] of cobalt nitrosyl by reaction between NO and ammoniacal cobalt (II) complexes. It has been well accepted that there were two series of cobalt nitrosyl, black series formed at low temperature (273.2 K and lower) and red series at high temperatures (room temperature or higher) [70]. However, there had been debates primarily on (1) the oxidation state of cobalt atom in the black nitrosyl and (2) the molecular structures of the two series. The former did not terminate until

Asmussen et al. [67] reported that both series contained cobalt in the oxidation state of +3. The erroneous designation of cobalt oxidation state by others were caused by impurity hexamminecobalt(II) chloride, $Co(NH_3)_6Cl_2$. As to the structure, although researchers commonly deemed one isomer to be a monomer and the other to be a dimer, dispute arose over whether the red or the black isomer was the dimer. To the author's best knowledge, almost all the researchers who considered polymerization believed that red isomer was the μ-hyponitrite dicobalt complex with a formula of $[(NH_3)_5Co(NO)_2Co(NH_3)_5]^{4+}$ as shown in Reactions 2.19 and 2.20 [68, 74, 77, 78, 80, 82, 83] with only one exception [84].

$$2NO + 2[Co(NH_3)_6]^{2+} \rightleftharpoons [Co(NH_3)_5N_2O_2(NH_3)_5Co]^{4+} + 2NH_3 \quad (2.19)$$

$$2NO + 2[Co(NH_3)_5]^{2+} \rightleftharpoons [Co(NH_3)_5N_2O_2(NH_3)_5Co]^{4+} \quad (2.20)$$

As experimental results showed that ammoniacal cobalt (II) solution was a promising option for NO abatement, it is of significance to determine the two key parameters, equilibrium constant and reaction rate constant, for better understanding of NO absorption mechanisms. Furthermore, Astarita [85] pointed out that the absorption rate of a gas-liquid reaction in a reactor can be presented as below in Eq. 2.21.

$$R_A a \propto a^{k_1}(1-\varepsilon_G)^{k_2} k_L^{k_3} r^{k_4} c_A^{*k_5} \quad (2.21)$$

where a = specific gas-liquid interfacial area, m^{-1};

c_A^* = saturated concentration of gas A, $mol \cdot L^{-1}$;

k_n (n= 1-5) = correlation coefficient in Eq. 2.21, -;

k_L = liquid-phase mass transfer coefficient, $m \cdot s^{-1}$;

r = reaction rate constant, units dependent upon on reaction orders;

R_A = the absorption rate of gas A, $mol \cdot m^{-2} \cdot s^{-1}$;

ε_G = gas holdup, -.

2.5 Equilibrium Constant for NO Absorption into Solvents

It is universal to use bubble column reactor to determine the equilibrium constant of reaction between absorbent and NO [30, 57, 86]. Teramoto et al. [30] bubbled dilute NO at flow rates ranging from 300 to 600 $mL \cdot min^{-1}$ through 80 mL aqueous Fe(II)-EDTA solution in a 2.5 cm I.D. batch bubble column. The concentration of NO was continuously monitored by a Shimadzu CLM-201 type NOx monitor. The equilibrium constant of reaction between NO and Fe(II)-EDTA was then determined by its

definition with equilibrium NO concentration given by Henry's Law and the product nitrosyl concentration provided by integration over the NO absorption efficiency curve.

Due to the disagreement between researchers, Nymoen et al. [86] later on re-determined the equilibrium constant of NO absorption into Fe(II)-EDTA using a method that was similar to Teramoto's but under much more extensively experimental conditions. All the investigations were conducted with inlet NO concentrations varying from 180 to 3000 ppmv and Fe(II)-EDTA solutions of 0.01 – 0.1 mol·L^{-1} at temperatures from 277.0 to 363.6 K.

Mao et al. [57] applied the same methodology to the NO absorption into hexamminecobalt(II) solution. They measured the equilibrium constant over temperatures ranged from 303.2 to 353.2 K under atmospheric pressure at pH = 9.14. Simulated flue gases with 200 – 800 ppmv NO passed through 250 mL 0.013 mol·L^{-1} solvent in forms of bubbles at 700 mL·min^{-1}. Finally the results were described in van't Hoff equation to give reaction enthalpy and to interpret temperature dependence. They ignored the analysis of cobalt (II) – ammonia system and stated that the product was a monomer of $[Co(NH_3)_5NO]^{2+}$ at temperatures higher than 303.2 K. This critical assumption conflicted with most aforementioned earlier publications. Therefore, it is worthwhile to determine the equilibrium constants of reactions between ammoniacal solutions and nitric oxide again by taking into account the analysis of cobalt (II) - ammonia system.

2.6 Kinetic Study for NO Absorption into Solvents

The chemical kinetics of NO absorption using aqueous absorbents was often studied in double-stirred tank reactors due to the fact that they are able to afford presumably perfect mixing for both phases. Sada's group used a baffled double-stirred tank reactor with two stirrers driven separately to investigate NO absorption by $NaClO_2$+NaOH, $FeSO_4$ and Fe(II)-EDTA solutions at 298.2 K. The absorber was tested continuously with respect to the gas phase and batchwise with respect to the liquid phase [28, 47, 87]. Teramoto et al. applied similar reactor and operational mode to study the NO absorption using Fe(II)-EDTA with and without Na_2SO_3 at temperatures between 288.2 and 308.2 K [30]. Later on, Chien et al. also adopted a reactor with similar dimensions while different shaft driving method for Fe(II)-EDTA at 323.2 K [88]. Recently, Du et al. reported that a similar dimensional reactor with same gas and liquid stirring speed gave satisfactory results for Fe(II)-EDTA at the temperatures of 298.2 – 323.2 K [89]. The related reaction rate constant was then determined by enhancement factor, E, which is the ratio of mass transfer coefficient accompanied by chemical reaction to that of physical absorption.

According to two-film theory [49], the physical gas absorption rate can be presented as

$$N_G = (\frac{1}{Hk_G} + \frac{1}{k_L})^{-1}(c_{Ai} - c_L) \quad (2.22)$$

where c_{Ai} = interfacial concentration of gas A, mol·L^{-1};

c_L = bulk concentration of gas A in the solution, mol·L^{-1};

H = Henry's Law constant, L·atm·mol^{-1};

k_G = gas-phase mass transfer coefficient, mol·s^{-1}·m^{-2}·atm^{-1};

k_L = liquid-phase mass transfer coefficient, m·s^{-1};

N_G = gas absorption rate into the solution, mol·m^{-2}·s^{-1}.

While for gas absorption accompanied by chemical reaction that usually occurs in the liquid phase, the gas bulk concentration in the liquid phase can be considered as zero and gas absorption rate can then be described with the introduction of enhancement factor, E,

$$N_G = (\frac{1}{Hk_G} + \frac{1}{Ek_L})^{-1}c_{Ai} \quad (2.23)$$

where E = enhancement factor, and E can be approximately given by film model in following equation [90],

$$E = \frac{1}{k_L}\sqrt{\frac{2}{m+1}k_{mn}D_A B^n c_{Ai}^{m-1}} \quad (2.24)$$

where B = bulk concentration of aqueous solution B, mol·L^{-1};

c_{Ai} = interfacial concentration of gas A, mol·L^{-1};

D_A = molecular diffusivity of solute gas A in liquid phase, m^2·s^{-1};

m, n = m-, n-th reaction order, -;

k_{mn} = reaction rate constant for (m+n)-th order reaction, L^{m+n-1}·mol^{1-m-n}·s^{-1}.

The major difference of using ammonical cobalt(II) solutions than other absorbents is that there are two reactive ions in the cobalt(II) – ammonia system; that is to say, two parallel reactions as shown in Reactions 2.19 and 2.20 take place in NO absorption.

Onda et al. [91] discussed the general case where the gas absorption was accompanied by two parallel irreversible reactions of m-th order and p-th order with respect to a gaseous species A and n-th and p-th orders with respect to the reactants B and C, respectively from the perspective of film theory and provided following asymptotic solution to enhancement factor of two-reaction process when they are pseudo mth- and p-th order respectively.

$$E_{parallel} = \sqrt{M(1 + \frac{m+1}{p+1} \cdot \frac{k_{pq} C_0^q c_{Ai}^{p-m}}{k_{mn} B_0^n})} \quad (2.25)$$

$$M = \frac{2}{m+1} \cdot \frac{k_{mn} D_A B_0^n c_{Ai}^{m-1}}{k_L^2} \quad (2.26)$$

where B_0 = bulk concentration of reactant B in liquid, $mol \cdot L^{-1}$;

C_0 = bulk concentration of reactant C in liquid, $mol \cdot L^{-1}$;

c_{Ai} = interfacial concentration of gas A, $mol \cdot L^{-1}$;

D_A = molecular diffusivity of solute gas A in liquid phase, $m^2 \cdot s^{-1}$;

$E_{parallel}$ = enhancement factor for parallel reactions, -;

k_L = liquid-phase mass transfer coefficient, $m \cdot s^{-1}$;

m, n, p, q = m-, n-, p-, q-th reaction order, -;

k_{mn} = reaction rate constant for (m+n)-th order reaction, $L^{m+n-1} \cdot mol^{1-m-n} \cdot s^{-1}$;

k_{pq} = reaction rate constant for (m+n)-th order reaction, $L^{p+q-1} \cdot mol^{1-p-q} \cdot s^{-1}$.

Specifically, Westerterp et al. [92] stated that the enhancement factor for a multiple reaction process containing pseudo first-order single reactions can be derived as,

$$E_{multiple} = \sqrt{\sum_{j=1}^{n} (E_{signle,j})^2} \quad (2.27)$$

where $E_{multiple}$ = enhancement factor for a multiple reaction process, -;

$E_{single,\ j}$ = enhancement factor for j-th single reaction in a multiple reaction process, -.

In order to take advantage of Eq. 2.25 and/or 2.27 for the determination of the forward reaction rate constants of Reactions 2.19 and 2.20, the concentrations of cobalt(II) complexes in the bulk liquid are maintained greatly in excess of the concentration of NO dissolved at the gas-liquid interface as Reactions 2.19 and 2.20 can be considered as irreversible [49] in this manner.

2.7 Mass Transfer in Various Industrial Absorbers

Bubble column (BC) [93, 94], conventional stirred tank reactor (CSTR) [95-97] and gas-inducing agitated tank (GIAT) [98, 99] are three types of frequently used industrial absorbers. Gas absorption can be achieved with or without chemical reaction. According to Eq. 2.21, the volumetric liquid-

phase mass transfer coefficient (k_La) is vital to the description of the gas absorption rate. It is well used to represent the rate of mass transportation across the gas-liquid interface from gas phase to liquid phase. In addition, the use of k_La can avoid the complexity of physical process taking place in the reactor as well as separate estimate of mass transfer coefficient (k_L) and specific interfacial area (a). It is a key parameter in the characterization, design and scale-up of gas-liquid contactors.

2.7.1 Bubble Column

In a bubble column (BC), the value of k_La is associated with numerous parameters such as gas superficial velocity, gas distributor design, bubble column diameter, and so on[100]. Meanwhile, it is commonly accepted that liquid velocity has insignificant or negligible effect on k_La value [101, 102]. A number of correlations have been proposed for the estimation of k_La. Generally, the dimensionless correlation developed by Akita and Yoshida [101] as shown in Eq. 2.28 for various gas-liquid systems in bubble columns with inner diameter up to 60 cm is applicable to simple gas sparger like a single hole or perforated plate [93, 102].

$$\frac{k_L a_B d_T^2}{D_L} = 0.6\left(\frac{\nu_L}{D_L}\right)^{0.5}\left(\frac{g d_T^2 \rho_L}{\sigma_L}\right)^{0.62}\left(\frac{g d_T^3}{\nu_L^2}\right)^{0.31}\varepsilon_G^{1.1} \tag{2.28}$$

in which the gas holdup in the bubble column is presented as,

$$\frac{\varepsilon_G}{(1-\varepsilon_G)^4} = 0.2\left(\frac{g d_T^2 \rho_L}{\sigma_L}\right)^{1/8}\left(\frac{g d_T^3}{\nu_L^2}\right)^{1/12}\left(\frac{U_G}{\sqrt{g d_T}}\right)^{1.0} \tag{2.29}$$

where d_T = diameter of bubble column reactor, m;

D_L = molecular diffusivity of solute gas in liquid phase, $m^2 \cdot s^{-1}$;

g = gravitational acceleration, $m \cdot s^{-2}$;

k_La_B = volumetric liquid-phase mass transfer coefficient in bubble column, s^{-1};

U_G = superficial gas velocity, $m \cdot s^{-1}$;

ε_G = gas holdup, -;

ν_L = liquid kinematic viscosity, $m^2 \cdot s^{-1}$;

ρ_L = liquid density, $kg \cdot m^{-3}$;

σ_L = liquid surface tension, $N \cdot m^{-1}$.

Effective distributors such as porous media give higher k_La values, which can be satisfactorily estimated by a semi-theoretical equation as described in Eq. 2.30. This equation was derived from Kolmogoroff's theory of isotropic turbulence [103].

$$k_L a_B = c_1 U_G^{c_2} \tag{2.30}$$

The value of constants c_1 is greatly dependent upon liquid phase properties and gas distributor type, whereas that of c_2 remains comparatively constant around 0.80 - 0.82 [104]. For water system inside a bubble column equipped with porous media sparger with U_G=0.0025 – 0.08 m·s^{-1}, c_1=1.091 and c_2=0.8 were given by Deckwer et al. [103].

2.7.2 Conventional Stirred Tank Reactor (CSTR)

In a conventional stirred tank reactor (CSTR), four dispersion patterns (flooding, cavity formation, complete dispersion of gas, recirculation of gas-liquid mixture) can be observed. The minimum impeller speed for complete dispersion of gas phase, N_{cd}, is a key parameter. Gas-liquid contacting at impeller speeds below N_{cd} leads to a poor reactor performance as the lower part of reactor is wasted due to the incomplete gas dispersion. From an economical and practical viewpoint, it is meaningless to operate a CSTR at speeds below N_{cd}. The flow regime transitions have been correlated in the literature by gas flow number *Fl* and Froude number *Fr* [105-107].

$$Fl_{cd} = 0.2 Fr_{cd}^{0.5} \left(\frac{d_I}{d_T}\right)^{0.5} \tag{2.31}$$

$$Fl_r = 13 Fr_r^2 \left(\frac{d_I}{d_T}\right)^5 \tag{2.32}$$

where d_I = impeller diameter, m;

d_T = stirred tank diameter, m;

N_I = impeller speed, Hz;

Q_G = volumetric gas flow rate, m^3·s^{-1};

$Fl = \frac{Q_G}{N_I d_I^3}$, gas flow number;

$Fr = \frac{N_I^2 d_I}{g}$, Froude number.

Researchers commonly correlated k_La with superficial gas velocity and power input per unit liquid volume or relative gas dispersion parameter [108-110]. Among proposed empirical correlations, Eq.

2.33 developed by Yawalkar [110] based on 178 literature data points is one of the most applicable correlations.

$$k_L a_C = 3.35 \left(\frac{N_I}{N_{cd}}\right)^{1.464} U_G \tag{2.33}$$

It can predict k_La within 22% of the observed values over a wide range of $0.39 < d_T < 2.7$ m for coalescing gas-liquid system regardless of type, size and position of the impeller and sparger.

In addition to N_I/N_{cd}, U_G, Kapic and Heindel [107] also included the ratio of tank diameter to impeller diameter, d_T/d_I, as a parameter based on 282 available data points. The correlation is presented in Eq. 2.34 and it can correlated most data within ±20% with R^2=0.97.

$$k_L a_C = 1.59 \left(\frac{N_I}{N_{cd}}\right)^{1.342} U_G^{0.93} \left(\frac{d_T}{d_I}\right)^{0.415} \tag{2.34}$$

where d_I = impeller diameter, m;

d_T = stirred tank diameter, m;

k_La_C = volumetric liquid-phase mass transfer coefficient of CSTR, s^{-1};

N_I = impeller speed, Hz;

N_{cd} = minimum impeller speed for complete dispersion of gas phase, Hz;

U_G = superficial gas velocity, $m \cdot s^{-1}$.

2.7.3 Gas-Inducing Agitated Tank (GIAT)

Apart from BCs and CSTRs, gas-inducing agitated tanks (GIATs) are well accepted as continuous degassers owing to their friendly operational condition, short residence time and high capacity. In a GIAT degasser, inert gas is induced into the reactor in the form of gas bubbles when impeller shaft is rotating at a speed beyond a critical value, which is greatly related to impeller submergence. The inert gas bubbles then collect undesired dissolved gas in liquid attributable to target gas concentration difference between inside and outside inert gas bubbles. Afterwards, target gas diffusing into the inert gas bubbles and travels to the liquid surface with the bubbles and is expelled into the headspace.

Like the description of k_La in a CSTR, the k_La in a GIAT can also be expressed in either power input per liquid volume (P_c/V_L) or relative gas dispersion parameter (N_I/N_{cd}) [111]. In particular, superficial gas velocity in a GIAT is determined from the gas induction rate, which depends on impeller speed, submergence and diameter. Meanwhile, both P_c/V_L and N_I/N_{cd} are related to impeller speed and diameter and vessel size [106, 112]. Yu and Tan [111] reported two new correlations for

the estimation of k_La in a GIAT after compiling 44 available literature data points and validated the correlations by their experimental data collected in a 40.64 cm × 40.64 cm vessel equipped with a 4-blade straight impeller. Comparatively, the correlation in P_c/V_L criterion, presented in Eqs. 2.35 – 2.38 as follows, gives a better performance. This work has been published in an international journal and the full article is appended to this thesis.

$$k_L a_{GI} = 1.212 \left(\frac{P_c}{V_L}\right)^{0.0816} \left(\frac{Q_I}{d_T^2}\right)^{0.692} \left(\frac{s}{d_T}\right)^{-0.390} \tag{2.35}$$

$$Q_I = 0.0021(N_I^2 - N_{cr}^2)^{0.75} d_I^3 \tag{2.36}$$

$$\frac{N_{cr}^2 d_I^2}{gs} = 0.21 \tag{2.37}$$

$$\frac{P_c - 1.767(2\pi N_I)}{\rho_L W N_I^3 R_I^4} = 22.24 - 6.71\left[1 - \frac{2gs}{0.84(\pi d_I N_I)^2}\right]^3 \tag{2.38}$$

where d_I = impeller diameter, m;

d_T = diameter of a GIAT, m;

k_La_{GI} = volumetric liquid-phase mass transfer coefficient of GIAT, s^{-1};

N_{cr} = critical impeller speed for gas induction, Hz;

P_c = power consumption in a GIAT, W;

Q_I = gas induction rate, $m^3\ s^{-1}$;

R_I = impeller radius, m;

s = impeller submergence, m;

V_L = liquid volume, m^3;

W = impeller vertical width, m.

Akita and Yoshida [113] stated that in terms of mass transfer characteristic a square bubble column offered the same performance as a cylindrical one with an inner diameter that is equal to the side length of the square column. Similar findings have also been reported for CSTRs. Leentvaar and Ywema [114], Kresta et al. [115] and Yu and Tan [111] proved that satisfactory results regarding mixing performance would be given if taking the side length of a square tank as the "diameter".

Unlike conventional BCs and CSTRs, modified BC and CSTR were used in Yu and Tan's study, which involved a pipe before the reactor due to the use of bubble generator. A number of studies

regarding horizontal gas-liquid two-phase flow (TPF) have been conducted, which primarily focused on the determination of flow regime and the estimations of gas (or liquid) holdup and frictional pressure drop. Mandhane et al [116] developed a well fitted flow regime map for gas-liquid two-phase based on 5935 observations in the multiphase pipe flow data bank. Taitel and Dukler [117] first theoretically predicted the flow regime transition with the application of momentum balance to each phase.

Gas holdup is one important parameter in TPF. It facilitates theoretical determination of flow pattern and is required for the estimate of frictional pressure drop. Many correlations for gas holdup and pressure drop have been proposed by Spedding's group [118-120].

Other researchers showed their interests in the mass transfer process within a horizontal pipe. Heuss et al [121] studied the absorption of ammonia and oxygen into water in a horizontal pipe with ID of 25.4 mm at superficial liquid velocities between 2.71 and 4.34 m/s and superficial gas velocities between 4.74 and 17.08 m/s. With the use of estimation of specific interfacial area, an empirical correlation for k_La was proposed as follows:

$$\frac{k_{Lp}d_{vs}}{D_L} = 0.0316\left(\frac{d_p(u_{SL}+u_{SG})\rho_L}{\mu_L}\right)^{0.9}\varepsilon_{Gp}^{-3} \tag{2.39}$$

where d_p = pipe diameter, m;

d_{vs} = Sauter mean bubble diameter, m;

k_{Lp} = liquid-phase mass transfer coefficient in a horizontal pipe, $m \cdot s^{-1}$;

u_{sG} = superficial gas velocity, $m \cdot s^{-1}$;

u_{sL} = superficial liquid velocity, $m \cdot s^{-1}$;

ε_{Gp} = gas holdup in a horizontal pipe, -;

μ_L = liquid dynamic viscosity, Pa·s.

Jepsen [122] conducted a series of experiments in a 25.4 mm ID pipe at superficial water velocities from 0.30 to 2.26 m/s and superficial air velocities from 0.76 to 10.97 m/s and developed a correlation for k_La, as shown in Eq. 2.40, based on the frictional energy dissipation.

$$k_L a_p = 3.47\epsilon^{0.40}D_L^{0.50}\sigma^{0.50}\mu_L^{0.05}d_p^{-0.68} \tag{2.40}$$

where k_La_p= volumetric liquid-phase mass transfer coefficient in a horizontal pipe, s^{-1};

ϵ = frictional energy dissipation, Pa s^{-1}.

Kress and Keyes [123] studied the desorption of oxygen from five different mixtures of glycerol and water into helium bubbles in a 50.8 mm I.D. pipeline. With the photographic determination of bubble size distribution, a recommended correlation for mass transfer coefficient was presented as

$$\frac{k_{Lp}d_p}{D_L} = 0.34\left(\frac{\mu_L}{\rho_L D_L}\right)^{0.5}\left(\frac{d_p(u_{SL}+u_{SG})\rho_L}{\mu_L}\right)^{0.94}(d_{vs}/d_p)^{1.0} \quad (2.41)$$

2.8 Regeneration of Ammoniacal Cobalt(II) Absorbent

In addition to fast reaction rate and capacity with nitric oxide, another important criterion for absorbent selection is the regeneration of absorbent. Long's group also investigated the regeneration of ammoniacal cobalt(II) absorbent. They focused primarily on the addition of (modified) activated carbon [34, 124-126] and the use of iodide with and without ultraviolet light [32, 127]. Furthermore, Taube et al. reported that persulfate ion can easily react with hexamminecobalt (III) ion to form nitrogen or oxygen [128-130], making persulfate ion a potential candidate for the regeneration of ammoniacal cobalt (II).

2.8.1 Activated Carbon (AC)

Long et al. [126] conducted batch experiments in a stirred glass flask of 500 mL to study the reduction of 0.01 mol·L^{-1} hexamminecobalt (III) with the use of coconut activated carbon. The experiments were conducted at an agitation speed of 200 rpm with liquid sample analyzed every 3 minutes. Besides, continuous measurements for simultaneous removal of SO_2 and NO were also performed in an 18 mm I.D., 1000 mm long counter-current packed column at atmospheric pressure. Gas entered from the bottom and exited from the top, while liquid was sprayed into the column from the top and circulated from the bottom of the tank. The gas and liquid flow rates were set at 200 mL·min^{-1} and 25 mL·min^{-1}, respectively. The regeneration reactor was a fixed-bed with a diameter of 20 mm and a height of 800 mm. In the regeneration process, used absorbent in the circulation tank first flew into the regeneration reactor upwardly and then into the packed column scrubber.

The effects of temperature, pH, size of activated carbon and liquid flow rate on the reduction of hexaamminecobalt (III) was investigated. The results of batch experiments showed that temperature had a positive effect on hexamminecaobalt(III) conversion. The suitable pH range was from 3.5 and 6.5. For the fixed-bed reactor, they reported that change of liquid flow rate greatly impacted the spray performance. And a relatively high yield of cobalt (II) was achieved at pH less than 9.0. The nitric oxide removal efficiency could be maintained between 70% and 80% for 100 hours or so.

Further investigations have been conducted by Long's group with minor improvement such as type of activated carbon [125] and modification of activated carbon with KOH solution [34]. The experimental methodologies in these two studies are almost the same as that used by Long et al. [126]. Chen et al. [125] concluded that for the batch experiments, pitch-based spherical activated carbon (PBSAC) performed much better than palm shell activated carbon (PSAC) as a hexaamminecobalt (III) reduction catalyst. The reduction rate of hexaamminecabalt(III) increased with PBSAC when PBSAC dose was 7.5 g/L or less and with its initial concentration. The optimum pH values ranged between 2.0 and 6.0. High temperature is desirable in the reduction reaction. A nitric oxide removal efficiency of around 90% had been maintained for over 200 hours. In addition, Cheng et al. [34] stated that treatment of activated carbon with KOH solution favored the reduction of hexaamminecabalt(III). The optimum KOH concentration was approximately 0.5 $mol \cdot L^{-1}$; the best impregnation duration was 9 hours; high temperatures were in favor of the conversion of hexaamminecabalt(III). The NO removal efficiency remained constant at 75% for a period of 110 hours.

2.8.2 Combination of Iodide and UV Radiation

Apart from activated carbon and its modifications, Long et al. [32, 127] also employed iodide (both with and without ultraviolet light) for the regeneration of hexaamminecabalt(II). Experiments were carried out in a packed column with 18 mm I.D. and a length of 1000 mm. The temperature was regulated by a jacket through which water was circulated from a thermostatic bath. The simulated flue gas (with NO concentration between 250 and 900 ppmv and SO_2 concentration 800-2500 ppmv) was fed into the reactor at the bottom, whereas liquid was sprayed into the column countercurrently at a flow rate of 25 $mL \cdot min^{-1}$ from the top. With the use of a 500 mL glass circulation tank, liquid could be recycled to form a closed loop. At the same time, UV lamps of 250 and 360 nm wave lengths were placed over the tank for the reduction of hexaamminecabalt(III).

They concluded that iodide could be considered as an effective co-catalyst at the iodide to cobalt (II) ratio of 0.25 for the regeneration of hexaamminecabalt(II), and UV irradiation at 360 nm could further improve the overall removal process. The optimal temperature was around 323.2 K. Increasing SO_2 and O_2 concentrations favored the NO removal efficiency. The NO removal efficiency maintained at 97.5% or higher for a period of 10 hours at the following conditions: T= 323.2 K, KI/Co^{2+} = 0.25, SO_2 = 2500 ppmv, O_2 = 5.2% and UV = 360 nm.

2.8.3 Persulfate Ion

Thusius and Taube [128] and White and Taube [130] repported that Persulfate ion could react with hexaamminecabalt(III). Their interests were in the reduction of hexamminecobalt (III) only. However, the deterioration of NO removal efficiency primarily is caused by the formation of inactive hexaamminecabalt(III) due to the existence of oxygen. Therefore, reagent that can react with hexaamminecabalt(III) provides a potentiality for the regeneration of hexaamminecabalt(II) absorbent to achieve a high NO removal efficiency for a long duration. Moreover, persulfate ion is quite commonly used as a low-cost food additive and is safe to handle. They investigated reactions between penta- and hexa- amminecobalt(III) perchlorate and potassium sulfate. The major component of the gaseous product of the reduction of Co(III) to Co^{2+} was oxygen with silver nitrate present as catalyst, whilst that without silver nitrate as catalyst was nitrogen. The mechanism was believed to be oxiding Co(III) to Co(IV) intermediate state, which then being reduced by coordinated NH_3 by a $2e^-$ change to Co^{2+}. At low Co(III) concentration, the rate of Co^{2+} production increased with Co(III), but when it is in millimole range, the rate reached a saturation value. The main net change in the rate saturation region for the pentaammine as substrate is

$$H^+ + [Co(NH_3)_5 \cdot H_2O]^{3+} + S_2O_8^{2-} = Co^{2+} + \frac{1}{2}N_2 + 4NH_4^+ + H_2O + 2{SO_4}^{2-} \qquad (2.42)$$

2.9 Summary

A great amount of NO_x is produced in fossil fuel combustion, and 95% of NO_x is NO. Combination of a combustion modification technology and a FGT is the optimum measure to tackle NO_x emissions. Wet scrubbing has been well developed for SO_2 removal from the flue gases, and it is expected to be cost-effective if wet scrubbing can be developed for simultaneous removal of NOx and SO2. Selection of the right absorbent is the key to this goal. The selection of an ideal absorbent rests primarily on a compromise of following points: (1) ability to react with insoluble nitric oxide (NO), (2) ease of regeneration or complete utilization of absorbent, (3) low operating cost, (4) easy disposal of liquid waste, and (5) zero or even positive effect of oxygen. Ammoniacal cobalt(II) complexes have been reported to meet these criteria.

However, the mechanism behind the NO absorption into ammonicacal cobaltous solutions was not well understood. And the equilibrium constant and kinetics of related chemicals reactions are missing in literature. In addition, there has been limited information on the mass transfer coefficient in industrial absorbers. Bubble column, conventional stirred tank reactor and gas-inducing agitated tank are three frequently used types of industrial absorbers. The mass transfer coefficient and reaction rate

constant are two important parameters in determination of NO absorption rate in these absorbers. Therefore, the correlations for evaluation of volumetric liquid-phase mass transfer coefficient were systematically reviewed.

The thesis work aims at addressing these missing information in literature. They are reported in the coming chapters. As the first step of this thesis work, the selection of optimum absorbent is reported in the next chapter. It was achieved by comparing the NO absorption performances of several popular absorbents such as H_2O_2, Fe(II)-EDTA and ammoniacal cobalt(II) solutions over a 165-minute continuous operation.

Chapter 3
Selection of Absorbent

3.1 Introduction

In this chapter, the experimental setup and procedures are first described. The performances of three absorbents (or systems) are compared. The selected optimal agent is then evaluated in terms of NO removal efficiency at different temperatures, pH values, and initial inlet absorbent concentrations.

3.2 Experimental Setup

Figure 3-1 shows the experimental setup of the bubble column system for the comparison/selection of NO absorbent. The experiments were conducted in acrylic column reactors under atmospheric pressure. Two identical reactors were used in series to increase the residence time. Each reactor was 500 mm long with an inner diameter of 30 mm. The liquid volume was maintained at 500 mL and no fresh aqueous solution was allowed to enter the absorbers during the experiments. Temperature of the column reactor was maintained by using a jacket through which water from a thermostatic bath was circulated. The variation of the temperature was within 0.01 ℃. The simulated flue gas was a mixture of N_2, O_2 and NO with a constant flow rate of 500 mL·min^{-1}. Concentrations of NO were measured at both the inlet and the outlet of the reactor system using a flue gas analyzer (Testo 350 XL) and also used to determine the NO removal efficiency, exchangeable with absorption efficiency herein, as shown in Eq. 3.1.

$$\eta = \frac{c_{in} - c_{out}}{c_{in}} \times 100\% \qquad (3.1)$$

where η = the NO removal efficiency, %;

c_{in} = the NO concentration at inlet, ppmv;

c_{out} = the NO concentration at outlet, ppmv.

The flue gas analyzer was able to measure oxygen and nitric oxide in the range of 0-25% vol. and 0-3000 ppmv, respectively. The corresponding resolutions were 0.1 vol. % and 1 ppmv. Due to the low flow rate of the simulated flue gas, it could take up to 20 minutes to take the first stable reading from the flue gas analyzer. During this period, the simulated flue gas was directly introduced to the scrubbing bottle. When the system became stable, the outlet flue gas was analyzed every 15 minutes. All data were repeated at least twice to check the repeatability, and the values used in the figures below are based on the average of all measurements.

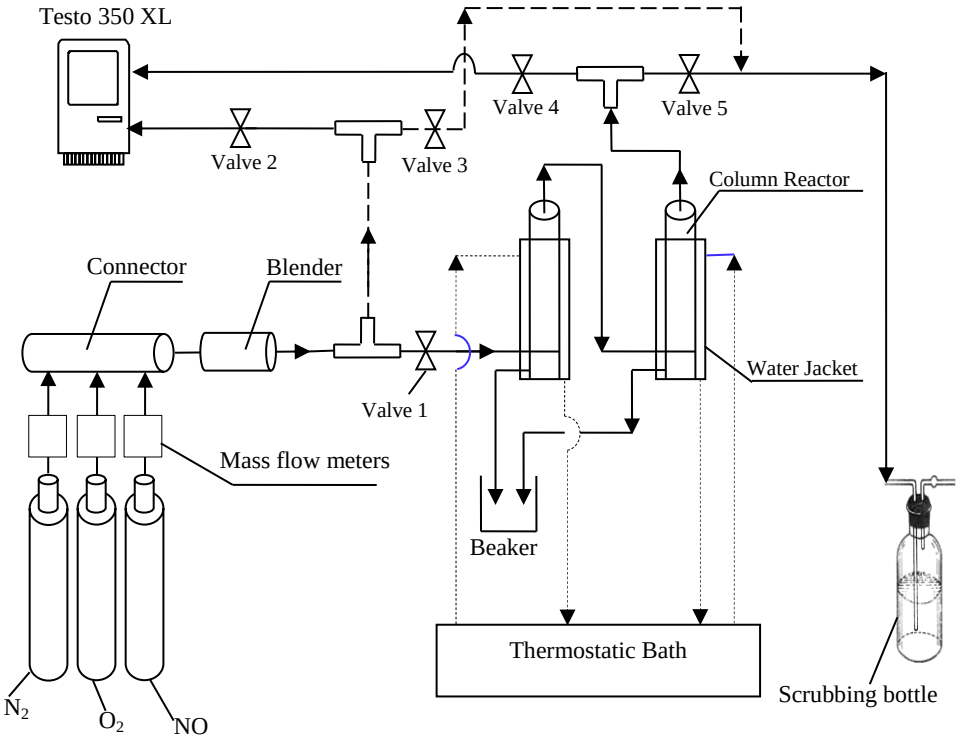

Figure 3-1: Experimental setup of the dual bubble column system

Penta- and hexamminecobalt(II) chloride ($[Co(NH_3)_5]Cl_2$ and $[Co(NH_3)_6]Cl_2$), Fe(II)-EDTA and H_2O_2 were selected for comparison. The initial concentrations of ammoniacal cobalt(II) solution and Fe(II)-EDTA were 0.060 and 0.075 $mol \cdot L^{-1}$, respectively. And the concentration of hydrogen peroxide (H_2O_2) was 30% by weight. As to be introduced shortly, the de-NO efficiency did not increase any more when the initial concentration of $[Co(NH_3)_6]Cl_2$ reached 0.060 $mol \cdot L^{-1}$. 30% of the H_2O_2 was the maximum concentration commercially available. The penta- and hexa-ammine system was prepared in a conical beaker with a volume of 500 mL by reaction between cobalt (II) chloride hexahydrate (analytically pure) and excessive aqueous ammonia (30% of concentration, AP) with the existence of ammonium chloride (NH_4Cl) (AP), which was used to form $NH_4Cl/NH_3 \bullet H_2O$ buffer solution in favour of the supply of NH_3 ligand. Since ammoniacal cobalt(II) complexes are not stable and easy to be oxidized, this process needs to be done quickly. The pH values of the liquids were measured by a pH meter (pHS-25C), which was made by Shanghai Yulong Instrument Co. Ltd. Buffer solutions with pH value of 4 and 7 were used to calibrate the pH meter before its first use. The pH value of hexamminecobalt(II) solution was adjusted by the addition of aqueous ammonia. The Fe(II)-EDTA solutions were prepared through reaction between equimolar amounts of $FeSO_4$ and EDTA-Na_2 (both analytical pure) in deionized water at atmosphere pressure. Its pH value was

regulated by the addition of NaOH or H_2SO_4. All the chemicals mentioned above were supplied by Tianjin Guangfu Fine Chemical Research Institute, China. The gases, NO (2.54% in N_2), N_2 (>99.99%), and O_2 (>99.99%) were from Harbin Limin Gas Co. Ltd., China. They were used to produce simulated flue gas with set flow rate of 500 mL·min^{-1} during the experiments. 2.54% of NO in nitrogen and O_2 are supplied from cylinders and further diluted with N_2 to the desired concentration of 500 ppmv of NO and 5.0% of O_2.

3.3 Results and Discussion

3.3.1 Uncertainty Analysis

Optimum absorbent was determined on the basis of NO absorption performance at given experimental conditions of gas flow rate of 500 mL·min^{-1}, 500 ppmv of NO and 5.0% of O_2. The time-series NO absorption efficiency into aqueous solutions measured at different points was the only indication of performance comparison. From Eq. 3.1 it can be seen that the uncertainty in the NO absorption arises due to the propagation of uncertainties in measured NO concentrations at both inlet and outlet, and it can be described by standard ANSI/ASME uncertainty analysis methodology as follows [131, 132]. It is noted that only general uncertainty analysis is conducted herein.

$$U_\eta{}^2 = \left(\frac{1}{c_{in}} U_{c_{out}}\right)^2 + \left(\frac{c_{out}}{c_{in}{}^2} U_{c_{in}}\right)^2 \tag{3.2}$$

where $U_{c_{in}}$, $U_{c_{out}}$ = uncertainties in the NO concentrations at inlet and outlet, respectively, in ppmv.

According to the specifications of Testo 350 XL provided by the supplier, $\frac{U_{c_{out}}}{c_{out}} = \frac{U_{c_{in}}}{c_{in}} = 5\%$. In this study, the inlet NO concentration remained constant at 500 ppmv. Therefore, $U_{c_{in}}$ = 25 ppmv, and $U_{c_{out}}$ = 0.05c_{out} ppmv.

Substituting these known variables into 3.2 and rewriting give

$$U_\eta{}^2 = \sqrt{2} \cdot 5\% \cdot \frac{c_{out}}{c_{in}} = 0.014\% \cdot c_{out} \tag{3.3}$$

Obviously, there is a linear relationship between the uncertainty in the NO removal efficiency and the measured outlet NO concentration whose slope is 0.014 %.

3.3.2 Selection of Optimal Absorbent (System)

Figure 3-2 shows the NO removal efficiencies of different absorbents over time. Overall it can be seen that ammoniacal cobalt(II) solution performed better than Fe(II)-EDTA and H_2O_2. The initial

NO removal efficiency, which is defined as the removal efficiency of the fresh absorbent, of hexamminecobalt(II) was 96.45% at the beginning and remains close to 80% over 165 minutes of continuous operation. The NO initial removal efficiency of H_2O_2 used herein was lower than 45% and decreases to about 28% in 165 minutes. As for Fe(II)-EDTA, the NO removal efficiency was close to 97.7% at the beginning and drops gradually to 90% in 75 minutes.

After 75 minutes of continuous operation, the NO removal efficiency of Fe(II)-EDTA dropped abruptly and eventually ended up with a negative de-NO efficiency, which means that extra NO had been produced, likely through the reaction in Eq. 3.4.

$$\mathrm{Fe(II)-EDTA + NO \rightleftharpoons Fe(II)(NO)-EDTA} \qquad (3.4)$$

The NO concentration measured at the outlet of the reactor reaches 866 ppmv whereas the inlet NO concentration was 500 ppmv. Note that all these data points were repeated at least four times and were deemed to be consistent. The absorption of nitric oxide by Fe(II)-EDTA follows Eq. 3.4. This reaction is reversible as proven by Hishinuma [133]. According to Nymoen's[86], this reaction took place fast and spontaneously. If the operating condition is free of oxygen, with the consumption of Fe(II)EDTA, there will be an equilibrium. And no more NO would have been absorbed after the equilibrium. Thus, the NO concentration at the outlet should have been the same as that of inlet. While in this work, 5.0% of oxygen existed in the simulated flue gas. Besides the reaction with NO, Fe(II)EDTA also reacted with oxygen as well to form inactive Fe(III)EDTA [134-136], whereas the oxygen would first react with penta- and hexa-amminecobalt(II) to create a strong oxidant rather than the $[Co(NH_3)_6]Cl_3$ without catalyst. This will be elaborated shortly. The reduction of Fe(II)EDTA due to the formation of Fe(III)EDTA would break and shift the established equilibrium to the left so that the originally bound NO released. This is consistent with the abnormal phenomenon occurring after 150 min shown in **Figure 3-2**. The outlet NO concentration was greater than the inlet one. The Addition of sulphite such as Na_2SO_3 may somewhat resolve this problem with increased operational cost.

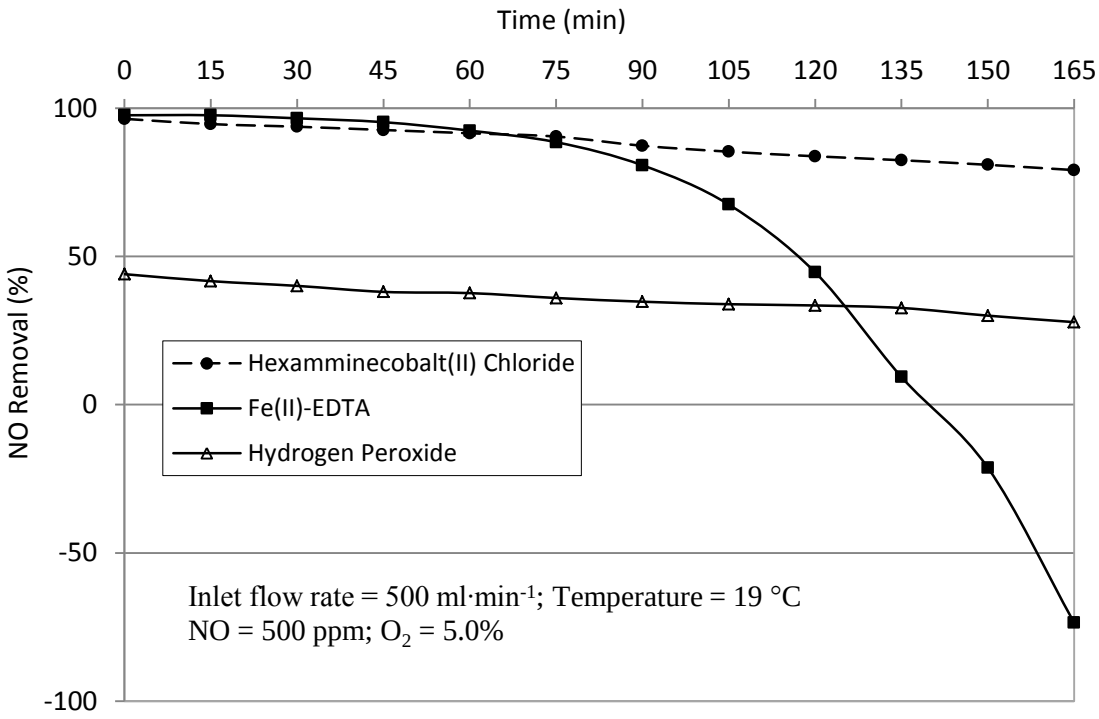

Figure 3-2: The continuous NO removal efficiency of different absorbents

The relatively high and consistent NO removal efficiency of ammoniacal cobalt(II) solution might be associated with the fact that it has the capability to not only bind with NO but also activate the oxygen molecule as well. As shown in Eqs. 3.5 and 3.6, penta- and hexa-amminecobalt(II) chloride can react with NO to form a μ-hyponitrite dicobalt nitrosyl complex, $[Co(NH_3)_5N_2O_2(NH_3)_5Co]Cl_4$.

$$2NO + 2[Co(NH_3)_5]^{2+} \rightleftharpoons [Co(NH_3)_5N_2O_2(NH_3)_5Co]^{4+} \quad (3.5)$$

$$2NO + 2[Co(NH_3)_6]^{2+} \rightleftharpoons [Co(NH_3)_5N_2O_2(NH_3)_5Co]^{4+} + 2NH_3 \quad (3.6)$$

Penta- and hexa-amminecobalt(II) chloride can also be oxygenated to produce a diamagnetic salt of a binuclear cobalt complex ion, $[(NH_3)_5Co\text{-}O\text{-}O\text{-}Co(NH_3)_5]^{4+}$, in which the O-O bridging group is a peroxide bond similar to that in hydrogen peroxide. This mechanism has been proven by thermodynamics theory by Ochiai [137] and experimentally by Schaefer [138].

$$O_2 + 2[Co(NH_3)_5]^{2+} \rightleftharpoons [Co(NH_3)_5O_2(NH_3)_5Co]^{4+} \quad (3.7)$$

$$O_2 + 2[Co(NH_3)_6]^{2+} \rightleftharpoons [Co(NH_3)_5O_2(NH_3)_5Co]^{4+} + 2NH_3 \quad (3.8)$$

This diamagnetic complex is a strong oxidant similar to hydrogen peroxide. It will react with the nitrosyl product in Reactions 3.5 and 3.6 to form a nitro complex, which will finally be transformed into soluble nitrate and nitrite [32].

Absorption of NO using H_2O_2 follows different mechanisms depending on whether ammonia exists or not. Azuhata et al. [139, 140] reported that NO absorption was a coordination reaction in the presence of NH_3. A NO removal efficiency of as high as 90% could be reached at a NH_3 to NO ratio of 5 and a H_2O_2 to NO ratio of 1 when the temperature was 550 ℃. However, two side reactions would happen to reduce the NO absorption efficiency if oxygen were to be added to the system. Zamansky et al. [141] also reported that NO absorption would be improved in terms of conversion rate (up to 90-98%) of NO into NO_2 when NH_3 was absent and with a temperature of at least 476 ℃. For room temperature of approximately 20 ℃, the addition of nitric acid into hydrogen peroxide was necessary [142]. Therefore, either high temperature or extra acidic acids is needed in order for H_2O_2 to achieve high NO absorption efficiency. It is normal to see a low NO absorption efficiency in our experiments under the conditions of temperature level at only 19 ℃.

Regarding the performance of ammoniacal cobalt(II) system, the results herein is quite different from what has been previously reported in literature [32]. In this experimental study, hexamminecobalt(II) chloride maintained a relatively high NO absorption efficiency. The reason for this was probably due to the higher volume and concentration of the absorbents in the system herein. Furthermore, greater differences were observed for hydrogen peroxide and Fe (II)-EDTA, the efficiencies of which were much lower than previously reported [32]. It takes about 135 minutes to show the effect of reversible reaction between Fe(II)-EDTA and NO in the experiments herein. Long et al. [32] did not see this phenomena most likely because they only ran the experiments for 60 minutes with Fe (II) –EDTA. Nonetheless, since the methodology was not available in their publication with respect to the tests for Fe (II)-EDTA and H_2O_2, there might be other reasons for these differences.

Overall, the experimental results herein identified ammoniacal cobalt(II) system as the best absorbent for the system used. Therefore, the following experiments were focused on this sorbent alone.

3.3.3 Effect of Fresh Absorbent Composition on NO Removal Efficiency

Figure 3-3 shows the effect of the overall concentration of ammoniacal cobalt(II) system on the NO removal efficiency at different durations of operation. During the first 30 minutes, the reductions in NO removal efficiency were 8.82%, 6.81%, 4.30%, 2.66% and 3.43% as the concentration of absorbent increased from 0.030 to 0.080 $mol \cdot L^{-1}$. The experimental results indicated that the NO

removal efficiency rose steadily with the increase in concentration of the hexamminecobalt(II) from 0.030 to 0.060 mol·L^{-1}. After 0.060 mol·L^{-1}, the efficiency will remain more or less constant. This implied that the absorption process had become mass transfer limited. Results in **Figure 3-3** indicate that excessive Co(II) did not further increase the de-NOx performance of a system. From an engineering economics point of view, it is better to maintain the Co(II) concentration around 0.060 mol·L^{-1}.

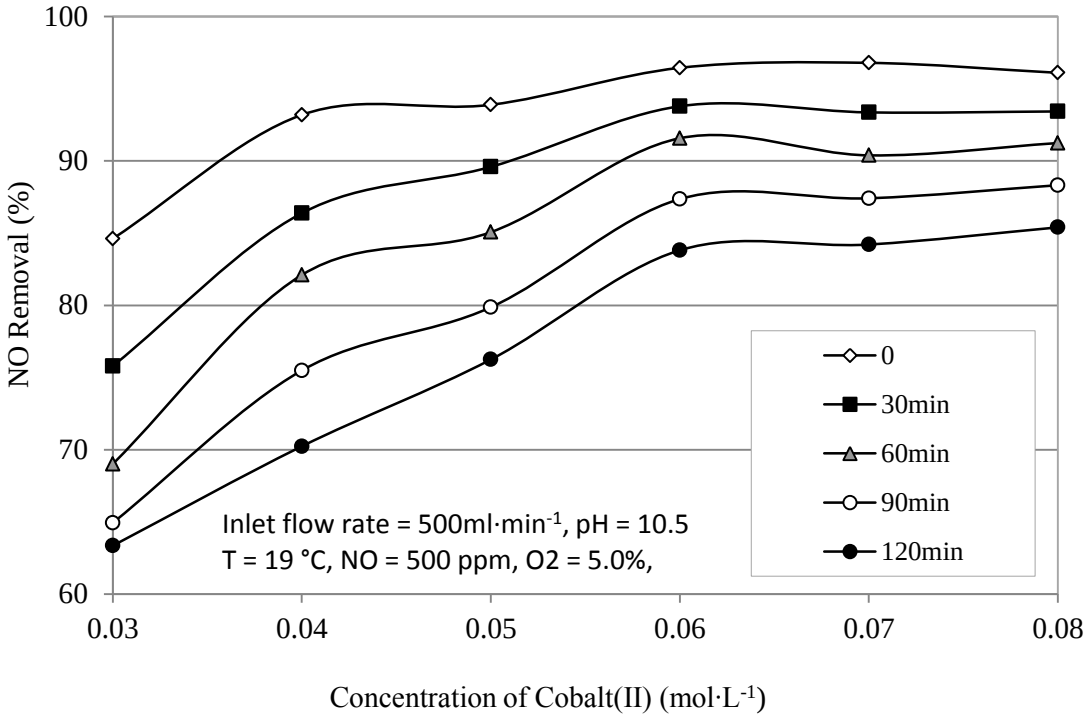

Figure 3-3: Effect of concentration of cobalt(II) on NO removal efficiency

The change in NO removal efficiency with concentration of hexamminecobalt(II) chloride shared the same tendency as that reported previously by Mao et al. [56] but with different optimum absorbent concentration. Mao et al. reported that the optimum absorbent concentration was 0.040 mol·L^{-1} instead of 0.060 mol·L^{-1} as it was in our experiment. The difference was likely caused by the experimental apparatus. In this thesis work, bubble column reactors were used. The double-stirred reactor used in Mao's work boasts higher efficient as stirring provides better gas-liquid dispersion thus improving mass transfer and reaction area. It would be useful to compare different reactors in terms of NO removal efficiency in the future.

3.3.4 Effect of pH Value on NO Removal Efficiency

Figure 3-4 shows the effect of pH value on the NO removal efficiency of absorbent at the end of different operation durations. It is worthwhile to mention that ammoniacal cobalt (II) chloride is not stable and can only be freshly prepared for use. And the effect of pH value is exerted through the determination of the productivity of penta- and hexa-amminecobalt (II) chloride of the reaction between $CoCl_2$ and NH_3 [36]. In order to compare the pH effect, in present research, the amount of $CoCl_2 \cdot 6H_2O$ (NOT the $[Co(NH_3)_6]Cl_2$) applied at different pH value were the same. The inlet NO concentration was 500 ppmv with 5.0% of O_2. The experimental results showed that the operating pH value had a noticeable effect on the NO absorption efficiency. For instance, the initial NO absorption efficiency increased by 40% from 53.1% to 92.5% when pH value increased from 9.75 to 10.46, rendering the change with pH insignificant at greater alkalinity. After 15 minutes of operation, the efficiency followed the same tendency, rising from 49.80% to 88.52% over the pH between 9.75 and 10.46, and remaining more or less constant then. Results in **Figure 3-4** indicate that the optimum pH value was at 10.50 regardless of the residence time. Excessive ammonia could not improve the performance. However, since ammonia is not an expensive chemical, it is recommended to have extra ammonia in practice.

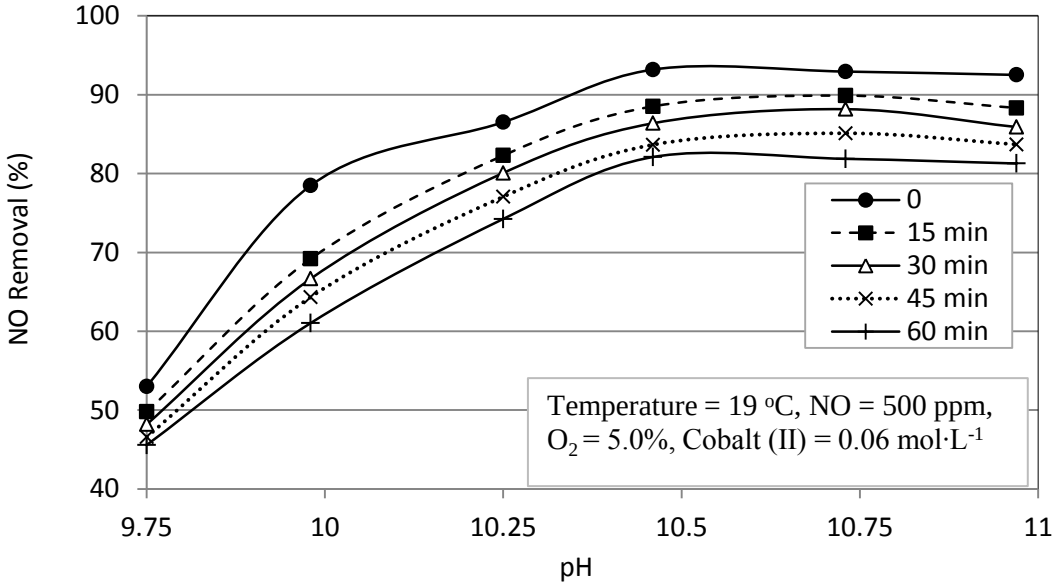

Figure 3-4: Effect of pH on NO removal efficiency at different operation time

This observation is consistent with the theoretical analyses. According to Ji et al., synthesis of penta and hexa-amminecobalt(II) chlorides needs to be performed at high pH values [36]. The ultimate

product of the reaction between cobalt (II) chloride hexahydrate and ammonia is highly pH dependent. Based on the stepwise complex stability constants in **Table 2-2** given by Yatsimirskii and Volchenskova [63] and Ji et al. [36], with the addition of 1 $mol \cdot L^{-1}$ of ammonia chloride, the portion of hexamminecobalt(II) ion in the cobalt(II)-ammine complexes was 81.48% at a pH value of 10.46, while 42.43% at pH of 9.75, which was just above half of 81.48%. This well explains why the initial efficiency at pH of 9.75 was also just over half of that of 10.46.

In addition, different from cobalt (II) nitrate used in Ji's study, chloridion of present $CoCl_2$ was a ligand for transition-metal cobalt. The concentration of the free ammonia in the aqueous solution can be calculated by using Eq. 2.17. A lack of free ammonia in the aqueous solution caused by the decrease in pH value would result in the existence of $[Co(NH_3)_5Cl]Cl$, which could not effectively coordinate with nitric oxide. Hence, a low pH value did not favour the absorption of NO. However, like cobalt salen-type complexes, there would be a deprotonation of OH^- group in the reaction leading to decomposition of cobalt complex at the very high pH value [143]. This explains why a very slight reduction in NO removal efficiency actually occurred at the pH value that was nearly 11. Therefore, careful balancing the amount of hydroxyl is important to this process because at very high OH^- concentrations the cobalt complex will start decomposing while at low concentrations it can exist as an inactive species.

On the other hand, the variation trend in the NO removal efficiency with pH value differed significantly from what had been previously reported in literature [56]. As shown in **Figure 3-5**, the NO absorption efficiency (indicated by the absorption rate on the y-axis) increased dramatically as pH value increased from 8.5 to 11.5 or so. It seems that NO absorption rate would increase at an even greater rate with an increase in pH values of more than 11. This seems to be against the aforementioned theoretical analysis. Further investigation is needed in order to explain the difference.

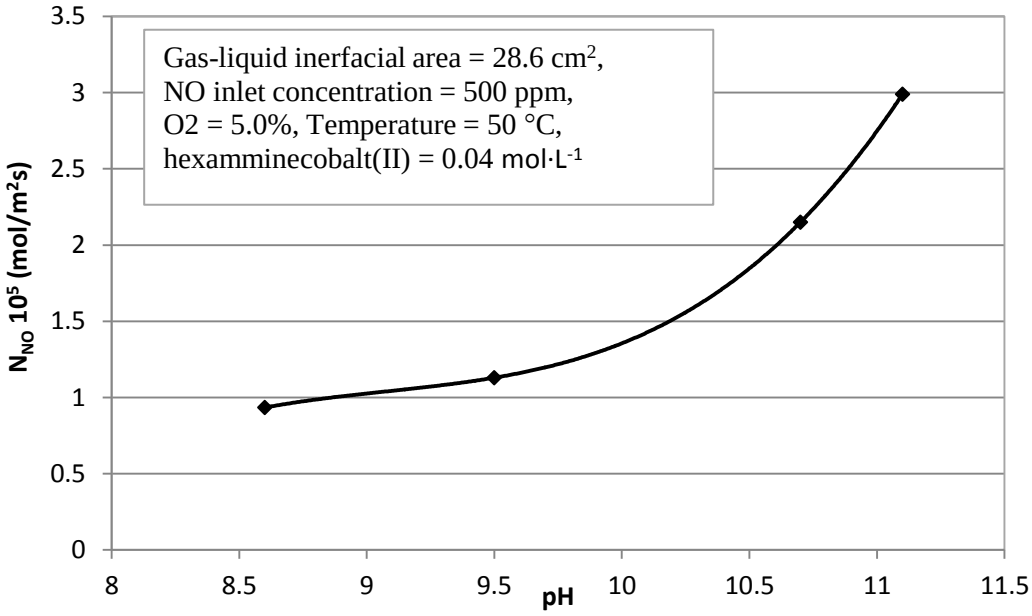

Figure 3-5: Effect of pH on NO absorption rate

3.3.5 Effect of Temperature on NO Removal Efficiency

Figure 3-6 shows the NO removal efficiencies of hexammminecobalt (II) solution over time at three different operating temperatures of 292.2, 308.2 and 323.2 K. The concentration of the ammoniacal cobalt (II) was still 0.060 mol·L^{-1} and the simulated flue gas contained 500 ppmv of NO and 5.0% of O_2. The experimental results show that the operating temperature had comparable effects on the NO absorption efficiency for the temperatures of 19 ℃ and 35 ℃. However, the NO absorption into the ammonia-cobalt system decreased approximately 14% initially when temperature increased from 35 to 50 ℃. It can be concluded that both the coordination and oxidation of NO into ammoniacal cobalt(II) chlorides decreased with the increase of temperature. As a result the absorption of NO dropped. Results shown in **Figure 3-6** indicate that excessive heating was not necessary for the absorption of NO in practice.

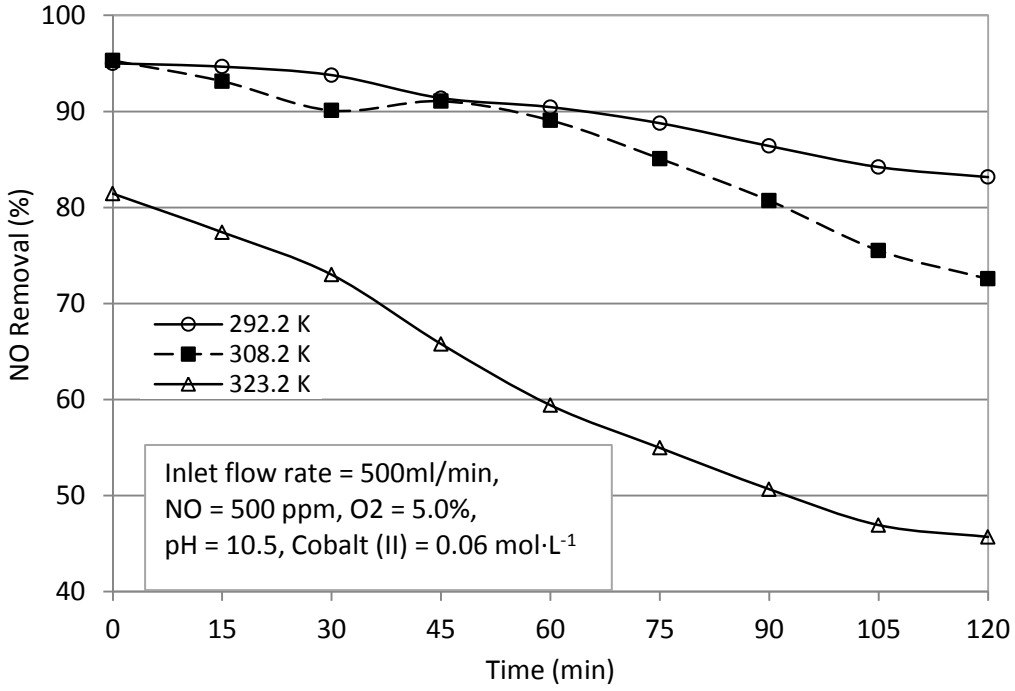

Figure 3-6: Effect of temperature on NO removal efficiency

The maximum efficiency of 96.45% indicates that the chemical reactions within the bubbles were faster than the mass transfer rate at the interface between liquid and gas bubbles. From the engineering application point of view, it is necessary to increase the mass transfer rate in order to improve the efficiency. One option is to reduce the bubble size to increase the specific interfacial areas between liquid and bubbles. But the volumetric gas-liquid mass transfer coefficient k_La is a product of liquid side mass transfer coefficient, k_L and the gas-liquid specific area, a, extremely small bubbles may reduce the k_La because k_L decreases as bubble size decreases. There should be an optimum bubble size corresponding to the highest volumetric mass transfer coefficient. This should be investigated quantitatively in the future.

3.4 Summary

Based on the experimental work within in this Chapter, ammoniacal cobalt(II) system was found to perform better than Fe(II)-EDTA and H_2O_2 in terms of NO removal efficiency, although all test subject efficiencies dropped with operating time. The NO removal efficiency of ammoniacal cobalt(II) system was highly affected by operating conditions such as temperature, pH value and initial concentration. It decreased with the increase in temperature, and rose to the maximum before it

levelled off as pH value and concentration of absorbent increased. The highest initial NO removal efficiency of 96.45% corresponded to inlet flow rate of 500 $mL \cdot min^{-1}$, temperature of approximately 19 ℃, pH value of around 10.5, and the concentrations of $[Co(NH_3)_6]Cl_2$, NO and O_2 of 0.06 $mol \cdot L^{-1}$, 500 ppmv and 5.0%, respectively.

Although the superiority of ammonical cobalt(II) ions to other absorbent has been experimentally proven, the real mechanism behind the NO absorption remains unknown or unwarranted. For insight into such mechanism, information of relevant equilibrium and kinetics is desired. In the next chapter, the equilibrium constants are measured in a bubble column based on cobalt(II) – ammonia system.

Chapter 4
Determination of Equilibrium Constants

4.1 Introduction

Equilibrium constants of reactions between nitric oxide and ammoniacal solutions (namely penta- and hexa-amminecobalt(II) solutions) are essential to understanding the mechanism of nitric oxide absorption and the design of a gas-liquid reactor. These constants, however, were unknown or incorrectly analyzed in literature. This chapter reports the determination of the equilibrium constants in a bubble column reactor. Experimental setup, absorbent preparation, and experimental procedures are first described in detail. Then original data are summarized, followed by data analysis. At last, equilibrium constants at different temperatures are presented in the van't Hoff equation.

4.2 Theoretical

As introduced above, penta- and hexa-amminecoblat(II) ions are most likely to react with nitric oxide; therefore, following equilibria might take place in the cobalt(II) - ammonia system,

$$2NO + 2[Co(NH_3)_5]^{2+} \rightleftharpoons [Co(NH_3)_5N_2O_2(NH_3)_5Co]^{4+} \tag{4.1}$$

$$2NO + 2[Co(NH_3)_6]^{2+} \rightleftharpoons [Co(NH_3)_5N_2O_2(NH_3)_5Co]^{4+} + 2NH_3 \tag{4.2}$$

Recall the last step reversible equilibrium in **Table 2-2**,

$$Co(NH_3)_5(H_2O)^{2+} + NH_3 \rightleftharpoons Co(NH_3)_6{}^{2+} + H_2O \tag{4.3}$$

The equilibrium constants of Reactions 4.1 – 4.3 then can be defined as:

$$K_{NO}^5 = \frac{[(NH_3)_5Co(N_2O_2)Co(NH_3)_5{}^{4+}]_e a_w^2}{[Co(NH_3)_5(H_2O)^{2+}]_e^2[NO]_e^2} \tag{4.4}$$

$$K_{NO}^6 = \frac{[(NH_3)_5Co(N_2O_2)Co(NH_3)_5{}^{4+}]_e[NH_3]_e^2 f_{NH_3}^2}{[Co(NH_3)_6{}^{2+}]_e^2[NO]_e^2} \tag{4.5}$$

$$K_6 = \frac{[Co(NH_3)_6{}^{2+}]_e a_w}{[Co(NH_3)_5(H_2O)^{2+}]_e[NH_3]_e f_{NH_3}} \tag{4.6}$$

And from Eqs. 4.4 – 4.6 following equation can be obtained.

$$K_{NO}^5 = (K_6)^2 K_{NO}^6 \tag{4.7}$$

where $[\ ]_e$ = corresponding concentration at equilibrium, mol·L^{-1};

a_w = water activity, -;

f_{NH_3} = the activity coefficient of the ammonia, -;

K_6 = equilibrium constant of Reaction 4.3;

K_{NO}^5 = equilibrium constant of Reaction 4.1;

K_{NO}^5 = equilibrium constant of Reaction 4.2.

In Eq. 4.4, the solution of K_{NO}^5 necessitates the knowledge of water activity, a_w, and the concentrations of NO, $(NH_3)_5Co(N_2O_2)Co(NH_3)_5{}^{4+}$ and $Co(NH_3)_5(H_2O)^{2+}$ at equilibrium. Water activity, a_w, is a measure of the energy status of the water in a system. It can be assumed unity in 2 mol·L^{-1} NH_4NO_3 solution at low ammonia concentration (less than 1 mol·L^{-1}). Nevertheless, assuming a_w equal to unity will lead to errors at higher ammonia concentrations [61, 62]. The values at ammonia concentrations of 1.01 - 10.57 mol·L^{-1} can be estimated [62, 65].

The equilibrium NO concentration in water can be obtained from its solubility in terms of the Henry's constant of NO in water which can be presented as [144],

$$H_w = 526.32\exp(-1400\left(\frac{1}{T}-\frac{1}{298.15}\right)) \tag{4.8}$$

where H_w = Henry's constant of NO dissolved in water, L·atm·mol^{-1}; T = temperature, K.

The solubility in an electrolyte solution can then be predicted by taking ionic strength into account. In this study, the solution can be regarded as a mixed solution of cobaltous nitrate and ammonium nitrate, where the concentration of NH_4NO_3 is excessively higher than that of $Co(NO_3)_2$. According to Sada et al. [47] and Onda et al. [145], Busen absorption coefficient in an electrolyte can be associated with that in water at the same temperature by following equation,

$$log_{10}\left(\frac{\alpha}{\alpha_w}\right) = -(k_1I_1 + k_2I_2) \tag{4.9}$$

in which the ionic strength of a solution can be expressed by

$$\mathrm{I} = 1/2\sum c_i z_i^2 \tag{4.10}$$

where k_1 = salting-out parameter of aqueous NH_4NO_3 solution, L·mol^{-1};

k_2 = salting-out parameter of aqueous $Co(NO_3)_2$ solution, L·mol^{-1};

I_1 = ionic strength of aqueous NH_4NO_3 solution, mol·L^{-1};

I_2 = ionic strength of aqueous $Co(NO_3)_2$ solution, mol·L^{-1};

c = concentration of aqueous solution;

z = valence, -;

α = Busen absorption coefficient in electrolyte solution, cm^3 of gas · cm-^{3} of solution;

α_w = Busen absorption coefficient in water, cm^3 of gas · cm-^{3} of water;

And the salting-out parameter, k, is the summation of contributions of cation, anion and gas, respectively:

$$k = x_c + x_a + x_G \tag{4.11}$$

The values of x_c, x_a and x_G are summarized in **Table 4-1** [26, 47, 145].

Table 4-1: Values of x_c, x_a and x_G

Symbol	$x_{NH_4^+}$	$x_{Co^{2+}}$	$x_{NO_3^-}$	x_{NO}
Value	-0.0737	-0.0534	0.3230	-0.1825

Henry's constant is another parameter commonly used to represent gas solubility in liquid solution, the conversion between Busen absorption coefficient and Henry's constant can be realized by [146]

$$\alpha_i = 22.4 \cdot \frac{1}{H_i} \cdot \frac{\rho}{M} \tag{4.12}$$

where M = molar mass of the solution, g·mol^{-1}; ρ = density, kg·m^{-3}.

Substituting Eq. 4.12 into 4.9 gives

$$log_{10}\left(\frac{H}{H_w}\right) = k_1 I_1 + k_2 I_2 \tag{4.13}$$

Then the equilibrium NO concentration in the solution is described in

$$[NO]_e = \frac{P_T y_{in}}{H} \tag{4.14}$$

where $[NO]_e$ = NO concentration in the liquid phase at equilibrium, mol·L^{-1};

P_T = total pressure, atm;

y_{in} = NO concentration at inlet, ppmv.

Secondly, the concentration of $(NH_3)_5Co(N_2O_2)Co(NH_3)_5^{4+}$ at equilibrium is equal to half of the amount of NO absorbed based on the stoichiometry in Reactions 4.1 and 4.2. The total amount of NO absorbed can be calculated through the graphic integration of a NO absorption efficiency curve, which is given by the continuous measurement of outlet NO concentration, by using Trapezoid method. A typical absorption curve can be found in **Figure 4-1**.

$$n = G_m y_{in} \int_0^{\infty} \eta dt \tag{4.15}$$

where G_m = total molar flow rate of NO, mol·s^{-1};

n = amount of NO absorbed, mol;

t = time, s;

η = NO removal efficiency, %.

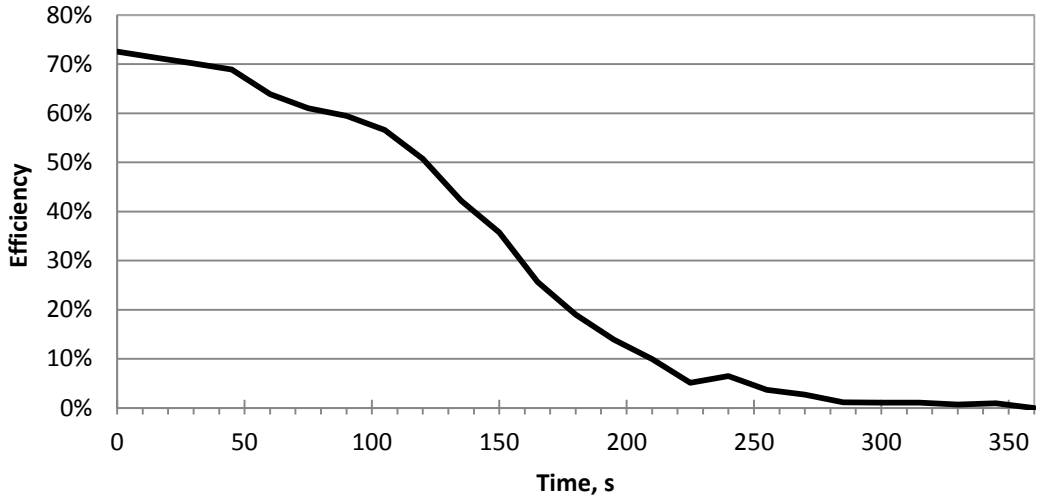

Figure 4-1: A typical NO absorption curve

According to the ideal gas law,

$$G_m = \frac{P_T Q_G}{RT} \tag{4.16}$$

where Q_G = volumetric NO flow rate, m^3·s^{-1};

R = gas constant, 0.08205 L·atm·K^{-1}·mol^{-1};

T = temperature, K.

Then the amount of NO absorbed by chemical reaction is

$$n_{chem} = G_m y_{in} \int_0^{\infty} \eta dt - V_L[NO]_e \tag{4.17}$$

where n_{chem} = the amount of NO absorbed by chemical reaction, mol;

V_L = liquid volume, m^3.

Furthermore, the equilibrium concentration of $(NH_3)_5Co(N_2O_2)Co(NH_3)_5{}^{4+}$ can be described as,

$$[(NH_3)_5Co(N_2O_2)Co(NH_3)_5{}^{4+}]_e = \frac{1}{2}(\frac{G_m y_{in}}{V_L}\int_0^\infty \eta dt - [NO]_e) \qquad (4.18)$$

Lastly, the combination of ammonia – cobalt(II) analysis based on **Table 2-2** or Eqs. 2.8 -2.13 in Section 2.4.1 and the known equilibrium concentration of $(NH_3)_5Co(N_2O_2)Co(NH_3)_5{}^{4+}$ provides the concentration of $Co(NH_3)_5(H_2O)^{2+}$ at equilibrium. As a result, the value of K_{NO}^5 can be obtained following Eq. 4.4 and K_{NO}^6 is then given by Eq. 4.16.

4.3 Experimental

All the chemicals mentioned herein were purchased from Sigma-Aldrich Co. LLC. A continuous water purification system (Model S-99253-10) from Thermo Scientific Inc. was used to produce deionized water. The key to a successful solvent preparation was to establish an oxygen-free environment, because cobalt(II) complexes were able to react with oxygen. Therefore, deionized water was degassed by pure nitrogen (Grade 4.8 from Praxair Inc.) for around 30 minutes before use. As the oxidation rates of cobaltous complexes was relatively slow without catalysts, it was reasonable to assume that the oxidation of cobalt (II) complexes was negligible in a short period [16]. The cobalt (II) - ammonia system was prepared in a 500 mL beaker by step reversible reactions between cobalt(II) nitrate hexahydrate ($Co(NO_3)_2{\cdot}6H_2O$, ACS reagent) and aqueous ammonia ($NH_3{\cdot}H_2O$, ACS reagent, 28-30% NH_3 basis) with the addition of 2 mol·L^{-1} ammonium nitrate (NH_4NO_3, ACS reagent), which in this case was used to form $NH_4NO_3/NH_3{\cdot}H_2O$ buffer solution. This solution was produced to ensure a ready supply of NH_3 ligand while avoiding the formation of hydroxide and the precipitation of cobalt hydroxide.

Certain amount of $Co(NO_3)_2{\cdot}6H_2O$ and NH_4NO_3 were weighed by an analytical balance with readability of 0.1 mg (Model RK-11422-01 from Denver Instrument Inc.) and a top-loading balance with readability of 0.01 g (Model RK-11421-93 from Denver Instrument Inc.), respectively, and dissolved in the 500 mL beaker placed on a stirring hot plate (Model SP142025Q from Thermo Scientific Cimarec Inc.) by deionized water to around 100 mL. The pH values of the liquids were measured by a bench top pH meter with accuracy of ± 0.01 (Model pH 700) manufactured by Oakton Instruments. The reading was taken under mild magnetic stirring. Aqueous ammonia was added to make a pH value just slightly above the desired value. Then water was used to dilute or ammonia to concentrate alternatively, until the solution ended up with 300 mL volume of pH value between 9.06 and 9.37. As an example, a prepared solution with 2 mol·L^{-1} NH_4NO_3 at pH = 9.23 is depicted in

Figure 4-2. Its color is light yellow. At the same time, a picture of precipitation (most likely green according to literature) occurring without the addition of NH_4NO_3 is shown in **Figure 4-3** for comparison.

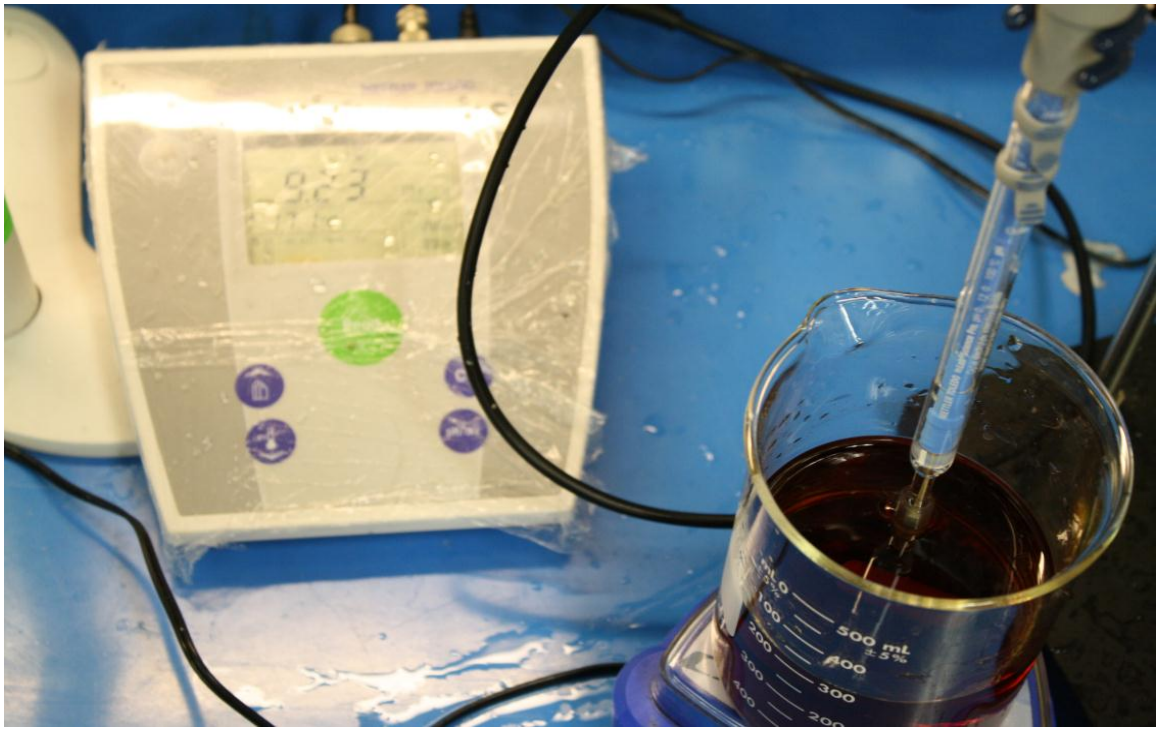

Figure 4-2: Prepared solution with 2 $mol \cdot L^{-1}$ NH_4NO_3 at pH = 9.23

The prepared solution was then transferred to a PYREX 500 mL bubble column reactor with coarse fritted disc (cylinder) distributor (Product #31770-500C from Corning Inc.). The glass bubble column reactor with a 29/40 standard taper stopper, which incorporated a central vertical tube with a 12 mm diameter coarse fritted cylinder as distributor in the lower end, was used to seal the top to the base. The gas entered the bottom of bottle through the top of the tube in the form of bubbles and exited via the sidearm of the bottle stopper. This coarse fritted cylinder had a nominal pore distribution of 40 to 60 μm and provided greater efficiency and more uniform dispersion of gas bubbles for complete absorption. Most importantly, it could be conveniently seated in the water bath for temperature regulation. The concentration of total cobalt (II) was between 0.04 and 0.05 $mol \cdot L^{-1}$.

Figure 4-3: Occurrence of precipitation without NH_4NO_3

Figure 4-4 shows the experimental setup for the determination of equilibrium constants. The operation was performed continuously with respect to the gas phase and batch-wise with respect to the liquid phase. All gases were from Praxair Inc. The compressed air cylinder was of grade zero for ozone generation. In order to eliminate error, a certified 605 ppmv nitric oxide cylinder with nitrogen balance was used. A regulator relieved deliver pressure of each cylinder before entering the process line. Then a mass flow controller provided the flow rate of gases from Cole-Parmer (Model S-32648-16), which had a range of 5 $L \cdot min^{-1}$ and an accuracy of ±1.5% full-scale. The flow controller was regulated by a bellows-sealed metering valve (Model SS-4BMG) purchased from Swagelok Inc. The gas was fed at flow rate of approximately 2.60 $L \cdot min^{-1}$.

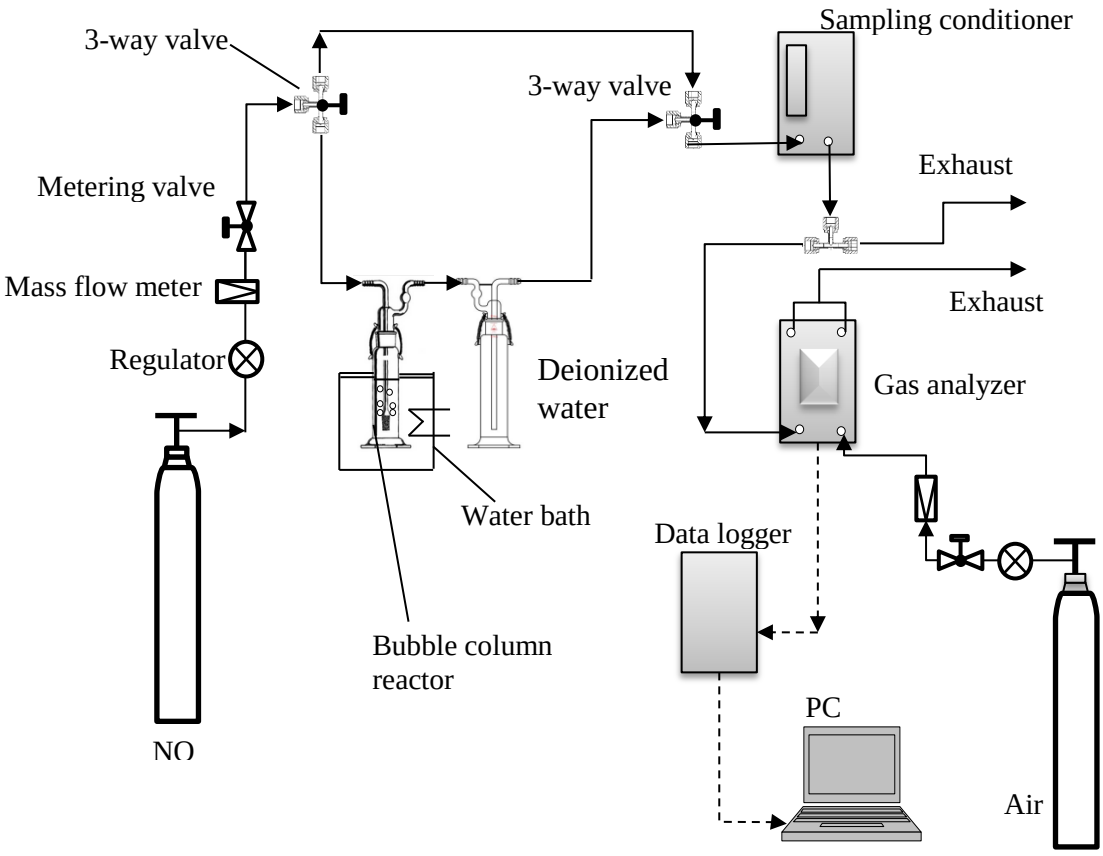

Figure 4-4: The experimental setup of the 500 mL bubble column system

Downstream the metering valve was a 3-way valve that could be switched between by-pass and gas feeding. The nitrosyl formation reactions took place in the bubble column reactor mentioned above. Due to the volatilization of concentrated aqueous ammonia, a glass bottle filled with deionized water was placed to absorb NH_3 to eliminate its interference before the exhaust entered gas analyzer. The NO concentrations at the outlet were measured by a gas analyzer (Model CAI 650 NOXYGEN which had a range of 3000 ppmv and repeatability of around 0.5% of full scale) from California Analytical Instruments Inc. Since the CAI 650 NOXYGEN analyzer could only work properly under atmospheric pressure, a "Tee" conjunction was added for pressure dump whose flow rate was around 1 $L \cdot min^{-1}$. The analyzer required an extra air or oxygen supply for ozone generation. A data logger was used to collect data every 2 seconds. The main section and devices are illustrated in **Figure 4-5**.

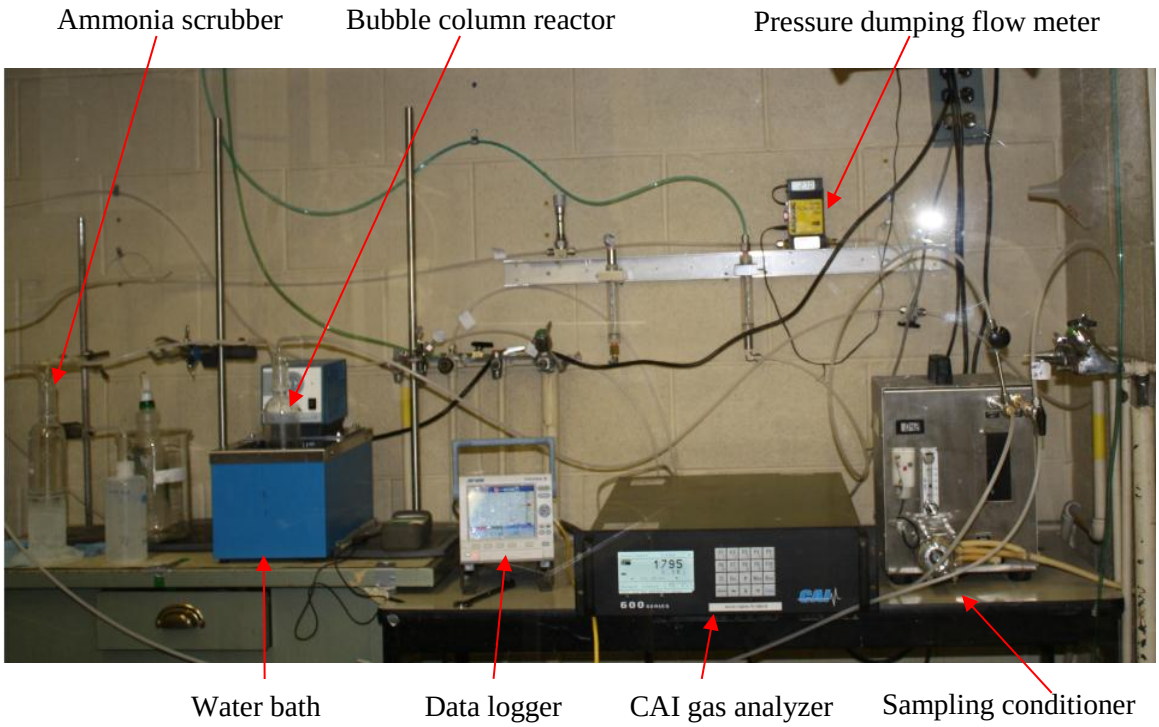

Figure 4-5: Picture of main section of laboratorial setup for equilibrium

The operation terminated when the outlet concentration reached 605 ppmv or so and remained invariable, which indicated that the reaction reached equilibrium. The same pH meter measured the final pH value of used solvent. The corresponding NO absorption efficiency was then described as:

$$\eta = \frac{y_{in} - y_{out}}{y_{in}} \tag{4.19}$$

This measured efficiency will be used in Eq. 4.18 for $[(NH_3)_5Co(N_2O_2)Co(NH_3)_5{}^{4+}]_e$ calculation.

4.4 Results and Discussion

4.4.1 Determination of Reactive Complexes in Cobalt(II) – Ammonia System

In order to validate the assumption that only penta- and hexa-amminecobalt (II) nitrates contribute to NO absorption, a stream of 605 ppmv NO standard gas with nitrogen balance was bubbled through absorbent of pH = 7.63 at T = 304.2 K. The total cobalt (II) concentration of aqueous absorbent was 0.04 mol·L^{-1}; the concentration of ammonium nitrate was 2 mol·L^{-1}. According to the calculation scheme described in Section 2.4.1, the cobalt (II) – ammonia system is summarized in **Table 4-2**; it

shows that complexes of coordination number less than five constitutes 99.65% of the system, with 0.35% of penta-amminecobalt (II) nitrate. The ineffectiveness of small coordination number complexes can be proved if there is no evident NO absorption taking place.

Table 4-2: Cobalt (II) –ammonia system at pH = 7.63, T = 304.2 K, $[NH_4^+] = 2\ mol \cdot L^{-1}$

Co^{2+}	$Co(NH_3)^{2+}$	$Co(NH_3)_2^{2+}$	$Co(NH_3)_3^{2+}$	$Co(NH_3)_4^{2+}$	$Co(NH_3)_5^{2+}$	$Co(NH_3)_6^{2+}$
4.30%	24.01%	44.38%	21.58%	5.38%	0.35%	0

Figure 4-6 shows the changes of outlet NO and oxygen concentrations with time. It can be seen that the outlet NO concentration reached 605 ppmv in 2.5 minutes. The relatively low NO concentrations in the first minute was a result of the existence of oxygen in the headspace at the beginning of the test. The NO concentration was then diluted. The glass bubble column was open to the air at each absorbent loading and the volume of solution inside was 300 mL out of 500 mL column capacity; therefore, there might be some residual oxygen present in the headspace.

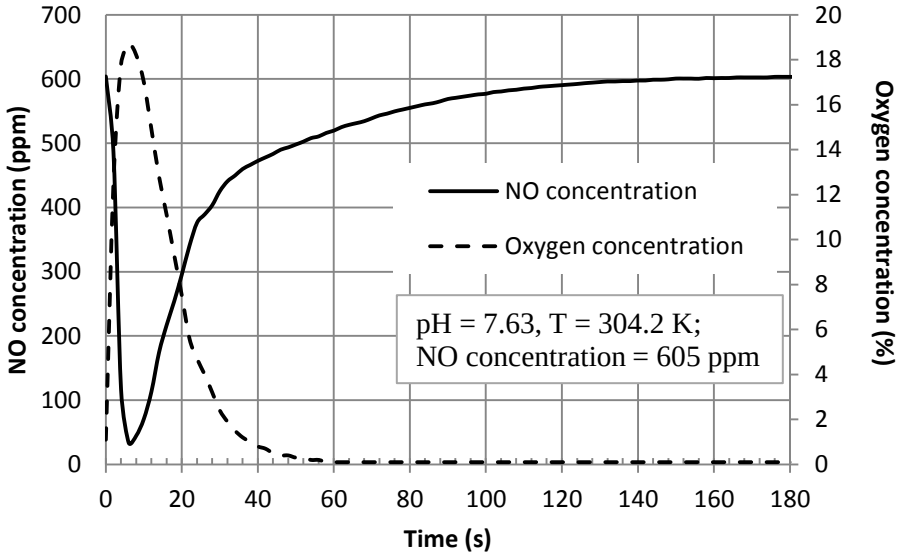

Figure 4-6: The time series plot of outlet NO and oxygen concentrations

The presence of 520 ppmv NO in sixtieth second could be attributed to two contributions. Firstly, according to **Table 4-2** the solution still contained 0.35% of pentaamminecobalt (II) nitrate, which could react with NO. Another possible reason was that some NO dissolved into aqueous solvent even though its solubility was low. Since the NO concentration was in the order of ppmv, these two

contributions to the NO absorption could not be neglected. Therefore, it was reasonable to conclude that only penta- and hexa-amminecaoblt (II) nitrates in a cobalt(II) - ammonia system reacted with NO to form nitrosyl products.

The research findings in **Figure 4-6** can be successfully explained via the analysis of cobalt (II) – ammonia system on the basis of the reversible step reactions proposed by Bjerrum [62], and the assumption made in the analyses by Mao et al. [57] was questionable.

4.4.2 Equilibrium Constants

Based on the calculation scheme in Section 4.1, the equilibrium constants of Reactions 4.1 and 4.2 at different temperatures from 298.2 to 310.2 K and pH values between 9.06 and 9.37 are tabulated in **Table 4-3**. There are 4 replicates for each temperature. In order to eliminate experimental error, the outliers were first detected and abandoned using Grubbs' test [147, 148] at the significance level, α, of 0.1. Then the mean value of remaining data at each temperature was used for further analysis. The maximum ratio of standard deviation to corresponding mean was less than 13.6%, and most of the ratios were within 5%. As for equilibrium constant, its order of magnitude is more practical as it is usually presented in terms of logarithm format. It can be seen that K_{NO}^5 has an order of magnitude of 10^{12} and K_{NO}^6 of 10^{13}.

Table 4-3: Equilibrium constants at NO = 605 ppmv, NH_4NO_3 = 2 mol·L^{-1}, A=NH_3

T K	$[Co]_T$ mol·L^{-1}	pH	$[NH_3]$ mol·L^{-1}	$[CoA_5N_2O_2A_5Co]$ mol·L^{-1}	$[CoA_5]$ mol·L^{-1}	$[CoA_6]$ mmol·L^{-1}	a_w	K_6	10^{-12} K_{NO}^5	10^{-13} K_{NO}^6
298.2	0.04	9.35	1.39	1.15E-03	0.0204	7.72	0.98	0.26	3.87	5.89
		9.23	1.06	8.31E-04	0.0198	5.58	0.98		3.01	4.57
	0.05	9.06	0.71	8.98E-04	0.0212	3.89	1.00		2.88	4.50
		9.21	1.01	1.36E-03	0.0241	6.46	0.98		3.37	5.12
304.2	0.04	9.17	1.51	7.21E-04	0.0209	8.03	0.98	0.24	2.78	4.86
		9.21	1.65	6.99E-04	0.0210	8.86	0.98		2.68	4.68
	0.05	9.20	1.61	1.01E-03	0.0261	1.08	0.98		2.53	4.41
309.2	0.04	9.16	2.22	4.99E-04	0.0209	1.18	0.97	0.23	2.19	4.28
	0.05	9.17	2.27	7.17E-04	0.0259	1.50	0.96		2.06	4.03
		9.37	3.59	5.93E-04	0.0222	2.31	0.93		2.15	4.22

It is well-acknowledged that the temperature dependence of chemical reaction equilibrium constant can be described by van't Hoff's equation [149].

$$\frac{dlnK_{NO}^{5}}{dT} = \frac{\Delta H^{5}}{RT^{2}} \tag{4.20}$$

$$\frac{dlnK_{NO}^{6}}{dT} = \frac{\Delta H^{6}}{RT^{2}} \tag{4.21}$$

where ΔH^5 = reaction enthalpy of Reaction 4.1, kJ·mol^{-1};

ΔH^6 = reaction enthalpy of Reaction 4.2, kJ·mol^{-1}.

This expression of temperature dependence has also been accepted by Nymoen et al. [86] who used Fe(II)-EDTA to absorb NO and by Mao et al. [57] for NO control utilizing hexamminecobalt(II) solution. Integration of Eq.s 4.20 and 4.21 gives

$$lnK_{NO}^{5} = -\frac{\Delta H^{5}}{R} \cdot \frac{1}{T} + constant5 \tag{4.22}$$

$$lnK_{NO}^{6} = -\frac{\Delta H^{6}}{R} \cdot \frac{1}{T} + constant6 \tag{4.23}$$

Regression analysis of the experimental data gives the following equilibrium constant equations.

$$lnK_{NO}^{5} = 3598.5 \cdot \frac{1}{T} + 16.759 \qquad (R^2=0.994) \tag{4.24}$$

$$lnK_{NO}^{6} = 1476.4 \cdot \frac{1}{T} + 26.597 \qquad (R^2=0.970) \tag{4.25}$$

They provide values of the standard enthalpy change, $\Delta H^5 = -29.92\ kJ \cdot mol^{-1}$ and $\Delta H^6 = -12.27\ kJ \cdot mol^{-1}$, which means that these two reactions are exothermic in nature. It indicates that high temperatures are not favourable to the removal of NO using ammoniacal cobalt (II) solutions. This is consistent with the experimental findings in our earlier publication [60]. Then the temperature dependence of K_{NO}^{5} and K_{NO}^{6} can be given by

$$K_{NO}^{5} = 1.90 \times 10^{7} \exp(\frac{3598.5}{T}) \tag{4.26}$$

$$K_{NO}^{6} = 3.56 \times 10^{11} \exp(\frac{1476.4}{T}) \tag{4.27}$$

These two equations can be used to calculate the equilibrium constant at certain temperatures between 298.2 and 309.2 K. In literature available to the public, only Mao et al. [57] have measured the equilibrium constant of reaction between NO and hexa-amminecobalt(II) ion in the temperature

interval from 303.2 to 353.2 K at pH = 9.14. Although our experimental setup was similar to theirs, the results were quite different. At the temperature of 303.2 K, for example, the value of K_{NO}^{6} calculated using Eq. 4.27 is 4.63×10^{13} L·mol^{-1} whereas that computed according to Mao et al. [57] would have been 5.16×10^{4} L·mol^{-1}. The main causes of this difference are explained as follows.

Firstly, Mao et al. did not consider the contribution of pentaamminecobalt (II) ion to NO absorption. Nevertheless, the rationality of using the method established by Bjerrum [62] to analyze the compound composition of a solution containing cobalt (II) ions and aqueous ammonia at high concentration ammonium salt has been proven in Section 4.3.1 and by other researchers [36, 61, 63]. Although Mao et al. [57] added ammonium salt (without concentration specified) when preparing the ammoniacal cobalt (II) solutions, they assumed that the end product of ammonical cobalt(II) complexes was hexa-amminecobalt(II) alone. But according to the calculation procedure described in Section 2.4.1, the complex distribution in a solution at pH = 9.14, T = 303.2 K and $[NH_4^+]$ = 2 mol·L^{-1} is tabulated in **Table 4-4**. It can be seen that the largest contributor is pentaamminecobalt (II) ion, which is 53.34%, whereas hexaamminecobalt(II) ion only accounts for 17.60%, even less than 25.61% of tetraamminecobalt (II) ion. Therefore, the assumption made by Mao et al. [57] that the end product was hexaamminecobalt (II) alone seemed problematic; unless otherwise they prepared the absorbent in a different way, which was not explicitly mentioned.

Table 4-4: Cobalt(II) -ammonia system at pH=9.14, T = 303.2 K and $[NH_4^+]$ = 2 mol·L^{-1}

Co^{2+}	$Co(NH_3)^{2+}$	$Co(NH_3)_2^{2+}$	$Co(NH_3)_3^{2+}$	$Co(NH_3)_4^{2+}$	$Co(NH_3)_5^{2+}$	$Co(NH_3)_6^{2+}$
0	0	0.21%	3.24%	25.61%	53.34%	17.60%

Secondly, the molecular structure of generated nitrosyl proposed by them is different from that in this study. They considered the product of reaction between hexamminecobalt (II) ion and NO as a monomer, $[Co(NH_3)_5NO]^{2+}$ in the following Eq. 4.28, while we believe that the nitrosyl is more likely to be a the μ-hyponitrite dicobalt complex with a formula of $[(NH_3)_5Co(NO)_2Co(NH_3)_5]^{4+}$ in Eq. 4.2

$$Co(NH_3)_6^{2+} + NO \rightleftharpoons [(NH_3)_5Co(NO)]^{2+} + NH_3 \qquad (4.28)$$

Actually the nitrosyl is more likely to be a μ-hyponitrite dicobalt complex with a formula of $[(NH_3)_5Co(NO)_2Co(NH_3)_5]^{4+}$ according to Eq. 4.2. As mentioned above, high temperature (room temperature or above) favours the formation of red series nitrosyl compound [68, 70]. It was also observed in this study as shown in **Figure 4-7** (b). Many previous investigations proved the molecular

structure of red series as μ-hyponitrite dimeric formulation $[(NH_3)_5Co(NO)_2Co(NH_3)_5]^{4+}$ from various aspects. Feltham [74] reported the red salt was a 4:1 electrolyte in the form of $[(NH_3)_5Co(NO)_2Co(NH_3)_5]X_4$ by conductivity measurement. Mercer et al. [77] stated that a dimeric structure had been definitely assigned to the red isomer through infrared and chemical investigation. The crystal structure study conducted by Hoskins et al. [78, 80] showed that the red nitrosyl ion was binuclear: the two crystallographically independent cobalt atoms, each surrounded by five ammonia molecules, were bridged asymmetrically through a hyponitrite ion. Raynor [83] determined the red nitrosylpentaammines of cobalt as $[(NH_3)_5Co(NO)_2Co(NH_3)_5]^{4+}$ with a trans hyponitrite bridging group and metal-nitrogen bond from infrared evidence. Chacon Villalba et al. [82] also confirmed by X-ray diffraction methods that the red nitrosyl compound as $[(NH_3)_5Co(NO)_2Co(NH_3)_5]^{4+}$. Hence, the square of $[NO]_e$ is present in the denominator in this study instead of $[NO]_e$. As $[NO]_e$ is in the order of 10^{-7} mol·L^{-1}, making the result in the order of 10^{13} instead of 10^4.

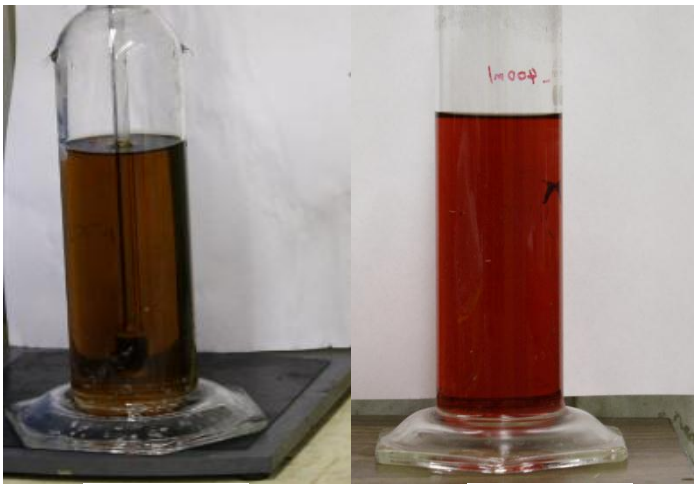

(a) (b)

Figure 4-7: Colors of aqueous absorbent (a) fresh absorbent (b) used absorbent

In addition, the omission of temperature dependence upon Henry's constant as shown in Eq. 4.8 and the negligence of effect of ionic strength on NO solubility as described in Eq. 4.9 might also lead to difference.

Although this thesis work gave acceptable results regarding equilibrium constants of reactions between NO and ammoniacal cobalt (II) complexes, the accuracy could be further enhanced by directly measuring corresponding concentrations at equilibrium with a liquid-phase Fourier transform

infrared spectroscopy (FTIR). It may reduce uncertainties caused by the empirical constants adopted in the concentration calculation scheme.

4.5 Uncertainty Analysis

Due to the complexity of this experimental system, only general uncertainty analysis which contains only propagation of bias errors will be elaborated for this section. In general, a data reduction equation as described in Eq. 4.29 for the determination of experimental result, r, from N measured variables X_i is needed before doing an uncertainty analysis.

$$r = r(X_1, X_2, \dots X_N) \tag{4.29}$$

Then the uncertainty in the result is given by Eq. 4.30 [131, 132],

$$U_r{}^2 = (\frac{\partial r}{\partial X_1} U_{X_1})^2 + (\frac{\partial r}{\partial X_2} U_{X_2})^2 + \cdots + (\frac{\partial r}{\partial X_N} U_{X_N})^2 \tag{4.30}$$

where U_r = the uncertainty in the experimental result;

U_{X_i} = the uncertainty in the measured variable X_i.

Dividing both sides of Eq. 4.30 by the square of the experimental result, r, gives,

$$(\frac{U_r}{r})^2 = (\frac{1}{r}\frac{\partial r}{\partial X_1} U_{X_1})^2 + (\frac{1}{r}\frac{\partial r}{\partial X_2} U_{X_2})^2 + \cdots + (\frac{1}{r}\frac{\partial r}{\partial X_N} U_{X_N})^2 \tag{4.31}$$

Specifically, the uncertainty of $K_{NO}{}^5$ described in Eq. 4.4 can be presented in Eq. 4.32, in which A denotes $[(NH_3)_5Co(N_2O_2)Co(NH_3)_5{}^{4+}]_e$ and B denotes $[Co(NH_3)_5(H_2O)^{2+}]_e$ for ease of presentation.

$$(\frac{U_{K_{NO}^5}}{K_{NO}^5})^2 = (\frac{U_A}{A})^2 + 4(\frac{U_{a_w}}{a_w})^2 + 4(\frac{U_B}{B})^2 + 4(\frac{U_{[NO]_e}}{[NO]_e})^2 \tag{4.32}$$

It can be seen from the RHS of Eq. 4.32 that the uncertainties of A, a_w, B and $[NO]_e$ are needed. a_w is the value of water activity experimentally given by Bjerrum [62]; however, information of its uncertainty is unavailable. It is well-accepted that a reasonable assumption can be taken if an uncertainty in quantity is unknown and/or unachievable. In the case where multiple uncertainties in quantities are unobtainable, it is natural and universal to assign the same value to all unknown uncertainties if possible [131]. The uncertainty in a_w is set to be a variable α% herein, and all the unknown uncertainties hereafter in this chapter will be assumed to be α% for simplicity.

4.5.1 Uncertainty in $[NO]_e$

The uncertainty in $[NO]_e$ presented in Eq. 4.14 can be given by

$$\left(\frac{U_{[NO]_e}}{[NO]_e}\right)^2 = \left(\frac{U_{P_T}}{P_T}\right)^2 + \left(\frac{U_{y_{in}}}{y_{in}}\right)^2 + \left(\frac{U_H}{H}\right)^2 \tag{4.33}$$

The uncertainty in total pressure $P_{T,}$ which is atmospheric pressure, can be assumed zero. The uncertainty in y_{in} of 2% was given by the gas supplier, Praxair Inc. Uncertainty in H is derived as follows.

Rewriting Eq. 4.13 gives,

$$H = H_w 10^{k_1 I_1 + k_2 I_2} \tag{4.34}$$

Then the uncertainty in H is described in the following equation.

$$\left(\frac{U_H}{H}\right)^2 = \left(\frac{U_{H_w}}{H_w}\right)^2 + 5.3(I_1 U_{k_1})^2 + 5.3(k_1 U_{I_1})^2 + 5.3(I_2 U_{k_2})^2 + 5.3(k_2 U_{I_2})^2 \tag{4.35}$$

Eq. 4.35 shows that the uncertainty in H depends not only on the uncertainties on H_w, k_1, I_1, k_2 and I_2, but also on the values of k_1, I_1, k_2 and I_2. According to **Table 4-1** and Eq. 4.11, k values for NH_4NO_3 and $Co(NO_3)_2$ are 0.0668 and 0.0871, respectively.

Propagation of the uncertainty in salting-out parameters to k described in Eq. 4.11 is expressed as

$$(U_k)^2 = (U_{x_c})^2 + (U_{x_a})^2 + (U_{x_G})^2 \tag{4.36}$$

Values of x_c, x_a, and x_G are available in literature without uncertainty; it is assumed again that $\left(\frac{U_{x_c}}{x_c}\right) = \left(\frac{U_{x_a}}{x_a}\right) = \left(\frac{U_{x_G}}{x_G}\right) = \alpha\%$ for further calculation.

Based on the definition of ionic strength in Eq. 4.10, the valence of ion for a given electrolyte solution is constant with an uncertainty of zero. Substituting the value of ion valence gives the solution to Eqs. 4.37 and 4.38 for NH_4NO_3 and $Co(NO_3)_2$, respectively. For simplicity, define the subscripts of 1= NH_4NO_3 and 2 = $Co(NO_3)_2$.

$$I_1 = c_1 \tag{4.37}$$

$$I_2 = 3c_2 \tag{4.38}$$

Thus,

$$(\frac{U_{I_1}}{I_1})^2 = (\frac{U_{c_1}}{c_1})^2 \tag{4.39}$$

$$(\frac{U_{I_2}}{I_2})^2 = (\frac{U_{c_2}}{c_2})^2 \tag{4.40}$$

As the concentrations of NH_4NO_3 and $Co(NO_3)_2$ are calculated from measured compound mass by balance and solution volume by

$$c = \frac{m}{MV_L} \tag{4.41}$$

Propagation of uncertainties in m, M and V to concentration can be written as

$$(\frac{U_c}{c})^2 = (\frac{U_m}{m})^2 + (\frac{U_M}{M})^2 + (\frac{U_{V_L}}{V_L})^2 \tag{4.42}$$

The repeatability of ±0.02 g is provided by Denver Instrument Inc. to the top-loading balance for weighing of NH_4NO_3. And a repeatability of ±0.0002 g is also provided by the manufacturer to the analytical balance for weighing of $Co(NO_3)_2 \cdot 6H_2O$. They can be taken as reasonable estimates of the uncertainty. All the glassware is from Corning Inc., and 5% is given as the bias limit of the volume. It is noted that the values of universal constants such as molecular weight, gas constant, etc. are known with a much greater accuracy than the measurements made in most experiments. So it is justifiable to assume the uncertainties in such quantities are negligible and to set them as zero. Assuming that U_M is zero and substituting it into Eq. 4.42 gives,

$$(\frac{U_c}{c})^2 = (\frac{U_m}{m})^2 + (\frac{U_{V_L}}{V_L})^2 \tag{4.43}$$

U_{Hw} is needed to determine U_H. The temperature dependence on Henry's Law constant of gas into water can be expressed as [144]

$$H_w = C_1 \exp(-C_2 \left(\frac{1}{T} - \frac{1}{298.15}\right)) \tag{4.44}$$

It can be seen from Eq. 4.8 that C_1 = 526.32 and C_2 = 1400 for NO. The uncertainties of these two empirical constants are unknown and assumed to be α% too. Then the uncertainty of H_w can be described in Eq. 4.45.

$$(\frac{U_{H_w}}{H_w})^2 = (\frac{U_{C_1}}{C_1})^2 + [(\frac{1}{298.15} - \frac{1}{T})U_{C_2}]^2 + (C_2 T^{-2} U_T)^2 \tag{4.45}$$

Although there is no information available on the calibration of thermometer, a comparison between the readings of the thermometer and a calibrated thermal couple shows a difference less than 0.5 ^{o}C. In the absence of any other information, it is assumed that U_T = 0.5 ^{o}C (or K).

4.5.2 Uncertainty in $[(NH_3)_5Co(N_2O_2)Co(NH_3)_5^{4+}]_e$

The data reduction expression of $[(NH_3)_5Co(N_2O_2)Co(NH_3)_5^{4+}]_e$ as shown in Eq. 4.18 is very complex due to the presence of the integral item. The partial derivative with respect to η is difficult to obtain. In practice, the calculation of the integral item is graphically solved by using trapezoid method. The time for the reaction to reach equilibrium is discretized into grids with interval of 2 seconds (which is the sampling interval). Then Eq. 4.18 can be numerically rewritten as in Eq. 4.46, in which A = $[(NH_3)_5Co(N_2O_2)Co(NH_3)_5^{4+}]_e$ for ease of presentation.

$$A = \frac{1}{2}\left\{\frac{G_m y_{in}}{V_L}\left(\sum_{i=1}^{N}\frac{1}{2}(\eta_i + \eta_{i+1})\Delta t\right) - [NO]_e\right\} \; where \; N = \frac{t_e}{\Delta t} \tag{4.46}$$

Rearranging and combining terms give

$$A = \frac{1}{2}\left\{\frac{G_m y_{in}\Delta t}{2V_L}(\eta_1 + 2\eta_2 + \cdots + 2\eta_N + \eta_{N+1}) - [NO]_e\right\} \; where \; N = \frac{t_e}{\Delta t} \tag{4.47}$$

Further simplification of Eq. 4.47 is performed by neglecting $[NO]_e$ as the value of $[NO]_e$ is much less than the first item in the bracket. Besides, in the calculation Δt is equal to 2 s, which is a constant. So the uncertainty of time interval Δt is zero. The data reduction expression of A then becomes

$$A = \frac{G_m y_{in}}{2V_L}(\eta_1 + 2\eta_2 + \cdots + 2\eta_N + \eta_{N+1}) \; where \; N = \frac{t_e}{2} \tag{4.48}$$

The propagation of uncertainties in quantities in the RHS of Eq. 4.47 to A is then described as

$$(\frac{U_A}{A})^2 = (\frac{U_{G_m}}{G_m})^2 + (\frac{U_{y_{in}}}{y_{in}})^2 + (\frac{U_{V_L}}{V_L})^2 + (\frac{U_{\eta_1} + 2U_{\eta_2} + \cdots + 2U_{\eta_N} + U_{\eta_{N+1}}}{\eta_1 + 2\eta_2 + \cdots + 2\eta_N + \eta_{N+1}})^2 \tag{4.49}$$

As mentioned above, $\frac{U_{y_{in}}}{y_{in}} = 2\%$ is provided by Praxair, and $\frac{U_{V_L}}{V_L} = 5\%$ by Corning Inc.

The uncertainty in G_m is computed based on Eq. 4.16,

$$(\frac{U_{G_m}}{G_m})^2 = (\frac{U_{Q_G}}{Q_G})^2 + (\frac{U_{P_T}}{P_T})^2 + (\frac{U_R}{R})^2 + (\frac{U_T}{T})^2 \tag{4.50}$$

It is well-acknowledged that quantities like atmospheric pressure and gas constant is quite accurate, and their uncertainties can be assumed to be zero. Then Eq. 4.50 further transforms into

$$(\frac{U_{G_m}}{G_m})^2 = (\frac{U_{Q_G}}{Q_G})^2 + (\frac{U_T}{T})^2 \quad (4.51)$$

According to product specifications given by manufacturers, the uncertainty in Q_G is 1.5% of full scale. Recall that U_T = 0.5 ^oC. The uncertainty in NO removal efficiency η is calculated by propagation of uncertainties in y_{in} and y_{out} as shown in following equation.

$$(U_\eta)^2 = (y_{out} y_{in}^{-2} U_{y_{in}})^2 + (-\frac{1}{y_{in}} U_{y_{out}})^2 \quad (4.52)$$

where $\frac{U_{y_{in}}}{y_{in}} = 2\%$, and $U_{y_{out}}$ is 0.5 % of full scale provided by CAI Inc.

4.5.3 Uncertainty in $[Co(NH_3)_5(H_2O)^{2+}]_e$

According to Eqs. 2.10 -2.15, the data reduction equation of $[Co(NH_3)_5(H_2O)^{2+}]_e$ is presented as

$$[Co(NH_3)_5(H_2O)^{2+}]_e = K_1K_2K_3K_4K_5 \cdot [NH_3]^5 \cdot (\frac{f_{NH_3}}{a_w})^5 \cdot [Co(H_2O)_6{}^{2+}] \quad (4.53)$$

The uncertainty in $[Co(NH_3)_5(H_2O)^{2+}]_e$ is then given by following equation where B = $[Co(NH_3)_5(H_2O)^{2+}]_e$.

$$(\frac{U_B}{B})^2 = (\frac{U_{K_1}}{K_1})^2 + (\frac{U_{K_2}}{K_2})^2 + (\frac{U_{K_3}}{K_3})^2 + (\frac{U_{K_4}}{K_4})^2 + (\frac{U_{K_5}}{K_5})^2 + 25(\frac{U_{[NH_3]}}{[NH_3]})^2 + 25(\frac{U_{f_{NH_3}}}{f_{NH_3}})^2 + 25(\frac{U_{a_w}}{a_w})^2 + (\frac{U_{[Co(H_2O)_6{}^{2+}]}}{[Co(H_2O)_6{}^{2+}]})^2 \quad (4.54)$$

Since there is no information on uncertainties in empirical constants K_1, K_2, K_3, K_4, K_5, f_{NH3} and a_w, it is assumed that $\frac{U_{K_1}}{K_1} = \frac{U_{K_2}}{K_2} = \frac{U_{K_3}}{K_3} = \frac{U_{K_4}}{K_4} = \frac{U_{K_5}}{K_5} = \frac{U_{f_{NH_3}}}{f_{NH_3}} = \frac{U_{a_w}}{a_w} = \alpha\%$.

Rewriting Eq. 2.17 to gives the data reduction expression for $[NH_3]$.

$$[NH_3] = \frac{k_{NH_4{}^+} \cdot [NH_4{}^+]}{[H^+]} \quad (4.55)$$

Thus, the corresponding uncertainty in $[NH_3]$ is shown as follows.

$$(\frac{U_{[NH_3]}}{[NH_3]})^2 = (\frac{U_{k_{NH_4{}^+}}}{k_{NH_4{}^+}})^2 + (\frac{U_{[NH_4{}^+]}}{[NH_4{}^+]})^2 + (\frac{U_{[H^+]}}{[H^+]})^2 \quad (4.56)$$

As usual, assumption of $\frac{U_{k_{NH_4{}^+}}}{k_{NH_4{}^+}} = \alpha\%$ is made, and $\frac{U_{[NH_4{}^+]}}{[NH_4{}^+]}$ is calculated by using Eq. 4.43.

The concentration of hydrogen ion in the aqueous solution is calculated by using pH value that is measured by a pH meter in the following equation.

$$[H^+] = 10^{-pH} \tag{4.57}$$

Hence, the uncertainty in $[H^+]$ is described as

$$(\frac{U_{[H^+]}}{[H^+]})^2 = (-ln10 \cdot U_{pH})^2 \tag{4.58}$$

The specification of the pH meter (Model pH-700) gives $U_{pH} = 0.01$.

From Eq. 4.54 one can see that the uncertainty in B necessitates the knowledge of uncertainty in $[Co(H_2O)_6{}^{2+}]$. The achievement of the data reduction expression for $[Co(H_2O)_6{}^{2+}]$ is summarized as follows. According to mass balance of Co^{2+},

$$\begin{aligned}[Co^{2+}]_T = \left[Co(H_2O)_6{}^{2+}\right] + \sum_{i=1}^{6}\left[Co(NH_3)_i(H_2O)_{6-i}{}^{2+}\right] \\ + 2[(NH_3)_5Co(N_2O_2)Co(NH_3)_5{}^{4+}]_e\end{aligned} \tag{4.59}$$

As defined in Eqs. 2.10 – 2.15, the concentration of different ammoniacal cobalt(II) complex is a function of $[Co(H_2O)_6{}^{2+}]$ and

$$\left[Co(NH_3)_i(H_2O)_{6-i}{}^{2+}\right] = \prod_{j=1}^{i} K_j \cdot [NH_3]^i \cdot \left(\frac{f_{NH_3}}{a_w}\right)^i \cdot \left[Co(H_2O)_6{}^{2+}\right], (i = 1-6) \tag{4.60}$$

Substituting Eq. 4.60 into Eq. 4.59 gives the data reduction expression of $[Co(H_2O)_6{}^{2+}]$.

$$\left[Co(H_2O)_6{}^{2+}\right] = \frac{[Co^{2+}]_T - 2A}{\beta} \tag{4.61}$$

where

$$A = [(NH_3)_5Co(N_2O_2)Co(NH_3)_5{}^{4+}]_e \tag{4.62}$$

$$\beta = 1 + \sum_{i=1}^{6}\left\{\prod_{j=1}^{i} K_j \cdot [NH_3]^i \cdot (\frac{f_{NH_3}}{a_w})^i\right\} \tag{4.63}$$

The uncertainty in $[Co(H_2O)_6{}^{2+}]$ is then described as

$$\left(\frac{U_{\left[Co(H_2O)_6{}^{2+}\right]}}{\left[Co(H_2O)_6{}^{2+}\right]}\right)^2 = \left(\frac{U_{[Co^{2+}]_T}}{[Co^{2+}]_T - 2A}\right)^2 + 4\left(\frac{U_A}{[Co^{2+}]_T - 2A}\right)^2 + \left(\frac{U_\beta}{\beta}\right)^2 \qquad (4.64)$$

The uncertainty in $[Co^{2+}]_T$ can be estimated by Eq. 4.43, and that in A has already been elaborated in Section 4.5.2. It is shown that data reduction expression of quantity β is very complex, and the task of obtaining the partial derivatives in Eq. 4.62 is tedious. In order to continue the uncertainty analysis of the equilibrium constant, it is assumed $\left(\frac{U_\beta}{\beta}\right) = 2\alpha\ \%$ to avoid the time consuming calculations. This simplification will then be validated by examining the sensitivity of $\left(\frac{U_\beta}{\beta}\right)$ to ultimate $\left(\frac{U_{K_{NO}^5}}{K_{NO}^5}\right)$. Eventually all the unknown variables in Eq. 4.32 can be determined.

As an example, **Figure 4-8** shows the uncertainties in measured equilibrium constant of Reaction 4.1, $K_{NO}{}^5$, with different assumed α values at T = 298.2 K, $[Co^{2+}]_T$ = 0.04 mol·L^{-1} and pH = 9.23. It can be seen that $\frac{U_{K_{NO}^5}}{K_{NO}^5}$ greatly depends on the assumed uncertainty in empirical constant, α%. The smallest $\frac{U_{K_{NO}^5}}{K_{NO}^5}$ of 57.3% is given at α=0 under which none of the empirical coefficients contributes to the ultimate uncertainty in $K_{NO}{}^5$. As α value increases from 0 to 6%, the uncertainty in $K_{NO}{}^5$, $\frac{U_{K_{NO}^5}}{K_{NO}^5}$, rapidly rises from 57.3 to 126.9 %. The sensitivity of $\frac{U_\beta}{\beta}$ to $\frac{U_{K_{NO}^5}}{K_{NO}^5}$ at α = 2% is summarized in **Table 4-5**. The uncertainty in $K_{NO}{}^5$ slightly rises from 68.2% to 71.0% with the uncertainty in β increasing from 2 % (= α) to 10% (= 5α). Therefore, it can be concluded that the effect of $\frac{U_\beta}{\beta}$ on $\frac{U_{K_{NO}^5}}{K_{NO}^5}$ is insignificant, which justify the assumption of $\frac{U_\beta}{\beta} = 2\alpha$.

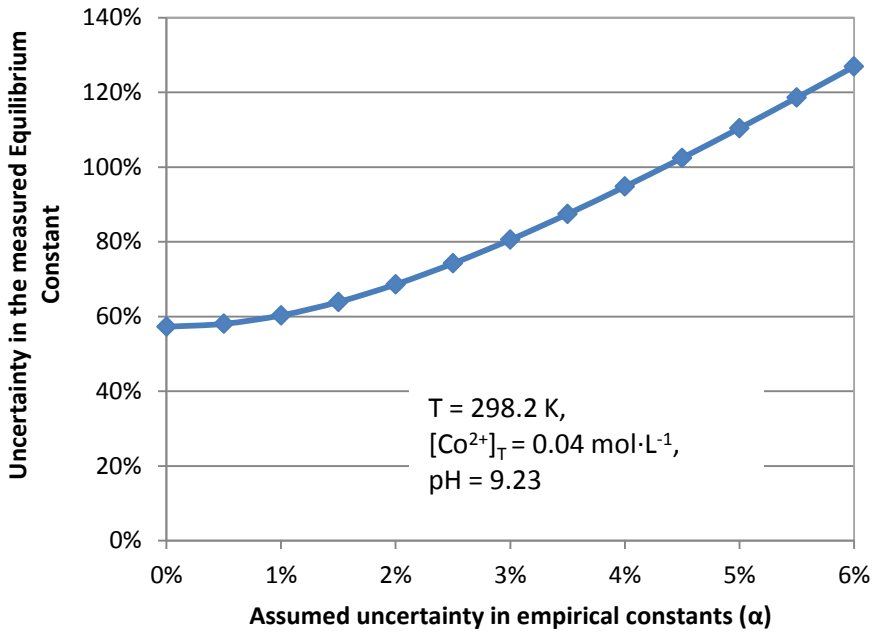

Figure 4-8: Uncertainties in measured equilibrium constant K_{NO}^{5} with different α values

Table 4-5: Uncertainties in measured K_{NO}^{5} with different (U_β/β) values at α = 2%

$\frac{U_\beta}{\beta}$	$\frac{U_{K_{NO}^5}}{K_{NO}^5}$
2%	68.2%
3%	68.4%
4%	68.6%
5%	68.8%
6%	69.2%
7%	69.5%
8%	70.0%
9%	70.5%
10%	71.0%

4.6 Summary

The analysis of cobalt (II) – ammonia system for solutions containing cobalt (II) nitrate, ammonium hydroxide and 2 $mol \cdot L^{-1}$ ammonium nitrate was reviewed. The characteristics of reactions between nitric oxide and ammoniacal cobalt (II) complexes were analyzed through the molecular structure of corresponding nitrosyl. It was validated that only penta- and hexa-amminecobalt (II) complexes had

the ability to react with NO as shown in Reactions 4.1 and 4.2. Moreover, the equilibrium constants of such reactions were determined. K_{NO}^{5} was in the order of magnitude of 10^{12} and K_{NO}^{6} of 10^{13}. All experimental data fitted Eqs. 4.26 and 4.27 well.

With equilibrium constants of reactions between NO and ammoniacal cobalt(II) solutions given by this chapter, the absorption capacity of this absorbent can be estimated. However, the knowledge of NO absorption rate could not be determined without related reaction rate constants. Therefore, the kinetic study of NO absorption into ammoniacal cobalt(II) solutions is conducted and this is the topic of the next chapter.

Chapter 5
Kinetic Study

5.1 Introduction

In this chapter, the kinetics of NO absorption into ammonicacal cobalt(II) solutions was investigated by using the enhancement factor, E, which is the ratio of NO absorption rate with chemical reaction to pure physical absorption rate. The reactions between nitric oxide and ammoniacal cobaltous solvents took place in a home-made double-stirred tank that was commonly utilized in gas absorption kinetics. The operating conditions were as follows. All experimentations were conducted at temperatures between 298.2 and 303.2 K because parameters for cobalt(II) – ammonia system analysis were only available in the temperature interval from 295.2 and 303.2 K and for ammonium nitrate concentrations up to 2 $mol \cdot L^{-1}$. Also, Yu et al. [60] reported that low temperature favored the NO absorption, making it less useful to perform experiments at temperatures higher than 303.2 K. The ammonium nitrate concentration was 2 $mol \cdot L^{-1}$ for all experimentations. As two parallel reactions exist due to the presence of penta- and hexa-amminecobalt(II) ions, two runs with different liquid compositions, which were dependent upon pH values, were necessitated at each temperature. In this work, one was performed at pH of 8.5 under which reactive agent was almost pentaamminecobalt(II) complex only. Nevertheless, the pH value of 12 at which 100% of hexaamminecoablt(II) ion occurred in the solution was too high to achieve and maintain. Instead, a pH value nearly 9.8 where both penta- and hexa-amminecobalt(II) solvents constitute approximately 50% was utilized. In order to maintain excessive absorbent compared to NO concentration, the cobalt(II) nitrate was 0.075 $mol \cdot L^{-1}$ at low pH value while 0.025 $mol \cdot L^{-1}$ at high pH value. Four gas streams with concentrations from 400 to 1400 ppmv were fed at 2.6 $L \cdot min^{-1}$ per pH value per temperature to determine the reaction order with respect to NO. The reaction rate constants of the two key reactions were determined to be 6.43×10^{6} and 1.00×10^{7} $L \cdot mol^{-1} \cdot s^{-1}$, respectively at 298.2 K, and increase to 7.57×10^{6} and 1.12×10^{7} $L \cdot mol^{-1} \cdot s^{-1}$, respectively at 303.2 K. Uncertainty analyses were also conducted for the results.

5.2 Experimental

A continuous water purification system (Model S-99253-10) from Thermo Scientific Inc. was used to produce deionized water. Because cobalt(II) complexes react with oxygen, the key to a successful preparation was to establish an oxygen-free condition. Therefore, deionized water was degassed by pure nitrogen (Grade 4.8 from Praxair Inc.) for about 30 min before use. As the oxidation rates of

cobaltous complexes was relatively slow without catalysts such as activated carbon, it was assumed that the oxidation of cobalt(II) complexes was negligible in a short period [60]. The cobalt(II) – ammonia system was prepared in a 500 mL flask by step reversible reactions between cobalt(II) nitrate hexahydrate ($Co(NO_3)_2 \cdot 6H_2O$, ACS reagent) and aqueous ammonia ($NH_3 \cdot H_2O$, ACS reagent, 28-30% NH_3 basis) with the addition of 2 $mol \cdot L^{-1}$ ammonium nitrate (NH_4NO_3, ACS reagent); it was used to form $NH_4NO_3/NH_3 \cdot H_2O$ buffer solution to ensure a ready supply of NH_3 ligand while avoiding the formation of hydroxide and the precipitation of cobalt hydroxide. All the chemicals mentioned in this Chapter were bought from Sigma-Aldrich Co. LLC. Certain amount of $Co(NO_3)_2 \cdot 6H_2O$ and NH_4NO_3 were weighed by an analytical balance with readability of 0.0001 g (Model RK-11422-01 from Denver Instrument Inc.) and a top-loading balance with readability of 0.01 g (Model RK-11421-93 from Denver Instrument Inc.), respectively, and dissolved in the 500 mL flask placed on a stirring hot plate (Model SP142025Q from Thermo Scientific Cimarec Inc.) by deionized water to around 100mL. The pH values of the liquids were measured by a benchtop pH meter with an accuracy of ± 0.01 (Model pH 700) manufactured by Oakton. The reading was taken under mild magnetic stirring. Aqueous ammonia was added to make a pH value slightly above the desired value. Then water was added to dilute or ammonia was added to concentrate alternatively until the solution ends up with 500 mL volume of desired pH value of 8.5 or 9.8.

The prepared solution was then transferred to a home-made double stirred tank reactor as illustrated in **Figure 5-1**. **Figure 5-2** was the picture of the home-made double stirred tank reactor and its support frame. The reactor was a vessel of 99.72 mm I.D. with an outer jacket of 152.4 mm I.D. through which temperatures were regulated. Four baffles of 9.5 mm width were equipped in the reactor to ensure a flat surface when rotating. Both stirrers were paddle-type impellers. The gas-phase stirrer was a 4-straight flat impeller with a diameter of 54.0 mm, and the liquid-phase stirrer an 8-straight flat impeller with a diameter of 38.1 mm. The reactor was sealed with TFE seals in order to avoid possible corrosion caused by the solvent. The top and bottom shafts were driven by two mixers bought from IKA Corp (Model RK-50705-00). Two love-joy couplings were employed to cope with vibration. The concentration of total cobalt (II) was either 0.025 or 0.075 $mol \cdot L^{-1}$.

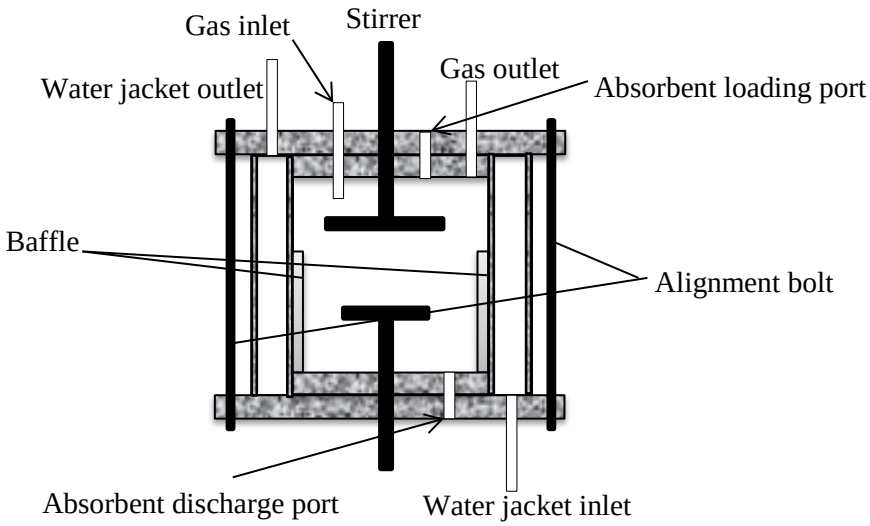

Figure 5-1: Schematic diagram of the double-stirred tank

Figure 5-2: Picture of the double stirred tank reactor

Figure 5-3 is the experimental setup for the kinetic study of reactions between nitric oxide and ammoniacal cobalt(II) solutions. The operation was performed continuously with respect to the gas phase and batch-wise with respect to the liquid phase. All gases were purchased from Praxair Inc. The compressed air cylinder was of grade zero for ozone generation. The nitrogen cylinder was of grade 4.8 and nitric oxide cylinder contained 2.54% balanced nitrogen. Deliver pressure of each cylinder was relieved by a regulator before entering the process line. A certain gas mixture was synthesized by regulating flow rates of different gases using gas mass flow controllers from Cole-Parmer. The body of the nitrogen mass controller (Model S-32648-16) was made of aluminum; mass flow meters for corrosive nitric oxide (Model S-32648-58) and active oxygen (Model S-32649-60) were made of 316 stainless steel. Their accuracy was ±1.5% full-scale. Ranges of flow meters for NO and N_2 were 200 $mL \cdot min^{-1}$ and 5 $L \cdot min^{-1}$, respectively. Each flow controller was regulated by a bellows-sealed metering valve (Model SS-4BMG) purchased from Swagelok Inc. A 316 stainless steel in-line pipe mixer (Model RK-04669-05) bought from Koflo Inc. was employed to produce a completely mixed output of the simulated flue gas. The effectiveness of this flue gas synthesis system was first validated through comparison between calculated and measured NO concentrations prior to further experimentations. Then simulated flue gas streams with NO concentrations ranged from 400 to 1400 ppmv were fed at a flow rate of approximately 2.60 $L \cdot min^{-1}$.

Downstream the mixer was a 3-way valve, which could be switched between by-pass and gas feeding. The nitrosyl formation reactions took place in the double-stirred tank reactor as mentioned above. As time spent for data collection in this kinetics experiment was around 3 minutes, the impact of volatilization of ammonia was insignificant and could be ignored; therefore, there was no absorbing bottle after the tank reactor. NO concentrations at both inlet and outlet were measured by a gas analyzer (Model CAI 650 NOXYGEN with range of 3000 ppmv and repeatability of around 0.5% of full scale) from California Analytical Instruments Inc. It is noteworthy that the inlet NO concentration was determined by measuring the bypass with the gas analyzer for 5 minutes before switching to the reactor because no flow rate change was found before and after switching. Since the CAI 650 NOXYGEN analyzer could only work properly under atmospheric pressure, a "Tee" conjunction was added for pressure relief at a flow rate of around 1 $L \cdot min^{-1}$. The analyzer still needed an extra air or oxygen supply for ozone generation. A data logger was used to collect data every 2 seconds. The operation normally lasted for 3-5 minutes after the reading of outlet concentration was stabilized. At this moment, the final pH value of used solvent was measured by the same pH meter again. The picture of actual laboratorial setup for kinetic study is shown in **Figure 5-4**.

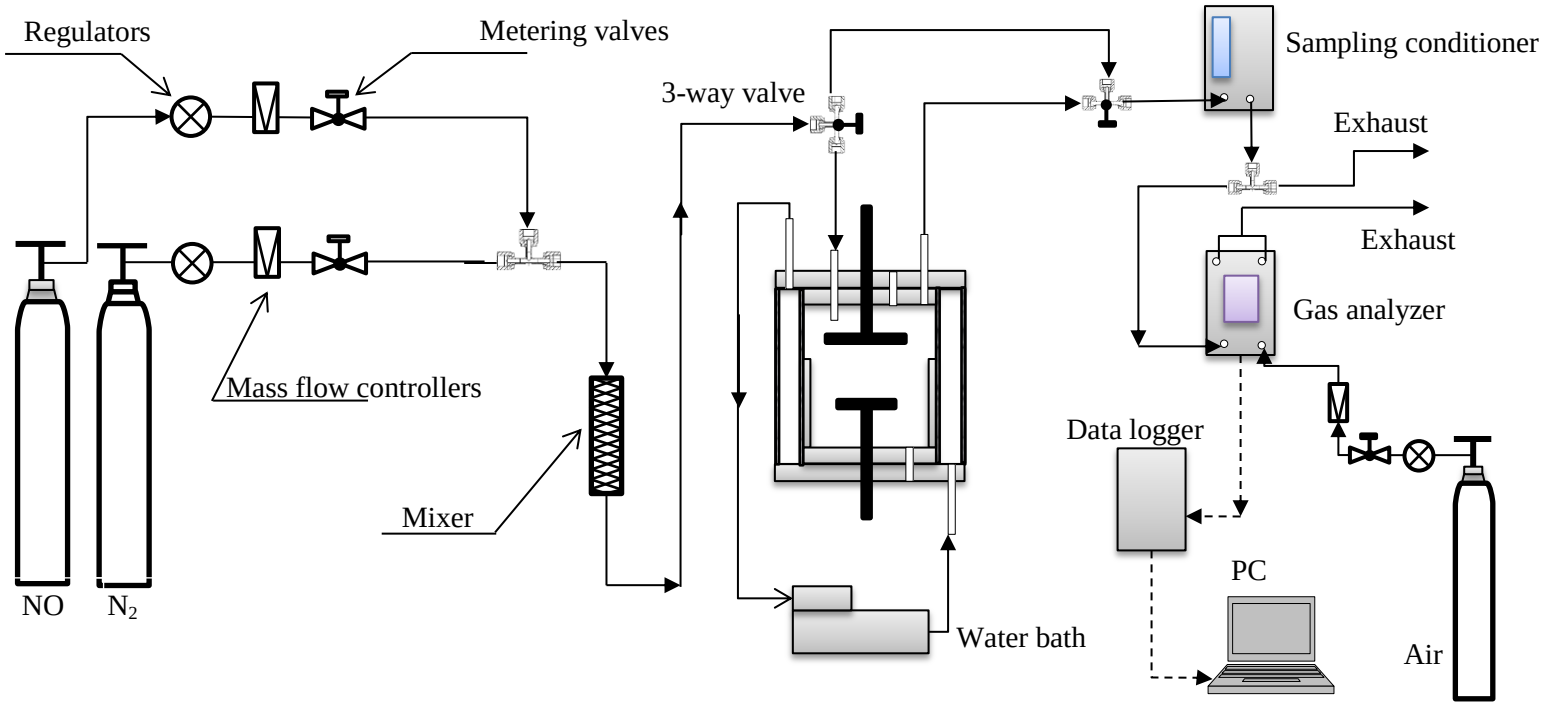

Figure 5-3: Laboratorial setup for the measurement of equilibrium constants

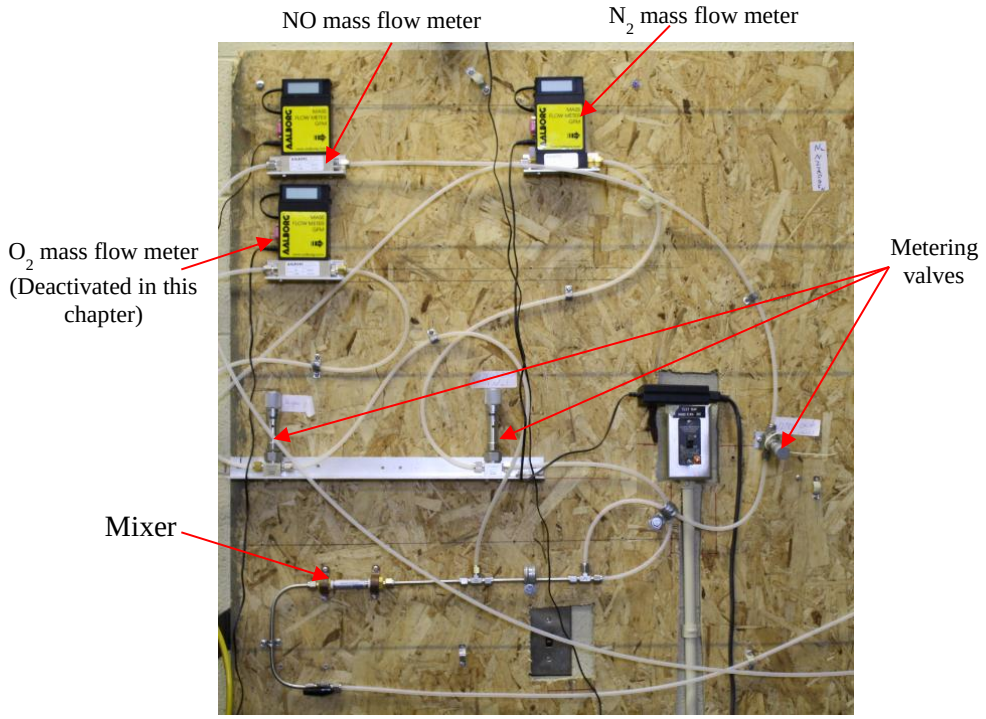

(a) flue gas simulation system

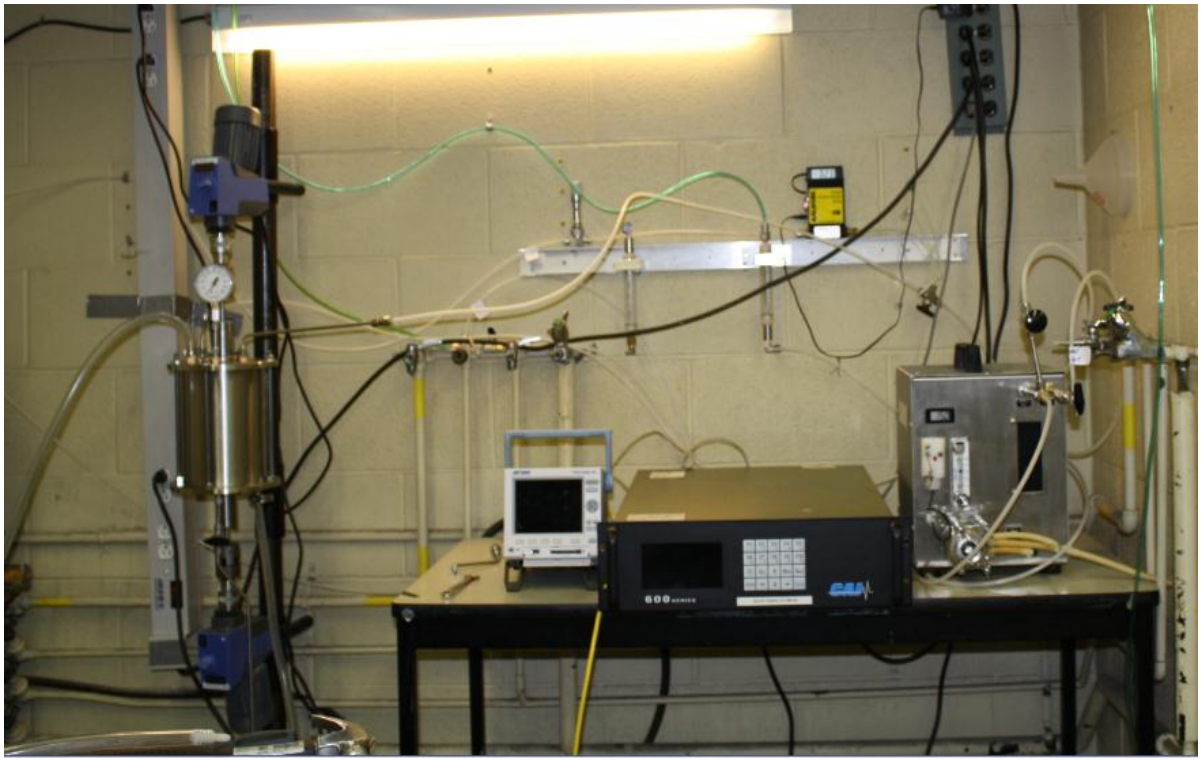

(b) double stirred tank section

Figure 5-4: Picture of actual laboratorial setup for kinetic study

According to mass balance and the ideal gas law, the corresponding NO absorption rate into ammoniacal cobalt(II) solutions is

$$N_{NO} = \frac{Q_G P_T}{RTS_A}(y_{in} - y_{out}) \quad (5.1)$$

where N_{NO} = NO absorption rate into ammoniacal cobalt(II) solutions, $mol \cdot m^{-2} \cdot s^{-1}$;

P_T = total pressure, atm;

Q_G = volumetric flue gas flow rate, $m^3 \cdot s^{-1}$;

R = gas constant, = 0.08205 $L \cdot atm \cdot K^{-1} \cdot mol^{-1}$;

S_A = cross-sectional area of the double-stirred reactor, m^2;

T = temperature, K;

y_{in}, y_{out} = NO concentrations at inlet and outlet, respectively, ppmv.

This measured NO absorption rate was used for the calculation of reaction rate constant as follows.

5.3 Calculation

For the ease of presentation, it is necessary to recall the reactions between NO and penta- and hexa-amminecobalt(II) ions, as described in Reactions 5.2 and 5.3.

$$2NO + 2[Co(NH_3)_5]^{2+} \rightleftharpoons [Co(NH_3)_5N_2O_2(NH_3)_5Co]^{4+} \quad (5.2)$$

$$2NO + 2[Co(NH_3)_6]^{2+} \rightleftharpoons [Co(NH_3)_5N_2O_2(NH_3)_5Co]^{4+} + 2NH_3 \quad (5.3)$$

Again the establishment of ammonia – cobalt(II) system can be executed following the procedure presented in Section 2.4.1. In Section 2.6, the pseudo mth- and p-th order rate constants, k_{mn} and k_{pq}, of Reactions 5.2 and 5.3 can be determined with the combination of Eqs. 2.23, 2.25 and 2.26 when the liquid absorbents are excessively used. Rewrite these three equations in Eqs. 5.4 – 5.6 as follows for the purpose of convenient citation and clear demonstration.

$$N_G = \left(\frac{1}{Hk_G} + \frac{1}{Ek_L}\right)^{-1} c_{Ai} \quad (5.4)$$

$$E_{parallel} = \sqrt{M\left(1 + \frac{m+1}{p+1} \cdot \frac{k_{pq} C_0^q c_{Ai}^{p-m}}{k_{mn} B_0^n}\right)} \quad (5.5)$$

$$M = \frac{2}{m+1} \cdot \frac{k_{mn} D_A B_0^n c_{Ai}^{m-1}}{k_L^2} \tag{5.6}$$

where c_{Ai} = interfacial concentration of gas A, $mol \cdot L^{-1}$;

B_0 = bulk concentration of reactant B in liquid, $mol \cdot L^{-1}$;

C_0 = bulk concentration of reactant C in liquid, $mol \cdot L^{-1}$;

D_A = molecular diffusivity of solute gas A in liquid phase, $m^2 \cdot s^{-1}$;

$E_{parallel}$ = enhancement factor for parallel reactions, -;

H = Henry's Law constant, $L \cdot atm \cdot mol^{-1}$;

k_G = gas-phase mass transfer coefficient, $mol \cdot s^{-1} \cdot m^{-2} \cdot atm^{-1}$;

k_L = liquid-phase mass transfer coefficient, $m \cdot s^{-1}$;

N_G = gas absorption rate into the solution, $mol \cdot m^{-2} \cdot s^{-1}$;

m, n, p, q = m-, n-, p-, q-th reaction order, -;

k_{mn} = reaction rate constant for (m+n)-th order reaction, $L^{m+n-1} \cdot mol^{1-m-n} \cdot s^{-1}$;

k_{pq} = reaction rate constant for (m+n)-th order reaction, $L^{p+q-1} \cdot mol^{1-p-q} \cdot s^{-1}$.

The specific results regarding reaction orders with respect to each reactant in Reactions 5.2 and 5.3 will firstly be finalized. With these known reaction orders, it still requires the knowledge of N_{NO}, H, c_{NOi}, k_G, k_L and D_{NO} for the solutions to reaction rate constants. The gas-liquid interfacial NO concentration can be predicted from Henry's law as

$$c_{NOi} = \frac{P_T y}{H} \tag{5.7}$$

where c_{NOi} = interfacial concentration of NO, $mol \cdot L^{-1}$;

H = Henry's constant, $L \cdot atm \cdot mol^{-1}$;

P_T = total pressure, atm;

y = NO concentration in the gas phase of the reactor, ppmv.

The temperature dependence of Henry's constant in water is given by the same method introduced in Section 4.1. Please refer to that section for more information.

As the dimensions of the reactor in this study were almost the same as those in Sada's works [28, 47, 87] and stirring speeds for both phases were close to theirs, their empirical correlations for gas- and liquid- mass transfer coefficients were employed. Firstly, the liquid-phase mass transfer

coefficient of carbon dioxide and the gas-phase mass transfer coefficient are correlated with corresponding stirring speed as [28, 47, 87].

$$k_{L,CO_2-H_2O} = 9.41 \times 10^{-7} n_L^{0.65} \quad (5.8)$$

$$k_{G,SO_2-N_2} = 1.22 \times 10^{-2} n_G^{0.61} \quad (5.9)$$

where k_{L,CO_2-H_2O} = liquid-phase mass transfer coefficient given by CO_2-H_2O system, $m \cdot s^{-1}$;

k_{G,SO_2-N_2} = gas-phase mass transfer coefficient given by SO_2-N_2 system, $mol \cdot s^{-1} \cdot m^{-2} \cdot atm^{-1}$;

n_G = gas-phase stirrer speed, rpm;

n_L = liquid-phase stirrer speed, rpm.

Then values of liquid- and gas-phase mass transfer for NO can be determined by Eqs. (26) and (27) with known k_{L,CO_2-H_2O} and k_{L,SO_2-N_2}, respectively [28, 47, 87, 89].

$$k_{L,NO} = k_{L,CO_2-H_2O}(D_{NO-H_2O}/D_{CO_2-H_2O})^{2/3} \quad (5.10)$$

$$k_{G,NO} = k_{G,SO_2-N_2}(D_{NO-N_2}/D_{SO_2-N_2})^{2/3} \quad (5.11)$$

where D_{NO-H_2O} = molecular diffusivity of NO in water, $m^2 \cdot s^{-1}$;

$D_{CO_2-H_2O}$ = molecular diffusivity of CO_2 in water, $m^2 \cdot s^{-1}$;

D_{NO-N_2} = molecular diffusivity of NO in N_2, $m^2 \cdot s^{-1}$;

$D_{SO_2-N_2}$ = molecular diffusivity of SO_2 in N_2, $m^2 \cdot s^{-1}$;

$k_{G,NO}$ = gas-phase mass transfer coefficient for NO, $mol \cdot s^{-1} \cdot m^{-2} \cdot atm^{-1}$;

$k_{L,NO}$ = liquid-phase mass transfer coefficient for NO, $m \cdot s^{-1}$.

The gas diffusivity in liquid can be well estimated by Wilke-Chang equation [150],

$$D_{AB} = 7.4 \times 10^{-12} (\emptyset M_B)^{0.5} \frac{T}{\mu_B V_{bA}^{0.6}} \quad (5.12)$$

where D_{AB} = the diffusivity of gas A in a solvent B, $m^2 \cdot s^{-1}$;

M_B = molar mass of B, $g \cdot mol^{-1}$;

T = temperature, K;

V_{bA} = molar volume of solute A at its normal boiling temperature, $cm^2 \cdot mol^{-1}$;

Φ = association factor of solvent, -;

μ_B = dynamic viscosity, Pa·s.

For water, the association factor is 2.26 (which is better than 2.6 originally proposed by Wilke and Chang) [151, 152]; the molar volumes of NO and CO_2 at its normal boiling temperature are 23.6 and 34 cm^3/mol, respectively. According to Incropera et al. [153], the water viscosities are tabulated every 5 K so that value at certain temperature can be obtained by interpolation.

Unlike Henry's law constant or solubility, ionic strength has no obvious impact on NO diffusivity. Zacharia and Deen [154] measured NO diffusivity in pure water and phosphate buffered saline at 298.2 K and found that they were the same. Therefore, the NO diffusivity in pure water was used for 2 mol·L^{-1} NH_4NO_3 solution in present study.

The gas diffusivity for binary gas system at low pressures can be theoretically predicted by using Chapman-Enskog equation [155].

$$D_{AB} = \frac{2.66 \times 10^{-7} T^{3/2}}{P M_{AB}^{1/2} \sigma_{AB}^2 \Omega_D} \tag{5.13}$$

in which

$$M_{AB} = \frac{2}{\frac{1}{M_A} + \frac{1}{M_B}} \tag{5.14}$$

$$\sigma_{AB} = \frac{\sigma_A + \sigma_B}{2} \tag{5.15}$$

$$\Omega_D = \frac{1.06036}{(T^*)^{0.15610}} + \frac{0.19300}{\exp(0.47635 T^*)} + \frac{1.03587}{\exp(1.52996 T^*)} + \frac{1.76474}{\exp(3.89411 T^*)} \tag{5.16}$$

$$T^* = \frac{kT}{(\epsilon_A \epsilon_B)^{1/2}} \tag{5.17}$$

where D_{AB} = the diffusivity of gas A in gas B, $m^2 \cdot s^{-1}$;

M_A, M_B = molecular weights of A and B, g·mol^{-1};

P = pressure, bar;

T = temperature, K;

σ = characteristic Lennard-Jones length, Å;

ϵ = characteristic Lennard-Jones energy, J;

Ω_D = diffusion collision integral, -.

κ = Boltzmann's constant, $J \cdot K^{-1}$;

The values of σ and ϵ/k for various gases are summarized in **Table 5-1** [155].

Table 5-1: Lennard-Jones potentials as determined from viscosity data

Gas species	**σ, Å**	**ϵ/k, K**
NO	3.492	116.7
N_2	3.798	71.4
SO_2	4.112	335.4

After the selection of required parameters in Eqs. 5.4 – 5.6, the solutions to reaction rate constants of Reactions 5.2 and 5.3 can be determined by graphical determination of reaction order with respect to NO and regression analysis.

5.4 Results and Discussion

5.4.1 Validation of Flue Gas Simulation

Due to the use of flue gas synthesis, it is necessary to check the performance of Koflo mixer to justify the effectiveness of simulation system before the systematic investigation, and to make sure all the data collected was reliable. **Table 5-2** presents the readings given by the CAI 650 NOXYGEN gas analyzer for flue gas streams with calculated NO concentration ranged from 203 to 1132 ppmv. The agreement between calculated and measured values was acceptable for the maximum error was less than 1.5%, indicating that the flue gas simulation process was warranted.

Table 5-2: Readings of gas analyzer in the absence of oxygen

Number	NO ($mL \cdot min^{-1}$)	N_2 ($L \cdot min^{-1}$)	Calculated NO concentration (ppmv)	Measured NO concentration (ppmv)
1	23	2.86	203	201
2	35	2.85	308	307
3	47	2.85	412	411
4	58	2.84	508	505
5	69	2.83	605	605
6	82	2.82	718	717
7	94	2.83	817	815
8	105	2.83	909	906
9	117	2.84	1005	997
10	132	2.83	1132	1121

5.4.2 The Determination of Pseudo Orders with respect to NO

In order to determine the pseudo orders with respect to NO, the NO absorption rate as described in Eq. 5.4 was used. Substitution of Eq.s 5.5 and 5.6 into Eq. 5.4 gives,

$$N_{NO} = \left(\frac{1}{Hk_G} + \frac{1}{\sqrt{D_{NO}}\sqrt{\frac{2}{m+1}k_{mn}^{5}B_5^{n}c_{NOi}^{m-1} + \frac{2}{p+1}k_{pq}^{6}B_6^{q}c_{NOi}^{p-1}}}\right)^{-1}c_{NOi} \qquad (5.18)$$

where B_5 = bulk concentration of pentaamminecobalt(II) nitrate in liquid, $mol \cdot L^{-1}$;

B_6 = bulk concentration of hexaamminecobalt(II) nitrate in liquid, $mol \cdot L^{-1}$;

c_{NOi} = interfacial concentration of NO, $mol \cdot L^{-1}$;

D_{NO} = molecular diffusivity of solute NO in liquid phase, $m^2 \cdot s^{-1}$;

H = Henry's Law constant, $L \cdot atm \cdot mol^{-1}$;

k_G = gas-phase mass transfer coefficient, $mol \cdot s^{-1} \cdot m^{-2} \cdot atm^{-1}$;

N_{NO} = gas absorption rate into the solution, $mol \cdot m^{-2} \cdot s^{-1}$.

m, n, p, q = m-, n-, p-, q-th reaction order, -;

k_{mn} = reaction rate constant for (m+n)-th order Reaction 5.2, $L^{m+n-1} \cdot mol^{1-m-n} \cdot s^{-1}$;

k_{pq} = reaction rate constant for (m+n)-th order Reaction 5.3, $L^{p+q-1} \cdot mol^{1-p-q} \cdot s^{-1}$.

At a certain experimental condition corresponding to set temperature, solvent concentration, pH value and stirring speed, the Henry's constant, gas-film mass transfer coefficient, NO diffusivity, reaction rate constants and orders were fixed. Then it can be seen from Eq. 5.18 that the absorption

rate of NO into the mixture of penta- and hexa-amminecobalt(II) solutions is only a function of the interfacial concentration of NO. A linear relationship between N_{NO} and c_{NOi} could exist only if m=p=1.

Figure 5-5 is the plot of N_{NO} versus c_{Noi} under two different experimental conditions, from which the evident linear relationship between N_{NO} and c_{Noi} can be observed in both situations. Therefore, the pseudo orders with respect to NO of Reactions 5.2 and 5.3 can be determined as m = p =1. Thus, Eq. 5.18 can be rewritten as in Eq. 5.19 after substituting m=p=1.

$$N_{NO} = \left(\frac{1}{Hk_G} + \frac{1}{\sqrt{D_{NO}}\sqrt{k_{1n}^5 B_5^n + k_{1q}^6 B_6^q}}\right)^{-1} c_{NOi} \tag{5.19}$$

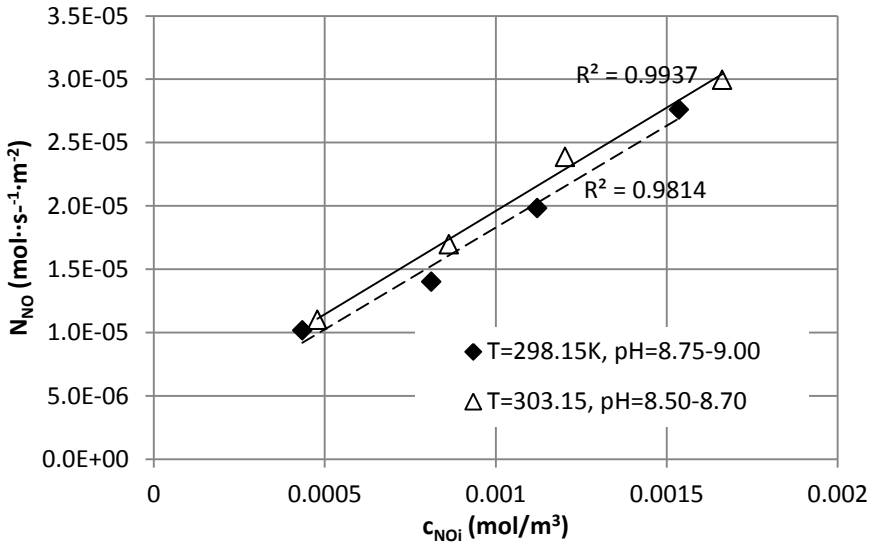

Figure 5-5: The plot of N_{NO} vs c_{Noi} at two experimental conditions

5.4.3 The Determination of Reaction Rate Constants

Further rearrangement of Eq. 5.19 gives

$$k_{1n}^5 B_5^n + k_{1q}^6 B_6^q = \frac{\left(\frac{c_{NOi}}{N_{NO}} - \frac{1}{Hk_G}\right)^{-2}}{D_{NO}} \tag{5.20}$$

Theoretically, the numerical solutions of the four unknown variables, namely k_{1n}^5, k_{1q}^6, n and q, in Eq. 5.20 can be found if four trials are conducted at each temperature to form a system of four non-linear

equations. However, according to the warning in Matlab software the Jacobean matrix generated by such a nonlinear equation system was badly scaled, thereby making Newton's method inapplicable. As an alternative approach, the multiple linear regression analysis can be utilized to avoid the complicated numerical calculation if the reaction orders with respect to liquid reactants, n and q, are known. Therefore, six tests using different solvent concentrations and/or gas concentrations are conducted at each temperature. The corresponding experimental results are summarized in **Table 5-3**.

The best way to determine the reaction order with respect to penta- and hexa-amminecobalt(II) is to have respective compounds react alone with NO. Nevertheless, according to cobalt(II)-ammonia analysis it is troublesome to prepare solutions that contain large amount of penta-amminecobalt(II) while no hexaamminecobalt(II). It is known that the product composition is greatly dependent upon pH value. The average coordinate number increases with pH value [36, 62]. The hexamminecobalt(II) ion does not appear in the system until pH = 8 at which the proportion of pentaamminecobalt(II) compound is only 2.75% or so and the ratio of penta- to hexa-ammiecobalt(II) ions is not large enough to ignore the contribution of hexa-ammiecobalt(II) to the calculation in Eq. 5.20. In practice, very small amount of ammonia easily results in pH value beyond 8, making it difficult to prepare solution with pH < 8. Furthermore, the preparation of solutions exclusively with hexaamminecobalt(II) is also unrealistic as the pH value of such a solution will reach approximately 12, which is difficult to achieve with addition of ammonia and at which the volatilization of ammonia is rather evident.

Table 5-3: The experimental results for the determination of reaction rate constants

T (K)	pH	c_{Noi} (mol·m^{-3})	N_{NO} (mol·s^{-1}·m^{-2})	B_5 (mol·L^{-1})	B_6 (mol·L^{-1})	$Y = \frac{\left(\frac{c_{NOi}}{N_{NO}} - \frac{1}{Hk_G}\right)^{-2}}{D_{NO}}$ (s^{-1})
298.2	9.00	4.78E-04	1.10E-05	3.06E-02	4.89E-03	2.44E+05
	9.87	8.81E-04	1.92E-05	9.04E-03	1.51E-02	2.18E+05
	8.84	8.63E-04	1.70E-05	2.34E-02	2.59E-03	1.75E+05
	8.83	1.20E-03	2.39E-05	2.30E-02	2.48E-03	1.76E+05
	9.77	1.73E-03	3.53E-05	1.07E-02	1.29E-02	1.88E+05
	8.75	1.66E-03	3.00E-05	1.93E-02	1.73E-03	1.45E+05
303.2	8.70	4.34E-04	1.02E-05	2.41E-02	2.74E-03	2.21E+05
	9.85	8.18E-04	1.98E-05	6.48E-03	1.82E-02	2.38E+05
	8.50	8.12E-04	1.40E-05	1.51E-02	1.08E-03	1.18E+05
	9.74	1.54E-03	3.88E-05	8.47E-03	1.58E-02	2.56E+05
	8.51	1.54E-03	2.76E-05	1.55E-02	1.14E-03	1.27E+05
	8.50	1.12E-03	1.98E-05	1.51E-02	1.08E-03	1.22E+05

Although there were numerous investigations on reactions between NO and ammoniacal cobalt(II) complexes, they primarily focused on the preparation and structural analysis of nitrosyl product. Mao et al. studied chemical equilibrium [57] and kinetics [56] without considering cobalt(II) – ammonia analysis. Moreover, they used a monomer nitrosyl as the reaction product, which contradicted with most existing studies. In terms of kinetics study, no data of rate constants were given due to the simplification of instantaneous reaction [56]. Recently, our research group experimentally determined the equilibrium constants of such reactions [156]. Thus, there is no information about the reaction order with respect to cobalt(II) solvents. However, the kinetics of absorption of oxygen into penta- and hexa-amminecobalt(II) reported by Simplicio and Wilkins [61] might shed some light onto the determination of reaction orders with respect to the liquid reactants when they were used to cope with NO. They stated that the reactions between oxygen and penta- and hexa-amminecobalt(II) ions held the second-order rate law. Specifically, the reactions were first order with respect to O_2, pents- and hexa-ammincecobalt(II) solutions, respectively. From the analysis in last section, the absorption of NO into ammonical cobalt(II) compounds is first-order with respect to NO; meanwhile, penta- and

hexa-amminecobalt(II) compounds are from the same family and probably have similar reactivity. Thus, it is assumed that they are first-order with respect to both liquid absorbents, n=p=1. Normally, reactions like Reactions 5.2 and 5.3 have n and p values ranged from 0 to 2. In addition to n=p=1, the possibilities of n=p=0, n=p=0.5 and n=p=2 are also analyzed. If these assumptions cannot give satisfactory results, unequal n and q values will be taken.

First of all, the possibility of n=q=0 can be eliminated because the right-hand side (RHS) of Eq. 5.20 changes with inlet gas concentration at the same temperature. It is well known that rate constant is a function of temperature; therefore, the value of RHS of Eq. 5.20 should be invariable if n=q=0. The regression analysis is then executed to three most possible sets of n and q values. The corresponding regression results are tabulated in **Table 5-4**.

Table 5-4: Reaction rate constants at various n, p values

Temperature	**n=q=0.5 ($L^{0.5}\cdot mol^{-0.5}\cdot s^{-1}$)**		**n=q=1 ($L\cdot mol^{-1}\cdot s^{-1}$)**		**n=q=2 ($L^{2}\cdot mol^{-2}\cdot s^{-1}$)**	
(K)	$k_{1.5}^{5}$	$k_{1.5}^{6}$	k_{2}^{5}	k_{2}^{6}	k_{3}^{5}	k_{3}^{6}
298.2	8.41E+05	1.04E+06	6.43E+06	1.00E+07	2.78E+08	8.79E+08
303.2	7.22E+05	1.43E+06	7.57E+06	1.12E+07	4.24E+08	7.53E+08

The assumption of n=q=0.5 is unjustifiable since the rate constant increases as temperature, whereas it can be seen from **Table 5-4** that the value of $k_{1.5}^{5}$ at 298.2 K is greater than that at 303.2 K if n=q=0.5. Likewise, the value of k_{3}^{6} is 8.79×10^{8} at 298.2 K while 7.53×10^{8} at 303.2 K if n=q=2. The superiority of n = q =1 can be further exhibited by comparison between the parity plots of Y for n=p=1 and n=p=2, respectively, as shown in **Figure 5-6**.

It can be seen that the regression analysis with the assumption of n=p=1 gives a rather desirable result which is much better than that of n=p=2. As for n=p=1, the deviations between predicted and experimental Y values are all within ±6% for both temperatures. When it comes to n=p=2, several predicted Y values are away from the y=x line with one residual even beyond 20%. Hence, it is unnecessary to perform other regression analyses with unequal n and q values and concluded that second-order law (i.e., n=q=1) holds the best for reactions between NO and penta- and hexa-amminecobalt(II) complexes. Eventually Eq. 5.20 can be rewritten as one of the following two equations.

$$k_2^5 B_5 = Y - k_2^6 B_6 \tag{5.21}$$

$$k_2^6 B_6 = Y - k_2^5 B_5 \tag{5.22}$$

where

$$Y = \frac{\left(\frac{c_{NOi}}{N_{NO}} - \frac{1}{Hk_G}\right)^{-2}}{D_{NO}} \tag{5.23}$$

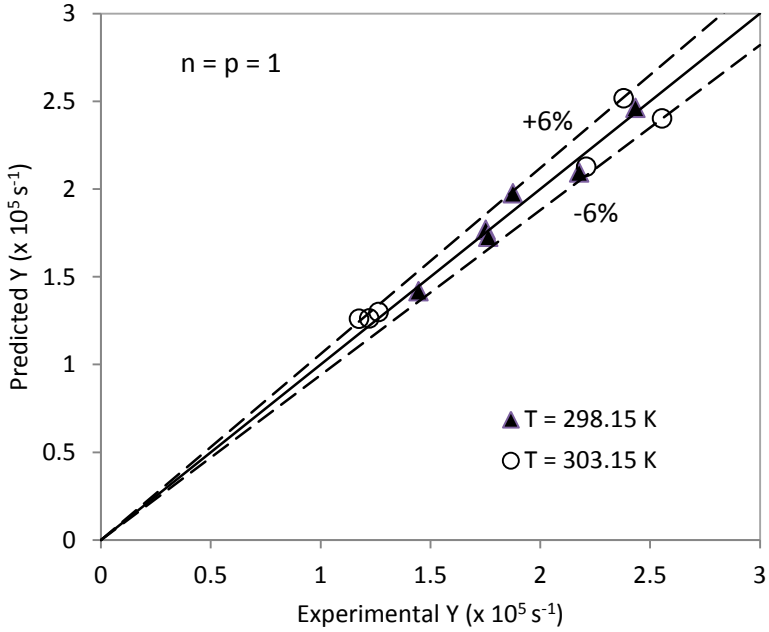

(a)

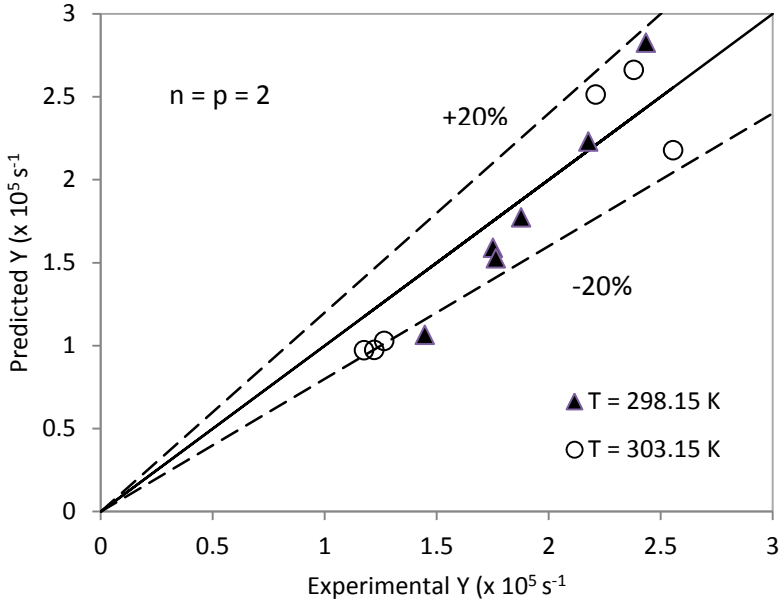

(b)

Figure 5-6: Parity plot of Y (a) n = p =1; (b) n = p =2

Further analyses by plotting $Y\text{-}k_2^6 B_6$ against B_5 and $Y\text{-}k_2^5 B_5$ against B_6 are shown in **Figure 5-7**. With the fitted values of k_2^5 and k_2^6 shown in **Table 5-4** substituted, the validities of Eqs. 5.21 and 5.22 are illustrated in **Figure 5-7**. In conclusion, Reaction 5.2 is of first order with respect to NO and penta-amminecobalt(II), respectively; Reaction 5.3 is of first order with respect to NO and hexa-amminecobalt(II), respectively. The second-order rate constants of Reaction 5.2 are 6.43×10^6 and 7.57×10^6 $L\cdot mol^{-1}\cdot s^{-1}$at 298.2 and 303.2 K, respectively, and the counterparts of Reaction 5.3 are 1.00×10^7 and 1.12×10^7 $L\cdot mol^{-1}\cdot s^{-1}$, respectively.

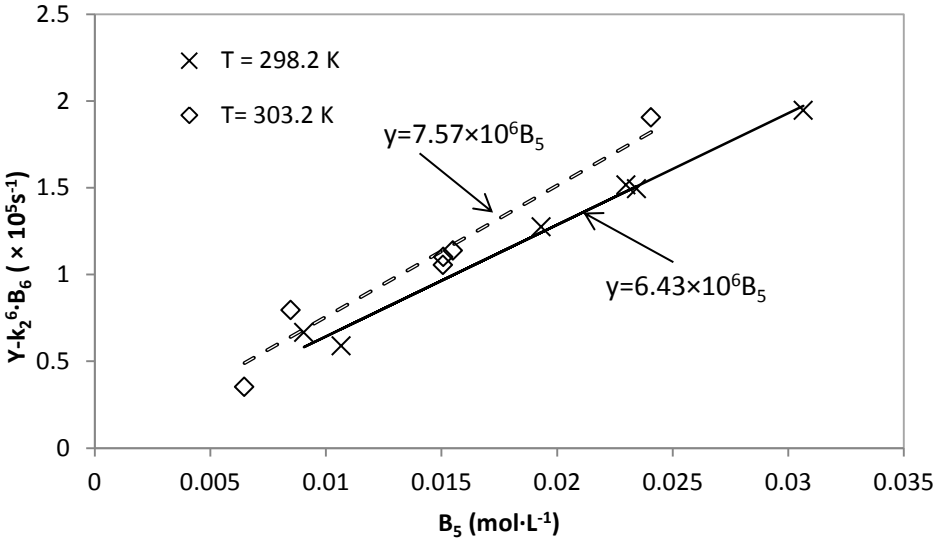

(a)

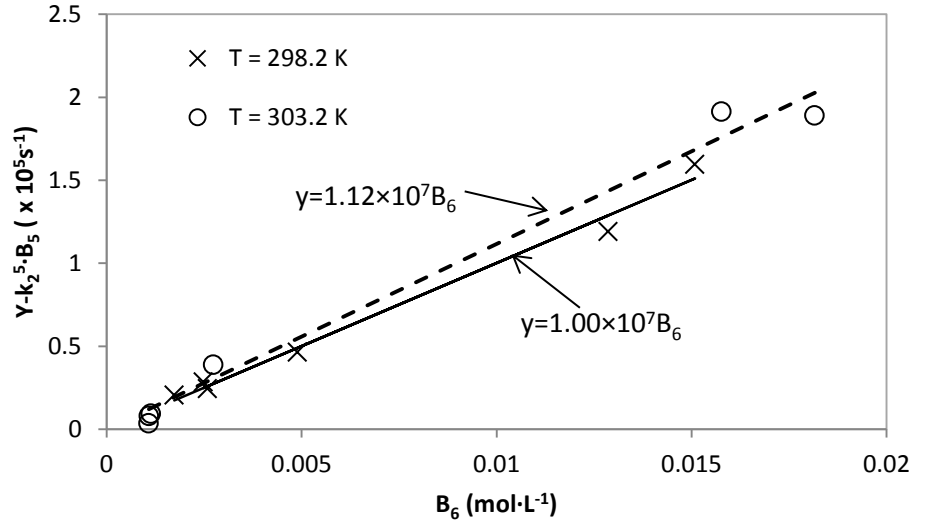

(b)

Figure 5-7: Analysis of reaction order with respect to pentaamminecobalt(II) ions (a) in terms of B_5; (b) in terms of B_6

5.4.4 Comparison with Fe(II)-EDTA Solution

Fe(II)-EDTA was known for its fast reaction rate with NO in the absence of oxygen; numerous studies showed that the reaction between NO and Fe(II)-EDTA was first order with respect to NO and Fe(II)-EDTA [30, 87-89]. The published values of this second order reaction rate constant slightly vary from researcher to researcher and are summarized in **Table 5-5**. It can be seen that the second order rate constant of NO absorption into Fe(II)-EDTA has an order of 10^8 $L \cdot mol^{-1} \cdot s^{-1}$, whereas it is known from **Table 5-4** that the counterparts of ammoniacal cobalt(II) complexes are in the order of

10^7 L·mol^{-1}·s^{-1}. This explains why Fe(II)-EDTA absorbs NO faster than ammoniacal cobalt(II) solutions do [60]. However, a typical flue gas from power plant contains excess oxygen remaining from intake combustion air, usually 2-6% by volume [52, 53] and the significantly negative effect exerted by oxygen may make Fe(II)-EDTA a less competitive NO absorbent. It was reported that 5% oxygen in a flue gas would greatly deteriorate the NO removal capacity by as high as 83% [25] due to the oxidation of Fe(II)EDTA to Fe(III)EDTA; Fe(III)EDTA is inactive with NO. On the other hand, the oxygen present in the flue gas favors the performance of NO absorption by using ammoniacal cobalt(II) complexes [32]. From this point of view, ammoniacal cobalt(II) solutions are more suitable for NO abatement.

Table 5-5: The 2nd –order rate constant of NO absorption into Fe(II)-EDTA at 298.2 K

Researcher	**pH**	**2nd reaction rate constant (L·mol^{-1}·s^{-1})**
Teramoto et al. [30]	4.6 – 8.0	1.70×10^8
Sada et al. [87]	1.5 – 2.5	3.29×10^7
	7.0	1.23×10^8
	9.5-10	1.04×10^8
Littlejohn and Chang [157]	5.1	6.00×10^7
Weisweiler et al. [158]	7.0	9.40×10^7
Chien et al. [88]	3.0 – 11.0	3.70×10^7
Du et al. [89]	1.5 – 2.5	1.14×10^8

5.5 Uncertainty Analysis

In this chapter, the two reaction rate constants k_2^5 and k_2^6 for parallel Reactions 5.2 and 5.3 were determined by multiple linear regression model based on following linear equation, which is the rewriting of Eq. 5.21.

$$Y = k_2^5 B_5 + k_2^6 B_6 \qquad (5.24)$$

where $Y = \frac{\left(\frac{c_{NOi}}{N_{NO}} - \frac{1}{Hk_G}\right)^{-2}}{D_{NO}}$. The experimental values of Y, B_5, and B_6 are tabulated in **Table 5-3**. There are six sets of (B_5, B_6) data for linear regression at each temperature. It can be seen that the intercept of Eq. 5.24 is zero; thus, only k_2^5 and k_2^6 are the parameters to be determined.

As the response Y is a measured experimental result given by Eq. 5.23. Its uncertainty is computed using error propagation method elaborated in Chapter 4. In addition, the uncertainty for the multiple linear regression model is also calculated.

5.5.1 Uncertainty in Y

According to Eq. 5.23, the propagation of uncertainties in c_{NOi}, N_{NO}, H, k_G and D_{NO} to Y is described as

$$\left(\frac{U_Y}{Y}\right)^2 = \left(\frac{U_{D_{NO}}}{D_{NO}}\right)^2 + 4\left[\frac{U_{c_{NOi}}}{N_{NO}\left(\frac{c_{NOi}}{N_{NO}} - \frac{1}{Hk_G}\right)}\right]^2 + 4\left[\frac{c_{NOi}U_{N_{NO}}}{{N_{NO}}^2\left(\frac{c_{NOi}}{N_{NO}} - \frac{1}{Hk_G}\right)}\right]^2 + 4\left[\frac{{k_G}^{-1}U_H}{H^2\left(\frac{c_{NOi}}{N_{NO}} - \frac{1}{Hk_G}\right)}\right]^2 + 4\left[\frac{H^{-1}U_{k_G}}{{k_G}^2\left(\frac{c_{NOi}}{N_{NO}} - \frac{1}{Hk_G}\right)}\right]^2 \tag{5.25}$$

where U = certainty into the subscript quantity in the same units as corresponding quantity.

It was found in the calculation that the value of $\left(\frac{c_{NOi}}{N_{NO}}\right)$ was at least 25 times greater than that of $\left(\frac{1}{Hk_G}\right)$; therefore, Eq. 5.25 can be simplified by neglecting $\frac{1}{Hk_G}$ from term $\left(\frac{c_{NOi}}{N_{NO}} - \frac{1}{Hk_G}\right)$ and

$$\left(\frac{U_Y}{Y}\right)^2 = \left(\frac{U_{D_{NO}}}{D_{NO}}\right)^2 + 4\left(\frac{U_{c_{NOi}}}{c_{NOi}}\right)^2 + 4\left(\frac{U_{N_{NO}}}{N_{NO}}\right)^2 + 4\left(\frac{N_{NO}/c_{NOi}}{Hk_G}\right)^2\left[\left(\frac{U_H}{H}\right)^2 + \left(\frac{U_{k_G}}{k_G}\right)^2\right] \tag{5.26}$$

The analysis of uncertainties in c_{NOi} and H has already been done in Section 4.5.1. Here emphasis is given to the estimation of uncertainties in D_{NO}, N_{NO} and k_G.

The data reduction expression for D_{NO} is presented in Eq. 5.13, from which the uncertainty in D_{NO} is described as

$$\left(\frac{U_{D_{NO}}}{D_{NO}}\right)^2 = 0.25\left(\frac{U_\emptyset}{\emptyset}\right)^2 + 0.25\left(\frac{U_{M_{NO}}}{M_{NO}}\right)^2 + \left(\frac{U_T}{T}\right)^2 + \left(\frac{U_{\mu_{NO}}}{\mu_{NO}}\right)^2 + 0.36\left(\frac{U_{V_{bA}}}{V_{bA}}\right)^2 \tag{5.27}$$

in which the uncertainties in molecular weight, NO viscosity, and V_{bA} can be assumed to be zero. Then Eq. 5.27 becomes

$$\left(\frac{U_{D_{NO}}}{D_{NO}}\right)^2 = 0.25\left(\frac{U_\emptyset}{\emptyset}\right)^2 + \left(\frac{U_T}{T}\right)^2 \tag{5.28}$$

The uncertainty in empirical association factor is then assumed as $\frac{U_\emptyset}{\emptyset} = 5\%$ again. As discussed in Section 4.5.1, U_T = 0.5 K.

The measured NO absorption rate into ammoniacal cobalt(II) solutions was calculated by Eq. 5.1; thus, the propagation of uncertainties in quantities at the RHS of Eq. 5.1 to N_{NO} is given as follows.

$$(\frac{U_{N_{NO}}}{N_{NO}})^2 = (\frac{U_{Q_G}}{Q_G})^2 + (\frac{U_{P_T}}{P_T})^2 + (\frac{U_R}{R})^2 + (\frac{U_{S_A}}{S_A})^2 + (\frac{U_T}{T})^2 + \left(\frac{1}{y_{in} - y_{out}}\right)^2 (U_{y_{in}}{}^2 + U_{y_{out}}{}^2) \quad (5.29)$$

where $\frac{U_{P_T}}{P_T} = \frac{U_R}{R} = 0$, and $U_{y_{in}} = U_{y_{out}} = 15\ ppmv$. Rewriting Eq. 5.29 with $\frac{U_{P_T}}{P_T} = \frac{U_R}{R} = 0$ subistituted gives,

$$(\frac{U_{N_{NO}}}{N_{NO}})^2 = (\frac{U_{Q_G}}{Q_G})^2 + (\frac{U_{S_A}}{S_A})^2 + (\frac{U_T}{T})^2 + \left(\frac{1}{y_{in} - y_{out}}\right)^2 (U_{y_{in}}{}^2 + U_{y_{out}}{}^2) \quad (5.30)$$

In this kinetic study, the flow rate of simulated flue gas is the sum of flow rates of gases from NO and N_2 cylinders.

$$Q_G = Q_{NO} + Q_{N_2} \quad (5.31)$$

where Q_{NO} = the flow rate of gas from NO cylinder, $m^3 \cdot s^{-1}$;

Q_{N2} = the flow rate of gas from N_2 cylinder, $m^3 \cdot s^{-1}$.

Further propagation of uncertainty on the basis of Eq. 5.31 generates,

$$U_{Q_G}{}^2 = U_{Q_{NO}}{}^2 + U_{Q_{N_2}}{}^2 \quad (5.32)$$

According to specifications of mass flow controller, $U_{Q_{NO}} = 1.5\% \times 200 = 3\ mL \cdot min^{-1}$, and $U_{Q_{NO}} = 1.5\% \times 5000 = 75\ mL \cdot min^{-1}$. Thus, $U_{Q_G} \simeq U_{Q_{NO}} = 75\ mL \cdot min^{-1}$.

As defined, the cross-sectional area of the double stirred tank reactor is calculated by

$$S_A = \frac{\pi}{4} d^2 \quad (5.33)$$

where d is the diameter of the double stirred tank reactor. Thus, the uncertainty in S_A doubles that in diameter.

$$\frac{U_{S_A}}{S_A} = 2\frac{U_d}{d} \quad (5.34)$$

The diameter of 99.72 mm is measured by a digital caliper with accuracy of ± 0.04 mm; that is to say, $\frac{U_d}{d} = 0.04$ %, and $\frac{U_{S_A}}{S_A} = 0.08$ %.

Then the uncertainty in k_G is last parameter needed to solve $\frac{U_Y}{Y}$. From Eq. 5.11 it can be seen that $k_{G,\,NO\text{-}N2}$ is a function of $k_{G,\,SO2\text{-}N2}$, $D_{NO\text{-}N2}$ and $D_{SO2\text{-}N2}$. The corresponding error propagation expression for $k_{G,\,NO\text{-}N2}$ is shown in Eq. 5.35.

$$(\frac{U_{k_{G,NO-N_2}}}{k_{G,NO}-N_2})^2 = (\frac{U_{k_{G,SO_2-N_2}}}{k_{G,SO_2}-N_2})^2 + \frac{4}{9}(\frac{U_{D_{NO-N_2}}}{D_{NO-N_2}})^2 + \frac{4}{9}(\frac{U_{D,SO_2-N_2}}{D_{,SO_2-N_2}})^2 \qquad (5.35)$$

The value of $k_{G,\,SO2\text{-}N2}$ is given by Sada et al. [28, 47, 87] by empirical correlation. The uncertainty is not given; hence, the assumption of $\frac{U_{k_{G,SO_2-N_2}}}{k_{G,SO_2-N_2}} = 5\%$ is taken again. Eq. 5.26 shows that the ultimate $\frac{U_Y}{Y}$ is not sensitive to the value of $\frac{U_{k_{G,SO_2-N_2}}}{k_{G,SO_2-N_2}}$ as the calculated value of coefficient $(\frac{N_{NO}/c_{NOi}}{Hk_G})^2$ is extremely small. So it is justifiable to make this assumption.

The gas diffusivity for binary gas system is theoretically predicted by Chapman-Enskog equation as shown in Eq. 5.13. If all the uncertainties in quantities involved are assumed to be zero, $\frac{U_{D_{NO-N_2}}}{D_{NO-N_2}} = \frac{U_{D,SO_2-N_2}}{D_{,SO_2-N_2}} = 1.5\frac{U_T}{T}$. Likewise, the ultimate $\frac{U_Y}{Y}$ is insensitive to the value of $\frac{U_{D_{NO-N_2}}}{D_{NO-N_2}}$ due to the extremely small calculated value of coefficient $(\frac{N_{NO}/c_{NOi}}{Hk_G})^2$, justifying the assumption.

Eventually, the uncertainty in Y can be obtained by Eq. 5.26. A sample calculation was done for the trial conducted at T = 298.2 K, pH = 9.87 and $[Co^{2+}]_T$ = 0.025 mol·L^{-1}. The measured NO concentrations at inlet and out were 717 and 640 ppmv, respectively, and $\frac{N_{NO}/c_{NOi}}{Hk_G} = 0.039$. Assuming all relative uncertainty in empirical coefficient equal to 5%, $(\frac{U_H}{H})^2 = 0.0104$ and$(\frac{U_{c_{NOi}}}{c_{NOi}})^2 = 0.0108$, the results are summarized in detail in **Table 5-6**.

Table 5-6: Results of uncertainty in Y at T = 298.2 K, pH = 9.87 and $[Co^{2+}]_T$ = 0.025 mol·L^{-1}

Uncertainty in Quantity	**Value**
$\frac{U_{\emptyset}}{\emptyset}$	5.00 %
$\frac{U_T}{T}$	0.17 %
$\frac{U_{D_{NO}}}{D_{NO}}$	2.51 %
$\frac{U_{c_{NOi}}}{c_{NOi}}$	10.39 %
$\frac{U_{Q_G}}{Q_G}$	2.63 %
$\frac{U_{S_A}}{S_A}$	0.08 %
$\frac{U_{N_{NO}}}{N_{NO}}$	27.68 %
$\frac{U_H}{H}$	10.20%
$\frac{U_{k_{G,SO_2-N_2}}}{k_{G,SO_2}-N_2}$	5.00%
$\frac{U_{D_{NO-N_2}}}{D_{NO-N_2}}$	0.25%
$\frac{U_{D,SO_2-N_2}}{D,_{SO_2-N_2}}$	0.25%
$\frac{U_{k_G}}{k_G}$	5.01%
$\frac{U_Y}{Y}$	59.18%

In addition to uncertainty in the response variable, Y, the uncertainty for the multiple linear regression model and corresponding test for the significance of regression are of more interest to engineers as the correlated regression equation can be used to estimate parameters and is of practical significance.

5.5.2 Uncertainty for Multiple Linear Regression

The standard error of estimate (SEE) represents a measure of the variation around the fitted line of regression and it is described in Eq. 5.36 [159].

$$SEE = \left\{ \frac{\sum_{i=1}^{6} [Y_i - (k_2^5 B_{5i} + k_2^6 B_{6i})]^2}{4} \right\}^{1/2} \tag{5.36}$$

It is worthwhile to mention that the 4 in the denominator is given by (6-2), in which 2 subtracted from 6 arises because two degrees of freedom are lost from N observations when k_2^5 and k_2^6 are determined by least squares. According to Schenck [160], the uncertainty for the straight-line curve-fit can be chosen as 2(SEE) for most cases as a ±2(SEE) band around the regression line contains approximately 95% of the data points. The values of SSE are 7.05×10^3 and 1.22×10^4 s^{-1} at 298.2 and 303.2 K, respectively. Therefore, the uncertainties for this multiple linear regression are 1.41×10^4 and 2.44×10^4 s^{-1} at 298.2 and 303.2 K, respectively.

5.5.3 Hypothesis Tests

What is more important in the case of multiple linear regression analysis is the test for the significance of regression by using the analysis of variance. This test is usually used to check if there is a linear relationship between the response variable and the explanatory variable. The statements for the hypotheses are [159]:

$$H_0: k_2^5 = k_2^6 = 0$$
$$H_1: At\ least\ one\ of\ k_2^5\ and\ k_2^6 \neq 0 \tag{5.37}$$

Rejection of H_0 in Eq. 5.37 indicates that at least one of k_2^5 and k_2^6 significantly contributes to the regression model. The indicator F_o for this test is described in Eq. 5.38. The hypothesis H_0 is rejected if $F_0 > F_{0.05,\,2,\,4} = 6.94$. The analysis of variance (ANOVA) for significance of regression can be given by Microsoft Excel, and corresponding information is summarized in **Table 5-7**.

$$F_o = \frac{MSR}{MSE} \tag{5.38}$$

where

$$MSR = \frac{\sum_{i=1}^{6}[(k_2^5 B_{5i} + k_2^6 B_{6i}) - \bar{Y}]^2}{2} \quad (5.39)$$

$$MSE = \frac{\sum_{i=1}^{6}[Y_i - (k_2^5 B_{5i} + k_2^6 B_{6i})]^2}{4} \quad (5.40)$$

Table 5-7: Analysis of variance for significance of regression

(a) T = 298.2 K

Source of variation	**Degrees of freedom**	**Sum of squares**	**Mean squares**	**F_0**
Regression	2	2.25E+11	1.12E+11	2256.69
Residual	4	1.99E+8	4.98E+07	
Total	6	2.25E+11		

(b) T = 303.2 K

Source of variation	**Degrees of freedom**	**Sum of squares**	**Mean squares**	**F_0**
Regression	2	2.15E+11	1.08E+11	721.98
Residual	4	5.96E+08	1.49E+08	
Total	6	2.16E+11		

Both values of F_0 at 298.2 and 303 K are excessively greater than $F_{0.05, 2, 4} = 6.94$; therefore, the hypothesis H_0 is rejected for both temperatures. And it is concluded that at least one coefficient out of k_2^5 and k_2^6 is significant.

Furthermore, t-test can be individually conducted to check the significance of k_2^5 or k_2^6 in the multiple linear regression model with following hypotheses:

$$H_0: k_2^5 = 0$$
$$H_1: k_2^5 \neq 0 \quad (5.41)$$

and

$$H_0: k_2^6 = 0$$
$$H_1: k_2^6 \neq 0 \quad (5.42)$$

This process can also be completed by MS Excel and the test results are tabulated in **Table 5-8**. In a typical engineering practice, the t-test is performed at a significance of 0.05. The p-value can then be used to rejected hypothesis H_0 if p value is less than the significance, 0.05. It can be seen from **Table 5-8** that both p values are greatly less than 0.05. Therefore, null hypotheses in Eqs. 5.41 and 5.42 at both temperatures are rejected, and it is concluded that both k_2^5 and k_2^6 are significant.

Table 5-8: Regression results for kinetic study at different temperatures

T	Item	Coefficient	Standard Error	t Stat	P-value	Lower 95%	Upper 95%
298.2 K	Intercept	0	N/A	N/A	N/A	N/A	N/A
	k_2^5	6.43E+06	1.65E+05	3.89E+01	2.60E-06	5.98E+06	6.89E+06
	k_2^6	1.00E+07	4.04E+05	2.48E+01	1.57E-05	8.90E+06	1.11E+07
298.2 K	Intercept	0	N/A	N/A	N/A	N/A	N/A
	k_2^5	7.57E+06	3.58E+05	2.11E+01	2.98E-05	6.57E+06	8.56E+06
	k_2^6	1.12E+07	5.50E+05	2.03E+01	3.48E-05	9.64E+06	1.27E+07

5.6 Summary

The reaction rate constants of Reactions 5.2 and 5.3 were determined with the use of the enhancement factor of NO absorption in a double-stirred reactor. Both reactions were first order with respect to NO and first order with respect to liquid absorbent. The forward reaction rate constants of Reactions 5.2 and 5.3 were 6.43×10^6 and 1.00×10^7 $L\cdot mol^{-1}\cdot s^{-1}$, respectively at 298.2 K, and increased to 7.57×10^6 and 1.12×10^7 $L\cdot mol^{-1}\cdot s^{-1}$, respectively at 303.2 K. The corresponding uncertainty analyses were also conducted.

The NO absorption into ammoniacal cobalt(II) under anaerobic condition now could be well understood by measured equilibrium constants and reaction rate constants. However, the presence of oxygen in flue gas is inevitable. Thus, it is of practical significance to investigate the effect of oxygen on NO reduction. Meanwhile, the regeneration of used absorbent will greatly boost absorbent's competition strength; therefore, effort is also made to conduct regeneration of absorbent. The next chapter is focused on this topic.

Chapter 6
Regeneration of Absorbent and Effect of Oxygen on NO Reduction

6.1 Introduction

After acquiring the knowledge of equilibrium and kinetics of NO absorption into ammoniacal cobalt(II) solutions, it is of importance to investigate the regeneration of the absorbents. Furthermore, the presence of oxygen in flue gas is inevitable; the effect of oxygen on NO absorption is then of concern in this study. Last but not least, the impact exerted by absorbent concentration was briefly examined in introduced in this chapter.

6.2 Experimental

Figure 6-1 shows the experimental setup for the observations of absorbent regeneration and the effects of oxygen in flue gas stream and absorbent concentration on NO absorption. It can be found by comparison with **Figure 4-4** that the reactor used herein was the same as that in equilibrium study. Roughly the section behind mixer is the same as described in Section 4.2; therefore, only the flue gas simulation part is elaborated as follows.

The operation was performed continuously with respect to the gas phase and batch-wise with respect to the liquid phase. All gases were from Praxair Inc. The compressed air cylinder was of grade zero for ozone generation. The nitrogen cylinder was of grade 4.8 and nitric oxide cylinder had content of 2.54% balanced in nitrogen. The pure oxygen for this study was also of grade 4.8. Deliver pressure of each cylinder was relieved by a regulator before entering the process line. A certain gas mixture was synthesized by regulating flow rates of different gases using gas mass flow controllers from Cole-Parmer. The nitrogen mass controller (Model S-32648-16) was made of aluminum whereas mass flowmeters for corrosive nitric oxide (Model S-32648-58) and active oxygen (Model S-32649-60) had 316 stainless steel bodies. They had an accuracy of ±1.5% full-scale. Ranges of flow meters for NO, O_2 and N_2 were 200 mL·min^{-1}, 500 mL·min^{-1} and 5 L·min^{-1}, respectively. Each flow controller was regulated by a bellows-sealed metering valve (Model SS-4BMG) purchased from Swagelok Inc. A 316 stainless steel in-line pipe mixer (Model RK-04669-05) bought from Koflo Inc. was installed to achieve a completely mixed output of the simulated flue gas. The simulated flue gas streams with NO concentrations ranged from 900 to 1060 ppmv were fed at flow rate of approximately 3.00 L·min^{-1}. The oxygen concentration in flue gas varied from 2.1 % to 8.7 % to observe the expected positive effect.

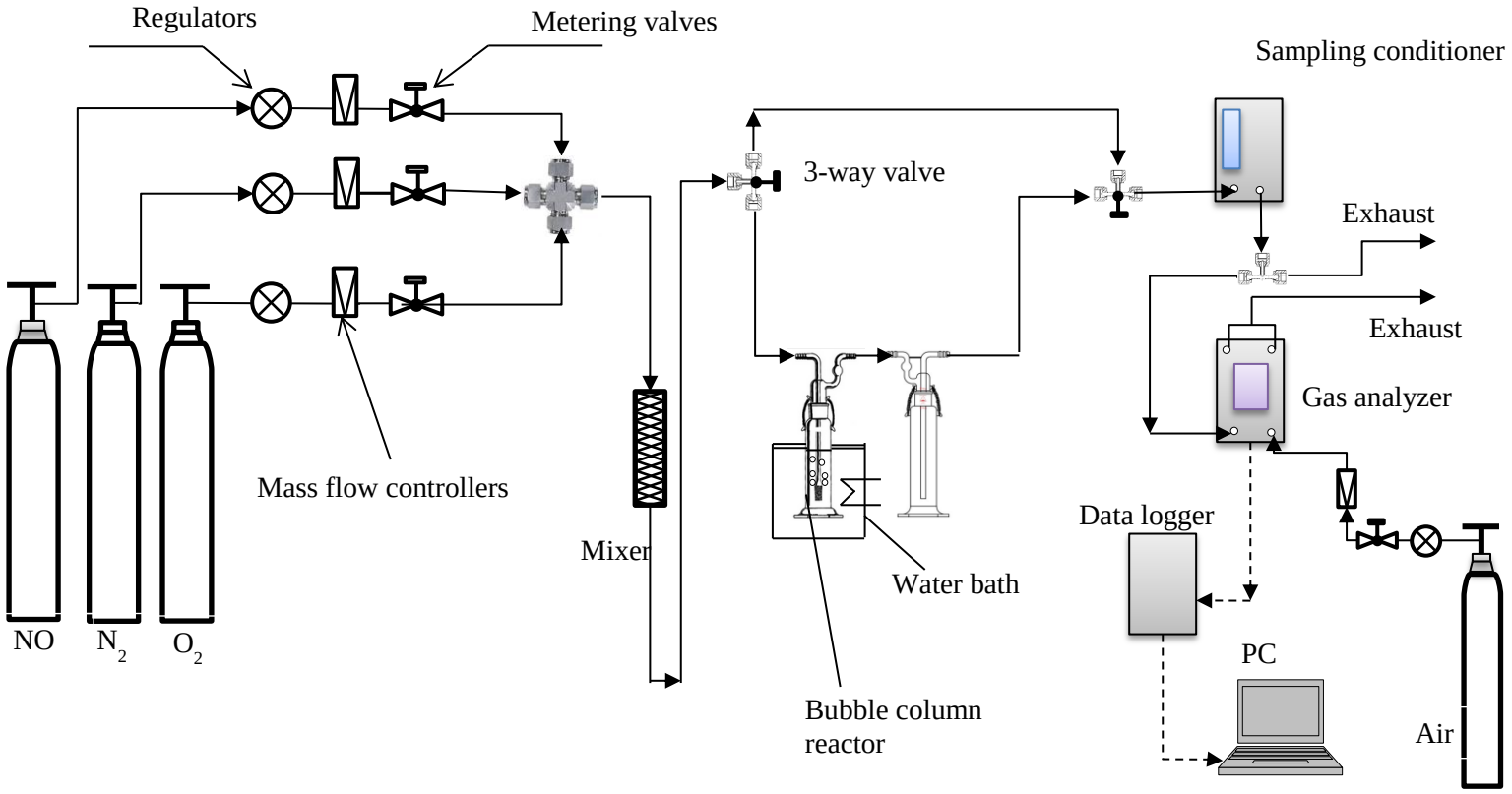

Figure 6-1: Laboratory setup for regeneration and effects of oxygen and absorbent concentration

Due to the presence of oxygen, the oxidation of NO into NO_2 by oxygen in the gas phase is of interest. Furthermore, the change in readings between with and without two bubble columns of 400 mL deionized water was also important to interpret experimental results. Thus, flue gas streams with calculated NO concentrations between 195 and 1110 ppmv and oxygen from 2.0 to 8.1 % were validated by CAI 650 NOXYGEN gas analyzer.

As mentioned in Section 2.8, potassium iodide (KI), sodium persulphate ($Na_2S_5O_8$) and activated carbon (AC) had been tested as potential regeneration additives. Thus, they were chosen to be investigated in current study. Firstly, the regeneration performances of KI and $Na_2S_5O_8$ were tested, respectively. Then the effect of AC on absorbent regeneration was examined by the combinations (KI + AC) and ($Na_2S_5O_8$ + AC).

6.3 Results and Discussion

6.3.1 Validation of Gas Readings

Simulated flue gases with calculated NO concentrations from 195 to 1110 ppmv were checked at 2.0%, 5.0% and 8.0 oxygen, respectively. Firstly, they entered CAI 650 NOXYGEN gas analyzer through by-pass route after Koflo mixer. Later on, they were directed into the columns in series before flowing into gas analyzer.

Tables 6-1 to 4 show the comparison between calculated and measured oxygen and NO concentrations at different oxygen contents and cases. Specifically, **Figures 6-2 and 3** illustrate the NO readings at different oxygen for by-pass route and bubble column scenario. When the readings are taken without bubble columns (by-pass route), although the agreement is not as excellent as that given by absence of oxygen in **Table 5-2**, which is reproduced in **Table 6-1**, all the deviations are within -5%. As the difference increased with oxygen concentration, this divergence might be caused by the conversion of NO into NO_2 by oxygen since the conversion rate increases with oxygen concentration. Data collected with two bubble columns resulted in greater deviations in comparison with by-pass route. It means the bubble columns of 400 mL deionized water slightly affected the readings. But this effect was negligible at small oxygen concentrations, especially with the absence of oxygen, in which case the deviation was covered by repeatability. The measured oxygen concentration was mostly somewhat higher than the corresponding calculated value. Fortunately, results in this chapter are only presented qualitatively within the conditions tested herein.

Table 6-1: Readings of gas analyzer in absence of oxygen

Number	Flow rates		Calculated NO concentration (ppmv)	Measured NO concentration (ppmv)	
	NO ($mL \cdot min^{-1}$)	N_2 ($L \cdot min^{-1}$)		Without columns or By-pass *	With columns
1	23	2.86	203	201	205
2	35	2.85	308	307	304
3	47	2.85	412	411	408
4	58	2.84	508	505	504
5	69	2.83	605	605	597
6	82	2.82	718	717	709
7	94	2.83	817	815	808
8	105	2.83	909	906	895
9	117	2.84	1005	997	991
10	132	2.83	1132	1121	1117

* Please refer to Table 5-2

Table 6-2: Readings of gas analyzer with approximately 2% oxygen

Number	Flow rate			Calculated concentration		Measured concentration with by-pass		Measured concentration with columns	
	NO ($mL \cdot min^{-1}$)	N_2 ($L \cdot min^{-1}$)	O_2 ($mL \cdot min^{-1}$)	NO (ppmv)	O_2 (%)	NO (ppmv)	O_2 (%)	NO (ppmv)	O_2 (%)
1	23	2.91	58	195	2.0	196	2.1	196	2.2
2	36	2.90	58	305	2.0	305	2.1	301	2.2
3	48	2.89	58	407	2.0	407	2.1	400	2.2
4	60	2.88	58	508	2.0	504	2.1	497	2.2
5	72	2.87	58	609	2.0	606	2.1	600	2.2
6	83	2.86	58	702	2.0	696	2.1	685	2.2
7	94	2.85	58	795	2.0	787	2.1	772	2.2
8	105	2.83	58	891	2.0	875	2.1	870	2.2
9	117	2.82	58	992	2.0	977	2.1	962	2.2
10	129	2.81	58	1093	2.0	1078	2.1	1058	2.2

Table 6-3: Readings of gas analyzer with approximately 5% oxygen

Number	Flow rate			Calculated concentration		Measured concentration with by-pass		Measured concentration with columns	
	NO ($mL \cdot min^{-1}$)	N_2 ($L \cdot min^{-1}$)	O_2 ($mL \cdot min^{-1}$)	NO (ppmv)	O_2 (%)	NO (ppmv)	O_2 (%)	NO (ppmv)	O_2 (%)
1	23	2.82	149	195	5.0	188	5.2	186	5.4
2	35	2.81	149	297	5.0	294	5.3	286	5.3
3	47	2.80	149	398	5.0	393	5.3	383	5.3
4	59	2.79	149	500	5.0	491	5.4	479	5.4
5	71	2.78	149	601	5.0	593	5.4	577	5.4
6	83	2.77	149	702	5.0	692	5.4	670	5.4
7	95	2.75	149	806	5.0	789	5.4	765	5.4
8	107	2.74	149	907	5.0	888	5.4	858	5.4
9	119	2.73	149	1008	5.0	981	5.3	952	5.4
10	131	2.72	149	1109	5.0	1078	5.3	1040	5.3

Table 6-4: Readings of gas analyzer with approximately 8% oxygen

Number	Flow rate			Calculated concentration		Measured concentration with by-pass		Measured concentration with columns	
	NO ($mL \cdot min^{-1}$)	N_2 ($L \cdot min^{-1}$)	O_2 ($mL \cdot min^{-1}$)	NO (ppmv)	O_2 (%)	NO (ppmv)	O_2 (%)	NO (ppmv)	O_2 (%)
1	24	2.73	242	203	8.1	196	8.6	193	8.7
2	36	2.72	242	305	8.1	299	8.6	291	8.7
3	48	2.71	242	406	8.1	398	8.6	384	8.7
4	60	2.70	242	507	8.1	498	8.7	477	8.7
5	72	2.69	242	609	8.1	591	8.7	570	8.7
6	84	2.67	242	712	8.1	688	8.7	660	8.7
7	96	2.66	242	813	8.1	787	8.7	749	8.7
8	108	2.65	242	914	8.1	884	8.8	836	8.7
9	120	2.64	242	1015	8.1	977	8.8	920	8.7
10	132	2.63	242	1116	8.1	1075	8.8	1005	8.7

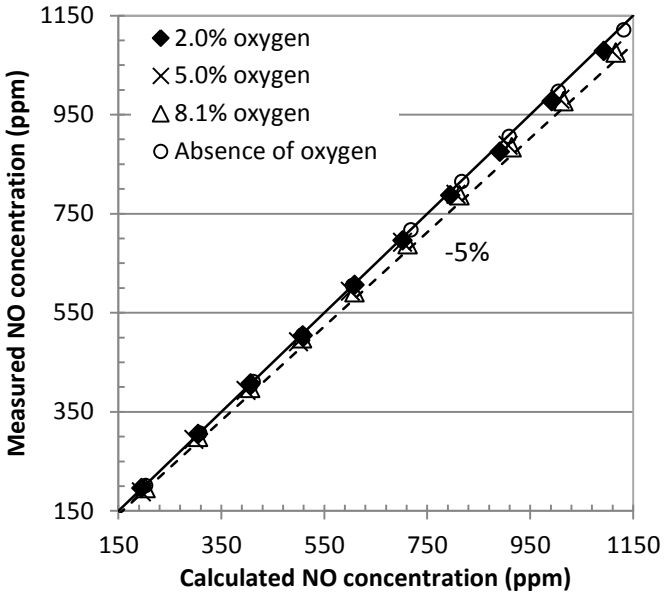

Figure 6-2: Parity plot of NO concentration at different oxygen concentrations through by-pass

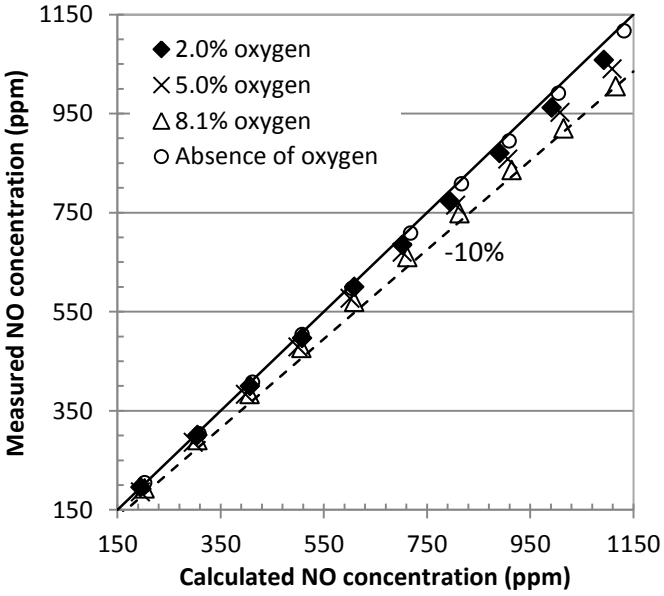

Figure 6-3: Parity plot of NO concentration at different O_2 concentrations with two columns

6.3.2 Regeneration by using Various Additives

Figure 6-4 depicts the regeneration of $Na_2S_5O_8$ at room temperature and KI at both room temperature and 325.2 K. The NO concentration was maintained at around 930 – 960 ppmv and oxygen 5.2% or so. It can be seen that $Na_2S_5O_8$ failed to function as a regeneration reagent; instead, it greatly reduced

the NO absorption efficiency. This was most likely due to the precipitation observed during the experiment. Considering the poor performance of $Na_2S_5O_8$, no further testing was conducted at 325.2 K.

As for KI, it did not contribute to absorbent regeneration either. In fact, the performances between conditions with and without KI were almost the same at room temperature, and the corresponding curves almost collapsed on each other. The divergence at the very beginning is probably attributable to instrument error. The CAI 650 NOXYGEN gas analyzer had a range of 3000 ppmv and repeatability of around 0.5% of full scale. Thus, the minor deviations could be covered. Even worse, at the higher temperature 325.2 K, the addition of KI impaired the absorption. All in all, KI or $Na_2S_5O_8$ alone did not work as an effective regeneration agent for the tests within this study.

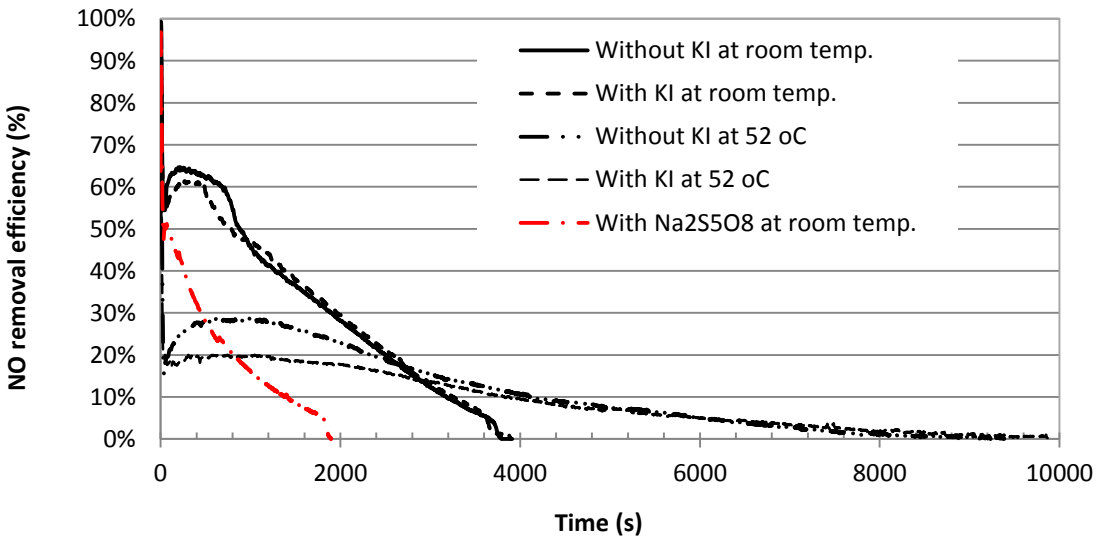

Figure 6-4: Regeneration performances of different additives at various temperatures

Further experimentations aiming at testing the combination of AC and $Na_2S_5O_8$ or AC and KI were also performed. For the combination of AC and $Na_2S_5O_8$, 1.02 g AC and 0.1780 g $Na_2S_5O_8$ were fed into the aqueous solution with 0.0075 mol·L^{-1} cobaltous ions and pH value of 9.8 after the absorption reached equilibrium. The mixture was then stirred on a magnetic stirrer for approximately 45 minutes. The corresponding results are shown in **Figure 6-5**; it can be seen that after addition of new agents the outlet NO concentration remained 949 ppmv, the same as the equilibrium NO before the addition. It indicates that the combination of AC and $Na_2S_5O_8$ failed to regenerate absorbents either.

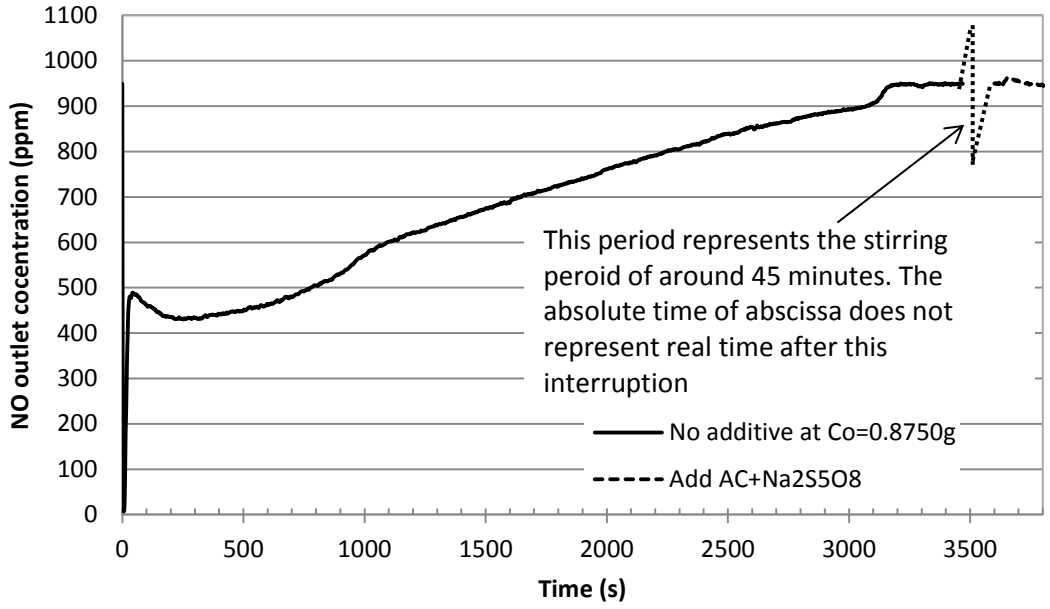

Figure 6-5: Regeneration test results by using combination of AC and $Na_2S_5O_8$

Similar test was also conducted to check the effectiveness of combination of AC and KI on absorbent regeneration. In this test, 8 g of AC was added into an absorbent system containing 0.010 $mol \cdot L^{-1}$ cobalt(II) nitrate and 0.0025 $mol \cdot L^{-1}$ KI at pH = 9.35 till the equilibrium of NO absorption. **Figure 6-6** shows the NO absorption with the use of combined AC and KI. Unfortunately, the concentration after addition remained almost unchanged from the equilibrium one, indicating that this combination did not contribute to regeneration immediately.

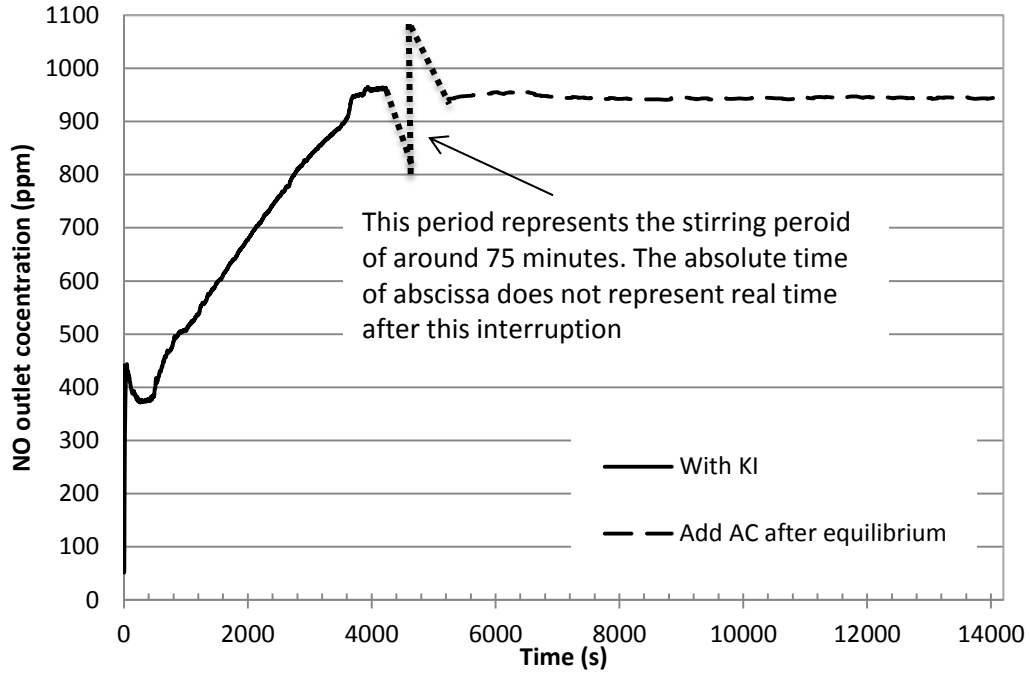

Figure 6-6: Regeneration by using combination of AC and KI

6.3.3 Effect of Oxygen on NO Removal Efficiency

Figure 6-7 shows the positive effect of oxygen on NO absorption using ammoniacal cobalt(II) ions. In order to compare the performance between each other, the flue gas flow rate remained at 3 $L \cdot min^{-1}$ and the pH value of the aqueous absorbent system maintained approximately 9.20. The inlet NO concentration varied between 900 and 1060 ppmv due to the adjustment of oxygen. Thus, it is more meaningful to compare NO reduction performances at different oxygen concentration in terms of absorption efficiency.

It can be seen that oxygen was helpful to NO absorption using ammoniacal cobaltous complexes as absorbents. 5% of oxygen could enhance the NO absorption at least 10 times than that without oxygen. As described in Section 3.2.1, penta- and hexa-amminecobalt(II) ions can react with oxygen to produce a diamagnetic salt of a binuclear cobalt complex ion, $[(NH_3)_5Co\text{-}O\text{-}O\text{-}Co(NH_3)_5]^{4+}$, which has a strong oxidizability that is very similar to that of hydrogen peroxide (H_2O_2). Thus, this diamagnetic complex reacts with the nitrosyl product $[(NH_3)_5Co\text{-}(NO)_2\text{-}Co(NH_3)_5]^{4+}$ to form a nitro complex, which might finally be transformed into soluble nitrate and nitrite [32].

The absorption of nitric oxide at an oxygen level of 2.1 % or higher seemed not different from that at 5% oxygen. It is likely because oxygen was excessively more than nitric oxide. NO was in the

order of 1000 ppmv, at least one order less than the oxygen concentration. According to stoichiometry, the ratio of NO to oxygen is 1:1; even 2% oxygen is 20 times greater than 1000 ppmv NO.

Furthermore, calculated amount of NO absorbed according to the integration of curve in **Figure 6-7** was nearly 0.003 mol, which responded to the summation of penta- and hexa-amminecobatl(II) at pH = 9.20 with original 0.01 mol·L^{-1} cobalt(II) in 400 mL aqueous solution. It indicates that with the amount of oxygen the reaction might be irreversible due to the reaction between nitrosyl product, $[(NH_3)_5Co\text{-}(NO)_2\text{-}Co(NH_3)_5]^{4+}$, and the binuclear cobalt complex ion, $[(NH_3)_5Co\text{-}O\text{-}O\text{-}Co(NH_3)_5]^{4+}$ at room temperature. In this case, there was nothing to do with regeneration. Probably that is why all the attempts to regenerations failed. In the future, regeneration can be tried again without oxygen.

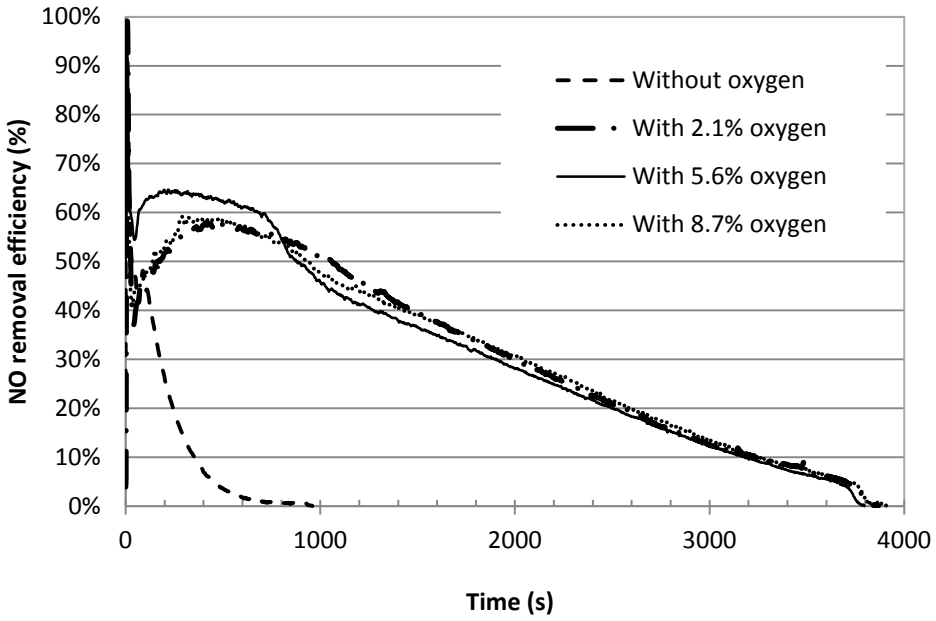

Figure 6-7: Effect of oxygen on NO absorption into ammoniacal cobalt(II) solutions

6.3.4 Effect of Absorbent Concentration on NO Removal Efficiency

Besides the effect of oxygen, the impact exerted by absorbent concentration is also investigated with the presence of approximately 5.5% oxygen. **Figure 6-8** shows the performance at different liquid concentrations. It can be seen that higher concentration gives better performance. And it responds again to the ammonia – cobalt(II) analysis. High pH value is in favor of the formation of cobalt

complexes with large coordination number, which are the effective reactants to NO absorption. When at the same pH value, as expected, the absorbent with concentration of 0.0075 mol·L^{-1} performs slightly inferior to 0.010 mol·L^{-1} system. And it is understandable that the best performance is given by the 0.050 mol·L^{-1} aqueous solvent.

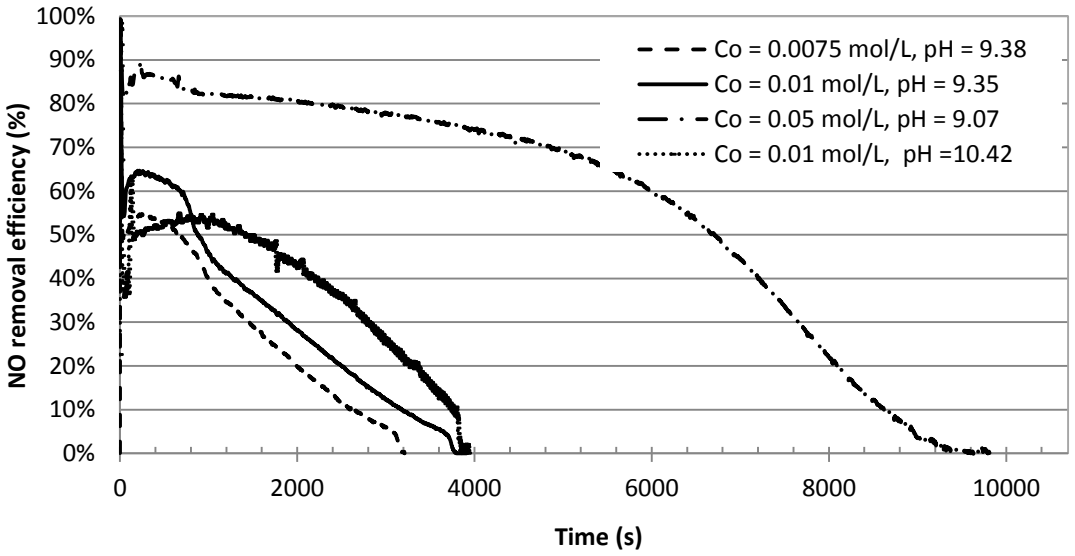

Figure 6-8: Effect of solvent concentration on NO absorption.

6.4 A Simple Economic Analysis

Based on the results in the previous chapters, a simple economic analysis is conducted to compare the capital cost between ammoniacal coalbt(II) solutions and its major competitor, Fe(II)-EDTA. As wet scrubber is expected to be employed for both absorbents, the comparison of operating costs of these two absorbents is the main subject of this economic analysis.

In this study, the ammoniacal cobalt(II) complexes were prepared by reaction between cobalt(II) nitrate hexahydrate ($Co(NO_3)_2 \cdot 6H_2O$) and aqueous solution ($NH_3 \cdot H_2O$). For the simplicity of comparison, it is assumed that adequate ammonia is added to make sure the product in the ammonia-cobalt(II) system is primarily hexa-amminecobalt(II) nitrate. And the overall reaction of the step reversible reactions summarized in the **Table 2-2** as shown in Reaction. 6.1 are used for analysis.

$$Co(NO_3)_2 + 6NH_3 \rightleftharpoons Co(NH_3)_6(NO_3)_2 \qquad (6.1)$$

Fe(II)-EDTA is usually produced by the reaction between ferrous sulfate heptahydrate ($FeSO_4 \cdot 7H_2O$) and ethylenediaminetetraacetic acid disodium salt dehydrate (EDTA-$Na_2 \cdot 2H_2O$).

$$FeSO_4 + EDTA - Na_2 \rightleftharpoons Fe(II) - EDTA + Na_2SO_4 \quad (6.2)$$

Assume that absorbent can be fully used to react with NO either by regeneration or with the presence of oxygen. According to stoichiometry in Reactions 2.9 and 4.2, 1 kmol of $Co(NH_3)_6(NO_3)_2$ or 1 kmol of $Fe(II) - EDTA$ is needed to react with 1 kmol of NO. Reactions 6.1 and 6.2 also show that for absorption of 1 kmol of NO, 1 kmol of $Co(NO_3)_2 \cdot 6H_2O$ and 6 kmol of NH_3 are required when using ammoniacal cobalt(II) solutions; 1 kmol of $FeSO_4 \cdot 7H_2O$ and 1 kmol of EDTA-$Na_2 \cdot 2H_2O$ are necessitated when using Fe(II)-EDTA. A sample price list of the chemicals is summarized in **Table 6-5**.

Table 6-5: Chemical expenses for the absorption of 1 kmol NO (absence of oxygen)

Absorbent	Chemical	Mass (t)	Price ($\$ \cdot t^{-1}$)	Expense (US $)	Manufacturer and Online Link
Fe(II)-EDTA	$FeSO_4 \cdot 7H_2O$	0.278	100	27.8	Tianjin Ruifengtiantai International Trade Co., Ltd. (http://rftt.en.alibaba.com/product/685724579-0/Ferrous_sulfate.html)
	EDTA-$Na_2 \cdot 2H_2O$	0.372	3000	1116.0	SJZ Chenghui Chemical Co., Ltd. (http://www.alibaba.com/product-gs/690656652/sale_product_EDTA_2NA_EDTA_disodium.html)
$Co(NH_3)_6(NO_3)_2$	$Co(NO_3)_2 \cdot 6H_2O$	0.291	550	160.1	Tianjin Ruifengtiantai International Trade Co., Ltd. (http://www.alibaba.com/product-gs/694390334/cobalt_nitrate.html)
	$NH_3 \cdot H_2O$ (30%)	0.210	400	280.0	Adinath Chemicals (http://www.alibaba.com/product-free/134926069/Aqueous_Ammonia.html)

It can be seen that for the absorption of 1 kmol of NO without presence of oxygen, the total chemical expenses of Fe(II)-EDTA and $Co(NH_3)_6(NO_3)_2$ are US$1143.8 and US$440.1, respectively. The chemical expense of Fe(II)-EDTA is 2.6 times greater than that of $Co(NH_3)_6(NO_3)_2$. However, the complete use of Fe(II)-EDTA is achieved by an extra regeneration reagent, while the presence of 5% oxygen can make the absorption reaction NO and ammoniacal cobalt(II) solutions irreversible and lead to full consumption of absorbent. The addition of regeneration agent further increases the operational cost of a system using Fe(II)-EDTA.

6.5 Summary

The presence of oxygen significantly enhanced the efficiency of NO absorption using ammoniacal cobalt(II) solutions. Calculated NO amount of absorbed into the aqueous solution showed that with the oxygen the absorption reaction could be considered as irreversible. This was probably the reason for the failure of regeneration of various reagents. A rough economic analysis showed that $Co(NH_3)_6(NO_3)_2$ cost less than Fe(II)-EDTA as a NO absorbent.

So far, the thesis work had been primarily focused on the fundamental study; it requires some attention placed onto the design and scale-up of industrial absorbers. As volumetric liquid-phase mass transfer coefficient, k_La, is a paramount parameter for gas-liquid contactors, the evaluation of k_La values in different absorbers was conducted and reported in the next Chapter.

Chapter 7
Mass Transfer in Industrial Gas-Liquid Contactors

7.1 Introduction

Before commercialization of the NO scrubbing technology introduced above, it is necessary to continue with the study of NO absorption in pilot-scale reactors. According to Astarita [85], the absorption rate of a gas-liquid reaction in a reactor is a function of volumetric liquid-phase mass transfer coefficient (k_La), gas solubility and reaction rate constant, etc. The reaction rate constant is invariable for a given absorbent. It means that the NO absorption performance is then greatly dependent upon the k_La value of the absorber, and a reactor with a high k_La value is desired.

As bubble column (BC) [93, 94], conventional stirred tank reactor (CSTR) [95-97] and gas-inducing agitated tank (GIAT) [98, 99] are well accepted as industrial absorbers, this chapter primarily focuses on the determination and comparison of k_La values of these three types of gas-liquid contactors. Extensive studies have been conducted to understand mass transfer coefficients in all these reactors; however, the results differed from researcher to researcher, making it necessary to select optimum correlations for k_La evaluation before performing NO absorption.

In this study, it is favorable to conveniently switch between different reactor types in order to compare their performances in a laboratory setting. The main body of the current gas-liquid contactor was a GIAT equipped with a 4-bladed straight turbine impeller. A porous median bubble generator was then added upstream of the main body to modify it from a GIAT to a BC or a CSTR. In conclusion, the unit worked as a GIAT without gas injection from the bubble generator. When inert gas was fed into the system, the unit either acted as a CSTR with agitation or functions as a BC without agitation. The entire system will be introduced in detail shortly in the experimental section. It is noteworthy that the main body was a square tank. Nevertheless, Akita and Yoshida [113] stated that in terms of mass transfer characteristic a square bubble column offered the same performance as a cylindrical one with an inner diameter that was equal to the side length of the square column. Similar findings have also been reported for CSTRs. Leentvaar and Ywema [114], Kresta et al. [115] and Yu and Tan [111] proved that satisfactory results regarding mixing performance would be given if taking the side length of a square tank as the "diameter". Thus, the shape effect on mass transfer coefficient was not considered in this study.

The removal or desorption of oxygen from water by using nitrogen bubbles was tested both continuously and semi-batch-wise to examine the applicability of proposed k_La correlations in

literature. They were applied in the mathematical modelling of degassing performance of different reactors and validated by experimental data.

7.2 Experimental

Figure 7-1 shows the laboratorial liquid degassing system, which could be switched between reactor types. This unit primarily comprised water and nitrogen supplies, a bubble generator and an acrylic GIAT degasser, two sampling points, vacuum system and meters and gauges. It could be operated continuously or batch-wise with respect to both phases at atmospheric pressure and room temperature. The picture of the main components of the degassing system is shown in **Figure 7-2**.

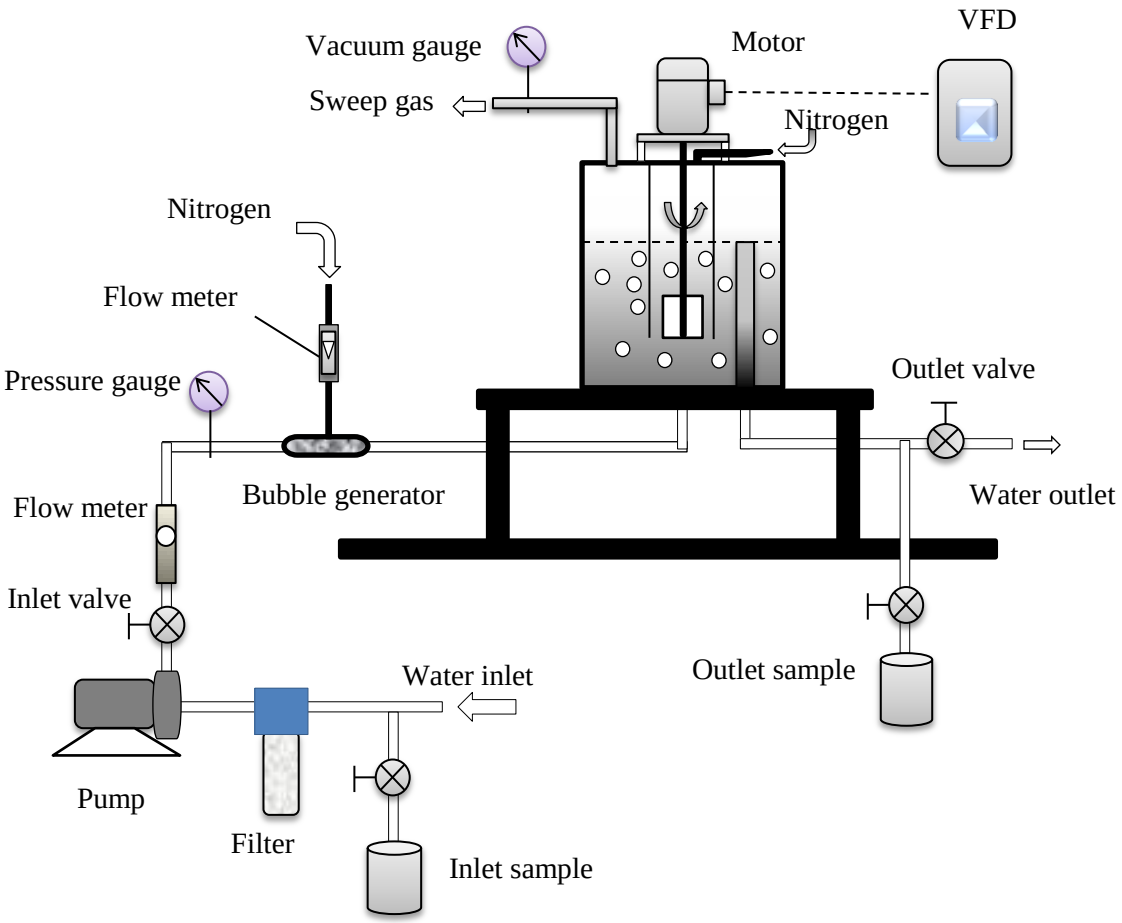

Figure 7-1: Experimental setup of the gas-liquid contactor system

Figure 7-2: Picture of the main fraction of degassing system

When the unit was operated in a continuous mode, water was first filtered to eliminate impurities before entering a water pump, which could be used when the tap water pressure was not high enough to reach the desired flow rate. The volumetric flow rate of water was set constant at 0.126 L/s by a vertical Cole-Parmer flow meter, followed by an Ashcroft pressure gauge. Nitrogen (99.5% from Praxair) bubbles were generated by a porous bubble generator (Model 7610-1/2-06-2-AB, Mott corporation). Purge nitrogen flow rate was regulated between 0 and 7.87 $\times 10^{-4}$ m^3/s by a gas flow meter from Cole-Parmer. Downstream the bubble generator, the aerated liquid traveled along a 0.4191m long PVC pipe of 25.4 mm inner diameter (ID) before it enters into an acrylic tank with dimensions of 457.2 mm $\times$ 406.4mm $\times$ 406.4mm (height $\times$ length $\times$ width) through an inlet at the bottom. The inside water level was maintained at 304.8 mm by a weir pipe of 50.8mm ID, and then 152.4mm was left as headspace. A DC motor equipped with a 4- bladed straight turbine impeller was centrally mounted on the top. This impeller had both diameter and vertical width of 101.6 mm. It was enclosed in a shrouded draft tube or stator perforated with 1.6mm or 9.5mm diameter holes and was submerged below liquid surface at 241.3mm. Agitation speed ranged from 0 to 16.7 Hz was adjusted

by a variable frequency drive (VFD). Therefore, the degasser acted as a GIAT without nitrogen injection. When nitrogen was fed into the system, the degasser either worked as a BC without mechanically agitation or functioned as a CSTR with stirring.

As a GIAT degasser, a shroud was used to allow for better induction of gas as it prevented froth accumulation on the free liquid surface. Due to the low pressure field created by impeller rotation, nitrogen entered the reactor from a gas inlet pipe on the top of the shroud. Meanwhile, gas-liquid interface was sheared by impeller blade when the forced vortex, which is also generated by impeller rotation, was sufficiently near the impeller, entrapping nitrogen bubbles and enabling the mixing of gas and liquid to occur. In a BC degasser, nitrogen gas was injected through the porous media bubble generator and present in the form of small bubbles, thereby giving a higher k_La value. It is noteworthy that there were two gas supplies to the CSTR degasser. One was the purge nitrogen injected through bubble generator; another was the nitrogen induced by impeller rotation.

With the nitrogen bubbles in the tank, dissolved oxygen diffused into the bubbles which float to the liquid surface and was released to headspace after burst of nitrogen bubbles and subsequently vacuumed out of the system through gas outlet. At the same time, degassed water continuously exited the tank from water outlet at the bottom. The concentrations of dissolved oxygen (DO) in water at both the inlet and outlet were analyzed by a Hach DO meter (Model WU-53013-10 from Cole-Parmer) with accuracy of ±1%. Three replicates were performed under a set condition to minimize experimental error. Then the experimental degassing efficiency was calculated as:

$$\eta = \frac{c_{Lin} - c_{Lout}}{c_{Lin}} \times 100\% \qquad (7.1)$$

where c_{Lin} = the dissolved oxygen in water at inlet, ppmm;

c_{Lout} = the dissolved oxygen in water at outlet, ppmm;

η = the efficiency of removal of dissolved oxygen from water, %.

Only CSTR system was operated in a batch-wise mode in order to determine the maximum oxygen removal efficiency as experimental results showed CSTR unit gave highest degassing efficiency. Shut off both inlet and outlet liquid valves after filling the agitated tank with filtered water. The purge nitrogen flow rate ranged from 3.93×10^{-4} to 5.90×10^{-4} m^3/s and agitation speed between 10.3 and 16.65 Hz. The water inside the tank was sampled and analyzed every minute initially and every 3-5 minutes later on over a 20-minute period. Corresponding degassing efficiency at different time was then calculated by using Eq. 7.1.

7.3 Mathematical Modeling

7.3.1 Continuous Bubble Degasser

Figure 7-3 is a simplified schematic diagram for the water de-oxygen unit. For simplification, the 17.78 cm long vertical pipe was treated as a horizontal one. Thus, the whole system was divided into a porous media bubble generator, a 41.91cm long horizontal pipeline with ID of 2.54cm and an acrylic GIAT mentioned previously.

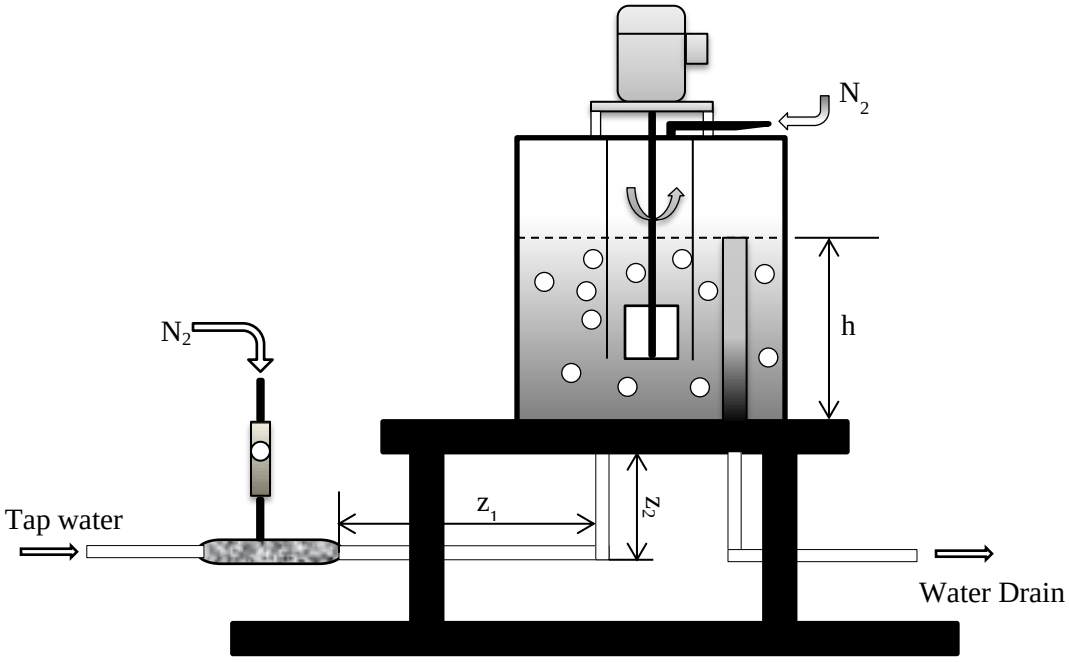

Figure 7-3: Schematic diagram for the continuous gas-liquid contactor

7.3.1.1 Degassing in a horizontal pipe

According to Mandhane et al [116], it is a stratified flow on the investigated superficial gas and liquid velocity ranges performed in current study. The ideal horizontal two-phase stratified flow is illustrated in **Figure 7-4**. Meanwhile, operational conditions such as superficial liquid and gas velocities and pipe diameter chosen for this degassing system fall into the applicable ranges used by Jepsen [122]; therefore, Eq. 2.38 is applicable to evaluate the horizontal pipe volumetric mass transfer

coefficient. The frictional energy dissipation, ϵ, of two-phase flow (TPF) in a horizontal pipe is expressed as

$$\epsilon = \left(\frac{dp}{dz}\right)_{TPF}(u_{SL} + u_{SG}) \tag{7.2}$$

where dp/dz = pressure drop per unit length of pipeline, Pa·m^{-1};

u_{sL} = superficial liquid velocity, m s^{-1};

u_{sG} = superficial gas velocity, m s^{-1}.

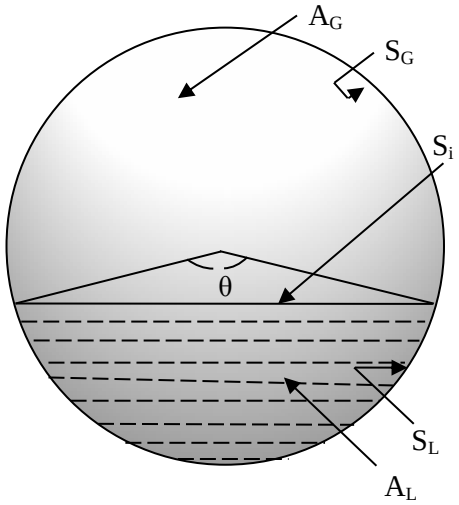

Figure 7-4: Ideal horizontal gas-liquid stratified flow

Based on **Figure 7-4**, imposing a force balance onto the liquid phase gives

$$(\frac{dp}{dz})_{TPF} = (\tau_{WL}S_L - \tau_i S_i)/A_L \tag{7.3}$$

in which

$$A_L = \frac{\pi}{4}(1 - \varepsilon_{Gp})d_p^2 \tag{7.4}$$

$$S_L = \frac{d_p}{2}\theta \tag{7.5}$$

$$S_i = d_p \sin(\frac{\theta}{2}) \tag{7.6}$$

where A_L = liquid-phase cross-sectional area, m^2;

d_p = horizontal pipe diameter, m;

S_i = interfacial perimeter, m;

S_L = liquid-phase perimeter, m;

ε_{GP} = gas holdup in the pipe, -;

Θ = subtended angle, rad;

τ_i = interfacial shear stress, Pa;

τ_{WL} = liquid-phase wall shear stress, Pa.

Gas holdup can be reliably estimated by Eq. 7.7 as below [118],

$$\varepsilon_{Gp} = 0.83[Q_G/(Q_G + Q_L)] \tag{7.7}$$

where Q_G = volumetric gas flow rate, $m^3 \cdot s^{-1}$;

Q_L = volumetric liquid flow rate, $m^3 \cdot s^{-1}$;

Then subtended angle, θ, shown in **Figure 7-4** is then calculated by solving Eq. 7.8 using Newton's method.

$$\theta - sin\theta - 2\pi(1 - \varepsilon_G) = 0 \tag{7.8}$$

Following the method suggested by Taital and Dukler [161], the shear stresses can be estimated as follows:

$$\tau_{WL} = f_L \frac{\rho_L u_{AL}^2}{2} \tag{7.9}$$

$$\tau_i = f_i \frac{\rho_G (u_{AG} - u_{AL})^2}{2} \tag{7.10}$$

in which

$$u_{AG} = u_{SG}/\varepsilon_G \tag{7.11}$$

$$u_{AL} = u_{SL}/(1 - \varepsilon_G) \tag{7.12}$$

where f_i = interfacial friction factor, -;

f_L = liquid friction factor, -;

u_{AG} = actual gas velocity, m s^{-1};

u_{AL} = actual liquid velocity, m s^{-1};

ρ_G = gas density, kg·m^{-3};

ρ_L = liquid density, kg·m^{-3}.

According to Spedding and Hand [162],

$$f_L = 0.0262[(1-\varepsilon_G)Re_{SL}]^{-0.139} \tag{7.13}$$

$$f_{SG} = 16/Re_{SG} \tag{7.14}$$

$$\frac{f_i}{f_{SG}} = 1.76\left(\frac{u_{SG}}{6}\right) + k_i \tag{7.15}$$

where Re = Reynolds number, -.

$$k_i = 2.7847\log_{10}(\frac{u_{SL}}{u_{SL}+6}) + 7.8035 \tag{7.16}$$

It is worthwhile to recall that a stratified flow can be obtained on the observed superficial gas and liquid velocity ranges under study based on flow map given by Mandhane et al. [116]. Assuming a plug flow was in the horizontal pipe and applying mass balance to the liquid phase in a differential element as shown in **Figure 7-5** provides

$$Q_L\frac{dc_{Lp}}{dz} = -k_L a_p\frac{\pi d_p^2}{4}(c_{Lp}-c_s) \tag{7.17}$$

where k_La_p = volumetric liquid-phase mass transfer coefficient in horizontal pipe, s^{-1};

c_{Lp} = concentration of dissolved gas in liquid in the pipe, mol·L^{-1};

c_s = saturated or interfacial concentration of dissolved gas in liquid in the pipe, mol·L^{-1};

z = axial distance, m.

The interfacial concentration cs in all cases can be evaluated by using Henry's Law and Ideal Gas Law,

$$c_s = \frac{c_G RT}{H} \tag{7.18}$$

where c_G = concentration of target gas in the gas phase, mol·L^{-1};

H = Henry's Law constant, L·atm·mol^{-1};

R = gas constant, = 0.08205 L·atm·K^{-1}·mol^{-1};

T = temperature, K.

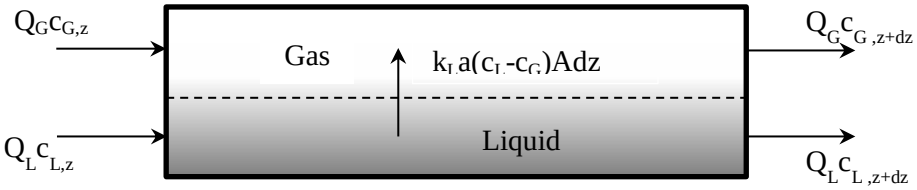

Figure 7-5: A differential element of the horizontal pipe

At steady state, mass conservation also gives

$$Q_G dc_{Gp} = -Q_L dc_{Lp} \tag{7.19}$$

Integrating Eq. 7.19 for $c_{Gp}=c_{Gin}$, when $c_{Lp}=c_{Lin}$,

$$c_{Gp} = \frac{Q_L}{Q_G}(c_{Lin} - c_{Lp}) + c_{Gin} \tag{7.20}$$

Because nitrogen gas cylinder used in present study was industrial purity 99.5% from Paraxair, it contained some contaminants which were mainly oxygen and rare argon. Assume the impurity was only oxygen and ideal gas law applies,

$$P_{O_2 in} = 0.5\%(P_A + \rho g h) \tag{7.21}$$

where g = gravitational acceleration, $m \cdot s^{-2}$;

h = liquid height, m;

P_A = atmospheric pressure, Pa;

$P_{O_2 in}$ = oxygen partial pressure at inlet, Pa.

Then,

$$c_{Gin} = P_{O_2 in}/RT \tag{7.22}$$

Substituting Eq.s 7.18 and 7.20 into 7.17 gives,

$$\frac{dc_{Lp}}{dz} = -\frac{k_L a_p \frac{\pi d_p^2}{4}}{Q_L}\left[c_L\left(1 + \frac{RTQ_L}{Q_G H}\right) - \frac{RT}{H}\left(\frac{Q_L}{Q_G}c_{Lin} + c_{Gin}\right)\right] \tag{7.23}$$

Further integration of Eq. 7.23 for $c_L=c_{Lin}$ at z=0 provides

$$c_{Lp}(z) = \frac{c_{Lin} - \frac{RT}{H}c_{Gin}}{1 + \frac{RTQ_L}{HQ_G}} e^{-\frac{\pi d_p^2 k_L a_p}{4Q_L}\left(1+\frac{RTQ_L}{HQ_G}\right)z} + \frac{\frac{RT}{H}\left(\frac{Q_L}{Q_G}c_{Lin} + c_{Gin}\right)}{1 + \frac{RTQ_L}{HQ_G}} \tag{7.24}$$

Thus, in current study, the DO concentration of water at z=0.4191m is the inlet DO concentration of subsequent stirring tank, c_{LTin}.

$$c_{LTin} = c_{Lp}(0.4191) \tag{7.25}$$

7.3.1.2 Degassing in the Stirring Vessel

When there was no purge nitrogen injected into the system, the degasser functioned as a GIAT. As mentioned above, nitrogen gas could not be induced into the vessel until the impeller speed reached critical speed, Ncr; that is to say, no evident degassing effectiveness was found before N_{cr}. According to Eqs. 2.31 and 2.37, it is known that N_{cr} is often greater than N_{cd}. Thus, it is reasonable to consider the gas and liquid phases to be perfect mixed when the degasser works at speeds above N_{cd}.

If extra nitrogen gas is fed into the system, the degasser is then a CSTR instead of a GIAT as generally the purge nitrogen ahead of tank is dominant, whose gas flow rate is much greater than the gas induction rate. As mentioned above, it is advisable to operate a CSTR at agitation speed above N_{cd} to fully utilize the reactor. Therefore, it is reasonable to assume a perfect mixing in a CSTR in practice.

It is justifiable to deem the gas-liquid contact in the stirring vessel as a perfect mixing regardless of nitrogen injection. At the steady state, mass balance of the tank gives

$$c_{Lout} = \frac{Q_L c_{LTin} + k_L a_T V_L c_{sT}}{Q_L + k_L a_T V_L} \tag{7.26}$$

where c_{Lout} = dissolved gas concentration at outlet, $mol \cdot L^{-1}$;

c_{LTin} = dissolved gas concentration at the inlet, $mol \cdot L^{-1}$;

c_{sT} = interfacial gas concentration in the reactor, $mol \cdot L^{-1}$;

$k_L a_T$ = volumetric liquid-phase mass transfer coefficient of reactor, s^{-1};

Q_L = volumetric liquid flow rate, $m^3 \cdot s^{-1}$;

V_L = liquid volume, m^3.

For simplicity assume that the interfacial concentration c_{sT} remains constant and it is equal to $c_s(0.4191)$, which can be calculated from Eqs. 7.18, 7.20 – 7.22 and 7.24. The value of $k_L a_T$ is

determined in terms of reactor type. k_La_{GI}, calculated by Eqs. 2.35 – 2.38, is used for GIAT type when no nitrogen gas is added. Caution is needed for the prediction of k_La_T for a CSTR in which purge nitrogen is injected through bubble generator because two nitrogen sources contribute to the superficial gas velocity. Not only is the nitrogen injected into the reactor, it is also induced into the system by impeller rotation. The superficial gas velocity then can be attained by

$$U_G = \frac{Q_G + Q_I}{d_T^2} \tag{7.27}$$

where d_T = stirring tank diameter, m;

Q_G = volumetric gas flow rate, $m^3 \cdot s^{-1}$;

Q_I = gas induction rate, $m^3 \cdot s^{-1}$;

U_G = superficial gas velocity, $m\ s^{-1}$.

Thus for a CSTR, $k_La_{C\,,}$ given by Eqs. 2.31, 2.34, 2.36 and 2.37, is substituted into Eq. 7.26. The overall degassing efficiency of the continuous degasser is expressed as

$$\eta_{con} = \frac{c_{Lin} - c_{Lout}}{c_{Lin}} \times 100 \tag{7.28}$$

7.3.1.3 Degassing in the Bubble Column

The main body of the degassing system becomes a square BC in the scenario where there is no mechanical agitation in the tank. As explained above, a square bubble column performs the same in terms of mass transfer as a cylindrical one with an I.D. equal to the side length of the square column. The complete mixing model and axial dispersion model (ADM) are two well-accepted models for the evaluation of a BC's performance [163]. In general, the performance of a BC can be better interpreted by ADM; however, for a column with small length to diameter ratio between 1 and 3, the gas-liquid complete mixing model is able to give satisfactory predictions [104]. In this study, the ratio was only 0.75; therefore, it is justified to make the assumption of gas-liquid complete mixing inside the BC. Then, Eq. 7.26 is also applicable to BC degasser by replacing k_La_T with k_La_B predicted by Eq. 2.28 with Deckwer's proposed constants [103] and the overall degassing efficiency is given by Eq. 7.28.

7.3.2 Semi-batch Bubble Degasser

Besides the continuous operational model, a semi-batch model is also established to examine the degassing capacity, interchangeable with upper limit of degassing efficiency, of a CSTR since it has the best performance. From the continuous reactor model, the contribution of the horizontal pipe is

relatively small compared to that of a CSTR, which will be elaborated in the next section. Therefore, it is reasonable to neglect the contribution of horizontal pipe when establishing the semi-batch degasser model.

In practice, the agitated tank is usually operated at a speed much higher than N_{cd}. It is feasible to assume ideal mixing for both phases in a GIAT and a negligible resistance of the gas phase to oxygen across the interface [164]. According to literature [165], the change in gas phase was also negligible attributable to the flushing of the original gas with the supplied gas and could be considered as steady state without triggering errors. Solute mass balance for both phases, thus, gives,

$$\frac{dc_L}{dt} = k_L a_{SB}(c_s - c_L) \tag{7.29}$$

$$Q_G(c_{Gin} - c_G) = k_L a_{SB} V_L(c_s - c_L) \tag{7.30}$$

where c_L = concentration of target gas in the liquid phase, mol·L^{-1};

c_s = interfacial concentration of target gas, mol·L^{-1};

c_G = concentration of target gas in the gas phase, mol·L^{-1};

c_{Gin} = concentration of target gas in the gas phase at inlet, mol·L^{-1};

$k_L a_{SB}$ = volumetric liquid-phase mass transfer coefficient of semi-batch reactor, s^{-1}.

V_L = liquid volume, m^3.

And c_s is computed by Eq. 7.18 and c_{Gin} by Eq.s 7.21 and 7.22. The expression of c_G in terms of c_L can be given by substituting Eq. 7.18 into Eq. 7.30,

$$c_G = \frac{k_L a_{SB} V_L c_L + Q_G c_{Gin}}{Q_G + k_L a_{SB} V_L \frac{RT}{H}} \tag{7.31}$$

Integrating Eq. 7.29 after substituting Eqs. 7.18 and 7.31 gives

$$c_L = \left(c_{Lin} - c_{Gin}\frac{RT}{H}\right) e^{-\frac{Q_G k_L a_{SB}}{Q_G + k_L a_{SB} V_L \frac{RT}{H}} t} + c_{Gin}\frac{RT}{H} \tag{7.32}$$

Then the degassing efficiency is presented as

$$\eta_{SB} = [1 - \frac{\left(c_{Lin} - c_{Gin}\frac{RT}{H}\right) e^{-\frac{Q_G k_L a_{SB}}{Q_G + k_L a_{SB} V_L \frac{RT}{H}} t} + c_{Gin}\frac{RT}{H}}{c_{Lin}}] \times 100 \tag{7.33}$$

7.4 Results and Discussion

7.4.1 Effect of Agitation Speed on Degassing Efficiency

In order to investigate the effect of agitation speed on the degassing efficiency, the degassing system was performed without and with nitrogen injection, respectively. The degassing unit was in fact operated in the GIAT mode without nitrogen injection. Because the critical impeller speed for the onset of gas induction, N_{cr}, is 6.94 Hz, it is meaningless to conduct investigation at speeds below N_{cr}. The agitation speed varies from 8.32 to 16.70 Hz. Besides, two shrouds perforated with 1.6 mm and 9.5 mm orifices are used in GIAT mode to see if orifice dimension has impact on degassing efficiency. After feeding nitrogen gas at $Q_G = 3.93 \times 10^{-4}$ m^3/s, the system turned into a CSTR. Since the N_{cd} calculated according to Eq. 4 was 6.14 Hz at this feeding rate, the observed impeller speed was, hence, set greater than 6 Hz to effectively use the unit. And the diameter of orifice in shroud for CSTR investigation was 9.5 mm.

Figure 7-6 shows the change of degassing efficiency with agitation speed in both cases. In a GIAT, the efficiency steadily increases with impeller speed and remains nearly unchanged after certain impeller speed. Additionally, the orifice dimension of shroud has no significant effect on degassing efficiency. This point is supported by many researchers [110, 166] who believed that volumetric liquid-phase mass transfer coefficient, k_La, is independent of disperser type and its orifice diameter as well. The k_La is a product of k_L and a, in which the variation in k_L is rather small and the change in k_La almost depends on the variation of specific interfacial area, which is highly related to bubble size [167]. Considerations based on forces affecting bubble size in turbulent regime show that the ultimate bubble diameter will be determined by turbulence intensity in the continuous phase caused by energy dissipated by mechanical agitation and is independent of orifice dimensions of disperser [167-169]. As bubble size and hence specific interfacial area depend on turbulence intensity, volumetric gas-liquid mass transfer coefficient is also dependent upon turbulence intensity[110]. Thus, it is reasonable that efficiency difference between these two shrouds is very small.

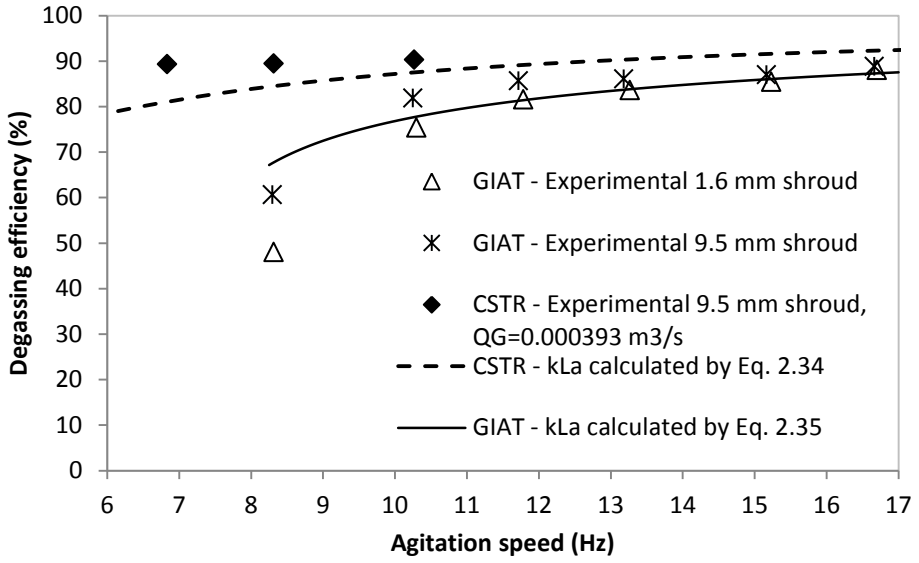

Figure 7-6: Effect of impeller speed on degassing efficiency in GIAT and CSTR

The combination of Eqs. 2.35 – 2.38 predicts degassing efficiency fairly well with the exception of the first point. This is because the correlation accepted for the estimation of gas induction rate is not suitable for the speed close to N_{cr}. The specific reason for this deviance is that at the beginning of gas induction, the gas is induced in the regions of the impeller where the fluid density is drastically reduced and the pressure driving force formed is much lower compared to in the absence of gas. Therefore, the actual value of the rate of gas induction is much lower than is predicted, resulting in overestimation of degassing efficiency which strongly depends on the gas induction rate [170]. Deviations of the other 5 predicted values are within ±5%.

As the effect of orifice size of a shroud is insignificant in a stirring vessel, no further comparison between different sizes will be conducted in a CSTR. The CSTR offers better performance than GIAT in terms of efficiency. However, its advantage over GIAT decreases as impeller speed increases and remained invariable. The variation in degassing efficiency is not evident in observed speed range. The degassing efficiency almost immediately reaches the maximum at the speed close to N_{cd} and remains unchanged. Although the agreement between Eq. 2.34 and related experimental data is not as excellent as the counterpart of the GIAT, the largest deviation is merely 9.3%, which is a satisfactory prediction.

Mechanical agitation is the largest contributor to energy consumption in this degassing unit and a higher speed requires more on quality of shaft material; thus, a speed slightly above N_{cd} is desired for a CSTR. Although a GIAT cannot work as efficient as a CSTR, it is preferred in dealing with hazardous gases due to the ability to complete utilize them [99]. More importantly, an acceptable efficiency can be attained at a moderately greater speed. From energy and economical perspectives, a

GIAT operated at a medium speed of about 10 Hz is also a suitable alternative for gas-liquid contact practice.

7.4.2 Effect of Purge Nitrogen Flow Rate on Degassing Efficiency

The effect of purge nitrogen flow rate was comprehensively observed both with and without mechanical agitation. Firstly, the unit was operated without agitation as a BC. Two types of gas sparger were applied in such module. The porous media bubble generator acted as a gas sparger if nitrogen was added prior to the main vessel. The second tested gas distributor was a multi-orifice sparger mounted at the bottom of the vessel. When the porous media bubble generator was used, the nitrogen gas was fed at flow rate between 1.97×10^{-4} and 9.83×10^{-4} m^3/s. As multi-orifice sparger was not as effective as porous media, higher nitrogen feeding rates ranged from 4.72×10^{-4} to 23.6×10^{-4} m^3/s were adopted. Then the degasser functioned as a CSTR with stirring at 10.3 Hz, in which the purge nitrogen gas was injected through the porous media bubble generator at rates varying between 1.97×10^{-4} and 7.87×10^{-4} m^3/s.

Figure 7-7 shows the degassing efficiencies of different reactors at various purge nitrogen volumetric flow rates. It can be seen that the gas sparger has a significant effect on degassing efficiency. The porous media distributor provides much better performance in comparison with multi-orifice type. For porous media, the efficiency dramatically increases from 24.7% to 69.4% as gas flow rate increases from 1.97×10^{-4} to 3.93×10^{-4} m^3/s, and steadily rose to 82% or so then levelled off. When it comes to multi-orifice design, the efficiency is approximately 20% less than that of porous media at the same rate. It gradually grows by 29.4% from 50.2 % to 79.6% in the gas flow rate interval between 4.72×10^{-4} and 23.6×10^{-4} m^3/s. This is mainly because the bubble size generated by porous media is smaller than that by orifice distributor, providing greater specific interfacial area. It is found that the CSTR rotating at 10.3 Hz gives highest efficiencies among investigated reactors. There is a slight increase of 5.7% over rates ranging from 1.97×10^{-4} to 7.87×10^{-4} m^3/s.

The predictions of the CSTR at N_I = 10.3 Hz given by model based on $k_L a_C$ calculated by Eq.2.32 match the experimental data rather well. The discrepancy is successfully limited to ±3.3 % or less. Unlike CSTR, BC's degassing performance is strongly related to sparger type. As far as less effective multi-orifice sparger is concerned, Eq. 2.28 developed by Akita and Yoshida [101] is accepted during modelling calculation. A good agreement with largest deviation of 10.7% can be found between predicted and experimental data. Porous media is well-acknowledged as an efficient gas distributor. Its mass transfer coefficient is usually evaluated by Eq.2.30. In this study, c_1=1.091 and c_2=0.8 proposed by Deckwer et al. [103] are used. The corresponding model then can predict most efficiency within ±9.1% of experimental data except for the first data point. This mismatch arises probably

because the first data point is collected at Q_G = 1.97 10^{-4} m^3/s, under which U_G =0.0012 m/s. It is out of the applicable superficial gas velocity range of Eq. 2.30, 0.0025 – 0.08 m/s. But interestingly, the first data point falls onto the curve drawn on the basis of Eq. 2.28, which is for inferior gas distributor. It means that at a lower gas flow rate, the porous media cannot be completely utilized and gas cannot be effectively distributed into the system. It functions as a simple orifice-type sparger. Thus, it is not suggested to work at lower gas flow rates for porous media.

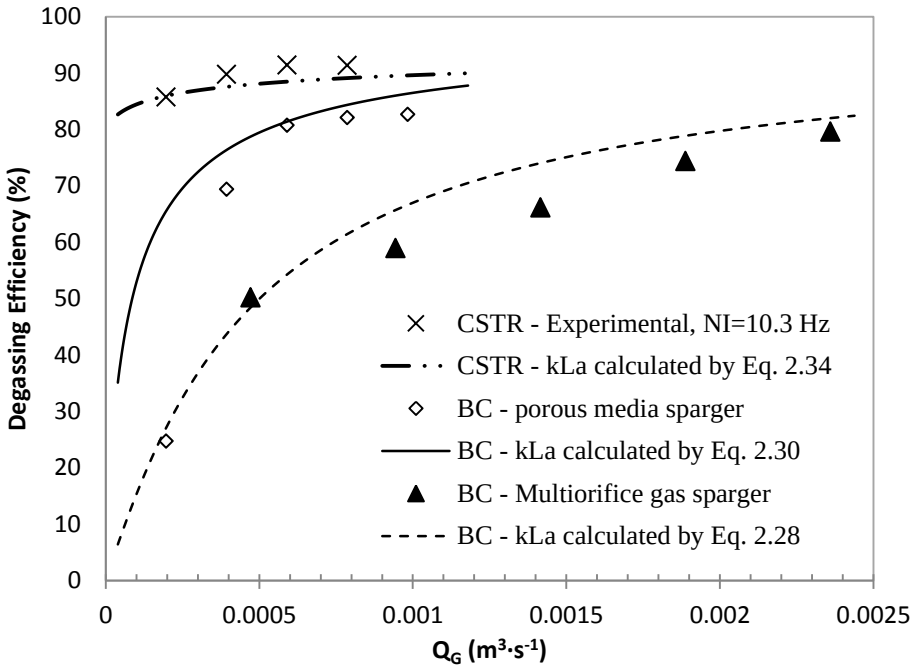

Figure 7-7: Effect of purge nitrogen flow rate on degassing efficiency for CSTR and BC

It is indicated that CSTR can afford best performance and its optimum gas flow rate can be set at around 3.93 $\times 10^{-4}$ m^3/s, beyond which the enhancement in degassing efficiency is minor. The BC equipped with orifice-type gas distributor is not recommended as its degassing efficiency is far less than the other two reactors. Although a BC with porous media sparger offers inferior results to a CSTR, it can achieve competitive efficiency, which is very close to that of a CSTR at a relatively higher gas flow rates. Considering advantages such as no movement part, less maintenance and footprint, efficient BCs performed at gas flow rates around 7.87 $\times 10^{-4}$ m^3/s are also of great energy-saving and practical significance, making them an ideal candidate for gas absorber.

7.4.3 Contribution of Pipe to Overall Continuous Degassing Performance

After evaluating the entire system with additional purge nitrogen injection, it is meaningful to identify the contribution of each section, namely the horizontal pipe and the square tank. This will provide useful information for further improvement, for example, the bubble generator location. In present research, the bubble generator is installed with a set distance of 0.4191m from the tank inlet due to plot limitation in the lab. According to mathematical model developed in section 7.2.1, the contribution of the horizontal pipe to the degassing efficiency is 2.46% under a typical operating condition of z = 0.4191 m, $Q_G = 3.93 \times 10^{-4}$ m^3/s, $Q_L = 1.26 \times 10^{-4}$ m^3/s. At this condition, the overall degassing efficiency is 76.34 % for a BC where there is no agitation and is 87.55% for a CSTR at N_I = 10.3 Hz. The ratio of the pipe contribution to overall efficiency is quite small in both reactors. Thus, a simplification by ignoring the horizontal part can be made without causing significant error in the semi-batch model.

7.4.4 Degassing Efficiency of A Semi-batch Reactor

Figure 7-8 shows the variation in degassing efficiency with residence time in a semi-batch bubble degasser where the unit is operated batchwise with respect to liquid phase while continuously with respect to gas phase. In order to verify its applicability, experimental observations obtained under two various conditions are used. The proposed model is able to fit data from both experimentations rather well; that is, the differentiations between predicted values by Eq. 7.33 and experimental results are within 9.1 % at $Q_G = 0.000393$ m^3/s and N_I=10.3 Hz and within 8.4 % with an exception of the first data point at $Q_G = 0.00059$ m^3/s and N_I = 16.65 Hz.

The degassing capacity, also known as upper limit of degassing efficiency depends on the purity of nitrogen gas utilized and initial dissolved oxygen concentration as well. For industrial nitrogen of 99.5% purity used in present study, a theoretical capacity of 97.57% with an ultimate liquid concentration of 0.236 ppmm can be achieved if initial dissolved oxygen concentration is 9.7 ppmm, whereas an experimental capacity of 92% with an ultimate liquid concentration of 0.72 ppmm is observed. This is probably due to the instrument error. The Hach DO meter used here has an accuracy of ±0.2 ppmm.

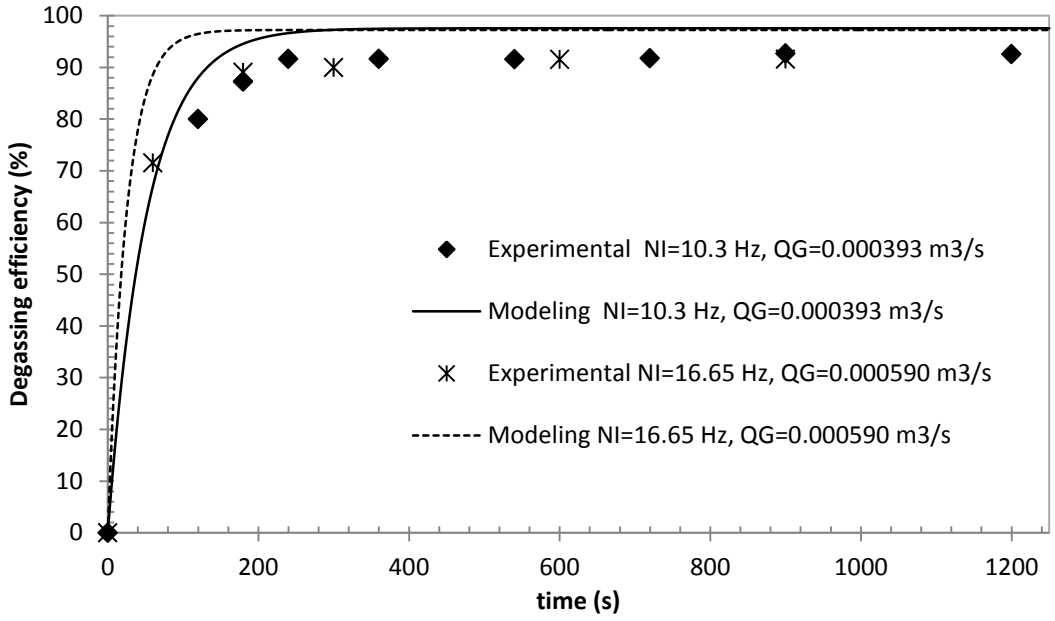

Figure 7-8: Degassing efficiency of the semi-batch degasser at different conditions

7.5 Summary

The mass transfer coefficient varying from reactor to reactor is the key to reactor design and scale-up. The continuous reactor model based on complete mixing assumption can satisfactorily interpret effects of parameters such as impeller speed and purge nitrogen flow rate within ±10 % for all three types of reactor. The semi-batch model evaluates the degasser performance within 9.1% at Q_G = 0.000393 m^3/s and N_I=10.3 Hz and within 8.4% except for the first data point at Q_G = 0.00059 m^3/s and N_I = 16.65 Hz.

The CSTR reactor affords better performance than GIAT and BC do. A speed slightly above N_{cd} and a gas flow rate around 3.93 $\times 10^{-4}$ m^3/s are desired for a CSTR in practice. However, due to the ability to completely absorb hazardous gases, a GIAT operated at a medium speed of about 10 Hz is also a suitable alternative for gas-liquid contactor. Furthermore, BCs equipped with porous media spargers at gas flow rates around 7.87 $\times 10^{-4}$ m^3/s are also of great energy-saving and practical significance as an ideal candidate of degassing technology on account of their unique advantages such as no movement part, less maintenance and footprint.

Eventually following correlations have been proven to be applicable to current study.

1) For CSTR:

$$k_L a_C = 1.59\left(\frac{N_I}{N_{cd}}\right)^{1.342} U_G^{0.93}\left(\frac{d_T}{d_I}\right)^{0.415} \tag{7.34}$$

2) For GIAT:

$$k_L a_{GI} = 1.212\left(\frac{P_c}{V_L}\right)^{0.0816}\left(\frac{Q_I}{d_T^2}\right)^{0.692}\left(\frac{s}{d_T}\right)^{-0.390} \tag{7.35}$$

3a) For BC equipped with efficient gas sparger:

$$k_L a_B = 1.091 U_G^{0.8} \tag{7.36}$$

3b) For BC equipped with simple gas sparger:

$$\frac{k_L a_B d_T^2}{D_L} = 0.6\left(\frac{\nu_L}{D_L}\right)^{0.5}\left(\frac{g d_T^2 \rho_L}{\sigma_L}\right)^{0.62}\left(\frac{g d_T^3}{\nu_L^2}\right)^{0.31}\varepsilon_G^{1.1} \tag{7.37}$$

Chapter 8
Conclusions and Future Work

8.1 Conclusions

The selection of an ideal absorbent for NO absorption rests primarily on a compromise of three points: (1) ability to react with inactive nitric oxide (NO), (2) ease of regeneration or complete utilization of absorbent and (3) zero or even positive effect of oxygen. Based on the work in this study, ammoniacal cobalt(II) system was found to be a better candidate than Fe(II)-EDTA and H_2O_2 in terms of NO removal efficiency. The NO removal efficiency of ammoniacal cobalt(II) system was highly affected by operating conditions such as temperature, pH value and initial solvent concentration. It decreased with the increase of temperature, and rose to the maximum then levelled off as pH value and concentration of absorbent increased. The highest initial NO removal efficiency of 96.45% corresponds to the inlet flow rate of 500 mL·min^{-1}, the temperature of 292.2 K, the pH value of 10.5, and the concentrations of $[Co(NH_3)_6]^{2+}$, NO and O_2 of 0.06 mol·L^{-1}, 500 ppmv and 5.0%, respectively.

The analysis of cobalt (II) – ammonia system for solutions containing cobalt (II) nitrate, ammonium hydroxide and 2 mol·L^{-1} ammonium nitrate was reviewed and introduced in the equilibrium study. The characteristics of reactions between nitric oxide and ammoniacal cobalt (II) complexes were analyzed through the molecular structure of corresponding nitrosyl. It was validated that only penta- and hexa-amminecobalt (II) complexes could react with NO as shown in Reactions 4.1 and 4.2.

$$2NO + 2[Co(NH_3)_5]^{2+} \rightleftharpoons [Co(NH_3)_5N_2O_2(NH_3)_5Co]^{4+} \quad (4.1)$$

$$2NO + 2[Co(NH_3)_6]^{2+} \rightleftharpoons [Co(NH_3)_5N_2O_2(NH_3)_5Co]^{4+} + 2NH_3 \quad (4.2)$$

The equilibrium constants of such reactions were determined. K_{NO}^5 had an order of magnitude of 10^{12} and K_{NO}^6 of 10^{13}. All experimental data fitted Eqs. 4.26 and 4.27 well.

$$K_{NO}^5 = 1.90 \times 10^7 \exp(\frac{3598.5}{T}) \quad (4.26)$$

$$K_{NO}^6 = 3.56 \times 10^{11} \exp(\frac{1476.4}{T}) \quad (4.27)$$

Kinetics of NO absorption into ammoniacal cobalt(II) solutions were studied in a home-made double-stirred reactor. The reaction rate constants of Reactions 4.1 and 4.2 were calculated based on the enhancement factor derived for gas absorption accompanied by parallel chemical reactions. Both

reactions were first order with respect to NO and first order with respect to liquid absorbent. The forward reaction rate constants of Reactions 4.1 and 4.2 were 6.43×10^6 and 1.00×10^7 $L\cdot mol^{-1}\cdot s^{-1}$, respectively, at 298.2 K, and increased to 7.57×10^6 and 1.12×10^7 $L\cdot mol^{-1}\cdot s^{-1}$, respectively, at 303.2 K

All attempts at regeneration of used absorbent failed under room temperature and atmospheric pressure. Oxygen in flue gas was found to have positive effect on NO absorption using ammoniacal cobalt(II) solutions. Calculated NO amount absorbed into the aqueous solution showed that with the oxygen the absorption reaction could be considered as irreversible. This was probably the reason for the failure of regeneration of various reagents. In addition, a simple economic analysis showed that $Co(NH_3)_6(NO_3)_2$ was of economic superiority to Fe(II)-EDTA as a NO absorbent.

Lastly, correlations for estimate of k_La values in some popular industrial absorbers such as bubble column (BC), conventional stirred tank reactor (CSTR) and gas-inducing agitated tank (GIAT) were determined through modeling removal of dissolved oxygen from water. The continuous reactor model based on complete mixing assumption could satisfactorily interpret effects of parameters such as impeller speed and purge nitrogen flow rate within ±10 % for all three types of reactors. The semi-batch model evaluated the degasser performance within 9.1% at Q_G = 393 cm^3/s and N_I=10.3 Hz and within 8.4% except for the first data point at Q_G = 590 cm^3/s and N_I = 16.65 Hz.

The CSTR reactor performed better than GIAT and BC did. A speed slightly above N_{cd} and a gas flow rate around 393 cm^3/s were desired for a CSTR in practice. However, due to the ability to completely absorb hazardous gases, a GIAT operated at a medium speed of about 10 Hz was believed to be a suitable alternative for gas-liquid contactor. Furthermore, BCs equipped with porous media spargers at gas flow rates around 787 cm^3/s were also of great energy-saving and practical significance as an alternative candidate for the unique advantages such as no movement part, less maintenance and small footprint.

Eventually the following correlations have been proven to be applicable to current study.

1) For CSTR:

$$k_La_C = 1.59\left(\frac{N_I}{N_{cd}}\right)^{1.342} U_G^{0.93}\left(\frac{d_T}{d_I}\right)^{0.415} \tag{7.34}$$

2) For GIAT:

$$k_La_{GI} = 1.212\left(\frac{P_c}{V_L}\right)^{0.0816}\left(\frac{Q_I}{d_T^2}\right)^{0.692}\left(\frac{s}{d_T}\right)^{-0.390} \tag{7.35}$$

3a) For BC equipped with efficient gas sparger:

$$k_L a_B = 1.091 U_G^{0.8} \tag{7.36}$$

3b) For BC equipped with simple gas sparger:

$$\frac{k_L a_B d_T^2}{D_L} = 0.6\left(\frac{\nu_L}{D_L}\right)^{0.5}\left(\frac{g d_T^2 \rho_L}{\sigma_L}\right)^{0.62}\left(\frac{g d_T^3}{\nu_L^2}\right)^{0.31}\varepsilon_G^{1.1} \tag{7.37}$$

8.2 Recommendations for Future Work

Motivated by simultaneous absorption of NOx and SO2 using wet scrubbing, this thesis project primarily focused on the mechanism of NO absorption into ammoniacal cobalt(II) solutions, the experimental investigation of effect of oxygen on NO absorption and the determination of mass transfer coefficients for several industrial absorbers. Future work should focus on understanding the effects of other co-existing air pollutant such as CO_2 and SO_2 on NOx absorption. Specific recommendations are summarized as follows.

Firstly, detailed qualitative and quantitative analyses of used absorbent by using analytic facilities such as HPLC, liquid-phase FTIR and Ion Chromatograph are necessitated to clarify the uncertainty that lingers over the fact of reaction between the nitrosyl product, $[Co(NH_3)_5N_2O_2(NH_3)_5Co]^{4+}$, and the binuclear cobalt complex ion, $[(NH_3)_5Co\text{-}O\text{-}O\text{-}Co(NH_3)_5]^{4+}$. With the knowledge of ultimate compound composition in the used liquid, the picture of reaction path can be clear. Furthermore, such information is quite important to the liquid disposal and treatment in practice.

Secondly, the simultaneous removal of SO_2 and NO using ammoniacal cobaltous ions deserves more attention. The ability to simultaneously absorb SO_2 and NO will allow us to utilize the existing FGD scrubbers that are commonly accepted in numerous industrial practices, thereby making this approach competitive. Although experimental findings in literature showed that the presence of SO_2 led to enhancement in NO absorption. However, the mechanisms behind this behavior remain unknown. In order to fill in this gap, investigations would be first performed in the scenario of SO_2 absorption alone following the methodology described in this thesis to acquire paramount parameters like equilibrium constants and reaction rate constants. Then extensive observations can be extended to the co-existence of CO_2, SO_2 and NO.

In the far future, with the acquisition of knowledge accumulated using simulated flue gas containing SO_2, oxygen and NO_x, the pilot tests can be conducted using real flue gases. And considerable field experimentations and accumulated industrial experiences will be useful in evaluating the commercialization of this technology.

Permissions

P. 1 Permission from Elsevier

ELSEVIER LICENSE
TERMS AND CONDITIONS

Jan 18, 2013

This is a License Agreement between Hesheng Yu ("You") and Elsevier ("Elsevier") provided by Copyright Clearance Center ("CCC"). The license consists of your order details, the terms and conditions provided by Elsevier, and the payment terms and conditions.

All payments must be made in full to CCC. For payment instructions, please see information listed at the bottom of this form.

Supplier	Elsevier Limited The Boulevard,Langford Lane Kidlington,Oxford,OX5 1GB,UK
Registered Company Number	1982084
Customer name	Hesheng Yu
Customer address	B1-01 Waterloo, ON N2L 3X1
License number	2911400961852
License date	May 17, 2012
Licensed content publisher	Elsevier
Licensed content publication	Applied Energy
Licensed content title	Absorption of nitric oxide from simulated flue gas using different absorbents at room temperature and atmospheric pressure
Licensed content author	Hesheng Yu,Qunyi Zhu,Zhongchao Tan
Licensed content date	May 2012
Licensed content volume number	93
Licensed content issue number	
Number of pages	6
Start Page	53
End Page	58
Type of Use	reuse in a thesis/dissertation
Portion	full article
Format	both print and electronic
Are you the author of this Elsevier article?	Yes

Will you be translating?	No
Order reference number	
Title of your thesis/dissertation	Absorption of Nitric Oxide from Flue Gas Using Ammoniacal Cobalt(II) Solutions in a Spray Tower
Expected completion date	Oct 2012
Estimated size (number of pages)	180
Elsevier VAT number	GB 494 6272 12
Permissions price	0.00 USD
VAT/Local Sales Tax	0.0 USD / 0.0 GBP
Total	0.00 USD
Terms and Conditions	

INTRODUCTION

1. The publisher for this copyrighted material is Elsevier. By clicking "accept" in connection with completing this licensing transaction, you agree that the following terms and conditions apply to this transaction (along with the Billing and Payment terms and conditions established by Copyright Clearance Center, Inc. ("CCC"), at the time that you opened your Rightslink account and that are available at any time at http://myaccount.copyright.com).

GENERAL TERMS

2. Elsevier hereby grants you permission to reproduce the aforementioned material subject to the terms and conditions indicated.

3. Acknowledgement: If any part of the material to be used (for example, figures) has appeared in our publication with credit or acknowledgement to another source, permission must also be sought from that source. If such permission is not obtained then that material may not be included in your publication/copies. Suitable acknowledgement to the source must be made, either as a footnote or in a reference list at the end of your publication, as follows:

"Reprinted from Publication title, Vol /edition number, Author(s), Title of article / title of chapter, Pages No.,

Copyright (Year), with permission from Elsevier [OR APPLICABLE SOCIETY COPYRIGHT OWNER]." Also Lancet special credit - "Reprinted from The Lancet, Vol. number, Author(s), Title of article, Pages No., Copyright (Year), with permission from Elsevier."

4. Reproduction of this material is confined to the purpose and/or media for which permission is hereby given.

5. Altering/Modifying Material: Not Permitted. However figures and illustrations may be altered/adapted minimally to serve your work. Any other abbreviations, additions, deletions and/or any other alterations shall be made only with prior written authorization of Elsevier Ltd. (Please contact Elsevier at permissions@elsevier.com)

6. If the permission fee for the requested use of our material is waived in this instance, please be advised that your future requests for Elsevier materials may attract a fee.

7. Reservation of Rights: Publisher reserves all rights not specifically granted in the combination of (i) the license details provided by you and accepted in the course of this licensing transaction, (ii) these terms and conditions and (iii) CCC's Billing and Payment terms and conditions.

8. License Contingent Upon Payment: While you may exercise the rights licensed immediately upon issuance of the license at the end of the licensing process for the transaction, provided that you have disclosed complete and accurate details of your proposed use, no license is finally effective unless and until full payment is received from you (either by publisher or by CCC) as provided in CCC's Billing and Payment terms and conditions. If full payment is not received on a timely basis, then any license preliminarily granted shall be deemed automatically revoked and shall be void as if never granted. Further, in the event that you breach any of these terms and conditions or any of CCC's Billing and Payment terms and conditions, the

license is automatically revoked and shall be void as if never granted. Use of materials as described in a revoked license, as well as any use of the materials beyond the scope of an unrevoked license, may constitute copyright infringement and publisher reserves the right to take any and all action to protect its copyright in the materials.

9. Warranties: Publisher makes no representations or warranties with respect to the licensed material.

10. Indemnity: You hereby indemnify and agree to hold harmless publisher and CCC, and their respective officers, directors, employees and agents, from and against any and all claims arising out of your use of the licensed material other than as specifically authorized pursuant to this license.

11. No Transfer of License: This license is personal to you and may not be sublicensed, assigned, or transferred by you to any other person without publisher's written permission.

12. No Amendment Except in Writing: This license may not be amended except in a writing signed by both parties (or, in the case of publisher, by CCC on publisher's behalf).

13. Objection to Contrary Terms: Publisher hereby objects to any terms contained in any purchase order, acknowledgment, check endorsement or other writing prepared by you, which terms are inconsistent with these terms and conditions or CCC's Billing and Payment terms and conditions. These terms and conditions, together with CCC's Billing and Payment terms and conditions (which are incorporated herein), comprise the entire agreement between you and publisher (and CCC) concerning this licensing transaction. In the event of any conflict between your obligations established by these terms and conditions and those established by CCC's Billing and Payment terms and conditions, these terms and conditions shall control.

14. Revocation: Elsevier or Copyright Clearance Center may

deny the permissions described in this License at their sole discretion, for any reason or no reason, with a full refund payable to you. Notice of such denial will be made using the contact information provided by you. Failure to receive such notice will not alter or invalidate the denial. In no event will Elsevier or Copyright Clearance Center be responsible or liable for any costs, expenses or damage incurred by you as a result of a denial of your permission request, other than a refund of the amount(s) paid by you to Elsevier and/or Copyright Clearance Center for denied permissions.

LIMITED LICENSE

The following terms and conditions apply only to specific license types:

15. Translation: This permission is granted for non-exclusive world English rights only unless your license was granted for translation rights. If you licensed translation rights you may only translate this content into the languages you requested. A professional translator must perform all translations and reproduce the content word for word preserving the integrity of the article. If this license is to re-use 1 or 2 figures then permission is granted for non-exclusive world rights in all languages.

16. Website: The following terms and conditions apply to electronic reserve and author websites:
Electronic reserve: If licensed material is to be posted to website, the web site is to be password-protected and made available only to bona fide students registered on a relevant course if:
This license was made in connection with a course,
This permission is granted for 1 year only. You may obtain a license for future website posting,
All content posted to the web site must maintain the copyright information line on the bottom of each image,
A hyper-text must be included to the Homepage of the journal from which you are licensing at

http://www.sciencedirect.com/science/journal/xxxxx or the Elsevier homepage for books at http://www.elsevier.com , and
Central Storage: This license does not include permission for a scanned version of the material to be stored in a central repository such as that provided by Heron/XanEdu.

17. Author website for journals with the following additional clauses:

All content posted to the web site must maintain the copyright information line on the bottom of each image, and the permission granted is limited to the personal version of your paper. You are not allowed to download and post the published electronic version of your article (whether PDF or HTML, proof or final version), nor may you scan the printed edition to create an electronic version. A hyper-text must be included to the Homepage of the journal from which you are licensing at http://www.sciencedirect.com/science/journal/xxxxx . As part of our normal production process, you will receive an e-mail notice when your article appears on Elsevier's online service ScienceDirect (www.sciencedirect.com). That e-mail will include the article's Digital Object Identifier (DOI). This number provides the electronic link to the published article and should be included in the posting of your personal version. We ask that you wait until you receive this e-mail and have the DOI to do any posting.

Central Storage: This license does not include permission for a scanned version of the material to be stored in a central repository such as that provided by Heron/XanEdu.

18. Author website for books with the following additional clauses:
Authors are permitted to place a brief summary of their work online only.
A hyper-text must be included to the Elsevier homepage at http://www.elsevier.com . All content posted to the web

site must maintain the copyright information line on the bottom of each image. You are not allowed to download and post the published electronic version of your chapter, nor may you scan the printed edition to create an electronic version.

Central Storage: This license does not include permission for a scanned version of the material to be stored in a central repository such as that provided by Heron/XanEdu.

19. Website (regular and for author): A hyper-text must be included to the Homepage of the journal from which you are licensing at http://www.sciencedirect.com/science/journal/xxxxx. or for books to the Elsevier homepage at http://www.elsevier.com

20. Thesis/Dissertation: If your license is for use in a thesis/dissertation your thesis may be submitted to your institution in either print or electronic form. Should your thesis be published commercially, please reapply for permission. These requirements include permission for the Library and Archives of Canada to supply single copies, on demand, of the complete thesis and include permission for UMI to supply single copies, on demand, of the complete thesis. Should your thesis be published commercially, please reapply for permission.

21. Other Conditions:

v1.6

If you would like to pay for this license now, please remit this license along with your payment made payable to "COPYRIGHT CLEARANCE CENTER" otherwise you will be invoiced within 48 hours of the license date. Payment should be in the form of a check or money order referencing your account number and this invoice number RLNK500781440. Once you receive your invoice for this order, you may pay your invoice by credit card. Please follow instructions provided at that time.

Make Payment To:
Copyright Clearance Center
Dept 001
P.O. Box 843006
Boston, MA 02284-3006

For suggestions or comments regarding this order, contact RightsLink Customer Support:

customercare@copyright.com or +1-877-622-5543 (toll free in the US) or +1-978-646-2777.

Gratis licenses (referencing $0 in the Total field) are free. Please retain this printable license for your reference. No payment is required.

P. 2 Permission from DE GRUYTER

Hesheng Yu

From: tiziana.ziesing@degruyter.com on behalf of rights@degruyter.com
Sent: January-03-13 5:39 AM
To: h48yu@uwaterloo.ca
Subject: AW: Request copyright of my publication in De Gruyter

Follow Up Flag: Follow up
Flag Status: Flagged

Dear Hesheng Yu,

Thank you for your permission request and your interest in reprinting the mentioned article
We would not object to the reprint In your doctoral dissertation, provided that full credit is given to the original source and the publisher de Gruyter, that the dissertation is not made available as open access and that you refer to the availability of the Journal article on our online platform www.degruyter.com.

Please notice that our permission is granted for the mentioned use only.
We wish you all the best for your dissertation and its publication.

With kind regards
Anne Reuter

Anne Reuter
Rights & Licenses

DE GRUYTER
Mies-van-der-Rohe-Straße 1
80807 München, Germany
T +49 (0)89.76902-474
F +49 (0)89.76902-350
anne.reuter@degruyter.com
www.degruyter.com

Von: Hesheng Yu [mailto:h48yu@uwaterloo.ca]
Gesendet: Dienstag, 27. November 2012 17:51
An: Degruyter, Rechte
Betreff: Request copyright of my publication in De Gruyter

1

Dear Sir or Madam,

My name is Hesheng Yu, a PhD student at the University of Waterloo in Canada. I am preparing for my PhD dissertation entitled "Absorption of Nitric Oxide from Flue Gas Using Ammoniacal Cobalt(II) Solutions", and planning to incorporate my publication with title of "New Correlations of Volumetric Liquid-Phase Mass Transfer Coefficients in Gas-Inducing Agitated Tank Reactors" in your International Journal of Chemical Reactor Engineering into the dissertation.

Therefore, I am writing to request permission of 100% use of my publised work. Please find the attached copyright request form and review.
Thank you very much for your time and consideration.

Regards,
Hesheng

Hesheng Yu
PhD candidate
Department of Mechanical & Mechatronics Engineering
University of Waterloo
Mailing address: ERC-3024, 200 University Ave. W., Waterloo, ON , N2L 3G1
Office: (519) 888-4567 ext. 38723
Cell: (519) 807-8927

References

1. U.S. EPA, *Control techniques for nitrogen oxides emissions from stationary sources - revised second edition*, U.S. EPA, Editor. 1983: Washington.
2. U.S. EPA, *Nitrogen oxides (NOx), why and how they are controlled*, U.S. EPA, Editor. 1999: North Carolina.
3. Abu-Ramadan, E., K. Saha, and X.G. Li, *Modeling the depleting mechanism of urea-water-solution droplet for automotive selective catalytic reduction systems.* AIChe Journal, 2011. **57**(11): p. 3210-3225.
4. Visakhamoorthy, S., Tzanetakis, T., Haggith. D., Sobiesiak, A., and J.Z. Wen, *Numerical study of a homogeneous charge compression ignition (HCCI) engine fueled with biogas.* Applied Energy, 2012. **92**: p. 437-446.
5. Visakhamoorthy, S., Wen, J.Z., Sivoththaman, S., and C.R. Koch, *Numerical study of a butanol/heptane fuelled Homogeneous Charge Compression Ignition (HCCI) engine utilizing negative valve overlap.* Applied Energy, 2012. **94**: p. 166-173.
6. U.S. EIA, *Electric power annual 2008*, U.S. DOE, Editor. 2010: Washington.
7. Hassan, S.M.N., P.L. Douglas, and E. Croiset, *Techno-economic study of CO2 capture from an existing cement plant using MEA scrubbing.* International Journal of Green Energy, 2007. **4**(2): p. 197-220.
8. Shar, A., *NOx emission specifications from stationary sources.* Pollution Engineering, 2001: p. 16-21.
9. Forzatti, P., *Present status and perspectives in de-NO_x SCR catalysis.* Applied Catalysis A : General, 2001. **222**(1-2): p. 221-236.
10. WBG, ed. *Pollution prevention and abatement handbook*. Nitrogen oxides: pollution prevention and control. 1998: Washington D. C.
11. Croiset, E., K. Thambimuthu, and A. Palmer, *Coal combustion in O_2/CO_2 mixtures compared with air*. Canadian Journal of Chemical Engineering, 2000. **78**(2): p. 402-407.
12. Croiset, E. and K.V. Thambimuthu, *Coal combustion with flue gas recirculation for CO_2 recovery*. Greenhouse Gas Control Technologies, 1999: p. 581-586.
13. Croiset, E. and K.V. Thambimuthu, *NO_x and SO_2 emissions from O_2/CO_2 recycle coal combustion.* Fuel, 2001. **80**(14): p. 2117-2121.
14. Singh, D., Croiset, E., Douglas, P.L., and M.A. Douglas, *Techno-economic study of CO_2 capture from an existing coal-fired power plant: MEA scrubbing vs. O_2/CO_2 recycle combustion.* Energy Conversion and Management, 2003. **44**(19): p. 3073-3091.
15. Tan, Y.W., Croiset, E., Douglas, M.A., and K.V. Thambimuthu, *Combustion characteristics of coal in a mixture of oxygen and recycled flue gas.* Fuel, 2006. **85**(4): p. 507-512.
16. Reese, J.L., *State of art of NOx emission control technology*, in *ASME Joint International Power Generation Conference*. 1994: Phoenix, Az. USA.
17. Bounicore, A.J. and T.D. Wayne, eds. *Air pollution engineering manual*. 1992, Van Nostrand Reinhold: New York, USA.
18. Chang, M.B., M.J. Kushner, and M.J. Rood, *Gas-phase removal of NO from gas streams via dielectric barrier discharges.* Environmental Science & Technology, 1992. **26**(4): p. 777-781.
19. Chang, M.B., M.J. Kushner, and M.J. Rood, *Removal of SO_2 and NO from gas streams with combined plasma photolysis.* Journal of Environmental Engineering-Asce, 1993. **119**(3): p. 414-423.
20. Chattopadhyaya, G., Macdonald, D.G., Bakhshi, N.N., Mohammadzadeh, B.J.S.S., and A.K. Dalai, *Removal of nitric oxide over Saskatchewan lignite and its derivatives.* Catalysis Letters, 2006. **108**(1-2): p. 1-5.

21. Ma, S.C., Yao, J.J., Gao L., Ma X.Y., and Y. Zhao, *Experimental study on removals of SO_2 and NO_X using adsorption of activated carbon/microwave desorption.* Journal of the Air & Waste Management Association, 2012. **62**(9): p 1012-1021.
22. Rubel, A.M., J.M. Stencel, and S.N. Ahmed, *Activated carbon for selective removal of nitrogen oxide from combustion flue gas*, in *Symposium on chemistry of flue gas cleanup processes for preprints of the fuel chemistry division* 1993: Denver, Co. p. 726-733.
23. Rubio, B., Izquierdo, M.T., Mayoral, M.C., M.T. Bona, and J.M. Andres, *Unburnt carbon from coal fly ashes as a precursor of activated carbon for nitric oxide removal.* Journal of Hazardous Materials, 2007. **143**(1-2): p. 561-566.
24. Perlmutter, H.D., H.H. Ao, and H. Shaw, *Absorption of NO promoted by strong oxidizing agents - organic tertiary hydroperoxides in N-hexadecane.* Environmental Science & Technology, 1993. **27**(1): p. 128-133.
25. Pham, E.K. and S.G. Chang, *Removal of NO from flue gases by absorption to an iron(II) thiochelate complex and subsequent reduction to ammonia.* Nature, 1994. **369**(6476): p. 139-141.
26. Sada, E., Kumazawa, H., Hayakawa, N., Kudo, I., and T. Kondo, *Absorption of NO in aqueous solutions of $KMnO_4$.* Chemical Engineering Science, 1977. **32**(10): p. 1171-1175.
27. Sada, E., Kumazawa, H., Kudo, I. and T. Kondo, *Absorption of lean NOx in aqueous solutions of $NaClO_2$ and NaOH.* Industrial & Engineering Chemistry Process Design and Development, 1979. **18**(2): p. 275-278.
28. Sada, E., Kumazawa, H., Kudo, I., and T. Kondo, *Absorption of NO in aqueous mixed solutions of $NaClO_2$ and NaOH.* Chemical Engineering Science, 1978. **33**(3): p. 315-318.
29. Baveja, K.K., D.S. Rao, and M.K. Sarkar, *Kinetics of absorption of nitric oxide in hydrogen peroxide solutions.* Journal of Chemical Engineering of Japan, 1979. **12**(4): p. 322-325.
30. Teramoto, M., Hiramine, S.I., Shimada, Y., Sugimoto, Y. and H. Teranishi, *Absorption of dilute nitric monoxide in aqueous solutions of Fe(II)-EDTA and mixed solutions of Fe(II)-EDTA and Na_2SO_3.* Journal of Chemical Engineering of Japan, 1978. **11**(6): p. 450-457.
31. Bosio, S., Ravella, A., Saracco, G.B., and G. Genon, *NOx absorption by ferrous sulfate solutions.* Industrial & Engineering Chemistry Process Design and Development, 1985. **24**(1): p. 149-152.
32. Long, X.L., W.D. Xiao, and W.K. Yuan, *Simultaneous absorption of NO and SO2 into hexamminecobalt(II)/iodide solution.* Chemosphere, 2005. **59**(6): p. 811-817.
33. Deshwal, B.R., Jin, D.S., Lee, S.H., Moon, S.H., Jung, J.H., and H.K. Lee, *Removal of NO from flue gas by aqueous chlorine-dioxide scrubbing solution in a lab-scale bubbling reactor.* Journal of Hazardous Materials, 2008. **150**(3): p. 649-655.
34. Cheng, J.Y., Yang, L., Dong, L., Long, X.L. and W.K. Yuan, *Regeneration of hexamminecobalt(II) catalyzed by activated carbon treated with KOH solutions.* Journal of Hazardous Materials, 2011. **191**(1-3): p. 184-189.
35. Kustin, K., I.A. Taub, and Weinstoc.E, *A kinetic study of formation of ferrous-nitric oxide complex.* Inorganic Chemistry, 1966. **5**(6): p. 1079-1082.
36. Ji, X.B., Buzzeo, M.C., Banks, C.E., and R.G. Compton, *Electrochemical response of cobalt(II) in the presence of ammonia.* Electroanalysis, 2006. **18**(1): p. 44-52.
37. IEA, *CO_2 capture and storage --- A key carbon abatement option*. 2008: Paris, France.
38. Feron, P.H.M., *Exploring the potential for improvement of the energy performance of coal fired power plants with post-combustion capture of carbon dioxide.* International Journal of Greenhouse Gas Control, 2010. **4**(2): p. 152-160.
39. Gao, X., Ding, H.L., Du, Z., Wu, Z.L., Fang, M.X., Luo, Z.Y., and K. Cen, *Gas-liquid absorption reaction between $(NH4)_2SO_3$ solution and SO_2 for ammonia-based wet flue gas desulfurization.* Applied Energy, 2010. **87**(8): p. 2647-2651.
40. Horn, R.J. and J.F. Bent, *Performance of dry flue gas desulfurization on a petroleum coke kiln application.* Journal of the Air Pollution Control Association, 1984. **34**(9): p. 982-986.

41. Pakrasi, A., Davis, W.T., and G.D. Reed, *A combined $Ca(OH)_2/NH_3$ flue gas desulfurization process for high sulfur coal: Results of a pilot plant study.* Journal of the Air & Waste Management Association, 1990. **40**(7): p. 987-992.
42. Faucett, H.L., J.D. Maxwell, and T.A. Burnett, *Technical assessment of NOx removal processes for utility application*. 1977: Washington. p. 37.
43. Baukal, C., *Everything you need to know about NO_x.* Pollution Control 2006: p. 18-24.
44. Bhardwaj, S., *Inventory of nitrogen oxide emissions and control technologies in Alberta's upstream oil and gas industry*. 2002: Edmonton.
45. Chang, M.B., Balbach, J.H., M.J. Rood, and M.J. Kushner, *Removal of SO_2 from gas streams using a dielectric barrier discharge and combined plasma photolysis.* Journal of Applied Physics, 1991. **69**(8): p. 4409-4417.
46. Hikita, H., Asai, S., H. Ishikawa, and S. Hirano, *Kinetics of absorption of nitric oxide in aqueous acidic solutions of ferrous sulfate.* Journal of Chemical Engineering of Japan, 1977. **10**(2): p. 120-124.
47. Sada, E., Kumazawa, H., Tsubol, N., I. Kudo, and T. Kondo, *Absorption of nitric oxide in aqueous ferrous sulfate sollutions.* Industrial & Engineering Chemistry Process Design and Development, 1978. **17**(3): p. 321-324.
48. Jethani, K.R., N.J. Suchak, and J.B. Joshi, *Selection of reactive solvent for pollution abatement of NOx.* Gas Separation & Purification, 1990. **4**: p. 8-28.
49. Smith, K., Lani, B., Berisko, D., Schultz, C., W., Carlson, and L.B. Benson, *Enhanced NO_x removal in wet scrubbers using metal chelates* U.S.D.o. Energy, Editor. 1992: Pittsburgh, Pennsylvania, USA.
50. Ji, X.B., Chevallier, F.G., Clegg, A.D., M.C. Buzzeo, and R.G. Comption, *The electrochemical reduction of aqueous hexamminecobalt(III): Studies of adsorption behaviour with fast scan voltammetry.* Journal of Electroanalytical Chemistry, 2005. **581**(2): p. 249-257.
51. Liu, D.K. and S.G. Chang, *Removal of nitric oxide from flue gas using water-soluble iron(II) dithiocarbamates.* Environmental Science & Technology, 1988. **22**(10): p. 1196-1200.
52. Granite, E.J., H.W. Pennline, and J.S. Hoffman, *Effects of photochemical formation of mercuric oxide.* Industrial & Engineering Chemistry Research, 1999. **38**(12): p. 5034-5037.
53. Xu, X., Song, C.S., Wincek, R., Andresen, J.M., B.G. Miller, and A.W. Scaroni, *Separation of CO_2 from power plant flue gas using a novel CO_2 "molecular basket" adsorbent.* Fuel Chemistry Division Preprints, 2003. **48**(1): p. 162-163.
54. Liu, D.K., L.P. Frick, and S.G. Chang, *A ferrous cysteine based recyclable process for the combined removal of NOx and SO_2 from flue gas.* Environmental Science & Technology, 1988. **22**(2): p. 219-223.
55. Sand, J. and O. Genssler, *Pentammine-nitroso-cobalt salts.* Berichte Der Deutschen Chemischen Gesellschaft, 1903. **36**: p. 2083-2086.
56. Mao, Y.P., Bi, W., Long, X.L., Xiao, W.D., W. Li, and W.K. Yuan, *Kinetics for the simultaneous absorption of nitric oxide and sulfur dioxide with the hexamminecobalt solution.* Separation and Purification Technology, 2008. **62**(1): p. 183-191.
57. Mao, Y.P., Chen, H., Long, X.L., Xiao, W.D., W. Li, and W.K. Yuan, *Experimental determination of equilibrium constant for the complexing reaction of nitric oxide with hexamminecobalt(II) in aqueous solution.* Journal of Hazardous Materials, 2009. **162**(1): p. 99-102.
58. Long, X.L., W.D. Xiao, and W.K. Yuan, *Removal of sulfur dioxide and nitric oxide using cobalt ethylenediamine solution.* Industrial & Engineering Chemistry Research, 2005. **44**(4): p. 686-691.
59. Long, X.L., Xin, Z.L., Chen, M.B. W.D. Xiao, and W.K. Yuan, *Nitric oxide absorption into cobalt ethylenediamine solution.* Separation and Purification Technology, 2007. **55**(2): p. 226-231.

60. Yu, H., Q. Zhu, and Z. Tan, *Absorption of nitric oxide from simulated flue gas using different absorbents at room temperature and atmospheric pressure.* Applied Energy, 2012. **93**: p. 53-58.
61. Simplicio, J. and R.G. Wilkins, *Uptake of oxygen by ammoniacal cobalt(II) solutions.* Journal of the American Chemical Society, 1969. **91**(6): p. 1325-1329.
62. Bjerrum, J., *Metal ammine formation in aqueous solution*. 1957, Copenhagen: P. Haase and Son. Denmark.
63. Yatsimirskii, K.B. and I.I. Volchenskova, *Absorption spectra and band type in Co(II) aquoamino complexes.* Theoretical and Experimental Chemistry, 1968. **6**(6): p. 808-815.
64. Goldberg, R.N., N. Kishore, and R.M. Lennen, *Thermodynamic quantities for the ionization reactions of buffers.* Journal of Physical and Chemical Reference Data, 2002. **31**(2): p. 231-370.
65. Perman, E.P., *Vapour pressure of aqueous ammonia solution Part II.* Journal of the Chemical Society, 1903. **83**: p. 1168-1184.
66. Ford, P.C. and I.M. Lorkovic, *Mechanistic aspects of the reactions of nitric oxide with transition-metal complexes.* Chemical Reviews, 2002. **102**(4): p. 993-1017.
67. Asmussen, R.W., O. Bostrup, and J.P. Jensen, *The magnetic properties of $[Co(NH_3)_5(NO)]Cl_2$ (black) and $[Co(NH_3)_5(NO)](NO_3)_2.1/2H_2O$ (red) - studies in Magnetochemistry .21.* Acta Chemica Scandinavica, 1958. **12**(1): p. 24-30.
68. Gans, P., *Reaction of nitric oxide with cobalt(II) ammine complexes and other reducing agents.* Journal of the Chemical Society a -Inorganic Physical Theoretical, 1967(6): p. 943-946.
69. Odell, A.L., R.W. Olliff, and A.A. Taggart, *Preparation and magnetic susceptibility of nitrosylpentamminecobalt chloride (Black).* Journal of the Chemical Society, 1965(Nov): p. 6024-6026.
70. Moeller, T. and G.L. King, *Nitrosylpentamminecobalt(II) chloride, black, and nitrosylpentamminecobalt(III) chloride, pink.* Inorganic Syntheses, 1953. **4**: p. 168-171.
71. Bostrup, O., *Nitrosylpentaamminecobalt(II) chloride.* Inorganic Syntheses, 1966. **8**: p. 191-195.
72. Milward, J.L., W. Wardlaw, and W.J.R. Way, *The constitution of the nitrosopentammine cobalt salts.* Journal of the Chemical Society (Resumed), 1938: p. 233-236.
73. Bertin, E.P., Mizushima, S.I., T.J. Lane, and J.V. Quagliano, *Infrared absorption studies of inorganic coordination complexes .XXI. Nitrosopentamminecobalt halides and nitrate.* Journal of the American Chemical Society, 1959. **81**(15): p. 3821-3823.
74. Feltham, R.D., *Metal nitrosyls.IV. On red and black isomers of cobalt nitrosopentaammines.* Inorganic Chemistry, 1964. **3**(7): p. 1038-1039.
75. Dale, D. and D.C. Hodgkin, *Crystal structure of black nitrosylpentamminecobalt dichloride.* Journal of the Chemical Society, 1965(Feb): p. 1364-1371.
76. Hall, D. and A.A. Taggart, *Crystal structure of nitrosylpentamminecobalt dichloride (black form).* Journal of the Chemical Society, 1965(Feb): p. 1359-1363.
77. Mercer, E.E., Mcallist.Wa, and J.R. Durig, *An infrared and chemical investigation of the two isomers of pentaammminenitrosylcobalt ion.* Inorganic Chemistry, 1967. **6**(10): p. 1816-1821.
78. Hoskins, B.F. and F.D. Whillans, *Crystal and molecular structure of a μ-hyponitrito-bisrpenta-amminecobalt(III) salt: the nature of the red nitrosylpenta-amminecobalt(III) cation.* Journal of Chemical Society Dalton Transactions, 1973(6): p. 607-611.
79. Pratt, C.S., B.A. Coyle, and J.A. Ibers, *Redetermination of structure of nitrosylpenta-amminecobalt(III) dichloride.* Journal of the Chemical Society A : Inorganic, Physical, Theoretical, 1971(13): p. 2146-2151.
80. Hoskins, B.F., Whillans, F.D., D.H. Dale, and D.C. Hodgkin, *The structure of the red nitrosylpenta-amminecobalt(III) cation.* Journal of the Chemical Society D: Chemical Communications, 1969(2): p. 69-70.

81. Noell, J.O. and K. Morokuma, *Relative stability of bent and linear coordination of the nitrosyl ligand in nitrosylpentaammine cobalt(III), $Co(NH_3)_5NO^{2+}$ - An ab initio investigation.* Inorganic Chemistry, 1979. **18**(10): p. 2774-2782.
82. Chacon Villalba, M.E., Navaza, A., Guida, J.A., E.L. Varetti, and P.J. Aymonino, *New structural study and reinterpretation of the vibrational spectra of the mu-N,O-hyponitrite bis[pentaamminecobalt(III)](4+) cation.* Inorganica Chimica Acta, 2006. **359**(2): p. 707-712.
83. Raynor, J.B., *Structure and reactivity of transition-metal complexes with polyatomic ligands. Part III. Nitric oxide complexes of cobalt and other transition metals with v(NO) 1195-1040 cm.-1.* Journal of the Chemical Society A: Inorganic, Physical, Theoretical, 1966: p. 997-1000.
84. Griffith, W.P., J. Lewis, and G. Wilkinson, *Infra-red spectra of transition metal-nitric oxide complexes. II. Complexes involving the NO^- ion.* Journal of Inorganic & Nuclear Chemistry, 1958. **7**(1-2): p. 38-44.
85. Astarita, G., *Mass transfer with chemical reaction*. 1967, Amsterdam: Elsevier. Netherlands.
86. Nymoen, H., D. Vanvelzen, and H. Langenkamp, *Absorption of NO in aqueous solutions of Fe(II)-EDTA - Determination of the equilibrium constant.* Chemical Engineering and Processing, 1993. **32**(1): p. 9-12.
87. Sada, E., Kumazawa, H., I. Kudo, and T. Kondo, *Individual and simultaneous absorption of dilute NO and SO_2 in aqueous slurries of $MgSO_3$ with Fe^{II}-EDTA.* Industrial & Engineering Chemistry Process Design and Development, 1980. **19**(3): p. 377-382.
88. Chien, T.W., Hsueh, H.T., B.Y. Chu, and H. Chu, *Absorption kinetics of NO from simulated flue gas using Fe(II)EDTA solutions.* Process Safety and Environmental Protection, 2009. **87**(5): p. 300-306.
89. Du, Q., Zhao, H.Y., Ming, L.L., Gao, J.M., G.B. Zhao, and S.H. Wu, *Experimental investigation on the kinetics of NO complex absorption through Fe(II)EDTA solvent in a double-stirred reactor.* Industrial & Engineering Chemistry Research, 2011. **50**(8): p. 4425-4431.
90. Danckwerts, P.V., *Gas-liquid reactions*. 1970, New York: McGraw-Hill Book Company. USA.
91. Onda, K., Sada, E., T. Kobayashi, and M. Fujine, *Gas absorption accompanied by complex chemical reactions - III Parallel chemical reactions.* Chemical Engineering Science, 1970. **25**(6): p. 1023-1031.
92. Westerterp, K.R., W.P. Van Swaaij, and A. Beenackers, *Chemical reactor design and operation*. 1984, New York: Wiley.
93. Deckwer, W.D., *Bubble column reactors*. 1992, Chichester: John Wiley & Sons Ltd. UK.
94. Alvarez, E., Gomez-Diaz, D., J.M. Navaza, and B. Sanjurjo, *Continuous removal of carbon dioxide by absorption employing a bubble column.* Chemical Engineering Journal, 2008. **137**(2): p. 251-256.
95. Petrissans, S.M., A. Petrissans, and A. Zoulalian, *Experimental study and modelling of mass transfer during simultaneous absorption of SO2 and NO2 with chemical reaction.* Chemical Engineering and Processing, 2005. **44**(10): p. 1075-1081.
96. Cheng, J., Yang, Z.R., Chen, H.Q., C.H. Kuo, and M.E. Zappi, *Simultaneous prediction of chemical mass transfer coefficients and rates for removal of organic pollutants in ozone absorption in an agitated semi-batch reactor.* Separation and Purification Technology, 2003. **31**(1): p. 97-104.
97. Uchida, S., Moriguchi, H., Maejima, H., K. Koide, and S. Kageyama, *Absorption of sulfur dioxide into limestone slurry in a stirred tank reactor.* Canadian Journal of Chemical Engineering, 1978. **56**(6): p. 690-697.
98. Scargiali, F., Russo, R., F. Grisafi, and A. Brucato, *Mass transfer and hydrodynamic characteristics of a high aspect ratio self-ingesting reactor for gas-liquid operations.* Chemical Engineering Science, 2007. **62**(5): p. 1376-1387.

99. Poncin, S., Nguyen, C., N. Midoux, and J. Breysse, *Hydrodynamics and volumetric gas-liquid mass transfer coefficient of a stirred vessel equipped with a gas-inducing impeller*. Chemical Engineering Science, 2002. **57**(16): p. 3299-3306.
100. Kantarci, N., F. Borak, and K.O. Ulgen, *Bubble column reactors.* Process Biochemistry, 2005. **40**(7): p. 2263-2283.
101. Akita, K. and F. Yoshida, *Gas holdup and volumetric mass-transfer coefficient in bubble columns - effects of liquid properties.* Industrial & Engineering Chemistry Process Design and Development, 1973. **12**(1): p. 76-80.
102. Shah, Y.T., Kelkar, B.G., S.P. Godbole, and W.D. Deckwer, *Design parameters estimations for bubble column reactors.* AIChE Journal, 1982. **28**(3): p. 353-379.
103. Deckwer, W.D., Burckhar.R, and G. Zoll, *Mixing and mass transfer in tall bubble columns.* Chemical Engineering Science, 1974. **29**(11): p. 2177-2188.
104. Deckwer, W.D., Nguyen-Tien, K., B.G. Kelkar, and Y.T. Shah, *Applicability of axial dispersion model to analyze mass transfer measurements in bubble columns.* AIChE Journal, 1983. **29**(6): p. 915-922.
105. Nienow, A.W., Warmoeskerken, M.M.C.G., J.M. Smith, and M. Konno, *On the flooding/loading transition and the complete dispersal condition in aerated vessels agitated by a Rushton-turbine*, in *Proc 5th European Conference on Mixing*. 1985: Wurtsburg, West Germany. p. 143–154.
106. Nienow, A.W., D.J. Wisdom, and J.C. Middleton, *Effect of scale and geometry on flooding, recirculation and power in gassed stirred vessels*, in *2nd European conference on mixing*. 1977: Cambridge, UK. p. 1-16.
107. Kapic, A. and T.J. Heindel, *Correlating gas-liquid mass transfer in a stirred-tank reactor.* Chemical Engineering Research & Design, 2006. **84**(A3): p. 239-245.
108. Van't Riet, K., *Review of measuring methods and results in nonviscous gas-liquid mass-transfer in stirred vessels.* Industrial & Engineering Chemistry Process Design and Development, 1979. **18**(3): p. 357-364.
109. Smith, J.M., K. van't Riet, and J.C. Middleton, *Scale-up of agitated gas-liquid reactors for mass transfer*, in *Proc 2nd European Conference on Mixing*. 1977: Cambridge, UK. p. 51-66.
110. Yawalkar, A.A., Heesink, A.B.M., G.F. Versteeg, and V.G. Pangarkar, *Gas-liquid mass transfer coefficient in stirred tank reactors.* Canadian Journal of Chemical Engineering, 2002. **80**(5): p. 840-848.
111. Yu, H.S. and Z.C. Tan, *New correlations of volumetric liquid-phase mass transfer coefficients in gas-Inducing agitated tank reactors.* International Journal of Chemical Reactor Engineering, 2012. **10:** p. 1-20.
112. Saravanan, K., Mundale, V.D., A.W. Patwardhan, and J.B. Joshi, *Power consumption in gas-inducing-type mechanically agitated contactors.* Industrial & Engineering Chemistry Research, 1996. **35**(5): p. 1583-1602.
113. Akita, K. and F. Yoshida, *Bubble size, interfacial area, and liquid-phase mass-transfer coefficient in bubble columns.* Industrial & Engineering Chemistry Process Design and Development, 1974. **13**(1): p. 84-91.
114. Leentvaar, J. and T.S.J. Ywema, *Some dimensionless parameters of impeller power in coagulation-flocculation processes.* Water Research, 1980. **14**(2): p. 135-140.
115. Kresta, S.M., D.M. Mao, and V. Roussinova, *Batch blend time in square stirred tanks.* Chemical Engineering Science, 2006. **61**(9): p. 2823-2825.
116. Mandhane, J.M., G.A. Gregory, and K. Aziz, *A flow pattern map for gas-liquid flow in horizontal pipes.* International Journal of Multiphase Flow, 1974. **1**(4): p. 537-553.
117. Taitel, Y. and A.E. Dukler, *A model for predicting flow regime transitions in horizontal and near horiztonal gas-liquid flow.* AIChe Journal, 1976. **22**(1): p. 47-55.
118. Chen, J.J.J. and P.L. Spedding, *An analysis of holdup in horizontal two-phase gas-liquid flow.* International Journal of Multiphase Flow, 1983. **9**(2): p. 147-159.

119. Spedding, P.L., E. Benard, and G.F. Donnelly, *Prediction of pressure drop in multiphase horizontal pipe flow.* International Communications in Heat and Mass Transfer, 2006. **33**(9): p. 1053-1062.
120. Watterson, J.K., R.K. Cooper, and P.L. Spedding, *Predicton of pressure loss and holdup in two-phase horizontal stratified roll-wave pipe flow.* Industrial & Engineering Chemistry Research, 2002. **41**(25): p. 6621-6622.
121. Heuss, J.M., C.J. King, and C.R. Wilke, *Gas-liquid mass transfer in cocurrent froth flow.* AIChe Journal, 1965. **11**(5): p. 866-873.
122. Jepsen, J.C., *Mass transfer in two-phase flow in horizontal pipelines.* AIChe Journal, 1970. **16**(5): p. 705-711.
123. Kress, T.S. and J.J. Keyes, *Liquid phase controlled mass transfer to bubbles in cocurrent turbulent pipeline flow.* Chemical Engineering Science, 1973. **28**(10): p. 1809-1823.
124. Long, X.L., H. Cheng, and W.K. Yuan, *Reduction of hexamminecobalt (III) catalyzed by coconut activated carbon.* Environmental Progress & Sustainable Energy, 2010. **29**(1): p. 85-92.
125. Chen, Y., Mao, Y.P., Zhu, H.S., Cheng, J.Y., X.L. Long, and W.K. Yuan, *Catalytic reduction of hexaminecobalt(III) by pitch-based spherical activated carbon (PBSAC).* Clean-Soil Air Water, 2010. **38**(7): p. 601-607.
126. Long, X.L., Xin, Z.L., Wang, H.X., W.D. Xiao, and W.K. Yuan, *Simultaneous removal of NO and SO_2 with hexamminecobalt(II) solution coupled with the hexamminecobalt(II) regeneration catalyzed by activated carbon.* Applied Catalysis B-Environmental, 2004. **54**(1): p. 25-32.
127. Long, X.L., W.D. Xiao, and W.K. Yuan, *Removal of nitric oxide and sulfur dioxide from flue gas using a hexamminecobalt(II)/iodide solution.* Industrial & Engineering Chemistry Research, 2004. **43**(15): p. 4048-4053.
128. Thusius, D.D. and H. Taube, *The oxidation of aquopentaammine and of hexaamminecobalt(III) ions.* Journal of Physical Chemistry, 1967. **71**(12): p. 3845-3857.
129. Thusius, D.D. and H. Taube, *Oxidation of water coordinated to cobalt(III).* Journal of the American Chemical Society, 1966. **88**(4): p. 850-851.
130. White, J.D. and H. Taube, *Reduction of cobalt(III) in cobaltammines induced by decomposition of persulfate Ion.* Journal of Physical Chemistry, 1970. **74**(23): p. 4142-4149.
131. Coleman, H.W. and W.G. Steele, *Experimentation and uncertainty analysis for engineers*. 1989: John Wiley & Sons, New York, USA.
132. *Measurement uncertainty*. ANSI/ASME PTC 19.1-1985 Part1, 1986.
133. Hishinuma, Y., Kaji, R., Akimoto, H., Nakajima, F., Mori, T., Kamo, T., A. Yoshijiro, and S. Nozawa, *Reversible binding of NO to Fe(II)EDTA.* Bulletin of the Chemical Society of Japan, 1979. **52**(10): p. 2863-2865.
134. Kurimura, Y., R. Ochiai, and N. Matsuura, *Oxygen oxidation of ferrous ions induced by chelation.* Bulletin of the Chemical Society of Japan, 1968. **41**(10): p. 2234-2239.
135. Wubs, H.J. and A. Beenackers, *Kinetics of the oxidation of ferrous chelates of EDTA and HEDTA in aqueous solution.* Industrial & Engineering Chemistry Research, 1993. **32**(11): p. 2580-2594.
136. Zang, V. and R. Vaneldik, *Kinetics and mechanism of the autoxidation of iron (II) induced through chelation by ethylenediaminetetraacetate and related ligands.* Inorganic Chemistry, 1990. **29**(9): p. 1705-1711.
137. Ochiai, E., *Oxygenation of cobalt(II) complexes.* Journal of Inorganic & Nuclear Chemistry, 1973. **35**(9): p. 3375-3389.
138. Schaefer, W.P., *The structure of decaammine-μ-peroxo-dicobalt disulfate tetrahydrate.* Inorganic Chemistry, 1968. **7**(4): p. 725-731.
139. Azuhata, S., H. Akimoto, and Y. Hishinuma, *Effect of H_2O_2 on homogeneous gas phase NO reduction reaction with NH_3.* AIChE Journal, 1982. **28**(1): p. 7-11.

140. Azuhata, S., Kaji, R., H. Akimoto, and Y. Hishinuma, *A study of the kinetics of the NH_3-NO-O_2-H_2O_2 reaction.* Symposium (International) on Combustion, 1981. **18**: p. 845-852.
141. Zamansky, V.M., Ho, L., P.M. Maly, and W.R. Seeker, *Oxidation of NO to NO_2 by hydrogen peroxide and its mixtures with methanol in natural gas and coal combustion gases.* Combustion Science and Technology, 1996. **120**(1-6): p. 255-272.
142. Thomas, D. and J. Vanderschuren, *The absorption-oxidation of NOx with hydrogen peroxide for the treatment of tail gases.* Chemical Engineering Science, 1996. **51**(11): p. 2649-2654.
143. Kervinen, K., Korpi, H., M. Leskela, and T. Repo, *Oxidation of veratryl alcohol by molecular oxygen in aqueous solution catalyzed by cobalt salen-type complexes: the effect of reaction conditions.* Journal of Molecular Catalysis a-Chemical, 2003. **203**(1-2): p. 9-19.
144. Lide, D.R. and H.P.R. Frederikse, eds. *CRC handbook of chemistry and physics*. 76th ed. 1995, CRC Press, Inc. : Boca Raton, FL, USA.
145. Onda, K., Sada, E., Kobayashi, T., S. Kito, and K. Ito, *Salting-out parameters of gas solubility in aqueous salt solutions.* Journal of Chemical Engineering of Japan, 1970. **3**(1): p. 18-24.
146. Sattler, K. and H.J. Feindt, *Thermal separation processes: Principles and Design*. 1995, New York: VCH Verlagsgesellschaft and VCH Publishers. 545.
147. Grubbs, F.E., *Sample criteria for testing outlying observations.* Annals of Mathematical Statistics, 1950. **21**(1): p. 27-58.
148. Grubbs, F.E., *Procedures for detecting outlying observations in samples.* Technometrics, 1969. **11**(1): p. 1-21.
149. Denbigh, K.G., *The principles of chemical equilibrium*. Fourth ed. 1981, Cambridge: Cambridge University Press. UK.
150. Wilke, C.R. and P. Chang, *Correlation of diffusion coefficients in dilute solutions.* AIChE Journal, 1955. **1**(2): p. 264-270.
151. Brodkey, R.S. and H.C. Hershey, eds. *Transport phenomena - A unified approach*. Chemical Engineering Series. 1988, McGraw-Hill: New York. USA.
152. Theodore, L. and F. Ricci, *Mass transfer operations for the practicing engineer*. 2010, Hoboken: John Wiley & Sons, Inc. USA.
153. Incropera, F.P., Dewitt, D.P., T.L., Bergman, and A.S. Lavine, *Fundamentals of heat and mass transfer*. Sixth ed. 2007: John Wiley & Sons Inc. Hoboken, USA.
154. Zacharia, I.G. and W.M. Deen, *Diffusivity and solubility of nitric oxide in water and saline.* Annals of Biomedical Engineering, 2005. **33**(2): p. 214-222.
155. Poling, B.E., J.M. Prausnitz, and J.P. O'Connell, *The properties of gases and liquids*. Fifth ed. 2000, New York: McGraw-Hill. USA.
156. Yu, H.S. and Z.C. Tan, *Determination of Equilibrium Constants for Reactions between Nitric Oxide and Ammoniacal Cobalt(II) Solutions.* Accepted by Industrial & Engineering Chemistry Research with Major Revision.
157. Littlejohn, D. and S.G. Chang, *Kinetic study of ferrous nitrosyl complexes.* Journal of Physical Chemistry, 1982. **86**(4): p. 537-540.
158. Weisweiler, W., R. Blumhofer, and T. Westermann, *Absorption of nitrogen monoxide in aqueous solutions containing sulfite and transition metal chelates such as Fe (II)-EDTA, Fe (II)-NTA, Co (II)-Trien and Co (II)-Treten.* Chemical Engineering and Processing, 1986. **20**(3): p. 155-166.
159. Montgomery, D.G., *Design and Analysis of Experiments*. 5thq ed. 2001, New York: John Wiley & Sons Inc. USA.
160. Schenck, H., *Theories of Engineering Experimentation*. 3rd ed. 1979, New York: McGraw-Hill. USA.
161. Taitel, Y. and A.E. Dukler, *A theoretical approach to the Lockhart-Martinelli correlation for stratified flow* International Journal of Multiphase Flow, 1976. **2**(5-6): p. 591-595.

162. Spedding, P.L. and N.P. Hand, *Prediction in stratified gas-liquid co-current flow in horizontal pipelines.* International Journal of Heat and Mass Transfer, 1997. **40**(8): p. 1923-1935.
163. Han, L. and M.H. Al-Dahhan, *Gas-liquid mass transfer in a high pressure bubble column reactor with different sparger designs.* Chemical Engineering Science, 2007. **62**(1-2): p. 131-139.
164. Linek, V., V. Vacek, and P. Benes, *A critical review and experimental verification of the correct use of the dynamic method for the determination of xxygen transfer in aerated agitated vessels to water, electrolyte solutions and viscous liquids.* Chemical Engineering Journal and the Biochemical Engineering Journal, 1987. **34**(1): p. 11-34.
165. Robinson, C.W. and C.R. Wilke, *Oxygen absorption in stirred tanks: A correlation for ionic strength effects.* Biotechnology and Bioengineering, 1973. **15**(4): p. 755-782.
166. Garcia-Ochoa, F. and E.G. Castro, *Estimation of oxygen mass transfer coefficient in stirred tank reactors using artificial neural networks.* Enzyme and Microbial Technology, 2001. **28**(6): p. 560-569.
167. Sideman, S., O. Hortacsu, and J.W. Fulton, *Mass transfer in gas-Liquid contacting systems.* Industrial and Engineering Chemistry, 1966. **58**(7): p. 32-47.
168. Miller, D.N., *Scale-up of agitated vessels gas-liquid mass transfer.* AIChE Journal, 1974. **20**(3): p. 445-453.
169. Calderbank, P.H., *Physical rate processes in industrial fermentation. Part II: mass transfer coefficients in gas-liquid contacting with and without mechanical agitation.* Transaction of the Institution of Chemical Engineers, 1959. **37**: p. 173-185.
170. Sawant, S.B., et al., *Mass transfer and hydrodynamic characteristics of the denver type of flotation cells.* Chemical Engineering Journal and the Biochemical Engineering Journal, 1981. **21**(1): p. 11-19.

Appendix A – Matlab Codes for Various Calculations

A. 1 For Cobalt(II) – Ammonia System Analysis

```
clc
clear all
% assume aw=1 and fNH3=1
K=[10^2.114;10^1.634;10^1.054;10^0.764;10^0.184;10^-0.616]; % at Temp=303.15K degrees
pH=3.5:0.01:12.5;
pH=pH';
for i=1:901
   cammonium=2; % concentration of ammonium chloride, mol/L
   cammonia(i)=cammonium*10^(pH(i)-9.329);% the acid dissociation of ammonium is 9.329 here, it will change with temperature and ammonium concentration
   A(i,1)=K(1)*cammonia(i);
   for j=2:6
      A(i,j)=A(i,j-1)*K(j)*cammonia(i);
   end

   cT=0.01; % the original concentration of cobal(II) nitrate, mol/L, this parameter is independent of calculation

   % c(1)=Co2+, c(2)=CoA, c(3)=CoA2, c(4)=CoA3, c(5)=CoA4, c(6)=CoA5,
   % c(7)=CoA6

   c(i,1)=cT/(1+A(i,1)+A(i,2)+A(i,3)+A(i,4)+A(i,5)+A(i,6));
   eff(i,1)=c(i,1)/cT*100;
   for k=2:7
```

```
    c(i,k)=A(i,k-1)*c(i,1);
    eff(i,k)=c(i,k)/cT*100;
    end
    eff;
end
plot(pH, eff)
```

A. 2. For GIAT – Effect of N_l at $Q_G = 0$

```
clc
clear all
format compact
format short
% constants first
cLin=10; %ppm
cLin=cLin/(32*1000) % mol/L

QL=0.000126;
DT=0.4064;
hL=0.3048;
A=DT^2; % to distinguish it from last AP for pipe
VL=hL*DT^2;
DI=4*0.0254;
RI=DI/2;
s=9.5*0.0254;
g=9.81;
Ncr=(0.21*g*s/DI^2)^0.5
rhoL=1000;% kg/m3
W=4*0.0254;

sn=99.5/100 %adjustable
so=1-sn
po=so*(1+1000*9.81*0.3048/101325)
```

```
R=8.205*10^-2;% L atm/ mol K
T=293.15; %K
H=769.23; % T=298.15, L atm/mol
H=H*exp(-1700*(1/T-1/298.15)); % L atm/mol

cGin=po/(R*T) % mol/L (=0.5% v%)
cs=cGin*R*T/H % mol/L, does not change

N=(495:2.5:1195)/60;% impeller speed
for i=1:281
   QI(i)=0.0021*(N(i)^2-Ncr^2)^0.75*DI^3;
   P(i)=(rhoL*W*N(i)^3*RI^4)*(22.24-6.71*(1-2*g*s/(0.84*(pi*N(i)*DI)^2))^3)+1.767*2*pi*N(i);
   kLaT(i)=1.212*(P(i)/VL)^0.0816*(QI(i)/A)^0.692*(s/DT)^-0.390;
   cLout(i)=(QL*cLin+kLaT(i)*VL*cs)/(kLaT(i)*VL+QL);
   effT(i)=(cLin-cLout(i))/cLin*100;
end
N=N';
effT=effT';
plot(N, effT)
```

A. 3 For CSTR – Effect of N_I at Q_G = 50scfm

```
clc
clear all
format compact
format short
% constants first
cLin=10; %ppm
cLin=cLin/(32*1000) % mol/L

QL=0.000126;% m3/s
orhL=1000; %kg/m3
orhG=1.429; %kg/m3
viscosityL=0.001; %Pa*s
viscosityG=       0.00002018; %Pa*s
```

```
D=0.0254;% pipe diameter, m
AP=pi/4*D^2; % pipe cross sectional area, m2
VSL=QL/AP; % liquid superficial velocity, m/s
ReSL=D*VSL*orhL/viscosityL; % liquid Reynolds number
Df=2.3*10^-9; %diffusivity; Df, m2/s
st=0.0728;%surface tension: st, N/m

R=8.205*10^-2;% L atm/ mol K
T=293.15; %K
H=769.23; % T=298.15, L atm/mol
H=H*exp(-1700*(1/T-1/298.15)); % L atm/mol

sn=99.5/100 %adjustable
so=1-sn
po=so*(1+1000*9.81*0.3048/101325)

cGin=po/(R*T) % mol/L (=0.5% v%)

c1=VSL/(VSL+6);
c2=2.7847*log10(c1)+7.8035;
z=0.4191; % horizontal pipe length

% variabls then
QG=7.86579*10^-6*50

VSG=QG/AP;
ReSG=D*VSG*orhG/viscosityG;
GHUp=0.83*(QG/(QG+QL));%GHUp = gas hold-up of pipe
LHUp=1-GHUp; %LHUp =liquid hold-up of pipe
% now comes the calculation of theta
theta = 3; % set an initial value to theta
for j=1:50
   f=theta-sin(theta)-2*pi*LHUp;
   g=1-cos(theta);
   theta=theta-f/g;
```

```
end
theta
AL=LHUp*pi/4*D^2;
SL=D/2*theta;
Si=D*sin(theta/2);
VLA=VSL/LHUp;
VGA=VSG/GHUp;
fL=0.0262*(LHUp*ReSL)^-0.139;
fSG=16/ReSG;
fi=(1.76*(VSG/6)+c2)*fSG;
twL=fL*orhL*VLA^2/2;
ti=fi*orhG*(VGA-VLA)^2/2;
deltaPL=(twL*SL-ti*Si)/AL;
FED=deltaPL*(VSL+VSG)/101325; % FED= friction energy dissipation
kLap=3.47*FED^0.4*(Df*10000)^0.5*(st*1000)^0.5*(viscosityL*1000)^0.05*(D*39.3701)^-0.68

k1=kLap*AP/QL;
k2=1+(R*T*QL)/(QG*H);
k3=(R*T/H)*(cLin*QL/QG+cGin);

%cLTin is the inlet concentration of tank,which is the pipe DO
%concentration at z=0.4191m

cLTin=((cLin-R*T*cGin/H)/k2)*exp(-k1*k2*z)+k3/k2



effp=(cLin-cLTin)/cLin*100 % pipe efficiency

cGTin=QL/QG*(cLin-cLTin)+cGin
cst=cGTin*R*T/H % cs' in the paper

% In the tank now

DT=0.4064;
hL=0.3048;
```

```
A=DT^2; % to distinguish it from last AP for pipe
VL=hL*DT^2;
DI=4*0.0254;
s=9.5*0.0254;
g=9.81;
Ncr=(0.21*g*s/DI^2)^0.5
N=(200:2.5:1200)/60;% impeller speed
QI=ones(401,1);
for i=1:87
   Ncd(i)=4*QG^0.5*DT^0.25/DI^2;
   %kLaT(i)=3.35*(N(i)/Ncd(i))^1.464*(QG)/A;
   kLaT(i)=1.59*(N(i)/Ncd(i))^1.342*(QG/A)^0.93*(DT/DI)^0.415;
   cLout(i)=(kLaT(i)*VL*cst+QL*cLTin)/(kLaT(i)*VL+QL);
   effT(i)=(cLin-cLout(i))/cLin*100;
end
for i=88:401
   QI(i)=0.0021*(N(i)^2-Ncr^2)^0.75*DI^3;
   Ncd(i)=4*(QG+QI(i))^0.5*DT^0.25/DI^2;
   %kLaT(i)=3.35*(N(i)/Ncd(i))^1.464*(QG+QI(i))/A;
   kLaT(i)=1.59*(N(i)/Ncd(i))^1.342*((QG+QI(i))/A)^0.93*(DT/DI)^0.415;
   cLout(i)=(kLaT(i)*VL*cst+QL*cLTin)/(kLaT(i)*VL+QL);
   effT(i)=(cLin-cLout(i))/cLin*100;
end

N=N';
Ncd=Ncd'
effT=effT';

plot(N,effT)
```

A. 4 For BC - Effect of Q_G at N_I = 0

```
clc
clear all
```

```
format compact
format short
% constants first
cLin=10; %ppm
cLin=cLin/(32*1000) % mol/L

QL=0.000126;%m3/s
orhL=1000; % kg/m3
orhG=1.429; % kg/m3
viscosityL=0.001; % Pa*s = Ns/m2
viscosityG=       0.00002018; % Pa*s
kviscosityL=viscosityL/orhL; % m2/s
D=0.0254;% pipe diameter, m
AP=pi/4*D^2;% pipe cross sectional area, m2
VSL=QL/AP; % liquid superficial velocity, m/s
ReSL=D*VSL*orhL/viscosityL;% liquid Reynolds number
Df=2.3*10^-9; %diffusivity; Df, m2/s, (or 1.97*10^-9,
http://compost.css.cornell.edu/oxygen/oxygen.diff.water.html)
st=0.0728;%surface tension, kg/s2

% refer to agitation .m file
R=8.205*10^-2;% L atm/ mol K
T=293.15; %K
H=769.23; % T=298.15, L atm/mol
H=H*exp(-1700*(1/T-1/298.15)) % L atm/mol

% inlet interfacial concentration caused by impurity of nitrogen (99.5%)
sn=99.5/100 %adjustable
so=1-sn
po=so*(1+1000*9.81*0.3048/101325)
cGin=po/(R*T) % mol/L (=0.5% v%)

c1=VSL/(VSL+6);
c2=2.7847*log10(c1)+7.8035;
z=0.4191; % horizontal pipe length
```

```
% variabls then
QG=7.86579*10^-6*(5:0.5:350);

for i=1:691
   VSG(i)=QG(i)/AP;
   ReSG(i)=D*VSG(i)*orhG/viscosityG;
   GHUp(i)=0.83*(QG(i)/(QG(i)+QL));%GHUp = gas hold-up of pipe
   LHUp(i)=1-GHUp(i); %LHUp =liquid hold-up of pipe
   % now comes the calculation of theta
   theta(i) = 3; % set an initial value to theta
   for j=1:50
      f=theta(i)-sin(theta(i))-2*pi*LHUp(i);
      g=1-cos(theta(i));
      theta(i)=theta(i)-f/g;
   end
   AL(i)=LHUp(i)*pi/4*D^2;
   SL(i)=D/2*theta(i);
   Si(i)=D*sin(theta(i)/2);
   VLA(i)=VSL/LHUp(i);
   VGA(i)=VSG(i)/GHUp(i);
   fL(i)=0.0262*(LHUp(i)*ReSL)^-0.139;
   fSG(i)=16/ReSG(i);
   fi(i)=(1.76*(VSG(i)/6)+c2)*fSG(i);
   twL(i)=fL(i)*orhL*VLA(i)^2/2;
   ti(i)=fi(i)*orhG*(VGA(i)-VLA(i))^2/2;
   deltaPL(i)=(twL(i)*SL(i)-ti(i)*Si(i))/AL(i);
   FED(i)=deltaPL(i)*(VSL+VSG(i))/101325; % FED= friction energy dissipation
   kLap(i)=3.47*FED(i)^0.4*(Df*10000)^0.5*(st*1000)^0.5*(viscosityL*1000)^0.05*(D*39.3701)^-
0.68;

   k1(i)=-kLap(i)*AP/QL;
   k2(i)=1+(R*T*QL)/(QG(i)*H);
   k3(i)=R*T/H*(QL*cLin/QG(i)+cGin);
```

```
%cLTin is the inlet concentration of tank,which is the pipe DO
%concentration at z=0.4191m

% cLTin(i)=(cLin-k3(i)/k2(i))*exp(k1(i)*k2(i)*z)+k3(i)/k2(i);
cLTin(i)=((cLin-R*T*cGin/H)/k2(i))*exp(k1(i)*k2(i)*z)+k3(i)/k2(i);

effp(i)=(cLin-cLTin(i))/cLin*100; % pipe efficiency

cGTin(i)=QL/QG(i)*(cLin-cLTin(i))+cGin;
cst(i)=cGTin(i)*R*T/H; % cs' in the paper

% In the square bubble column now

DT=0.4064; % so-called bubble column diameter, m
hL=0.3048;% m
A=DT^2; % to distinguish it from last AP for pipe
VL=hL*DT^2; %m3
g=9.81;
Bo=g*DT^2*orhL/st;
Ga=g*DT^3/kviscosityL^2;
UG(i)=QG(i)/A; %m/s
Fr(i)=UG(i)/sqrt(g*DT);
const1(i)=0.2*Bo^(1/8)*Ga^(1/12)*Fr(i);

% then it gives F(epsilon)=const1(i)*(1-epsilon(i))^4-epsilon(i)=0
% use Newton's method to solve

epsilon(i)=0.02;
for k=1:100
   F=const1(i)*(1-epsilon(i))^4-epsilon(i);
   G=-4*const1(i)*(1-epsilon(i))^3-1;
   epsilon(i)=epsilon(i)-F/G;
end
% Now we have the gas holdup in the bubble column "epsilon"
% Next comes the evaluation of volumetric mass transfer coefficient
```

```
    % epsilon(i)=1.07*Fr(i)^(1/3); this is too large
    % x(i)=3.43*UG(i)^1.03*100^1.03/100;
    Sc=kviscosityL/Df;

    %kLa(i)=0.6*Sc^0.5*Bo^0.62*Ga^0.31*epsilon(i)^1.1*(Df/DT^2);% this is for bubble column mass transfer coefficient estimate
    %kLa(i)=0.092/60*(UG(i)*3600)^0.516;
    kLa(i)=1.091*UG(i)^0.8;
    %kLa(i)=0.11/60*(UG(i)*3600)^0.615;
    cLout(i)=(kLa(i)*VL*cst(i)+QL*cLTin(i))/(kLa(i)*VL+QL);
    effT(i)=((cLin-cLout(i))/cLin)*100;
end
QG=QG';
effT=effT';
plot(QG, effT)
```

A. 5 For CSTR – Effect of Q_G at N_I = 618 rpm

```
clc
clear all
format compact
format short
% constants first
cLin=10; %ppm
cLin=cLin/(32*1000) % mol/L

QL=0.000126;%m3/s
orhL=1000; % kg/m3
orhG=1.429; % kg/m3
viscosityL=0.001; % Pa*s
viscosityG=       0.00002018; % Pa*s
D=0.0254;% pipe diameter, m
AT=pi/4*D^2;% pipe cross sectional area, m2
VSL=QL/AT; % liquid superficial velocity, m/s
ReSL=D*VSL*orhL/viscosityL;% liquid Reynolds number
```

```
Df=2.3*10^-9; %diffusivity; Df, m2/s, (or 1.97*10^-9,
http://compost.css.cornell.edu/oxygen/oxygen.diff.water.html)
st=0.0728;%surface tension: st

% refer to agitation .m file
R=8.205*10^-2;% L atm/ mol K
T=293.15; %K
H=769.23; % T=298.15, L atm/mol
H=H*exp(-1700*(1/T-1/298.15)) % L atm/mol

% inlet interfacial concentration caused by impurity of nitrogen (99.5%)
sn=99.5/100 %adjustable
so=1-sn
po=so*(1+1000*9.81*0.3048/101325)

cGin=po/(R*T) % mol/L (=0.5% v%)

c1=VSL/(VSL+6);
c2=2.7847*log10(c1)+7.8035;
z=0.4191; % horizontal pipe length

% variabls then
QG=7.86579*10^-6*(5:0.5:150);

for i=1:291
   VSG(i)=QG(i)/AT;
   ReSG(i)=D*VSG(i)*orhG/viscosityG;
   GHUp(i)=0.83*(QG(i)/(QG(i)+QL));%GHUp = gas hold-up of pipe
   LHUp(i)=1-GHUp(i); %LHUp =liquid hold-up of pipe
   % now comes the calculation of theta
   theta(i) = 3; % set an initial value to theta
   for j=1:50
      f=theta(i)-sin(theta(i))-2*pi*LHUp(i);
      g=1-cos(theta(i));
      theta(i)=theta(i)-f/g;
```

```
    end

    AL(i)=LHUp(i)*pi/4*D^2;
    SL(i)=D/2*theta(i);
    Si(i)=D*sin(theta(i)/2);
    VLA(i)=VSL/LHUp(i);
    VGA(i)=VSG(i)/GHUp(i);
    fL(i)=0.0262*(LHUp(i)*ReSL)^-0.139;
    fSG(i)=16/ReSG(i);
    fi(i)=(1.76*(VSG(i)/6)+c2)*fSG(i);
    twL(i)=fL(i)*orhL*VLA(i)^2/2;
    ti(i)=fi(i)*orhG*(VGA(i)-VLA(i))^2/2;
    deltaPL(i)=(twL(i)*SL(i)-ti(i)*Si(i))/AL(i);
    FED(i)=deltaPL(i)*(VSL+VSG(i))/101325; % FED= friction energy dissipation
    kLap(i)=3.47*FED(i)^0.4*(Df*10000)^0.5*(st*1000)^0.5*(viscosityL*1000)^0.05*(D*39.3701)^-
0.68;

    k1(i)=-kLap(i)*AT/QL;
    k2(i)=1+(R*T*QL)/(QG(i)*H);
    k3(i)=R*T/H*(QL*cLin/QG(i)+cGin);

    %cLTin is the inlet concentration of tank,which is the pipe DO
    %concentration at z=0.4191m

   % cLTin(i)=(cLin-k3(i)/k2(i))*exp(k1(i)*k2(i)*z)+k3(i)/k2(i);
    cLTin(i)=((cLin-R*T*cGin/H)/k2(i))*exp(k1(i)*k2(i)*z)+k3(i)/k2(i);

    effp(i)=(cLin-cLTin(i))/cLin*100; % pipe efficiency

    cGTin(i)=QL/QG(i)*(cLin-cLTin(i))+cGin;
    cst(i)=cGTin(i)*R*T/H; % cs' in the paper

    % In the tank now

    DT=0.4064;
```

```
hL=0.3048;
A=DT^2; % to distinguish it from last AT for pipe
VL=hL*DT^2;
DI=4*0.0254;
s=9.5*0.0254;
g=9.81;
Ncr=(0.23*g*s/DI^2)^0.5;
N=618/60; % impeller speed
QI=0.0021*(N^2-Ncr^2)^0.75*DI^3;
Ncd(i)=4*(QG(i)+QI)^0.5*DT^0.25/DI^2;
%kLaT(i)=3.35*(N/Ncd(i))^1.464*(QG(i)+QI)/A;% since now the reactor is a conventional stirred tank, this equation is selected rather than others
kLaT(i)=1.59*(N/Ncd(i))^1.342*((QG(i)+QI)/A)^0.93*(DT/DI)^0.415;
cLout(i)=(kLaT(i)*VL*cst(i)+QL*cLTin(i))/(kLaT(i)*VL+QL);
effT(i)=((cLin-cLout(i))/cLin)*100;
end
QG=QG';
effT=effT';
plot(QG, effT)
```

A. 6 For Semi-batch Model for CSTR

A. 6.1 At N_I = 618 rpm, Q_G = 50 scfH

```
clc
clear all

cLin=9.7; %ppm
cLin=cLin/(32*1000) % mol/L

R=8.205*10^-2;% L atm/ mol K
T=293.15; %K
H=769.23; % T=298.15, L atm/mol
H=H*exp(-1700*(1/T-1/298.15)); % L atm/mol

DT=0.4064;
```

```
hL=0.3048;
A=DT^2; % to distinguish it from last AT for pipe
VT=hL*DT^2;

DI=4*0.0254;
s=9.5*0.0254;
g=9.81;
Ncr=(0.21*g*s/DI^2)^0.5;
QG=7.86579*10^-6*50%gas flow rate, adjustable

sn=99.5/100 %adjustable
so=1-sn
po=so*(1+1000*9.81*0.3048/101325)

cG1=po/(R*T) % mol/L (=0.5% v%)

N=618/60;% impeller speed, adjustable
QI=0.0021*(N^2-Ncr^2)^0.75*DI^3
Ncd=4*(QG+QI)^0.5*DT^0.25/DI^2;

%kLa=3.35*(N/Ncd)^1.464*(QG+QI)/A
kLa=1.59*(N/Ncd)^1.342*((QG+QI)/A)^0.93*(DT/DI)^0.415

k1=QG*kLa/(QG+kLa*VT*R*T/H)
k2=cLin-cG1*R*T/H
k3=cG1*R*T/H*32*1000

t(1)=0
cL(1)=cLin

for i=1:2500
   t(i+1)=t(i)+0.5;
   cL(i+1)=k2*exp(-k1*t(i+1))+cG1*R*T/H;
   eff(i+1)=(1-cL(i+1)/cL(1))*100;
end
```

```
t=t';
eff=eff';
plot(t,eff)

eff(2501)
```

A. 6.2 At N_I = 999 rpm, Q_G = 75 scfH

```
clc
clear all

cLin=8.55; %ppm
cLin=cLin/(32*1000) % mol/L

R=8.205*10^-2;% L atm/ mol K
T=293.15; %K
H=769.23; % T=298.15, L atm/mol
H=H*exp(-1700*(1/T-1/298.15)); % L atm/mol

DT=0.4064;
hL=0.3048;
A=DT^2; % to distinguish it from last AT for pipe
VT=hL*DT^2;

DI=4*0.0254;
s=9.5*0.0254;
g=9.81;
Ncr=(0.21*g*s/DI^2)^0.5;

QG=7.86579*10^-6*75%gas flow rate, adjustable

sn=99.5/100 %adjustable
so=1-sn
po=so*(1+1000*9.81*0.3048/101325)
```

```
cG1=po/(R*T) % mol/L (=0.5% v%)

N=999/60;% impeller speed, adjustable
QI=0.0021*(N^2-Ncr^2)^0.75*DI^3
Ncd=4*(QG+QI)^0.5*DT^0.25/DI^2;

%kLa=3.35*(N/Ncd)^1.464*(QG+QI)/A
kLa=1.59*(N/Ncd)^1.342*((QG+QI)/A)^0.93*(DT/DI)^0.415

k1=QG*kLa/(QG+kLa*VT*R*T/H)
k2=cLin-cG1*R*T/H
k3=cG1*R*T/H*32*1000

t(1)=0
cL(1)=cLin

for i=1:2500
   t(i+1)=t(i)+0.5;
   cL(i+1)=k2*exp(-k1*t(i+1))+cG1*R*T/H;
   eff(i+1)=(1-cL(i+1)/cL(1))*100;
end
t=t';
eff=eff';
plot(t,eff)

eff(2501)
```

Appendix B – Other Relevant Publication

INTERNATIONAL JOURNAL OF CHEMICAL REACTOR ENGINEERING

Volume 10 2012 *Article* A50

New Correlations of Volumetric Liquid-Phase Mass Transfer Coefficients in Gas-Inducing Agitated Tank Reactors

Hesheng Yu* Zhongchao Tan†

*University of Waterloo, h48yu@uwaterloo.ca

†University of Waterloo, tanz@uwaterloo.ca

ISSN 1542-6580
DOI: 10.1515/1542-6580.1

New Correlations of Volumetric Liquid-Phase Mass Transfer Coefficients in Gas-Inducing Agitated Tank Reactors*

Hesheng Yu and Zhongchao Tan

Abstract

Volumetric liquid-phase mass transfer coefficient (kLa) is one of the most important parameters for the evaluation of the performance of a gas-inducing agitated tank (GIAT). In this paper, two equations in terms of power input per unit liquid volume (P/VL) and relative gas dispersion parameter (NI/Ncd), respectively, are developed according to data in literature. They can correlate existing kLa values within ±20% of measured ones for bladed impellers with different impeller submergence to tank diameter ratios in the range of 0.5 -1.23. In order to validate these equations, the liquid phase mass transfer coefficients in a continuous GIAT equipped with a 4-blade straight impeller were measured by removal of oxygen from water. It was found that the equation in P/VL criterion could correlate kLa values within ±12% of the experimental data, and the equation in NI/Ncd criterion could correlate kLa values within ±15.6% with an exception of 26.8% for NI = 16.7 Hz.

KEYWORDS: volumetric liquid-phase mass transfer coefficient, gas-inducing impeller, agitated tank

---

*Authors:
Hesheng Yu: Department of Mechanical & Mechatronics Engineering, University of Waterloo.
Zhongchao Tan*: Department of Mechanical & Mechatronics Engineering, Department of Civil & Environmental Engineering, University of Waterloo.

Corresponding author: Dr. Z. Tan, 200 University Avenue West, Waterloo, Ontario, Canada N2L 3G1; Phone: (519) 888-4567 ext. 38718; Email: tanz@uwaterloo.ca

The authors would like to acknowledge financial support provided by Natural Sciences and Engineering Research Council (NSERC) of Canada, Imperial Oil Ltd., Enersul Inc. and assistance of Mr. Harry Lei in experimental data collection.

1. Introduction

Gas-liquid stirred tank reactors (STRs) have been widely used in chemical, biochemical and petroleum industries owing to their low capital cost, excellent mixing effect and great mass transfer rate (Dhainaut *et al.*, 2005; Pinelli *et al.*, 2010). As a special STR, a gas-inducing agitated tank (GIAT) is characterized by its unique gas dispersion process. Gas is induced into a GIAT by its rotating impeller at a speed beyond a critical value instead of being sparged into the system through a distributor (Forrester *et al.*, 1998). The advantages of a GIAT are manifested in unit operations where a dead-end mode is wanted. Applications of GIATs include, but are not limited to, alkylation, ethoxylation, hydrogenation, chlorination, ammonolysis, and oxidation (Joshi and Sharma, 1977; Patwardhan and Joshi, 1999). They are also employed for froth flotation in mineral processing (Sawant *et al.*, 1981) and in wastewater treatment (Sardeing *et al.*, 2006).

The volumetric liquid-phase mass transfer coefficient, denoted as k_La in most publications, is one of the most important parameters for the evaluation of the performance of a GIAT. It quantifies the rate of interfacial mass transfer of a substance in a gas-liquid system. It is well acknowledged that k_La is an intensive variable (Hallaile and Merchuk, 1986), which primarily depends on the geometry and operation of the reactor. However, it is independent of the volume of liquid in the reactor. Several empirical equations have been developed by other researchers. Morsi's group provided correlations of k_La in a GIAT through statistics analysis; these correlations were presented in relatively complicated formats (Tekie *et al.*, 1997; Fillion and Morsi, 2000; Lemoine *et al.*, 2004; Lemoine and Morsi, 2005). They focused on organic solution systems at high pressures and temperatures, which are not the subject of present study.

Heim *et al.* (1995) proposed a dimensionless correlation (Eq. 1 below) for a disc impeller in an oxygen-water system at Froude numbers (Fr) of 0.28-1.49 and modified Reynolds numbers (Re^*) of 33,000-260,000. Zieverink *et al.* (2006) studied the effects of fluid properties on mass transfer in a small GIAT (0.064-meter inner diameter autoclave) and concluded that the values of k_La were best represented by a dimensionless correlation containing a Froude group ($Fr\text{-}Fr_{cr}$), Reynolds number and Schmidt number (Sh).

$$Sh = 1.04 \times 10^{-4}\left(1 - \exp\left(-1331.20 Re^{*-0.557} Fr^{0.869}\right)\right) \qquad (1)$$

Similar to the approach for a sparged STR, Joshi's group correlated k_La with the impeller power input per unit volume of liquid (P/V_L) as

$$k_La = C\left(\frac{P}{V_L}\right)^{c_1}(U_G)^{c_2} \qquad (2)$$

where C, c_1 and c_2 are empirical constants. Joshi and Sharma (1977) proposed that C=0.0068, c_1=0.55 and c_2=0.5 for U_G < 0.005 m/s; C=0.00326, c_1=0.55 and c_2=0.25 for U_G>0.005 m/s. Later, Sawant *et al.* (1981) proposed different coefficients as C=0.000617, c_1=0.5 and c_2=0.

Solving Equation (2) requires a known gas induction rate, Q_I, and P/V_L. It is necessary to introduce the critical impeller speed, N_{cr}, which is also referred to as the minimum impeller speed for the onset of gas induction before the determination of gas induction rate. Gas is induced into a in a typical GIAT by a rotating impeller at a speed above the critical speed, which can be predicted by using Equation (3) within 10% of the measured values (Sawant and Joshi, 1979; Patil *et al.*, 2005),

$$Fr_{cr} = \frac{N_{cr}^2 d_I^2}{gs} = constant \qquad (3)$$

The constant was 0.21 ± 0.04 for different types of impellers including pipe impellers, flattened cylindrical impellers, covered turbine impellers, Wemco flotation cells, Denver flotation cells, and shrouded turbine. Unlike the critical impeller speed for gas induction, the rate of gas induction is dependent on the type of impeller. Generally there are two types of gas-inducing impellers, namely hollow shaft with hollow blades and the rotor-stator type.

Existing correlations for various impellers are summarized in Table 1, which shows that the gas induction rate is often correlated with the difference between Froude number and critical Froude number (Fr-Fr_{cr}) or the square difference between impeller speed and critical speed for the onset of gas induction (N_I^2-N_{cr}^2). As introduced above, gas can only be induced into a GIAT by a rotating impeller at a speed beyond the critical value, which is governed by Equation (3). Gas induction rate increases with increasing impeller speed because the pressure field and vortex intensity increase with impeller speed. As a result, it is natural to correlate the rate of gas induction with the difference between Froude number and critical Froude number. As Froude number is proportional to the square of impeller speed, gas induction rate can also be correlated with the square difference between impeller speed and critical speed for the onset of gas induction if the value of gravitational acceleration (9.81 m/s^2) is substituted.

Table 1 Correlations of gas induction rate for different impellers

Impeller system	Correlation	Reference
Denver with stator	$Q_I = 0.0021(N_I^2 - N_{cr}^2)^{0.75} d_I^3$	(Sawant *et al.*, 1981)
PBTD with stator	$Q_G^2 = 2.68 \times 10^{-4} (\Delta P D^2)^{1.184}$	(Raidoo *et al.*, 1987)
hollow pipe + disc	$N_A = C[1 - \exp(-CRe^{c1} Fr^{c2})]$	(Heim *et al.*, 1995)
PBTD with stator	$Q_G = 129.95 N_I R_I^2 \left(1 - \frac{2gs}{0.85(\pi N_I d_I)^2}\right) + 92.42 N_I R_I^3 (1 - 0.30(\frac{2gs}{0.85(\pi N_I d_I)^2})^{1.5})$	(Saravanan and Joshi, 1995)
hollow pipe + bladed concave	$-\Delta P_D = \Delta P_P + \Delta P_0 + \Delta P_\gamma + \Delta P_{KE}$	(Forrester *et al.*, 1998)
hollow pipe + double disc	$N_A = [23(1 + (Fr - Fr_{cr})^{-1.7})]^{-1}$	(Poncin *et al.*, 2002)

The prediction of power consumption has not been studied as extensively as critical impeller speed and gas induction rate. A correlation for power input per unit liquid volume (P/V_L) in a GIAT was developed by Saravanan *et al.* (1996) as follows.

$$\frac{P - 1.767(2\pi N_I)}{\rho_L W N_I^3 R_I^4} = 22.24 - 6.71[1 - \frac{2gs}{0.84(\pi d_I N_I)^2}]^3 \qquad (4)$$

This semi-empirical equation was obtained using GIATs equipped with pitched turbine impellers with vessel diameters between 0.57 and 1.5 m. The ratio of impeller diameter (d_I) to vessel diameter (d_T) was in the range of $0.13 < d_I/d_T < 0.59$ and the impeller speed (N_I) of $0.13 < N_I < 13.5$ Hz.

Different from those who correlated k_La in a conventional STR with P/V_L, Yawalkar *et al.* (2002a) proposed a correlation for k_La in the form of gas relative dispersion parameter, N_I/N_{cd}, as shown in Equation (5).

$$k_L a = K \left(\frac{N_I}{N_{cd}}\right)^{k_1} U_G^{k_2} \qquad (5)$$

where K, k_1 and k_2 are coefficient or exponents to be determined empirically. Yawalkar *et al.* (2002a) proposed K=3.35, k_1=1.464 and k_2=1 for tanks equipped with disk-type impellers. N_{cd} is the minimum impeller speed for complete dispersion of gas phase. They claimed that, for a coalescing system, Equation (5)

predicted k_La within 22% of experimental values for vessel diameters (d_T) of 0.39 - 2.7 m. In addition, gas-liquid contacting at an impeller speed below N_{cd} led to a poor reactor performance as the lower part of reactor was not used effectively due to incomplete gas dispersion.

Joshi's group reported that the expression of k_La for conventional STRs was also applicable to GIATs. Sawant (1981) and Forrester (1998) stated that k_La in a GIAT could be accurately predicted by the correlation for a conventional STR operating at similar specific power inputs. Therefore, k_La in a GIAT can be estimated by using Equation (5) too. More importantly, the prediction of N_{cd} has been well established. However, there has been no correlation of k_La of a GIAT in terms of N_I/N_{cd} in the literature that is publicly available.

With a large amount of experimental data using different system configurations and operations, Nienow *et al.* (1977) correlated N_{cd} in a bladed-turbine-type STR with the gas volumetric flow rate and the diameters of the impeller and the reactor body as follows.

$$N_{cd} = \frac{4Q_G^{0.5} d_T^{0.25}}{d_I^2} \tag{6}$$

Although Equation (6) was developed for a conventional STR, it is reasonable to assume that it can also be applied to a GIAT, which is essentially a specific type of STR. The only modification needed is the substitution of the gas induction rate Q_I given by one of the equations in Table 1 for Q_G.

Existing correlations for mass transfer coefficient in GIATs equipped with bladed-type impeller were developed under specific conditions with limited applicability; therefore, it is better to develop new correlations with accuracy and a broad applicability. In this paper, the applicability of the four aforementioned existing correlations was first examined by available experimental data in literature. Next, two new mass transfer correlations were developed according to the data, and these new correlations were experimentally validated by mass transfer data in a laboratory setting.

2. Experimental

Figure 1 shows the continuous GIAT for the removal of dissolved oxygen from water using nitrogen bubbles. The GIAT reactor was made of a square acrylic with a width of 406.4 mm. Its corners function as virtual baffles, which prevents the formation of a surface vortex and promotes vertical circulation. Its height was 457.2 mm. Water level inside the tank was maintained at 304.8 mm, above which was headspace. A 4-bladed straight turbine impeller with both height and diameter of 101.6 mm was chosen and enclosed in a shrouded draft tube

perforated with 1.6 mm diameter holes. The impeller and shroud were submerged 241.3 mm below the liquid surface. The speed of agitation was adjusted by a variable frequency driver (VFD). The shroud enabled better induction of gas as it prevented froth accumulation on the free liquid surface. Nitrogen (99.5% of purity from Praxair Inc.) was induced into the tank from a gas inlet pipe on the top of the shroud by a rotating impeller. Meanwhile, gas-liquid interface was sheared by impeller blade when the forced vortex, which was also generated by the rotating impeller, was sufficiently close to the impeller, entrapping nitrogen bubbles and enabling the mixing of gas and liquid.

Volumetric liquid phase mass transfer coefficient was calculated using the oxygen concentrations measured at the inlet and outlet of the tank. Oxygen concentration in water was measured by using a dissolved oxygen (DO) meter (Model WU-53013-10 from Cole-Parmer, Inc.) with accuracy of ±1% of full scale. Three replications were taken for each data point. The critical speed for gas induction, N_{cr}, was much greater than the minimum speed needed for complete gas dispersion, N_{cd}. Therefore, it was reasonable to assume that liquid was completely mixed during tests. Then a mass balance gives,

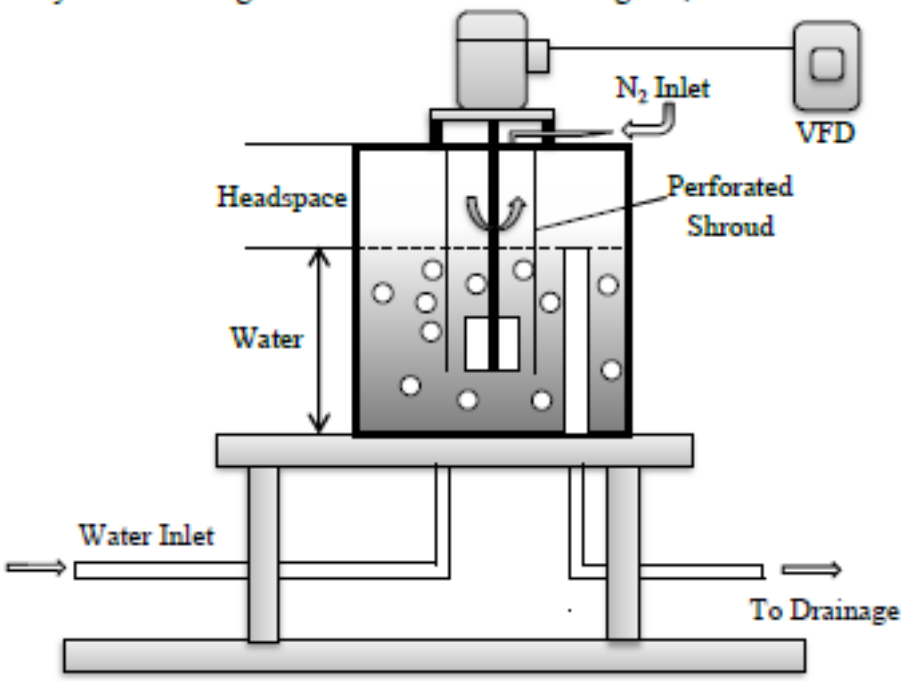

Figure 1: The GIAT for the removal of dissolved oxygen from water

$$Q_L c_{in} = Q_L c_{out} + k_L a V_L (c_{out} - c_s) \qquad (7)$$

Assuming the 0.5% impurity of nitrogen supply is all oxygen and neglecting the change in gas concentration in the tank, and one can get,

$$c_s = c_{sin} = 32000 \times 0.5\% P_T / H_{O_2} \quad (8)$$

The Henry's constant of oxygen is H_{O_2}=697.94 L·atm/mol and the total pressure is

$$P_T = (P_A + \rho g h_L)/101325 \quad (9)$$

Substituting P_A=101,325 Pa, ρ=1,000kg/m^3, g=9.81 m/s^2, h_L=0.3048 m into Equations (8) and (9) gives

$$c_s = c_{sin} = 0.236\ ppmm \quad (10)$$

Equation (7) can then be rewritten as,

$$k_L a = \frac{Q_L(c_{in} - c_{out})}{V_L(c_{out} - 0.236)} \quad (11)$$

3. Results and Discussion

3.1 Applicability of Existing Correlations

Most mass transfer coefficients in literature were presented in terms of specific power input (P/V_L) instead of impeller speed (N_I); the evaluation of P/V_L in a GIAT has not been well established. Therefore, limited data is available in the literature. To the authors' best knowledge, 44 data points were found in literature for coalescing (air-water) system in a GIAT equipped with bladed or disc-type impellers; they are summarized in Table 2. In order to minimize errors, values of superficial gas velocity, U_G, are derived from the known gas induction rate.

The deviations between measured and calculated k_La values of four available correlations are tabulated in Table 3. Equation (1), which is dimensionless, given by Heim *et al.* (1995) could only give acceptable predictions to the data of Forrester *et al.* (1998) with maximum error of -46.75%. The error could be as high as -95.70% for other studies. It was likely because the dimensionless variables in Equation (1) were not highly correlated. Its coefficient of determination, R^2 was 0.755. Furthermore, for the tank with a geometry of d_T = 0.3 m and s/d_T between 0.745 and 0.857, which was used by Heim *et al.* (1995), it did not fall into the range tabulated in Table 2. It is also worthwhile to point out

that the impeller adopted by Heim *et al.* (1995) is a disc turbine, which is slightly different from impellers in Table 2. This may lead to erroneous results.

Table 2: Available literature data for mass transfer scale-up correlation development

Researcher	d_T, m	s/d_T	$U_G \times 10^4$, m/s	N_I, Hz	P/V_L, W/m^3	N_I/N_{cd}	Impeller
Forrester *et al.* (1998)	0.45	0.5	4.9-13.46	5.71 - 10	625-2290	4.12 – 4.39	six-bladed concave
Poncin *et al.* (2002)	0.6	0.9, 1.23	17.68-145.01	8.33 - 16.67	209 - 698	2.94 – 4.23	double disk
Kasundra *et al.* (2008)	0.5	0.66	33.95-280.11	4 - 12	1692 - 8744	1.50 - 2.99	double disk, modified double disk, PBTD 45°, PBTD 60°

Table 3: Comparison between various correlations

Correlation	Deviation between measured and predicted k_La values		
	Forrester	Poncin	Kasundra
Joshi and Sharma	45.30 ~ 62.09%	70.59 ~ 78.40%	-15.55 ~45.26%
Sawant *et al.*	-21.67 ~ 18.20%	64.32 ~ 86.41%	47.97 ~ 80.87%
Heim *et al.*	-46.75 ~ 12.09%	-71.20 ~ -43.93%	-95.70 ~ -81.13%
Yawalkar *et al.*	-29.00 ~ 3.82%	-197.75 ~ -96.03%	-39.20 ~ 40.37%

However, the effect of impeller shape has already been included in terms of P/V_L and N_I/N_{cd} when evaluating the other three correlations. Generally speaking, a radial flow impeller such as disc turbine has a larger Power number than an axial flow impeller, e.g. pitched bladed impeller, and propeller (Bates *et al.*, 1963; Leentvaar and Ywema, 1980). Joshi and Sharma (1977) investigated the mass transfer characteristics of three such impellers as pipe, flattened cylindrical and disk turbine in a stirring tank. They found that at the same level of power consumption per unit liquid volume, comparable values of a and k_La could be obtained regardless of impeller type. Similar findings have also been reported by Sawant *et al.* (1981).

Furthermore, the minimum speed for gas complete dispersion, N_{cd}, is greatly associated with the turbulence intensity (Yawalkar *et al.*, 2002b), which depends on specific energy dissipation. According to Calderbank and Moo-Young (1961), turbulent flow first produces large eddies which will break into small eddies until energy dissipation is completed. The properties of these small eddies are exclusively dependent on the local energy dissipation rate per unit mass of

fluid. And the scale of these smallest eddies is related to liquid properties and specific energy dissipation. Therefore, the effect of impeller shape is represented by N_{cd} if mass transfer coefficient k_La is described in terms of N_T/N_{cd}.

The correlation of Sawant *et al.* (1981) estimated k_La within ±20% of measured values by Forrester *et al.* (1998); however, deviations of the other two were 64.32 - 86.41% and 47.97 - 80.87%, respectively. This might be due to the over simplification of their correlation in terms of only P/V_L. The relatively better correlation for the data of Forrester *et al.* (1998) was probably because the diameter of 0.45 m is closer to the diameters ranged from 0.1 m to 0.38 m used by Sawant *et al.* (1981).

Joshi and Sharma's formula (1977) performed better than the other two. Nonetheless, it did not match the data of Poncin *et al.* (2002), likely because this correlation did not take into account the effect of impeller submergence, which has been proven to be significant at a large ratio of submergence to tank diameter (Poncin *et al.*, 2002). Although the model of Yawalkar *et al.* (2002a) was fitted for conventional STRs with diameters from 0.39 to 2.7 m, its performance was comparable to that of Joshi and Shama (1977). Sawant *et al.* (1981) and Forrester *et al.* (1998) also reported similar findings when using correlations in specific power input criterion. They stated that k_La in a GIAT could be accurately predicted by a correlation for a conventional STR operating at similar specific power inputs. After all, a GIAT is one type of stirring tank reactor, and it is understandable if correlations for a conventional STR are applicable to a GIAT with certain geometric configuration and experimental conditions. The correlation of Yawalkar *et al.* (2002a) is more accurate for the study of Forrester *et al.* (1998) with deviations within ±20%, followed by ±40% for that of Kasundra *et al* (2008). For the same reason as Joshi and Sharma's model, it largely overestimates the k_La values of Poncin *et al* (2002).

3.2 New Correlations for Mass Transfer Coefficient in a GIAT

Existing correlations of mass transfer coefficient in a GIAT in Equations (2) and (5) do not include the ratio of impeller submergence to tank diameter, s/d_T, accounting for the effect of submergence. Nevertheless, Poncin *et al.* (2002) reported that this effect was significant. Thus, the term s/d_T is taken into account in the development of new mass transfer correlations herein. Accordingly, the volumetric liquid phase mass transfer coefficient k_La can be expressed as,

$$k_La = C\left(\frac{P}{V_L}\right)^{c_1}(U_G)^{c_2}\left(\frac{s}{d_T}\right)^{c_3} \qquad (12)$$

or

$$k_L a = K\left(\frac{N_I}{N_{cd}}\right)^{k_1} U_G{}^{k_2}\left(\frac{s}{d_T}\right)^{k_3} \quad (13)$$

Taking the natural logarithm of both left- and right-hand sides of Equations (12) and (13) transforms them to linear equations, respectively,

$$\ln(k_L a) = lnC + c_1 \ln\left(\frac{P}{V_L}\right) + c_2 \ln(U_G) + c_3 \ln\left(\frac{s}{d_T}\right) \quad (14)$$

$$\ln(k_L a) = lnK + k_1 \ln\left(\frac{N_I}{N_{cd}}\right) + k_2 \ln(U_G) + k_3 \ln\left(\frac{s}{d_T}\right) \quad (15)$$

The regression coefficients lnC, c_1, c_2, c_3 and lnK, k_1, k_2,k_3 are known. Ultimately, the correlations are described using Equations (16) and (17) with R^2 values of 0.980 and 0.978, respectively. Parity plots of these two correlations in Equations (16) and (17) for different studies are presented in Figures 2 and 3, respectively. It can be seen that both correlate almost all data within ±20% of measured ones, which is much lower than those listed in Table 3. These two equations are applicable to different bladed-type impellers including six-bladed concave, double disk, modified double disk, PBTD 45°, PBTD 60° impellers with a wide range of impeller submergence to tank diameter ratio, $0.5<s/d_T<1.23$.

$$k_L a = 1.212\left(\frac{P}{V_L}\right)^{0.0816} U_G{}^{0.692}\left(\frac{s}{d_T}\right)^{-0.390} \quad (16)$$

$$k_L a = 2.504\left(\frac{N_I}{N_{cd}}\right)^{-0.220} U_G{}^{0.691}\left(\frac{s}{d_T}\right)^{-0.630} \quad (17)$$

It can be seen that the exponent value of P/V_L in Equation (16) is much smaller than those given by Joshi and Sharma (1977) and Sawant *et al* (1981). Different from a conventional STR, the effects of P/V_L, s/d_T and U_G in a GIAT depend on each other. In a conventional STR, the gas supply is independent and adjustable. In a GIAT, however, gas is induced by a rotating impeller at a speed beyond a critical value (N_{cr}). Therefore, the superficial gas velocity is mainly dependent upon impeller diameter (d_I) and speed (N_I) and the critical speed for the onset of gas induction (N_{cr}). It can be seen from Equation (3) that N_{cr} depends primarily on d_I and impeller submergence (s). Meanwhile, Equation 4 shows that P/V_L is a function of N_I, d_I and s. Therefore, in a given tank the mass transfer coefficient (k_La) is controlled by such three factors as impeller speed, diameter and submergence. In the simplest correlation, all the effects on k_La can be combined and represented by P/V_L only as Sawant *et al* did (1981).

Although using P/V_L alone avoids complexity, the applicability of this correlation is still limited and needs further improvement. This is why we include the term s/d_T to describe k_La in a GIAT. The decrease in exponent value of P/V_L is likely because the significance of submergence from P/V_L is shared by term (s/dT), and the contribution of impeller speed is shared by term U_G.

As N_{cd} relies on the specific energy dissipation (P/V_L), similar interpretation explains why the exponent of N_I/N_{cd} in Equation (17) is smaller than that provided by Yawalkar *et al.* (2002 a).

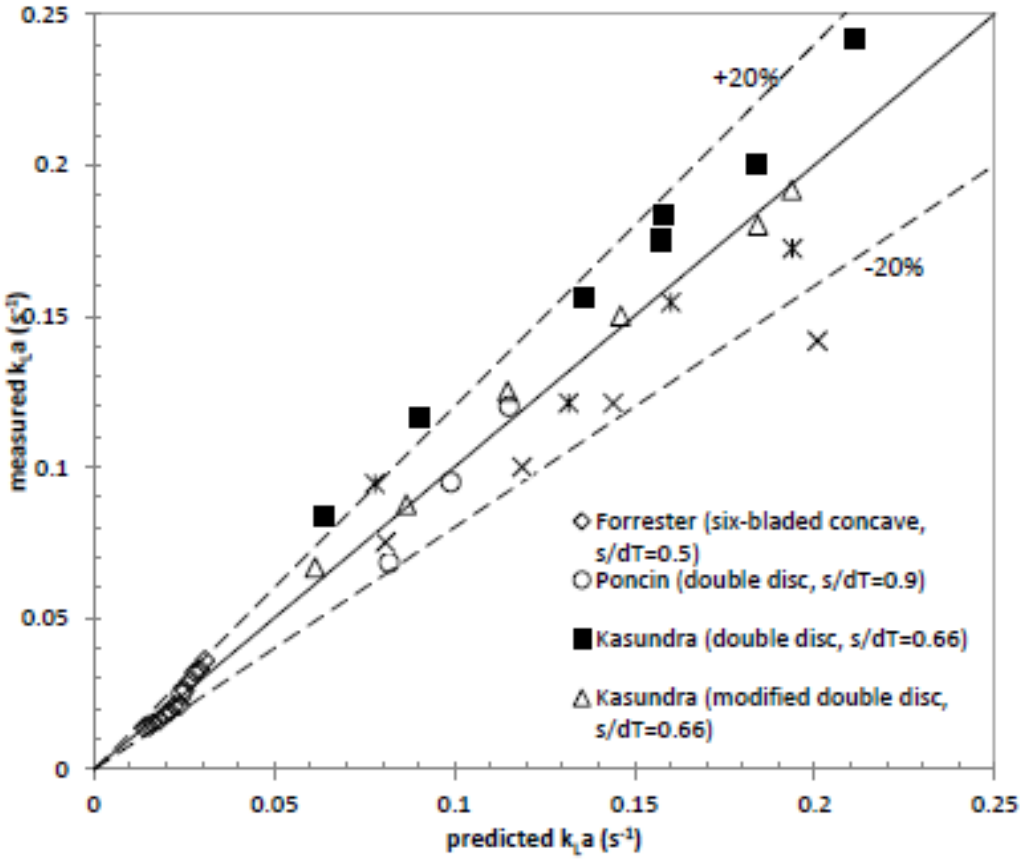

Figure 2: Comparison between measured k_La values and predicted k_La values by Equation (16)

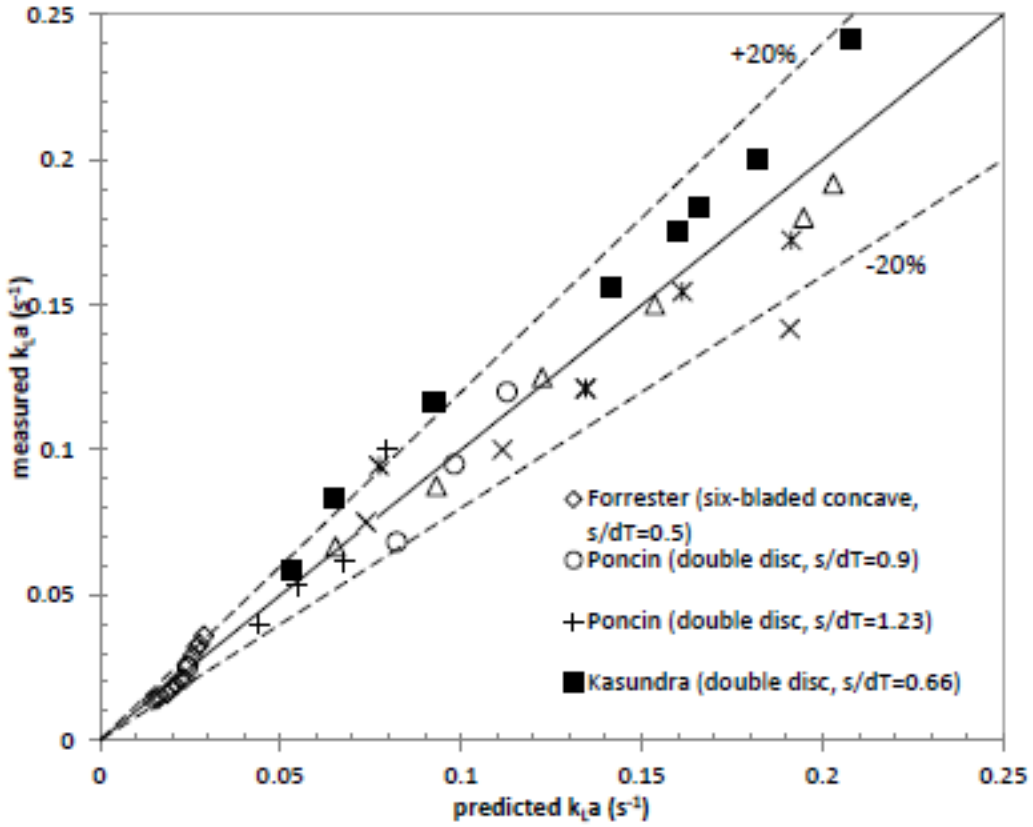

Figure 3: Comparison between measured k_La values and predicted k_La values by Equation (17)

3.3 Application of New Correlations to Our Experimental Data

3.3.1 Calculation Procedure

In order to compare the new correlations (Equations 16-17) with our experimental data, gas induction rate, power consumption and relative dispersion parameter of the 4-bladed straight impeller used in current study has to be determined. Cylindrical vessels equipped with four baffles are commonly used in literature while a square tank was utilized in the present work. A square tank can be considered as a cylindrical tank with four corners functioning as virtual baffles (Kresta *et al.*, 2006). As for the determination of "diameter" of a square tank, Leentvaar (1980) and Kresta (2006) proved that taking the side length of a square tank as the "diameter" would provide satisfactory results in terms of power consumption and mixing performance.

For specific power consumption, Leentvaar and Ywema (1980) investigated the effect of vessel geometry on impeller energy dissipation and

found that the dimensionless Power number for a square tank could be well estimated by the Power number of a baffled cylindrical tank with a distance between two baffles equal to the side length of the square tank. For example, baffles with width (B) of 10% of the vessel diameter (d_T) are evenly equipped in a cylindrical tank. Then this cylindrical tank is equivalent to a square tank with a side length of $0.8d_T$. Their experimental data showed for the same Reynolds number of 10^4, the Power number of a 126 mm i.d. cylindrical vessel was slightly higher than that of a 100 mm × 100 mm square tank. But they did not compare a cylindrical vessel to a square tank with a side length that equals the vessel diameter.

In addition, Kresta *et al.* (2006) compared the mixing performances between several square tanks and cylindrical tanks. They also concluded that the correlation of blend time for a cylindrical tank can also be used for a square tank if the "diameter" of the square tank was the side length and the Power number was assumed to be the same as that for a cylindrical tank.

Therefore, the tank shape (square or cylindrical) is believed to have a weak or even negligible effect on power consumption and mixing performance. Satisfactory results will be given if a square tank with a side length of d_{T_s} is treated as a cylindrical tank with a diameter of d_{T_s}. And, the value of side length of our square tank will be substituted into the corresponding equations for diameter in following calculations.

The effect of shroud on mass transfer coefficient is also insignificant and can be neglected. A shroud acts as a stator and is used to allow for better induction of gas as it prevented froth accumulation on the free liquid surface. In our gas-inducing rotor-stator system, nitrogen gas entered the reactor from a gas inlet pipe on the top of the shroud because of the low pressure field created by the rotating impeller. Gas-liquid interface was sheared by the impeller blade when the forced vortex was close enough to the impeller, entrapping nitrogen bubbles and enabling gas and liquid mixing (Patwardhan and Joshi, 1999).

Other researchers (Garcia-Ochoa and Castro, 2001; Yawalkar *et al.*, 2002a) believed that volumetric liquid-phase mass transfer coefficient, k_La, was independent of sparger/disperser type or its orifice diameter. The k_La is a product of k_L and a, in which the variation in k_L is rather small and the change in k_La depends mostly on the variation of specific interfacial area, which is highly related to bubble size (Sideman *et al.*, 1966). Considerations based on forces affecting bubble size in turbulent regime show that the optimum bubble diameter will be determined by turbulence intensity in the continuous phase caused by the energy dissipated by mechanical agitation and is independent of the dimensions of the orifice of the disperser (Calderbank, 1959; Sideman *et al.*, 1966; Miller, 1974). As bubble size and consequent specific interfacial area depend on turbulence

intensity, the volumetric gas-liquid mass transfer coefficient is also dependent primarily upon turbulence intensity (Yawalkar *et al.*, 2002a).

According to Calderbank and Moo-Young (1961), turbulence intensity is dependent upon properties of the liquid and specific energy dissipation. It is well-known that the specific energy dissipation can be described by Power number, which is constant at impeller speeds beyond a certain value (Leentvaar and Ywema, 1980). The energy dissipation per unit volume then becomes a function of impeller speed and diameter, liquid density, and tank diameter regardless of shroud.

As mentioned above, the gas induction rate is related to the impeller type and none of the equations in Table 1 are applicable to a 4-blade straight impeller. Therefore, a correlation for the closest type of impeller is used herein. The shrouded turbine system in this study is one type of rotor-stator impeller with the shroud acting as a stator. Therefore, the correlations for rotor-stator impellers are chosen over those for hollow shafts with hollow blades. The correlation of Sawant *et al.* (1981) holds a standard deviation of 3% for air-water system in Denver-type (which is a stator-rotor system) flotation cells with sizes from 100 mm×100 mm to 380 mm×380 mm. Since the reactor is a 406.4 mm × 406.4 mm square tank in our experimental setup, the correlation of Sawant *et al.* (1981) is chosen to estimate gas induction rate in our experiments. As for power consumption, Equation (4) is the only option although it was developed from pitched turbine impeller. And, our 4-blade impeller is basically a 90-degree pitched impeller. Hence, Equation (4) is deemed to give satisfactory results for power consumption prediction. In addition, the N_I/N_{cd} can be estimated by the combination of Equation (6) and the gas induction correlation of Sawant *et al.* (1981).

3.3.2 Validation of New Correlations with Our Experimental Data

The two correlations show that the effect of impeller speed is more significant than that of submergence. Therefore, the values of k_La corresponding to different impeller speeds are compared with those calculated using Equations (16) and (17). Figure 4 shows comparisons between predicted and experimentally determined values of k_La, and the error bars are corresponding standard deviations of the experimental data. It can be seen that both equations overestimate the k_La value for N_I=8.33 Hz. The difference might be caused by the prediction of gas induction rate. According to Sawant *et al.* (1981), correlation of gas induction rate is not applicable to the speed close to the critical speed for onset of gas induction, which is 6.94 Hz herein. At the beginning of gas induction, gas was induced in the region of impeller where the fluid density was drastically decreased and the pressure driving force arisen was much lower compared to that without induced gas. Therefore, the actual value of the rate of gas induction is much lower than is predicted, resulting in overestimation of k_La. For the other five speeds, values of

k_La calculated using both equations agree with the measured ones. Equations (16) and (17) can correlate the k_La values within ±12% and 15.6%, respectively, of experimental data with an exception of 26.8% calculated using Equation (17) for the last data point.

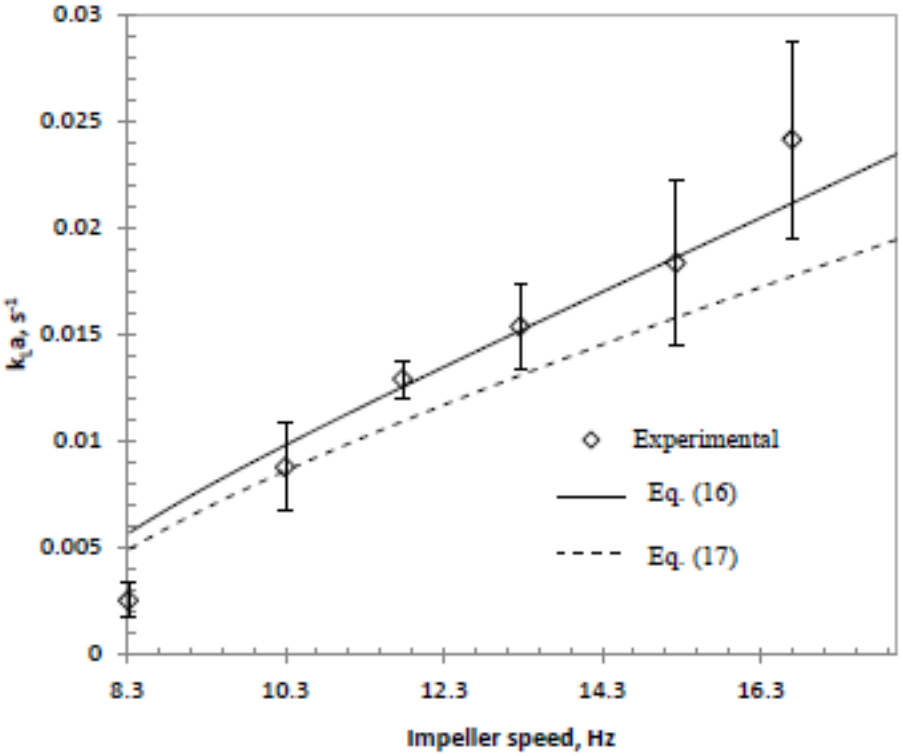

Figure 4: Validation of new correlations by effect of impeller speed

4. Conclusions

Based on the analyses within this paper, the following conclusions can be made. Two correlations (Equations (16) and (17)) are developed according to data in literature and include the ratio of submergence to tank diameter. They can be applied to a wide range of impellers with R^2 values of 0.980 and 0.978, respectively. Both equations are able to predict k_La values within ±20% of the measured ones. They can be applied to impellers with different types of blades including six-blade concave, double disk, modified double disk, PBTD 45°, PBTD 60° with a wide range of ratio of impeller submergence to tank diameter $0.5<s/d_T<1.23$. These two new correlations can also be used to calculate k_La in a GIAT equipped with a 4-blade straight impeller. Equation (16) correlates k_La values within ±12% of experimental data and Equation (17) performs slightly

worse, which provides deviations of 15.6% or less except for 26.8 % for N_I = 16.7Hz.

Notation

a	specific gas-liquid interfacial area, m^{-1}
C,c_1,c_2, c_3	empirical constants in Equations (2), (12) and (14)
c_{in}	dissolved concentration in tap water at inlet, ppmm
c_{out}	dissolved concentration in tap water at outlet, ppmm
c_s	gas-liquid interfacial concentration, ppmm
c_{sin}	inlet gas-liquid interfacial concentration, ppmm
d_I	impeller diameter, m
d_T	tank width or diameter, m
Fr	Froude number; $Fr = N_I^2 d_I^2/gs$
Fr_{cr}	critical Froude number; $Fr_{cr} = N_{cr}^2 d_I^2/gs$
g	gravitational acceleration, m/s^2
h_L	liquid height
H_{O_2}	Henry constant for oxygen in water, L·atm/mol
K, k_1, k_2, k_3	empirical constants in Equations (6), (13) and (15)
k_L	liquid-phase mass transfer coefficient, m/s
k_La	volumetric liquid-phase mass transfer coefficient, s^{-1}
N_A	aeration number; $N_A = Q_I/N_I D_I^3$
N_{cd}	minimum impeller speed for complete dispersion of gas phase, Hz
N_{cr}	critical impeller speed for the onset of gas induction, Hz
N_I	impeller speed, Hz
N_I/N_{cd}	relative dispersion parameter
P_A	atmospheric pressure, Pa
P_G	aerated power consumption, W
P_0	unaerated power consumption, W
P_T	total pressure, Pa
P/V_L	power input per unit volume of liquid, W/m^3
Q_G	volumetric sparged gas flow rate, m^3/s
Q_I	rate of gas induction, m^3/s
Q_L	volumetric liquid flow rate, m^3/s
Re*	modified Reynolds number; $Re^* = N_I d_I^2/v_a$, where $v_a = \frac{0.0065}{\rho}(4\pi N_I)^{-0.17}$
R_I	impeller radius, m
s	impeller submergence, m
Sh	Sherwood number; $Sh = k_L a/(g^2/v_a)^{1/3}$
T	temperature, K

U_G	gas superficial velocity, m/s
V_L	volume of the liquid in the tank, m^3
W	height of impeller, m
Greek letters	
μ	dynamic viscosity, Pa·s
ρ	density, kg/m^3
ΔP_D	total pressure driving force, $N \cdot m^{-2}$
ΔP_{KE}	pressure losses due to kinetic energy imparted to the liquid, $N \cdot m^{-2}$
ΔP_O	pressure losses across the orifice, $N \cdot m^{-2}$
ΔP_P	pressure losses due to friction along the gas pathway, $N \cdot m^{-2}$
ΔP_γ	pressure losses due to surface tension at the gas-liquid interface, $N \cdot m^{-2}$
Abbreviations	
GIAT	gas-inducing agitated tank
PBTD 45°	pitched-blade downflow turbine with blade angle of 45°
PBTD 60°	pitched-blade downflow turbine with blade angle of 60°
STR	stirred tank reactor
VFD	variable frequency driver

References

Calderbank, P.H., "Physical Rate Processes in Industrial Fermentation .Part II: Mass Transfer Coefficients in Gas-Liquid Contacting with and without Mechanical Agitation.", Transaction of the Institution of Chemical Engineers, 1959, 37, 173-185.

Calderbank, P.H., Moo-Young, M.B., "The continuous phase heat and mass-transfer properties of dispersions", Chemical Engineering Science, 1961, 16, 1-2, 39-54.

Dhainaut, M., Tetlie, P., Bech, K., " Modeling and experimental study of a stirred tank reactor", International Journal of Chemical Reactor Engineering, 2005, 3, 1, 1-17.

Fillion, B., Morsi, B.I., "Gas-liquid mass-transfer and hydrodynamic parameters in a soybean oil hydrogenation process under industrial conditions", Industrial & Engineering Chemistry Research, 2000, 39, 7, 2157-2168.

Forrester, S.E., Rielly, C.D., Carpenter, K.J., "Gas-inducing impeller design and performance characteristics", Chemical Engineering Science, 1998, 53, 4, 603-615.

Garcia-Ochoa, F., Castro, E.G., "Estimation of oxygen mass transfer coefficient in stirred tank reactors using artificial neural networks", Enzyme Microb Tech, 2001, 28, 6, 560-569.

Hallaile, M., Merchuk, J.C., "Operation Policies for a Gas-Liquid Stirred Tank Reactor" Chemical Engineering Communications, 1986, 46, 4-6, 179-196.
Heim, A., Kraslawski, A., Rzyski, E., Stelmach, J., "Aeration of Bioreactors by Self-Aspirating Impellers", Chemical Engineering Journal and the Biochemical Engineering Journal, 1995, 58, 1, 59-63.
Joshi, J.B., Sharma, M.M., "Mass transfer and hydrodynamic characteristics of gas inducing type of agitated contactors", Canadian Journal of Chemical Engineering, 1977, 55, 6, 683-695.
Kasundra, R.B., Kulkarni, A.V., Joshi, J.B., "Hydrodynamic and mass transfer characteristics of single and multiple impeller hollow self-inducing reactors", Industrial & Engineering Chemistry Research, 2008, 47, 8, 2829-2841.
Kresta, S. M., Mao, D. M., and Roussinova, V., "Batch blend time in square stirred tanks", Chemical Engineering Science, 2006, 61, 9, 2823-2825.
Leentvaar, J., and Ywema, T. S. J., "Some Dimensionless Parameters of Impeller Power in Coagulation-Flocculation Processes", Water Res, 1980, 14, 2, 135-140.
Lemoine, R., Fillion, B., Morsi, B., "Hydrodynamic and mass transfer parameters in agitated reactors Part I: critical mixing speed, induced gas flow rate, and wavy surface in SARs and GIRs", International Journal of Chemical Reactor Engineering, 2004, 2, 1, 1-31.
Lemoine, R., Morsi, B., "Hydrodynamic and mass transfer parameters in agitated reactors part II: Gas-holdup, sauter mean bubble diameters, volumetric mass transfer coefficients, gas-liquid interfacial areas, and liquid-side mass transfer coefficients", International Journal of Chemical Reactor Engineering, 2005, 3, 1, 1-47.
Miller, D.N., "Scale-up of Agitated Vessels Gas-Liquid Mass-Transfer", AIChE Journal, 1974, 20, 3, 445-453.
Nienow, A.W., Wisdom, D.J., Middleton, J.C., "Effect of scale and geometry on flooding, recirculation and power in gassed stirred vessels", 2nd European conference on mixing, 1977, Cambridge, UK, pp. 1-16.
Patil, S.S., Mundale, V.D., Joshi, J.B., "Mechanism of gas induction in a self-inducting impeller", Industrial & Engineering Chemistry Research, 2005, 44, 5, 1322-1328.
Patwardhan, A.W., Joshi, J.B., "Design of gas-inducing reactors", Industrial & Engineering Chemistry Research, 1999, 38, 1, 49-80.
Pinelli, D., Liu, Z.H., Magelli, F., "Analysis of KLa measurement methods in stirred vessels: the role of experimental techniques and fluid dynamic models", International Journal of Chemical Reactor Engineering, 2010, 8, 1, 1-38.
Poncin, S., Nguyen, C., Midoux, N., Breysse, J., "Hydrodynamics and volumetric gas-liquid mass transfer coefficient of a stirred vessel equipped with a gas-inducing impeller", Chemical Engineering Science, 2002, 57, 16, 3299-3306.

Raidoo, A.D., Rao, K.S.M.S.R., Sawant, S.B., Joshi, J.B., "Improvements in gas inducing impeller design", Chemical Engineering Communications, 1987, 54, 1-6, 241-264.

Saravanan, K., Joshi, J.B., "Gas-inducing-type mechanically agitated contactors: hydrodynamic characteristics of multiple impellers", Industrial & Engineering Chemistry Research, 1995, 34, 7, 2499-2514.

Saravanan, K., Mundale, V.D., Patwardhan, A.W., Joshi, J.B., "Power consumption in gas-inducing-type mechanically agitated contactors", Industrial & Engineering Chemistry Research, 1996, 35, 5, 1583-1602.

Sardeing, R., Xuereb, C., Poux, M., "Improvement of the performances of a gas-inducing system for application in wastewater treatment", International Journal of Chemical Reactor Engineering, 2006, 4, 1, 1-21.

Sawant, S.B., Joshi, J.B., "Critical impeller speed for the onset of gas induction in gas-inducing types of agitated contactors", Chemical Engineering Journal, 1979, 18, 87-91.

Sawant, S.B., Joshi, J.B., Pangarkar, V.G., Mhaskar, R.D., "Mass transfer and hydrodynamic characteristics of the denver type of flotation cells", Chemical Engineering Journal and the Biochemical Engineering Journal, 1981, 21, 1, 11-19.

Sideman, S., Hortacsu, O., Fulton, J.W., "Mass Transfer in Gas-Liquid Contacting Systems", Industrial and Engineering Chemistry, 1966, 58, 7, 32-47.

Tekie, Z., Li, J.J., Morsi, B.I., "Mass transfer parameters of O2 and N2 in cyclohexane under elevated pressures and temperatures: A statistical approach", Industrial & Engineering Chemistry Research, 1997, 36, 9, 3879-3888.

Yawalkar, A.A., Heesink, A.B.M., Versteeg, G.F., Pangarkar, V.G., "Gas-liquid mass transfer coefficient in stirred tank reactors", Canadian Journal of Chemical Engineering, 2002a, 80, 5, 840-848.

Yawalkar, A.A., Pangarkar, V.G., Beenackers, A., "Gas hold-up in stirred tank reactors", Canadian Journal of Chemical Engineering, 2002b, 80, 1, 158-166.

Zieverink, M.M.P., Kreutzer, M.T., Kapteijn, F., Moulijn, J.A., "Gas-liquid mass transfer in benchscale stiHe-Tanrred tankss-fluid properties and critical impeller speed for gas induction", Industrial & Engineering Chemistry Research, 2006, 45, 13, 4574-4581.